Vol. 164, October 1, 1984
Complete in one issue

ISSN 0003-2670

ANALYTICA CHIMICA ACTA

International journal devoted to all branches of analytical chemistry

ELSEVIER

ANALYTICA CHIMICA ACTA

International journal devoted to all branches of analytical chemistry
Revue internationale consacrée à tous les domaines de la chimie analytique
Internationale Zeitschrift für alle Gebiete der analytischen Chemie

PUBLICATION SCHEDULE FOR 1984

	J	F	M	A	M	J	J	A	S	O	N	D
Analytica Chimica Acta	156	157/1	157/2	158/1 158/2	159	160	161	162	163	164	165	166

Scope. *Analytica Chimica Acta* publishes original papers, short communications, and reviews dealing with every aspect of modern chemical analysis, both fundamental and applied.

Submission of Papers. Manuscripts (three copies) should be submitted as designated below for rapid and efficient handling:

Papers from the Americas to: Professor Harry L. Pardue, Department of Chemistry, Purdue University, West Lafayette, IN 47907, U.S.A.

Papers from all other countries to: Dr. A. M. G. Macdonald, Department of Chemistry, The University, P.O. Box 363, Birmingham B15 2TT, England. Papers dealing particularly with computer techniques to: Professor J. T. Clerc, Universität Bern, Pharmazeutisches Institut, Baltzerstrasse 5, CH-3012 Bern, Switzerland.

Submission of an article is understood to imply that the article is original and unpublished and is not being considered for publication elsewhere. Upon acceptance of an article by the journal, authors will be asked to transfer the copyright of the article to the publisher. This transfer will ensure the widest possible dissemination of information.

Information for Authors. Papers in English, French and German are published. There are no page charges. Manuscripts should conform in layout and style to the papers published in this Volume. Authors should consult Vol. 160 for detailed information. Reprints of this information are available from the Editors or from: Elsevier Editorial Services Ltd., Mayfield House, 256 Banbury Road, Oxford OX2 7DH (Great Britain).

Reprints. Fifty reprints will be supplied free of charge. Additional reprints (minimum 100) can be ordered. An order form containing price quotations will be sent to the authors together with the proofs of their article.

Advertisements. Advertisement rates are available from the publisher.

Subscriptions. Subscriptions should be sent to: Elsevier Science Publishers B.V., Journals Department, P.O. Box 211, 1000 AE Amsterdam, The Netherlands. Tel: 5803 911, Telex: 18582.

Publication. *Analytica Chimica Acta* appears in 11 volumes in 1984. The subscription for 1984 (Vols. 156–166) is Dfl. 2145.00 plus Dfl. 231.00 (p.p.h.) (total approx. U.S. $914.00). All earlier volumes (Vols. 1–155) except Vols. 23 and 28 are available at Dfl. 215.00 (U.S. $82.70), plus Dfl. 15.00 (U.S. $6.00) p.p.h., per volume.

Our p.p.h. (postage, packing and handling) charge includes surface delivery of all issues, except to subscribers in Australia, Brazil, Canada, China, Hong Kong, India, Israel, Japan, Malaysia, New Zealand, Pakistan, Singapore, South Africa, South Korea, Taiwan and the U.S.A. who receive all issues by air delivery (S.A.L. — Surface Air Lifted) at no extra cost. For the rest of the world, airmail and S.A.L. charges are available upon request.

Claims for issues not received should be made within three months of publication of the issues. If not they cannot be honoured free of charge.

For further information, or a free sample copy of this or any other Elsevier Science Publishers journal, readers in the U.S.A. and Canada can contact the following address: Elsevier Science Publishing Co., Inc., Journal Information Center, 52 Vanderbilt Avenue, New York, NY 10017, U.S.A., Tel: (212) 916-1250.

ELSEVIER is going ELSWARE

'Elsware' with its software.
Elsevier, publisher of many journals in all of the major scientific fields, is now going elsewhere with the launch of its first series of programs for both mini and micro-computers.

Unlike other software publishers, we have some unique features .....

programs are extensively refereed and operationally tested; program manuals usually include source code listings; free updates are provided for a year and comprehensive information is available before ordering.

PROGRAMS AVAILABLE

REFVALUE: calculates reference intervals from total hospital-patients laboratory data. (Baadenhuysen and Smit) **for PDP and HP 85 (and in prep. for IBM-PC).**
Price: Mini computer US$ 1080,00
Micro computer US$ 500,00

BALANCE: a program to statistically compare two series of measurements (Massart) **for IBM-PC and APPLE.**
Price: US$ 150,00

CLEOPATRA: Chemometrics Library: an Extendable set Of Programs as an Aid in Teaching, Research and Application. (Kateman) **for HP 9845 B (and in prep. for IBM-PC).**
Price: US$ 600,00

INSTRUMENTUNE-UP: helps the user to improve the performance of common scientific laboratory instruments (Deming and Morgan) **for IBM-PC and APPLE.**
Price: US$ 150,00

and in preparation:

CHEOPS: CHEmometrical OPtimization by Simplex. The program offers an intelligent, sequential experimental plan, based on the modified or super-modified simplex method. It optimizes the response of a system by varying up to ten instrumental parameters.

CLUE: a program for heirarchical divisive clustering.

ESS

Please send me further information on:

[ ] REFVALUE [ ] BALANCE [ ] CHEOPS
[ ] CLEOPATRA [ ] INSTRUMENTUNE-UP [ ] CLUE

ESS
ELSEVIER SCIENTIFIC SOFTWARE

Name .....
Address .....
City ..... Country .....

send this coupon to:

Keith Foley, Elsevier Scientific Software,
P.O. Box 330, 1000 AH Amsterdam,
The Netherlands. (Tel.: 020 - 5803 447)

or:
John Tagler, Elsevier Scientific Software (NASD)
52 Vanderbilt Ave, New York, NY 10017.
(Tel.: 212 867 9040)

ANALYTICA CHIMICA ACTA
VOL. 164 (1984)

ANALYTICA CHIMICA ACTA

International journal devoted to all branches of analytical chemistry

ELSEVIER Amsterdam–Oxford–New York–Tokyo

 0003-2670/84/$03.00

Printed in The Netherlands

Analytica Chimica Acta, 164 (1984) 1—21
Elsevier Science Publishers B.V., Amsterdam — Printed in The Netherlands

Review

THE VOLTAMMETRIC APPROACH IN TRACE METAL CHEMISTRY OF NATURAL WATERS AND ATMOSPHERIC PRECIPITATION

H. W. NÜRNBERG

Institute of Applied Physical Chemistry, Nuclear Research Center (KFA), D-5170 Jülich (Federal Republic of Germany)

(Received 29th May 1984)

SUMMARY

Advanced voltammetry, predominantly in the differential-pulse mode, has become one of the most significant and suitable methods for investigations of the level, fate and transfer of heavy metals with toxicological significance in the ecology of aquatic systems and atmospheric precipitations. In addition, voltammetry offers particular potentialities for studies of heavy metal speciation in natural waters. The salient aspects of the overall analytical procedure are discussed. The substantial possibilities for application are emphasized by a number of examples taken from recent work.

GENERAL ASPECTS OF ECOLOGICAL AND AQUATIC CHEMISTRY

Certain heavy metals have gained great significance in chemical and toxicological studies of the environment (see, e.g. [1—3]). Among those heavy metals are metals such as Cd, Pb and Hg which are generally toxic even at very low levels, and potentially toxic metals (e.g. Cu, Zn and Ni) which also have indispensable essential properties with different threshold levels for different types of plants and organisms, including man [4]. In contrast to most of the numerous other environmentally important chemicals, metals have the particular property of not being biologically degradable. Instead, they are accumulated by plants and organisms and undergo a biogeochemical cycle in the environment during which they are transformed into various chemical species (complexes and/or compounds). Of particular importance for the transfer of metals through the environment are all types of natural waters (rivers, lakes, ground water and the sea) as well as the atmosphere. From the atmosphere, the precipitations (rain and snow) can be an especially important mechanism for the transfer of heavy metals into terrestrial and aquatic systems (see Fig. 1).

In highly industrialized and/or densely populated regions, particularly in Europe, North America and Japan but also in other parts of the world, the sources of heavy metal emission are almost exclusively of anthropogenic origin. The input into inland waters (rivers and lakes) occurs either directly

0003-2670/84/$03.00

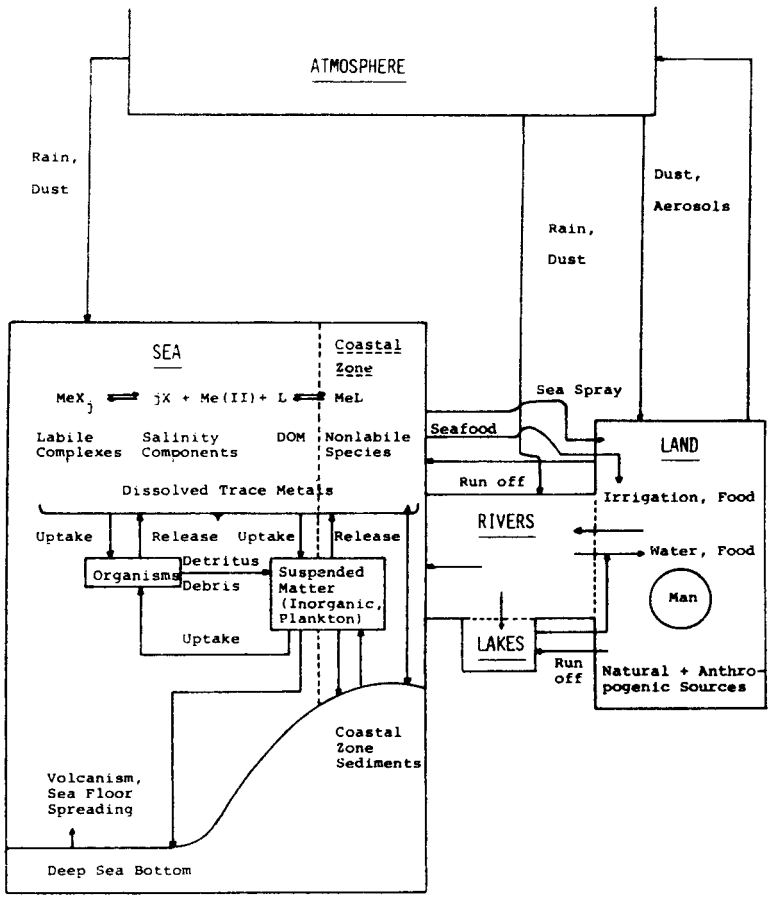

Fig. 1. Biogeochemical cycle of metals in the environment with details of fate in the sea. The interactions of dissolved metals and metals bound to suspended matter with the sediments in shallow water which are indicated for the coastal zone also apply to rivers and shore zones of lakes. The scheme depicted for the sea applies to rivers and lakes as well for the interactions of metals in the dissolved state with suspended matter and organisms.

by waste-water discharge and run-off water from polluted land or indirectly via emission into the atmosphere and subsequent wet and dry deposition. In other parts of the globe, natural sources of heavy metals, particularly volcanism and large bushfires, are of great significance.

If one considers the global biochemical cycle of the metals (Fig. 1), it is clear that there is a distinct tendency for metal transfer from the land to the sea which acts as a pseudo-sink. Again for the input into the sea, there are two main pathways, fluvial input and coastal run-off and deposition from the atmosphere. Nevertheless, the sea remains only a pseudo-sink, because the metal cycle is at least partly closed in two ways, by the marine food

chains that ultimately reach birds, land animals and man and by sea spray in coastal regions. While the fluvial input and the coastal run-off water is significant primarily for coastal and estuarine waters, heavy metal input into the open oceans probably occurs mainly by deposition from the atmosphere. In certain areas of the open sea, transport from coastal waters by currents can contribute. Furthermore, there are parts of the oceans, particularly the Pacific, where marine volcanism contributes to the heavy metal input into the deep oceanic bottom waters which are still largely uninvestigated. A further natural source at the ocean bottom is the sea floor spreading in the rift zones.

In all types of natural waters, the toxic heavy metal levels remain in the trace or even ultra-trace range. The typical range goes from several hundred $\mu g\ l^{-1}$ in highly polluted rivers to 0.001 $\mu g\ l^{-1}$ in unpolluted open ocean waters, depending also on the particular heavy metal. Rain in slightly to heavily polluted regions usually contains heavy metal levels between 0.1 and 1000 $\mu g\ l^{-1}$ depending again on the particular metal. Despite their occurrence at only trace levels, these toxic heavy metals constitute a group of prime significance among the chemicals of environmental importance in natural waters, because of their accumulation by aquatic organisms.

In the column of water, the total content of the heavy metals is distributed between the dissolved state and the suspended matter phase. The actual degree of this distribution differs for the various heavy metals and also depends on the composition of the suspended matter. This consists generally of particles of biological and organic nature (phytoplankton, bacteria) and their degradation products (detritus), fecal debris and possibly humic materials, as well as of inorganic (clay, silica) particles which can often be coated by a layer of organic matter sorbed on their surface that can exhibit specific complexation properties. Further, the dissolved phase of natural waters can contain significant amounts of dissolved organic matter (DOM), particularly if the biological productivity is high, and dissolved humic substances, particularly in some inland waters. The sources of DOM are mainly of natural origin as a result of metabolic exudation predominantly by plankton as well as their degradation after death. In polluted waters, however, a number of anthropogenic organic compounds can also contribute to the DOM. As a consequence of their complexation properties, DOM components can significantly affect the speciation pattern of dissolved heavy metals in natural waters.

The dissolved state is of great significance for the fate of the heavy metals in natural waters, because it is the phase in which heavy metal transfer between important fundamental components (suspended particles and organisms) of aquatic systems predominantly occurs. From the dissolved state, heavy metals can be taken up by phytoplankton and so enter the aquatic food chains. In addition, for higher organisms (molluscs, crustaceans and fish), direct heavy metal uptake from the water via the gills constitutes an important pathway in addition to the indirect uptake with food. For regulation of the concentration of the total heavy metal content (amounts in

the dissolved and suspended phases), the suspended matter is of prime importance as it provides efficient transfer to the surface layer of the bottom sediments and, when resuspension occurs, from sediments back into the water column. These interactions with the bottom sediments are of particular significance in rivers and estuaries as well as in the shallow waters of coastal zones of the sea or great inland lakes. But water loaded with elevated dissolved heavy metal levels may also be brought to surface waters by upwelling from the greater depths of the sea.

The aquatic chemistry of heavy metals is obviously a very demanding research area with a wide spectrum of aspects to be investigated for particular aquatic systems. From the methodological viewpoint, such investigations always require the methods and working approaches of advanced and often ambitious trace chemistry.

ASPECTS OF TRACE ANALYSIS

Instrumental methods of determination are needed which combine high sensitivity with high accuracy, i.e., small risks of systematic errors, and satisfactory precision. Reasonable rates of determination (especially simultaneous determinations), convenience in operation, compactness of instrumentation (for measurements on ships and boats) and reasonable costs for the necessary instrumentation are further important features of any really useful method.

Speciation is of prime importance in studies of the interactions of dissolved heavy metals with suspended particles, sediment surfaces and organisms. It is highly significant for concentration regulation in waters and for toxic effects. Thus species-sensitive methods of determination provide a much wider potential for applications than methods which are only element-specific.

Although numerous instrumental methods of determination are now available, very few correspond satisfactorily with all the general requirements outlined above. Among the most suitable methods for the determination of these heavy metals, advanced voltammetry, usually in the differential-pulse or sometimes the square-wave mode, is very attractive [5]. Voltammetry can be extremely sensitive and provides inherently high precision and potentialities for simultaneous determinations of various heavy metals. Moreover, voltammetry has the particular advantage of being, in principle, a species-sensitive method, not just an element-sensitive method, providing very significant and versatile opportunities for studies of heavy metal speciation in natural waters.

These potentialities, stemming fundamentally from the fact that voltammetry is based on Faraday's laws, have made the voltammetric approach a first choice for trace analysis and studies of trace chemistry of environmentally significant heavy metals in all types of natural waters [6, 7]. The most important alternatives are the relevant modes of atomic absorption spectrometry (a.a.s.). Critical assessment shows, however, that for the heavy metals considered, voltammetry usually provides the superior approach for natural

waters. An exception is mercury where the cold-vapour a.a.s. mode is somewhat more sensitive and also more convenient [8, 9]. The higher sample throughput often claimed for a.a.s. remains largely fictitious in practice, because a.a.s. is conventionally a single-element technique. In aquatic systems, several heavy metals (e.g. Cu, Pb, Cd, Zn or Ni and Co or Hg and Cu, etc.) usually have to be determined. The potential of voltammetry for simultaneous determinations thus balances the faster measurement rate of a.a.s. for a single element; moreover, if comparable precision is to be achieved, a.a.s. needs more test measurements than voltammetry. Yet, the a.a.s. technique undoubtedly has the advantage that it is very sensitive for a greater number of other metals. This aspect is also valid for various multi-element methods which are much more sophisticated in instrumental and cost requirements than voltammetry or a.a.s., such as atomic emission spectrometry with inductive-coupled plasma excitation (i.c.p.-a.e.s.), x-ray fluorescence (x.r.f.) or neutron activation analysis (n.a.a.). All these multi-element methods have the decisive drawback that they are usually not sensitive enough for direct determinations of heavy metals in natural waters. It should be noted that other metals, besides the considered toxic heavy metals, can be determined by voltammetry, but in most of these cases voltammetry has no, or few, advantages over other possible instrumental methods.

For most problems in the trace metal chemistry of natural waters, voltammetric determinations of the toxic heavy metals require prior preconcentration for low levels of concentration, in the same way as other instrumental methods. This is where the electrochemical approach provides its greatest inherent advantage because the preconcentration can be done electrochemically in the same cell as the final measurements. Thus, in contrast to common chemical preconcentration procedures there is little risk of additional contamination.

RELEVANT MODES OF VOLTAMMETRY

Stripping methods

Amalgam-forming heavy metals, such as Cu, Pb, Cd, Zn, are frequently determined by differential-pulse anodic stripping voltammetry (d.p.a.s.v.) at the mercury electrode. If the hanging (HMDE) or stationary (SMDE) mercury drop electrode can be applied, these four metals are determined simultaneously and preconcentration is achieved by applying a plating potential of −1.2 V vs. Ag/AgCl for several minutes with stirring of the solution (900 rpm). Precise adjustment of the plating potential excludes interference by hydrogen evolution even at pH 2 with this type of mercury working electrode. The HMDE or SMDE can be applied for heavy metal concentrations typically down to 0.1 $\mu g\ l^{-1}$ or even less [5, 10, 11]. Certain trace elements, such as selenium (IV), can be determined after electrochemical preconcentration at a rather positive potential (−0.2 V) as a HgSe layer by differential-pulse cathodic stripping voltammetry (d.p.c.s.v.) subsequently in the same run [10].

In the ultra-trace range, however, down to 0.001 $\mu g\ l^{-1}$, and for cadmium even 0.0001 $\mu g\ l^{-1}$, the mercury film electrode (MFE) formed in situ during the plating stage on a specially prepared glassy carbon substrate electrode is required. For this purpose, the analyte is spiked with mercury(II) nitrate, the mercury(II) ion concentration in the analyte being about 10^{-5} M. During the plating step the electrode is rotated at 1500 rpm to speed up mass transfer [12].

Figure 2 shows an example of the simultaneous determination of five metals in rain water. Usually, precise determinations require evaluation of the metal concentrations by standard additions for all types of natural waters. Frequently, two or three standard additions suffice. The use of calibration graphs is normally not to be recommended; the electrode processes and consequently the precise peak heights are very sensitive to inhibition effects of varying magnitude, caused by variations in the levels of traces of surface-active substances present in most natural waters. Therefore the safe way to ensure precise evaluation of concentrations is the standard additions approach. This is true also for all the other versions of voltammetric analysis discussed below.

With the HMDE or SMDE, precleaned glass or quartz cells can be used, but for the ultra-trace range (to which the application of the MFE is normally restricted) teflon cells are needed because quartz or glass cells can release minute amounts of the heavy metals to be determined. The MFE is predominantly used for sea water or pure inland fresh waters. For further prevention of contamination, reference and auxiliary electrodes are kept in special compartments of the teflon cell connected to the analyte by Vycor glass frits. Lead, cadmium and copper can be determined simultaneously at the MFE by d.p.a.s.v. [12]. Because of the lower hydrogen overvoltage of the MFE, less negative plating potentials of —1.0 V (Ag/AgCl) are applied in media at pH 2. Therefore, zinc has to be determined separately at pH 4.5.

During recent years, automation has been introduced in voltammetric analysis and various partly automated commercial systems have appeared.

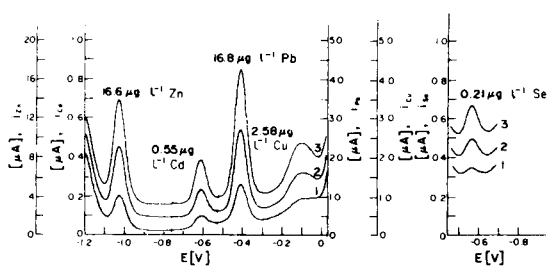

Fig. 2. Simultaneous d.p.a.s.v. determination at the SMDE of Zn, Cd, Pb and Cu in rain water (plating potential, E_d, —1.2 V; plating time, t_d, 3 min). Subsequently in same run, determination of Se(IV) by d.p.c.s.v. (E_d = —0.2 V, t_d = 5 min). Curves: (1) sample; (2, 3) first and second standard additions.

With these instruments, certain functions of the voltammetric measurement are automated and data are processed. Recently, a fully automated microprocessor-controlled instrument, the Voltammat was introduced for d.p.a.s.v. determinations of heavy metals at the SMDE [13]. All steps of the voltammetric procedure including standard additions and rinsing of the voltammetric cell before each run are automated. Voltammetric responses can be stored, compared and subtracted from each other and the results are displayed as voltammograms and in digital form. All stages of the sample pretreatment in the laboratory (filtration, acidification, u.v. irradiation) can, if necessary for the type of water, be included in the fully automated scheme if a photodigestion device [14] is combined with the Voltammat. Obviously, this fully automated approach will greatly simplify routine analysis and monitoring of toxic heavy metals in natural waters and atmospheric precipitations (rain and snow). This automated instrument can also be applied advantageously for heavy metal determinations in aqueous solutions obtained by digestion of biological materials (e.g., fish, mussels, crustaceans and plankton) from aquatic systems.

Mercury and copper can be determined simultaneously after acidification of the water sample to pH 1 by d.p.a.s.v. at an activated gold electrode [15–17]. For higher levels of copper, the gold electrode is even more suitable than the mercury electrode, because the problems connected with the limited solubility of copper as an amalgam in mercury are totally eliminated. In natural waters with chloride concentrations above 10^{-2} M, medium exchange after the plating stage becomes necessary. Before stripping, the water sample is replaced by a 0.1 M perchloric acid/2.5 $\times$ 10^{-3} M hydrochloric acid solution. Otherwise, the substantial response corresponding to chloride oxidation interferes and the chlorine formed damages the surface of the gold electrode.

For ultra-trace concentrations of mercury between 1 and 40 ng l^{-1}, which occur frequently in sea water, a more complicated voltammetric procedure is needed. During the plating stage, instead of the usual constant potential, a programmed polarization scheme with short intermittent anodic cleaning pulses to strip the copper from the plated mercury layer is required. After medium exchange, mercury is determined by subtractive d.p.a.s.v. at a twin gold electrode formed by splitting a gold disc into two halves insulated from each other [15, 17]. With this method, reliable data on the mercury levels in the German Bight have been obtained [17].

The normal gold-disc electrode has also been successfully applied for sensitive d.p.a.s.v. determinations of arsenic(III) down to 0.1 μg l^{-1} [18]. Arsenic(V) gives no response and requires prior chemical reduction to arsenic(III).

Adsorption voltammetry

A substantial number of heavy metals do not form stable amalgams and therefore cannot be determined by the stripping approach. Adsorption

voltammetry then becomes useful. It is based on electrochemical preconcentration by adsorption of a suitable species of the substance to be determined. This approach can be extended to a number of metals and inorganic and organic substances and has been widely studied. Recently, it has been applied successfully to the simultaneous determination of traces of nickel and cobalt [19—22]. For these two metals, the sample solution is adjusted to pH 9.2 with ammoniacal buffer and enough dimethylglyoxime (DMG) is added to give a concentration of about 10^{-4} M; a proportion of the Ni(II) and Co(II) present is complexed as $Ni(DMG)_2$ and $Co(DMG)_2$ while the rest of both metal ions are converted to their ammine complexes. The dimethylglyoxime complexes are surface-active and adsorb at the surface of a HMDE or SMDE. To attain optimal adsorption conditions, the electrode is held for several minutes at a potential of —0.7 V (Ag/AgCl), i.e., close to its zero charge potential, while the solution is stirred at 900 rpm to speed up mass transfer to the interface. Subsequently, stirring is stopped and the potential is scanned in the negative direction to the reduction potentials of nickel and cobalt. As there is no reversal in the potential scan, this method is not a stripping method. For ultra-trace concentrations of both metals, this scan to more negative potentials is done in the differential-pulse mode; the method may then be termed adsorption differential-pulse voltammetry (a.d.p.v.). As all complex equilibria in the sample solution are adjusted, as are the adsorption equilibria of the DMG complexes, the amount of metals adsorbed remains proportional to the overall bulk concentration of the metals provided that full coverage of the electrode surface is avoided. This can be achieved by appropriate selection of the ammonia buffer concentration and of the time allowed at the adsorption potential.

This adsorption approach provides very efficient electrochemical preconcentration and can be extended to many other cases [21, 22], whereas applications of the stripping approach are more restricted. Similar restrictions also apply to potentiometric stripping analysis [23].

Adsorption voltammetry has been extended to provide a sensitive, fast method for the determination of dissolved silica traces in natural waters and boiler feed water [24]; silica is preconcentrated by the formation of the heteropoly acid anion, $(SiMo_{12}O_{40})^{4-}$, after addition of molybdate to the solution, and adsorption of this species on the HMDE. The response resulting from the reduction of molybdenum(VI) in the adsorbed heteropoly acid anion allows silica to be determined down to 10^{-7} M. This approach is much faster than the conventional spectrophotometric determination based on molybdenum blue.

Limits of determination

The ultimate practical limits of determination that can be obtained with reasonable precision by operators with expertise in voltammetry and ultra-trace chemistry are listed in Table 1. It is emphasized that these limits are set by the presently remaining low blanks; the ultimate limits with the

TABLE 1

Limits of determination of differential-pulse methods (giving 20% or 10% relative standard deviations) for heavy metals in natural waters

Method	Limit of determination ($\mu g\ l^{-1}$)[a]								
	Cu	Pb	Cd	Zn	Ni	Co	Hg	Se(IV)	As(III)
D.p.s.v./ HMDE	0.05 (0.10)	0.02 (0.30)	0.02 (0.10)	0.02 (0.50)	—	—	—	0.01 (0.50)	—
D.p.s.v./ MFE	0.007 (0.05)	0.001 (0.0015)	0.0003 (0.0015)	—	—	—	—	—	—
D.p.s.v./ AuE	0.02 (0.10)	—	—	—	—	—	0.04[b] (0.20)	—	0.1 (1.0)
A.d.p.v./ HMDE	—	—	—	—	0.001 (0.02)	0.001 (0.02)	—	—	—

[a]The limits for 10% RSD are given in parentheses. [b]At twin AuE with subtractive d.p.a.s.v., 0.001 $\mu g\ l^{-1}$ can be determined.

differential-pulse modes, set by instrumental noise alone, would be substantially lower. Thus, in principle, further improvement of the sensitivity could be achieved by reducing the blanks further. This is, however, only worthwhile for special problems. For example, the determination limit for cadmium in snow from polar regions has been lowered to <0.1 ng kg^{-1} (i.e., 10^{-10} g kg^{-1}) with RSD of 50%, for baseline studies in Arctic snow deposits [25]. Other low baselines are under investigation for Antarctic snow deposits [26].

THE OVERALL ANALYTICAL PROCEDURE

The scheme of the overall procedure for voltammetric determinations is given in Fig. 3. It is obvious that quantitative methods giving high performance must be combined with adequate procedures of sampling and sample pretreatment. The overall reliability will depend on adequate minimization of contamination risks, particularly from trace levels of metals and elimination of losses of the heavy metal traces.

Sampling

Sampling is one of the most critical stages in any practical analysis. Any systematic errors introduced at this first stage will make the subsequent work unreliable and the final data will be useless, or even worse may lead to wrong chemical, geochemical and toxicological conclusions in environmental studies. Underestimation of the problems in the sampling stage are largely responsible for the fact that most of the data on trace elements in sea-water and many fresh-water systems obtained before 1975 have now to be regarded as obsolete or at least very doubtful [27].

More reliable sampling procedures have been introduced in very recent years in this and a few other laboratories and have become gradually more

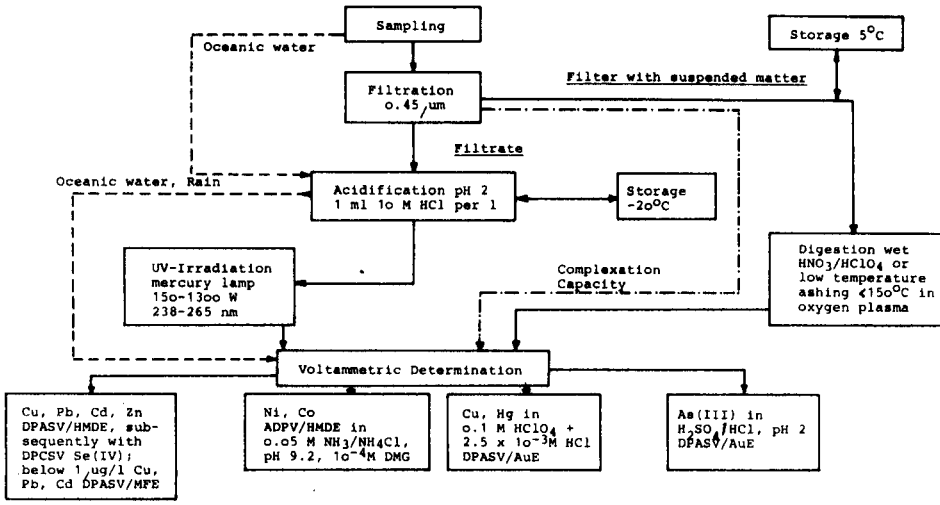

Fig. 3. Outline of the overall procedure for voltammetric analysis of natural waters.

widely adopted. Full details are available in the references cited below. Precleaned sampling flasks from polyethylene are used.

Surface water (0.3—1 m depth) is collected under special precautions from small fresh-water systems (rivers, creeks, ponds) from the banks with special sampling gear; in large rivers, lakes and in the sea, collection is done manually also, the hands being protected by polyethylene gloves, against the wind from the bow of small rubber or plastic boats [28, 29]. Collection of surface-water samples from on board larger research vessels will usually produce artefacts, because of the heavy metal contamination plume around any large ship.

Sample volumes between one and several litres are usually collected. Substantially larger volumes, as provided by the large water collectors common in conventional oceanography, cannot be collected and manipulated in the subsequent stages of sample pretreatment with sufficient minimization of contamination and are therefore unsuitable for trace metal studies.

Reliable deep-water sampling is a special and demanding art. For intermediate depths, down to typically 100 m, dynamic sampling with specially adapted GoFlo flasks yields satisfactory results. Special devices must be used for deep oceanic waters and for oceanic bottom water. In collection of deep waters, the principle of dynamic sampling has been applied, the opening of the sampler being brought into contact only with virgin uncontaminated water while the sampler is slowly lowered during sampling [30, 31].

For the reliable collection of rain and snow precipitation from the atmosphere, automated samplers which open only during the precipitation period have been introduced [32, 33]. In this manner, reliable discrimination between wet deposition and dry deposition of (by dust particles) has become possible.

For baseline studies in snow from polar and high alpine regions, meticulous manual sampling approaches with non-metallic equipment yield reliable results [25, 26].

It should be noted that for mercury determinations, aliquots from water samples collected in polyethylene flasks have to be transferred as soon as possible into glass bottles. Otherwise, losses of mercury during storage are inevitable [34].

Sample pretreatment

The subsequent sample pretreatment depends on the type of the natural water and on the purpose of the investigation, e.g., speciation studies or determination of the heavy metal levels in the dissolved and suspended matter phase.

Filtration. To separate the suspended matter from the water, the first step is filtration. To avoid contamination from dust in the ambient atmosphere, a closed system is needed for filtration [29, 35]. According to the usual convention in aquatic trace-metal chemistry, a cellulose acetate membrane filter with 0.45 μm pore size is used. Heavy metals contained in the filtrate are regarded as dissolved. Strictly speaking, this is an operational definition but at least it is usually a reasonably good approximation to reality. However, with some natural water samples, a fraction of small colloidal particles passes the 0.45-μm pore filter [36]. There are also some natural waters e.g., from certain regions in the oceans or certain creeks and fountains, in which the concentration of suspended matter is negligible [37]. In such cases, filtration is not necessary and this step can be omitted, in accordance with the general philosophy of avoiding all unnecessary handling of water samples so as to avoid contamination risks that lurk everywhere. As such natural waters usually contain only very low trace levels of heavy metals, this working principle becomes particularly important.

If speciation studies are intended, this separation of suspended matter from the water by filtration is the only permissible sample pretreatment [38, 39]. All further pretreatment procedures will inevitably alter the heavy metal species distribution in the sample of natural water. However, for analytical determinations of the overall levels of the heavy metals in the dissolved phase further pretreatment is necessary to adjust the water sample to the optimal conditions needed to attain fully the limits of determination given in Table 1.

The further treatment of the filtrate will be considered first. Usually, water from rivers, lakes and the sea has a natural pH between 6 and 8 (sea water). This pH is not optimal for exploiting the full sensitivity of voltammetry. As the pH must not be altered for speciation studies, such studies cannot be done at dissolved heavy metal levels lower than 10^{-9} M or about 0.1 μg l^{-1}. This level is close to reality for many natural waters, although in completely unpolluted waters the natural heavy metal levels might be still lower by a factor of 3—10 or more.

Adjustment of pH and storage. If the problem is simply to determine the dissolved heavy metal concentrations under the optimal sensitivity conditions,

the filtrate is acidified to pH 2 by adding small amounts (1 ml l^{-1}) of concentrated hydrochloric or perchloric acid (Merck, Suprapur). The increase in the heavy metal blank by the addition of such small quantities of ultrapure acids remains negligible. Filtration must always be done before acidification for samples containing noticeable concentrations of suspended matter, because otherwise heavy metals would be leached from the suspended matter and transferred to the dissolved state on acidification. The adjustment to acidic medium has also the important consequences that contamination by biological activity in the filtrate is prohibited and that heavy metal adsorption on the vessel wall is avoided. Therefore, such acidified samples can be stored unaltered in their heavy metal content for some time, particularly if they are stored at −20° C and in the dark [5, 11, 12].

Ultraviolet irradiation for photolytic decomposition of DOM. Samples from fresh-water systems (rivers, lakes, ponds), from estuaries and often from coastal waters and also from open ocean areas with high phytoplankton productivity, contain a certain amount of dissolved organic matter (DOM). Certain DOM components bind, predominantly by strong complexation, a certain fraction of the dissolved heavy metals in species not accessible (or accessible only at high overvoltages in rather irreversible electrode processes) to differential-pulse stripping or adsorption voltammetry. Moreover, significant DOM levels might cause interferences, because of adsorption at the electrode. Therefore, DOM must be decomposed before the voltammetric determination. This is achieved without contamination risk by u.v. irradiation which causes photolytic decomposition of DOM [11, 12, 16, 29]. Except for samples from the oceans, which contain only ultra-trace amounts of heavy metals, this photolysis can be speeded up by addition of some 30% hydrogen peroxide (Merck, Suprapur). In the past, 150-W mercury lamps have been applied, but recently the photolysis rate has been speeded up considerably by using high-intensity mercury lamps (1200 W) in an automated photodigestion device in which the concomitant problems of cooling the water samples have been solved [14]. This device can be used either separately or as a module of the fully automated Voltammat (see above) in the determination of heavy metals in natural and waste waters. In the photodigestion device, the pretreatment steps (filtration, acidification and photolysis of DOM in the filtrate) are automated. Yet, for samples with only ultra-trace amounts of heavy metals (e.g., oceanic water), the more time-consuming approach with the 150-W mercury lamp is safer (to exclude contamination), because the u.v. irradiation is done in the teflon voltammetric cell which is used with the MFE, simply by shining the u.v. light through a quartz cover onto the acidified filtrate; the quartz does not come in contact with the solution.

In large parts of the oceans, which are marine deserts, biological productivity is very low and consequently the DOM level remains negligible [37]. This is also true for fresh-water samples from certain small creeks and for rain-water samples, unless they are collected from zones with emissions of organic materials, e.g., regions where there are power plants burning fossil

fuels. In all such cases, where the DOM level remains negligible, the u.v. irradiation step is unnecessary, which not only saves time but also excludes any residual risk of contamination.

Digestion of suspended matter. The filtered-off suspended matter is digested together with the filter. A wet-digestion procedure can be applied which is rather general to all types of biological and organic materials [21, 22]. In this procedure, small amounts of nitric and perchloric acids (i.e., 0.2—0.5 ml of 70% $HClO_4$ and 0.4—1 ml of 65% HNO_3, Merck, Suprapur) are added to $\leqslant 0.5$ g of sample material. Such sample weights are usual for the suspended matter filtered off from the water volumes of 1 to several litres. As the amounts of acid, particularly perchloric acid, can be kept small, there are no safety risks.

A very reliable and convenient but more expensive alternative is low-temperature ashing at 120—150° C in a microwave-induced oxygen plasma [11, 12]. Both sorts of decomposition provide complete mineralization of the organic suspended matter, including any organic coatings on inorganic particles. Except for silica and clay particles, the mineralized sample is completely soluble, giving an acidified aqueous solution in which the heavy metals can be determined by voltammetry.

It should be emphasized that these decomposition processes release the total heavy metal content involved in interactions and possibly exchanges in the suspended matter. If any heavy metals were trapped inside inorganic insoluble particles, they would be of no relevance in this context; entrapped metals are irrelevant for pollution control and do not contribute to the metal content of natural waters either by sedimentation of suspended matter or by resuspension through advection. It should also be noted that the total concentration of a heavy metal in the water column is usually the feature of interest; thus the concentrations in the dissolved state and in the suspended matter are both referred to the unit volume of water. Only rarely are the metals in the suspended matter referred to the weight of that matter. The sum of the suspended and the dissolved heavy metal concentrations gives the total heavy metal concentration per litre in the water column.

The final stage of the procedure is the voltammetric determination, which has already been discussed.

Cleaning of laboratory ware and purity requirements for the laboratory

Scrupulous cleaning of all labware, sampling flasks and filters according to well established procedures is mandatory [29]. Reagents and standard solutions must be prepared with water having extremely low heavy metal blanks; thorough ion-exchange purification is usually satisfactory. Chemicals needed during sample pretreatment for digestion, acidification, etc., and as reagents must have the purity degree of the Merck Suprapur grade.

Care and precautions in handling samples and requirements for the cleanliness of the laboratory increase as the heavy metal contents in the waters studied decrease. Generally, it is recommended and it is often essential, to

run the determinations, including the preceding handling of water samples, in a clean bench with filtered laminar air flow. The general standard of the laboratory has to correspond to advanced trace analysis requirements [29]. This applies also to the general working philosophy of the staff; precleaned polyethylene gloves and possibly even sleeves should be worn to avoid contamination of samples. For work at ultra-trace levels, typically in the range 0.1—20 ng l^{-1}, a clean room laboratory becomes essential.

APPLICATIONS

The growing application of voltammetry in recent years has provided much reliable analytical data which has contributed significantly to the understanding and knowledge about the levels, behaviour, fate and transfer mechanisms of toxic heavy metals in the sea and in fresh-water systems, and about the contributions to the general levels made by atmospheric precipitation. The value of the voltammetric approach in this area of ecological chemistry is illustrated below by a number of important findings from the environmental research program in this Institute.

Oceans, coastal waters and inland waters

As a consequence of their exceptional sensitivity, the modes of voltammetry outlined above have proved excellent for investigation of the levels and distribution of cadmium, lead and copper in various parts of the oceans. So far, contours of the situation in the North Atlantic, the Eastern Arctic, the Western and Central Pacific oceans and in the shelf region of the Tasman Sea and parts of the Weddell Sea have been clarified [31, 37, 40]. Less extensive but similar work has been done for nickel and cobalt. Although the heavy metal levels are all in the ultra-trace range, there are significant differences for different geographic regions. This is connected with several influences, e.g., differences in deposition from the atmosphere, varying oceanographic parameters (currents, age and turnover rate of water masses, upwelling) and variations in biological productivity. Well-defined correlations of a similar type, but differing quantitatively according to the varying oceanographic parameters, between the vertical concentration profiles of nutrient-like metals such as cadmium and copper and the depth profiles of the nutrient concentrations (phosphate, nitrate, silicate) have been established for various ocean regions [37, 40, 41]. An example is shown in Fig. 4.

Detailed studies in Ligurian and Tyrrhenian coastal waters and along the Belgian, Dutch and German North Sea coasts, as well as in the German Bight, have provided reliable data on the heavy metal levels in these important coastal areas [42—44]. A recent study has revealed the distribution and transport of cadmium from the major fluvial input areas of cadmium pollution in the estuaries of the Scheldt, Rhine, Weser and Elbe with the northbound current over the North Sea and the Norwegian Sea into the North Atlantic and up to the Barents Sea [41].

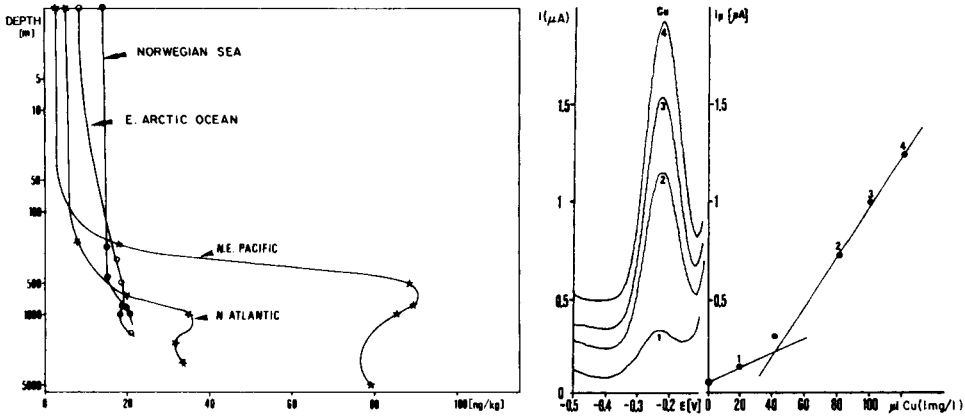

Fig. 4. Depth profiles of cadmium concentrations in various parts of the oceans. Because of different oceanographic conditions, increase of cadmium level below the euphotic zone differs considerably.

Fig. 5. D.p.a.s.v. determination of complexing capacity for copper in 0.45-μm filtered deep sea water (5600 m depth) from the southern tropical convergence (41° 55′S; 144° 58′W). (A) Reversible Cd(II) peak after increasing additions of Cu(II); (B) titration plot of peak heights vs. added μl of Cu(II) titrant (1 mg Cu(II) l^{-1}). The Cu(II) concentration in the sample at the equivalence point corresponds to the complexing capacity for Cu(II) of the water, i.e., the overall concentration Σ [L] of all organic ligands forming nonlabile complexes $Cu[L]_m$.

Important aspects of the concentration of heavy metals in the water column of estuaries and their distribution between dissolved state and suspended matter and the seasonal variation of these distributions have been elucidated for the Scheldt estuary [45, 46]. For the Tyrrhenian estuaries, including the Arno and Tiber, which belong to the simpler but rarer type of nontidal estuaries, it has been established that the overwhelming part of the fluvial heavy metal burden is transferred by sedimentation to the bottom sediments within the estuarine zone and the fluvial heavy metal input into the Mediterranean Sea remains marginal for these estuaries [47].

An extended study yielded the pattern of the burden of Cd, Pb and Cu for the River Rhine in 1979 and showed the contributions from tributaries [48]. Recently, the depth/concentration profiles of Cd, Pb and Cu in Lake Constance have been clarified [49, 50] as a first part of a continuing program on large European lakes.

Heavy metal speciation in natural waters

The particular feature that voltammetry is in principle a species-sensitive method has made it one of the most valuable approaches for speciation studies on toxic heavy metals in natural waters [36, 38, 39, 51—54]. Diagnostic studies such as the determination of the complexing capacities for various heavy metals (Cu, Pb, Cd, Zn) [51—57] and investigations on the

distribution of the overall dissolved concentrations of heavy metals over various complex categories of increasing stability (very labile, moderately labile, and nonlabile) by the application or omission of certain stages of sample pretreatment steps [36, 39, 54] have proved viable. Thus, the dissolved heavy-metal content present in very labile complexes can be measured at natural pH. Acidification to pH 1—2 releases further amounts of heavy metals bound in moderately stable complexes particularly with weakly complexing ligands. The determination of the heavy metals bound in nonlabile strong complexes and chelates, predominantly with organic ligands, requires the u.v. treatment for photolytic decomposition of the organic material.

In studies of complexing capacity, the natural water is titrated with a heavy metal M solution (usually Cu or Pb) to determine the total concentration of all ligands, $\Sigma[L]$, which form nonlabile complexes ML_m with the titrant metal. In this titration, the uncomplexed concentration of metal M is monitored voltammetrically by its reversible response (Fig. 5).

There is also a substantial potential for very elucidating investigations of various natural waters with regard to speciation features of general validity and fundamental physicochemical significance. From this area, the following examples may be mentioned. For lead and cadmium, the distribution between the relevant inorganic complexes in sea water has been established. It turns out that 97% of cadmium exists as very labile chloro complexes while lead is distributed as follows: 47% carbonato complexes, 7% hydroxy and 21% chloro complexes [39, 54]. Such speciation patterns should apply to large parts of the oceans where the DOM level is small.

In a number of coastal zones and in estuaries, however, the speciation patterns of both heavy metals are altered according to the respective elevated DOM-level, because strongly complexing organic ligands are now provided to a significant extent. In these studies on the inorganic speciation of lead and cadmium in sea water, the pseudo-polarogram approach [58] made it possible to evaluate the relationship between the reversible half-wave potential, $E_{1/2}$, and the ligand concentration, [X], from a.s.v. measurements at rather realistic overall trace levels (10^{-9} M) for dissolved lead and cadmium [59, 60]. From the measured shifts of $E_{1/2}$ with [X], the overall stability constants β_j and the ligand numbers j can be evaluated for the consecutive complex series MeX_j formed with a particular ligand X (Cl^-, CO_3^{2-}, HCO_3^-, OH^-, etc.). If these data are known for all significant complex species of the given heavy metal M in the type of natural water studied, the percentage species distribution of dissolved M in that water can be evaluated.

Studies with the well-defined ligands NTA (nitrilotriacetic acid) and EDTA have proved very elucidating in establishing the general features and boundary conditions for the formation of strong nonlabile complexes with organic ligands L in sea waters and fresh waters with different ionic strengths. Such investigations have been done for Cd, Pb and Zn [61—64]. For these studies of nonlabile heavy-metal complexes ML_m, a completely different

experimental approach was needed. The most important parameter, particularly for prognosis, is to establish for relevant or potentially relevant organic ligands L, the required concentration [L] needed to attain a certain degree of complexation of the heavy metal M in the natural water studied. These ligand concentrations required for ML_m formation are obtained by measuring the decrease of the reversible peak corresponding to the concentration of M remaining uncomplexed by L with increasing [L]. This is a kind of titration of [M] or, more precisely, of the sum $\Sigma[MX_j]$ of all labile inorganic MX_j species; increasing additions of L are made and voltammetry is used to monitor the concomitantly decreasing amount of $\Sigma[MX_j]$ by its reversible peak. It turned out that it is necessary to consider not only the general salt effect on the activity coefficients, which depends on the salinity of the natural water, but also strong specific effects exerted by certain chemical constituents present in substantial excess compared to the trace heavy metal. In this context, calcium and magnesium are of prime importance because they can compete with the heavy metals for the ligand or for the complexation sites on polymeric ligands. Therefore, substantially higher ligand concentrations are required to attain a certain degree of complexation of the particular heavy metal, compared to what one would expect from the ionic strength simply according to salinity (Fig. 6).

By monitoring the decrease of the reversible response corresponding to $\Sigma[MX_j]$ with time after addition of a strongly complexing ligand (e.g., EDTA), the kinetics and mechanism of formation of strong nonlabile heavy-metal complexes ML_m have been clarified in sea water and certain fresh waters [63, 65, 66]. The finding of most general significance was that the mechanism of ML_m formation prevailing in natural waters is not simple recombination of a free heavy metal ion with the ligand but a ligand-exchange mechanism in which the usually stronger complex-forming heavy metal displaces calcium and magnesium from its complexes with ligand L

$$MX_j + \begin{matrix} CaL_m \\ \downarrow\uparrow \\ MgL_m \end{matrix} \xrightarrow{k_f} ML_m + Ca + Mg + jX$$

(Charges are omitted for simplicity.)

Important prognostic predictions emerged from these studies with NTA and EDTA on the potential of other candidate ligands L (components of the DOM) to complex Cd, Pb and Zn, depending on the DOM levels in sea water and certain fresh waters. Thus, it could be predicted that the level of humic substances dissolved in open sea water is too low to affect significantly the speciation pattern of these three heavy metals [61—63]. Recent direct voltammetric studies with marine humic material in sea water and lake water have confirmed these predictions [67]. Other investigations have confirmed the expectation that amino acids are also of no significance, because their usual concentration level in natural waters is too low in relation to their moderate complexing power [68—70].

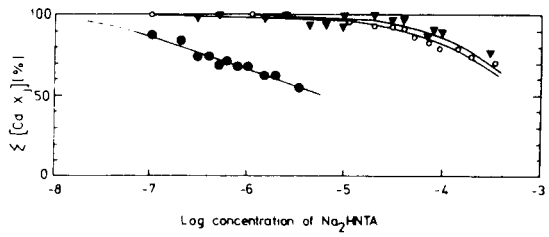

Fig. 6. Determination of ligand concentration [L] required to achieve a certain degree of complexation (%) of Cd(II) with NTA. D.p.a.s.v. is used to measure the decrease of the "free" Cd(II) present as labile inorganic species CdX_j including hydrated Cd(II), after increasing additions of NTA. Total Cd(II) concentration, 3×10^{-9} M. Curves:
(•) 0.59 M NaCl, borate buffer, pH 8.5;
(▾) artificial sea water, borate buffer, pH 7.9;
(○) Adriatic sea water, with preservation of natural carbonate buffer system, pH 7.9.

An example of an important application of these speciation studies is a highly sensitive method for monitoring $\geqslant 0.2\ \mu g\ l^{-1}$ NTA in natural waters by a voltammetric titration procedure with bismuth(III) [71]. Any traces of EDTA present ($\geqslant 0.1\ \mu g\ l^{-1}$) can be determined simultaneously. Monitoring of the NTA level in rivers, estuaries and coastal waters has gained significance, because NTA is used in laundry detergents as a substitute for phosphates, which cause eutrophication. However, there is a risk that excessive NTA levels would cause undesirable mobilization of heavy metals from the bottom sediments by dissolution through complex formation [72].

Deposition of heavy metals by atmospheric precipitation

In Western Europe and other heavy industrialized regions, a substantial amount of heavy metals is emitted into the atmosphere. As this emission occurs predominantly in the form of fine aerosol particles, it can travel some distance; the heavy metals are ultimately deposited on both land and sea. The atmosphere may provide a significant pathway for the distribution of heavy metal burdens in the environment. For Cd, Pb, Cu, Zn and probably also nickel, the most important deposition mode is precipitation with rain and snow. In this mode, most of the metals will descend in the dissolved form most favourable for uptake by vegetation, i.e., of greatest concern from the viewpoint of ecology. The above voltammetric methods seem obviously appropriate for investigating and monitoring the impact on the environment of the atmospheric precipitation of heavy metals.

The possibilities offered by voltammetry in this context, in combination with a reliable sampling procedure, are emphasized by the results obtained on the situation in Germany by a long-term study started in 1979 accompanied by further detailed investigations in certain regions [33, 73, 74]. A network of 20 automated samplers is distributed over the Federal Republic from the North Sea coast to the Alps, covering typical rural regions without strong industrial emission sources, as well as urban agglomerations, heavy

industrialized zones with strong emissions and two regions that have particular problems because of the operation of lead smelters or cadmium ore processing plants (Stolberg and Goslar). The automated sampler, initially made in the laboratory [32] but now available more widely (K. Bleymehl, D-5170 Jülich), operates only during the precipitation of rain and snow, remaining closed in dry periods; this eliminating interference by deposition of dry dust. Suspended particulate matter in rain water is filtered off by a built-in filtration device with a 0.45-μm membrane filter. Generally, the only necessary further preparation of the filtrate, which normally contains about 90% of the heavy metals in the precipitation, is acidification to pH 2. Subsequently, Cu, Pb, Cd and Zn are determined by d.p.a.s.v. at the HMDE and selenium(IV) by d.c.p.s.v. Nickel and cobalt can be determined by adsorption voltammetry after addition of DMG (see above).

Extended studies of this kind have revealed the contours, seasonal and meteorological dependencies and trends over the last four years for the atmospheric precipitation of heavy metals in various regions of the Federal Republic of Germany [73, 74]. Details of the problem locations of Stolberg and Goslar have also been clarified. Some general aspects of the atmospheric precipitation of heavy metals have been clarified, e.g., heavy metal concentrations in the deposited rain are higher in the initial 1—2 h of rainfall than in later rainfall where they become rather constant [10].

Important findings on pollution transport stem from participation in the Swedish polar expedition YMER-80 to the remote Arctic in the range north of Greenland, Spitsbergen and Franz-Josef-Land. Voltammetric ultra-trace analysis revealed significant differences in the heavy metal contents of snow deposited in summer and in the preceding winter. In good correlation with the meteorological situation in the northern hemisphere, it could be established that atmospheric transport of heavy metals (and presumably pollutants in general) occurs predominantly from Europe into the Arctic during fall and winter; usually in summer, the Arctic is meteorologically decoupled from Europe [25].

This paper was presented at the Sixth Australian Electrochemistry Conference, February 1984, Deakin University, Victoria, Australia.

REFERENCES

1 E. Merian, M. Geldmacher-v. Mallinckrodt, G. Machata, H. W. Nürnberg, H. Schlipköter and W. Stumm (Hrsg.), Metalle in der Umwelt, Verlag Chemie, Weinheim, 1984.
2 U. Förstner and G. Wittmann, Metal Pollution in the Aquatic Environment, Springer, Berlin, 1981.
3 R. M. Pytkowicz, Equilibria and Nonequilibria in Natural Waters, Wiley, New York, 1983, Vols. 1 and 2.
4 L. Friberg, G. F. Nordberg and B. Vouk (Eds.), Handbook on the Toxicity of Metals, Elsevier, New York, 1979.
5 H. W. Nürnberg, Pure Appl. Chem., 54 (1982) 853.
6 H. W. Nürnberg, Sci. Total Environ., 37 (1984) 9.
7 M. Stoeppler and H. W. Nürnberg, in E. Merian, M. Geldmacher-v. Mallinckrodt,

G. Machata, H. W. Nürnberg, H. Schlipköter and W. Stumm (Hrsg.), Metalle in der Umwelt, Verlag Chemie, Weinheim, 1984, Ch. 14a.
8 K. May and M. Stoeppler, Proc. Int. Conf. Heavy Metals Environ., Heidelberg, Sept. 1983, CEP Consultants, Edinburgh, 1983, Vol. 1, pp.241—244.
9 D. Schmidt and P. Freimann, Fresenius Z. Anal. Chem., 313 (1982) 200.
10 V. D. Nguyen, P. Valenta and H. W. Nürnberg, Sci. Total Environ., 12 (1979) 151.
11 P. Valenta and H. W. Nürnberg, Gewässerschutz-Wasser-Abwasser (Aachen), 44 (1980) 105.
12 L. Mart, H. W. Nürnberg and P. Valenta, Fresenius Z. Anal. Chem., 300 (1980) 350.
13 P. Valenta, L. Sipos, I. Kramer, P. Krumpen and H. Rützel, Fresenius Z. Anal. Chem., 312 (1982) 101.
14 W. Dorten, P. Valenta and H. W. Nürnberg, Fresenius Z. Anal. Chem., 317 (1984) 264.
15 L. Sipos, P. Valenta, H. W. Nürnberg and M. Branica, J. Electroanal. Chem., 77 (1977) 263.
16 L. Sipos, J. Golimowski, P. Valenta and H. W. Nürnberg, Fresenius Z. Anal. Chem., 298 (1979) 1.
17 L. Sipos, H. W. Nürnberg, P. Valenta and M. Branica, Anal. Chim. Acta, 115 (1980) 25.
18 F. G. Bodewig, P. Valenta and H. W. Nürnberg, Fresenius Z. Anal. Chem., 311 (1982) 187.
19 J. Golimowski, H. W. Nürnberg and P. Valenta, Lebensmittelchem. Gerichtl. Chem., 34 (1980) 116.
20 B. Pilhar, P. Valenta and H. W. Nürnberg, Fresenius Z. Anal. Chem., 307 (1981) 337.
21 P. Ostapczuk, P. Valenta, M. Stoeppler and H. W. Nürnberg, in S. S. Brown and J. Savory (Eds.), Chemical Toxicology and Clinical Chemistry of Metals, Academic Press, London, 1983, pp. 61—64.
22 P. Ostapczuk, M. Goedde, M. Stoeppler and H. W. Nürnberg, Fresenius Z. Anal. Chem., 317 (1984) 252.
23 D. Jagner, Anal. Chem., 50 (1978) 1924.
24 C. S. P. Iyer, P. Valenta and H. W. Nürnberg, Anal. Lett., Ser. A, 14 (1981) 921.
25 L. Mart, Tellus, 35B (1983) 131.
26 L. Mart, H. W. Nürnberg and G. Gravenhorst, Ber. Polarforsch. (Bremerhaven), 6 (1982) 68.
27 C. S. Wong, E. Boyle, K. W. Bruland, J. D. Burton and E. D. Goldberg (Eds.), Trace Metals in Sea Water, Plenum Press, New York, 1983.
28 L. Mart, Fresenius Z. Anal. Chem., 299 (1979) 97.
29 L. Mart, Talanta, 29 (1982) 1035.
30 B. Schaule and C. C. Patterson, in M. Branica and Z. Konrad (Eds.), Lead in the Marine Environment, Pergamon, Oxford, 1980, pp. 31—34.
31 L. Mart, H. W. Nürnberg and D. Dyrssen, in C. S. Wong, E. Boyle, K. W. Bruland, J. D. Burton and E. D. Goldberg (Eds.), Trace Metals in Sea Water, Plenum Press, New York, 1983, pp. 113—130.
32 H. W. Nürnberg, P. Valenta and V. D. Nguyen, Jahresber. 1979/80, Kernforschungsanlage Jülich, 1980, pp. 47—54.
33 H. W. Nürnberg, P. Valenta and V. D. Nguyen, in H. W. Georgii and J. Pankrath (Eds.), Deposition of Atmospheric Pollutants, D. Reidel, Dordrecht, 1982, pp. 143—157.
34 K. May, K. Reisinger, R. Flucht and M. Stoeppler, Vom Wasser, 55 (1980) 63.
35 L. Mart, Fresenius Z. Anal. Chem., 296 (1979) 350.
36 T. M. Florence and G. E. Batley, CRC Crit. Rev. Anal. Chem., 9 (1980) 219.
37 H. W. Nürnberg, L. Mart, H. Rützel and L. Sipos, Chem. Geology, 40 (1983) 97.
38 H. W. Nürnberg and P. Valenta, in C. S. Wong, E. Boyle, K. W. Bruland, J. D. Burton and E. D. Goldberg (Eds.), Trace Metals in Sea Water, Plenum, New York, 1983, pp. 671—697.
39 H. W. Nürnberg, Fresenius Z. Anal. Chem., 316 (1983) 557.
40 L. Mart, H. Rützel, P. Klahre, L. Sipos, U. Platzek, P. Valenta and H. W. Nürnberg, Sci. Total Environ., 26 (1982) 1.
41 L. Mart, H. W. Nürnberg and H. Rützel, Fresenius Z. Anal. Chem., 317 (1984) 201.

42 L. Mart, H. W. Nürnberg, P. Valenta and M. Stoeppler, Thalassia Jugosl., 14 (1978) 171.
43 L. Mart, H. W. Nürnberg and P. Valenta, in M. Branica and Z. Konrad (Eds.), Lead in the Marine Environment, Pergamon, Oxford, 1980, pp. 155—179.
44 H. W. Nürnberg, Acta Univ. Upsaliensis, Symp. Univ. Upsaliensis Annum Quinquentesimum Celebrantis, 12 (1978) 270.
45 P. Valenta, H. W. Nürnberg, P. Klahre, A. G. A. Merks, S. J. Reddy and H. Rützel, Mahasagar, in press.
46 P. Valenta, H. W. Nürnberg, H. Rützel and A. G. A. Merks, Vom Wasser, 62 (1984) 235.
47 R. Breder, R. Flucht and H. W. Nürnberg, Thalassia Jugosl., 18 (1982) 135.
48 R. Breder, H. W. Nürnberg, J. Golimowski and M. Stoeppler, in H. W. Nürnberg (Ed.), Pollutants and their Ecotoxicological Significance, Wiley, Chichester, 1984.
49 L. Sigg, M. Sturm, W. Stumm, L. Mart and H. W. Nürnberg, Naturwissenschaften, 69 (1982) 546.
50 L. Sigg, M. Sturm, J. Davis and W. Stumm, Thalassia Jugosl., 18 (1982) 293.
51 H. W. Nürnberg, Thalassia Jugosl., 16 (1980) 89.
52 P. Valenta, in G. G. Leppard (Ed.), Trace Element Speciation in Surface Waters and its Ecological Implications, Plenum, New York, 1983, pp. 49—69.
53 H. W. Nürnberg, in G. G. Leppard (Ed.), Trace Element Speciation in Surface Waters and its Ecological Implications, Plenum, New York, 1983, pp. 211—230.
54 H. W. Nürnberg, in C. J. M. Kramer, M. Branica, J. C. Duinker, J. Hart-Stam, R. F. C. Mantoura, H. W. Nürnberg and W. Stumm (Eds.), Complexation of Trace Metals in Natural Waters, M. Nijhoff/W. Junk, The Hague, 1984, pp. 95—115.
55 J. C. Duinker and C. J. M. Kramer, Mar. Chem., 5 (1977) 207.
56 T. M. Florence, Talanta, 29 (1982) 345.
57 A. Neubecker and H. E. Allen, Water Res., 17 (1983) 1.
58 M. Branica, D. H. Novak and S. Bubić, Croat. Chem. Acta, 49 (1977) 231.
59 L. Sipos, P. Valenta, H. W. Nürnberg and M. Branica, in M. Branica and Z. Konrad (Eds.), Lead in the Marine Environment, Pergamon, Oxford, 1980, pp. 61—76.
60 M. L. S. Simoes-Goncalves, M. C. T. A. Vaz and J. J. R. Frausto da Silva, Talanta, 28 (1981) 237.
61 B. Raspor, P. Valenta, H. W. Nürnberg and M. Branica, Sci. Total Environ., 9 (1978) 87.
62 B. Raspor, H. W. Nürnberg, P. Valenta and M. Branica, in M. Branica and Z. Konrad (Eds.), Lead in the Marine Environment, Pergamon, Oxford, 1980, pp. 181—195.
63 B. Raspor, H. W. Nürnberg, P. Valenta and M. Branica, Limnol. Oceanogr., 26 (1981) 54.
64 H. W. Nürnberg and B. Raspor, Environ. Technol. Lett., 2 (1981) 457.
65 B. Raspor, P. Valenta, H. W. Nürnberg and M. Branica, Thalassia Jugosl., 13 (1977) 79.
66 B. Raspor, H. W. Nürnberg, P. Valenta and M. Branica, J. Electroanal. Chem., 115 (1980) 293.
67 B. Raspor, H. W. Nürnberg, P. Valenta and M. Branica, in C. J. M. Kramer, M. Branica, J. C. Duinker, J. Hart-Stam, R. F. C. Mantoura, H. W. Nürnberg and W. Stumm (Eds.), Complexation of Trace Metals in Natural Waters, M. Nijhoff/W. Junk, The Hague, 1984, pp. 317—327.
68 M. L. S. Simoes-Goncalves and P. Valenta, J. Electroanal. Chem., 132 (1982) 357.
69 M. L. S. Simoes-Goncalves, P. Valenta and H. W. Nürnberg, J. Electroanal. Chem., 149 (1983) 249.
70 P. Valenta, M. L. S. Simoes-Goncalves and M. Sugawara, in C. J. M. Kramer, M. Branica, J. C. Duinker, J. Hart-Stam, R. F. C. Mantoura, H. W. Nürnberg and W. Stumm (Eds.), Complexation of Trace Metals in Natural Waters, M. Nijhoff/W. Junk, The Hague, 1984, pp. 357—366.
71 A. Voulgaropoulos, P. Valenta and H. W. Nürnberg, Fresenius Z. Anal. Chem., 317 (1984) 367.
72 W. Salomons and J. A. van Pagee, Proc. Int. Conf. Heavy Metals Environ., Amsterdam, Sept. 1981, CEP Consultants, Edinburgh, 1981, pp. 694—697.
73 H. W. Nürnberg, P. Valenta and V. D. Nguyen, Proc. Int. Conf. Heavy Metals Environ., Heidelberg, Sept. 1983, CEP Consultants, Edinburgh, 1983, Vol. 1, pp. 115—123.
74 H. W. Nürnberg, P. Valenta, V. D. Nguyen, M. Goedde and E. Urano de Carvalho, Fresenius Z. Anal. Chem., 317 (1984) 314.

Analytica Chimica Acta, 164 (1984) 23—39
Elsevier Science Publishers, B.V., Amsterdam — Printed in The Netherlands

AN EFFICIENT FLOW-INJECTION SYSTEM WITH ON-LINE ION-EXCHANGE PRECONCENTRATION FOR THE DETERMINATION OF TRACE AMOUNTS OF HEAVY METALS BY ATOMIC ABSORPTION SPECTROMETRY

ZHAOLUN FANG[a], J. RŮŽIČKA* and E. H. HANSEN

Chemistry Department A, Technical University of Denmark, Building 207, 2800 Lyngby (Denmark)

(Received 6th June 1984)

SUMMARY

A flow-injection system with on-line ion-exchange preconcentration on dual columns is described for the determination of trace amounts of heavy metals at $\mu g\ l^{-1}$ and sub-$\mu g\ l^{-1}$ levels by flame atomic absorption spectrometry. The degree of preconcentration ranges from 50- to 105-fold for different elements at a sampling frequency of 60 s h^{-1}. The detection limits for Cu, Zn, Pb and Cd are 0.07, 0.03, 0.5, and 0.05 $\mu g\ l^{-1}$, respectively. Relative standard deviations were 1.2—3.2% at $\mu g\ l^{-1}$ levels. The behaviour of the different chelating exchangers used was studied with respect to their preconcentration characteristics, with special emphasis on interferences encountered in the analysis of sea water.

Ion-exchange preconcentration has proved to be an effective means of increasing the sensitivity of atomic absorption spectrometry (a.a.s.) as well as a means of removing interferences. The concept has been utilized for many years and its practicality has recently been shown in the work of, for example, Kingston et al. [1], and Danielsson et al. [2]. However, the conventional column mode of ion-exchange preconcentration is tedious and so incompatible with the final rapid determination by a.a.s. Therefore, an attempt was made recently to apply an on-line flow-injection preconcentration technique by ion exchange to a.a.s. determinations with the aim of speeding up and simplifying the preconcentration step. This approach has undergone fast development since the first paper by Olsen et al. [3] was published. Valve designs have been improved; in addition to Chelex-100, other ion-exchange resins have been tested, and different flow systems have been proposed to increase the efficiency of the process [4—7]. These developments indicate that the new approach not only increases the speed of the preconcentration process, but could also ultimately rival the sensitivity and speed of graphite-furnace atomic absorption spectrometry. The designs suggested so far are

[a]Present address: Institute of Forestry and Soil Science, Academia Sinica, Shenyang, Box 417, China.

0003-2670/84/$03.00

TABLE 1

The development of flow-injection preconcentration systems

Basic configuration [3]:

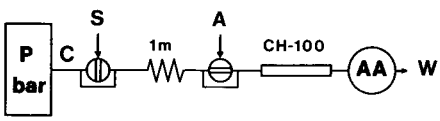

(P, pump; C, carrier; S, sample; A, eluent; CH-100, Chelex column; AA, a.a.s. detector; W, waste.)

Development	Concentration efficiency of system (x-fold min^{-1})	Ref.
Improved design: (1) no discharge of effluent into nebulizer (prevents blocking); (2) countercurrent elution (improves column operation); (3) confluenced buffer (improves mixing).	6	3
(1), (2) incorporated into design; (4) single valve design (simplifies construction and manipulation); (5) acid eluent flowing through nebulizer only during elution (lessens corrosion of nebulizer); (6) sampling by time and flow rate instead of by sample loop (increases efficiency, decreases sample dispersion).	9	4, 7
(1), (2), (4), (5) incorporated into system; (7) system with dual column operated alternately (increases efficiency).	13—18	5
(3), (5), (6) incorporated into system; (8) resin with surface bound immobilized functional groups (improves sensitivity).	20	6
(1—6), (8) incorporated into system; (9) parallel sampling, sequential elution dual-column system.	50—105	Present work

summarized in Table 1, including the present design. For comparison of the efficiency of the different systems, the degree of preconcentration attained in one minute (including sampling time and elution time) is taken as a measure for evaluation. Table 1 clarifies the main object of the present paper, i.e., to combine the advantages of the previous designs while avoiding the shortcomings as much as possible. The system described here is more efficient than the previous designs, being capable of attaining 50—105-fold preconcentration at a sampling frequency of 60 h^{-1}. A number of heavy metals can thus be determined at sub-$\mu g\ l^{-1}$ levels by flame a.a.s., the detection limits for Cu, Zn, Pb and Cd being 0.07, 0.03, 0.5 and 0.05 $\mu g\ l^{-1}$, respectively, with precisions ranging between 1.2 and 3.2%.

Previous studies have shown that the type of ion-exchange resin is important in the overall performances of the systems. Therefore, besides the study on the hardware of the system, the different types of resins applied for preconcentrations in f.i.a. were compared with respect to their behaviour when used for determinations of heavy metals in sea water.

EXPERIMENTAL

Apparatus

The atomic absorption spectrometer was a Varian AA-1275 Model connected to a Radiometer REC-80 recorder with a REA-112 high-sensitivity module. The sample uptake rate of the nebulizer was adjusted to 4 ml min^{-1}. Varian hollow-cathode lamps were used; the wavelengths used were Cu 324.7, Zn 213.8, Pb 217.0, Cd 228.8 nm.

Two Ismatec Model Mini-S-840 peristaltic pumps with tygon pump tubes were employed in the system. The stop-go intervals of the pumps were controlled synchronously by a laboratory-built timer which was triggered by a microswitch on the injector valve, being actuated at each turn of the valve rotor.

A two-layer valve with 8 channels was designed on the basis of a previous configuration by Krug et al. [7] to control the simultaneous uptake of analyte metals from two samples on two identical columns and to accomplish the subsequent elution of these two samples sequentially. Details of the valve are shown in Fig. 1. The rotor was made of teflon and the stator block was PVC. All connections were made with 0.5 mm i.d. Microline tubing (Thermoplastic Scientific).

The columns were made as described earlier [5] from suitable lengths of 2.8 mm i.d. tygon tubing. The section filled with resin was 35 mm long which accommodated 35 mg of Chelex-100 (in the ammonium form), or 10 mg of 8-quinolinol-based resin [6], or 110 mg of the 122 resin [5] in each column. With one of the column ends sealed with nylon gauze, the resins

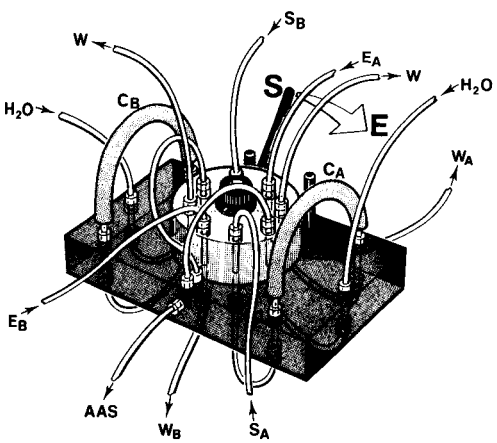

Fig. 1. Dual-column ion-exchange preconcentration valve. S_A, S_B, samples A and B; C_A, C_B, ion-exchange columns A and B; E_A, E_B, eluant (2 M nitric acid) for columns A and B; W_A, W_B, waste lines for samples and eluants A and B; W, waste lines; AAS, atomic absorption spectrometer. The dimensions of the base plate of the valve are 70 × 45 × 10 mm. For details of operation, see text and Fig. 2.

were fed as a slurry into the column with a 1-ml plastic syringe; the other end of the column was then sealed similarly. The ionic form of the resins during packing is not important except for Chelex-100, which should be in the H^+-form; this is different from the form used previously [3] and will be explained in more detail in the Discussion.

The entire setup of the system is shown in Fig. 2. The flow system will be discussed in more detail later.

Reagents

All chemicals were of analytical-reagent grade. Deionized water was used throughout. The reagents and standard solutions were stored in polyethylene bottles.

Standard solutions of copper(II) (5—20 $\mu g\ l^{-1}$), zinc(II) (5—20 $\mu g\ l^{-1}$), lead(II) (25—100 $\mu g\ l^{-1}$) and cadmium(II) (2.5—10 $\mu g\ l^{-1}$) were made by two-stage dilutions of 1000 $\mu g\ ml^{-1}$ aqueous standard solutions (BDH Chemicals). Because of the low concentration of the working standards, the dilutions had to be prepared fresh daily. When buffers were added to samples and not

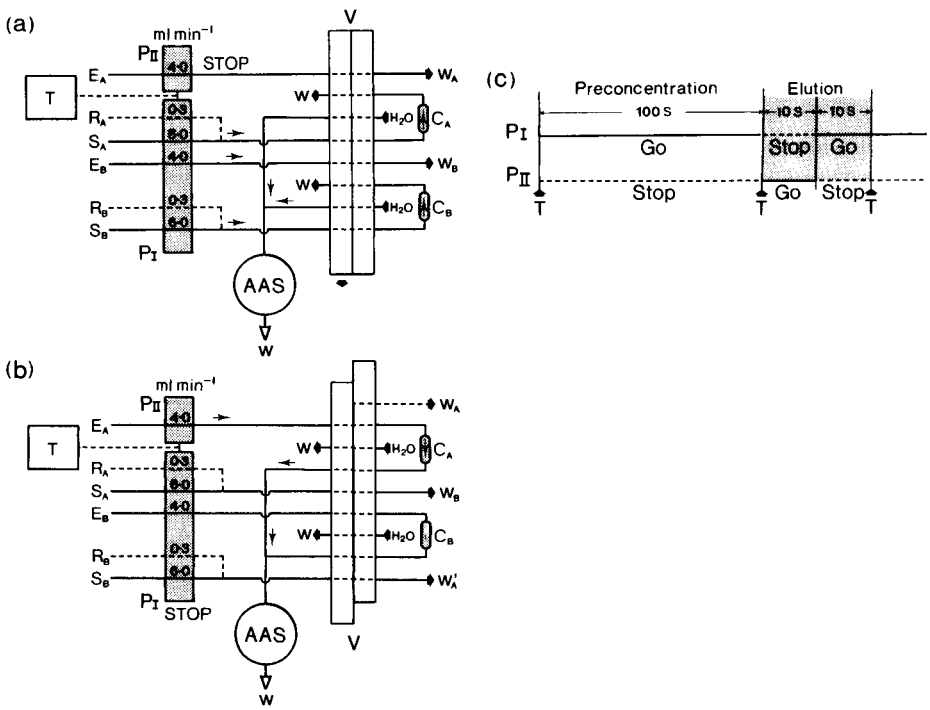

Fig. 2. Manifold for dual-column on-line ion-exchange preconcentration system with flame atomic absorption detection. (a) Sampling and preconcentration mode; (b) elution mode for column A. PI, PII, pumps I and II; T, timer; V, valve; because of the circular arrangement of the valve channels, $W_{A'}$ represents the same channel as W_A; other symbols are the same as for Fig. 1. (c) Time-sequencing program for valve operation. The points marked T indicate turn of valve. Note that the elution of both columns A and B takes place in position (b) of the valve, but with pumps PI and PII sequenced stop-go and go-stop, respectively.

mixed on-line into the samples, the buffer solution had to be added immediately prior to injection in order to avoid loss of analyte by adsorption. The ammonium acetate buffer solutions were prepared by diluting a 2 M ammonium acetate solution adjusted to pH 10 with 25% ammonia solution.

The Chelex-100 chelating resin was 50—100 mesh (sodium form; Bio-Rad Laboratories).

The 8-quinolinol chelating exchanger was from Pierce Chemicals Co. The 8-quinolinol was azo-immobilized to controlled pore glass (CPG, 50 nm pore size and 125—177 μm particle size). The weakly acidic 122 resin which had a phenol—formaldehyde base with salicylate functional groups was from the Institute of Chemical Engineering of Eastern China, Shanghai.

Procedure

The manifold was set up as shown in Fig. 2. The pumps were connected to the double timer; the sampling time was normally fixed to 100 s, while the elution time was set to 10 s for both columns. The sampling flow rate was 6.0 ml min^{-1} and the elution flow rate 4.0 ml min^{-1}.

With the valve in the elution position ((E) in Fig. 1 and (b) in Fig. 2), samples A and B in 0.025 M ammonium acetate buffer (final pH 9.5) were pumped by pump I through the pump tubes and valve to waste in order to wash out the previous sample. (This is a preparation step prior to the sampling stage and should be completed simultaneously with the elution of analyte from the previous sample on column A. If 10 s is insufficient for the washout of the previous sample, i.e., when carryover occurs, the elution period of column A should be lengthened. The pump tubes and connecting tube for the sampling should also be kept as short as possible to facilitate washout.) When the recorder returned to baseline following the elution of column A the valve was turned manually to the sampling position ((a) in Fig. 2), which actuated the microswitch initiating the monitoring of the sampling time. At the end of the sampling time, pump I was stopped automatically. The valve was at once returned manually to elution position (b) which actuated the second channel of the timer, starting pump II. The eluant, 2 M nitric acid, was pumped through column B, eluting the analyte directly into the nebulizer of the spectrometer and producing a transient signal which was recorded. The elution was stopped after 10 s, at which point pump I resumed its action, the 10-s stop period of pump I being used to change samples. Then elution of column A was effected by means of pump I producing a second signal. After the recorder had returned to baseline, which was about 10 s after the start of the elution, the preparative washout of the next two samples was completed and another turn of the valve commenced the next sampling sequence (cf. Fig. 2c). Distilled water was aspirated into the nebulizer during the sampling period to wash it out. During elution the water flowed to waste. Before closing down, the entire system was washed by pumping distilled water through the lines. This is particularly important because a chelating resin could be seriously damaged by being left in 2 M nitric acid

overnight. When Chelex-100 is used, the column should be washed in the H^+-form, as washing in the NH_4^+-form will create excessive swelling and pressure in the column (see Discussion).

RESULTS AND DISCUSSION

Studies on the swelling properties of the Chelex-100 resin

The Chelex-100 resin is one of the most studied chelating resins and has been widely used in the preconcentration of heavy metals from sea water prior to a.a.s. Recently, Olsen et al. [3] have used Chelex-100 for on-line preconcentration of heavy metals in a flow-injection system. Although the selectivity of the resin for heavy metals was very useful for such a purpose, it was reported that the undesirable swelling of the resin, which could amount to 100% of the volume during transformation from H^+-form to NH_4^+-form, and shrinking on acidification, considerably hampered the performance of the unidirectional flow system by progressively yielding tighter packing of the resin, which ultimately blocked the flow of liquid [3]. Olsen et al. solved the problem partially by altering the flow direction through the column by means of countercurrent elution which overcame the blocking of the flow. Yet the degree of the packing still underwent drastic changes during the course of each sampling/elution cycle. If the amount of resin and the extent of its swelling were not carefully controlled, the performance of the flow system during elution could be seriously affected through changes in flow rate, especially when preconcentration was done at high pH for longer times at high flow rates when increased sensitivity was needed. Thus, the swelling properties of the resin, although unimportant for conventional open columns, are very important in an on-line low-pressure system as required by f.i.a. Erratic blockages, leakages and flow-rate fluctuations caused by excessive changes in back-pressure can occur. The swelling properties of Chelex-100 were therefore studied more closely.

A slurry of Chelex-100 in the NH_4^+-form, corresponding to the amount in an actual column, half-filled a 1-ml plastic syringe barrel (5 mm i.d.). The resin was held in the syringe by a piece of nylon gauze, fixed at the bottom of the barrel by a section of tygon tubing. The top of the barrel was stoppered and connected to a peristaltic pump. Different concentrations of ammonium acetate buffered at different pH values, water and 2 M nitric acid were then pumped alternately through the resin at a rate of 6 ml min^{-1}. The change in volume was read off the scale on the syringe barrel and recorded at different times. The results are shown in Fig. 3.

It can be seen that buffer solutions of higher concentrations produce lower final volumes of resin and reach equilibrium faster, but no difference in swelling properties was observed for pH values in the range 5.5—10. It is interesting to note that the volume differences obtained with different concentrations of buffer was partially retained during the large volume change from the H^+ to the NH_4^+-form. Yet the percentage of swelling from the

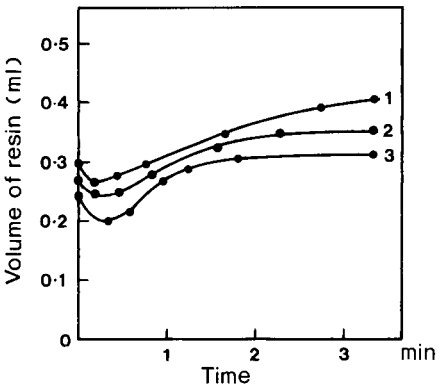

Fig. 3. Swelling properties of the Chelex-100 resin as a function of exposure to alkaline buffers of fixed pH (10) but different concentrations. The column used was 5 mm i.d., and contained 50 mg of resin; initial state, H^+-form; buffer concentration, 0.05 M ammonium acetate (1); 0.1 M (2); 0.5 M (3); buffer flow rate 6 ml min^{-1}. After 4 min of exposure, the resin was converted to the H^+ form by elution with 2 M nitric acid. The initial volume of the resin in the H^+-form depends on the concentration of the buffer to which the resin has previously been exposed.

initial H^+-form (volume at 0 min in Fig. 3) to the NH_4^+ form at equilibrium was still larger when lower concentrations of ammonium acetate buffer were used, being 40% for 0.05 M buffer and less than 30% for the 0.5 M buffer. Moreover, the lowest volume of the resin was not observed in the H^+-form, but at an early stage of substitution by NH_4^+ ions, with more intense shrinking for the higher NH_4^+ concentration. Hence, when the difference between the lowest and highest volume was considered, the percentage swelling amounted to 50% of the lower volume, independent of the NH_4^+ concentration. When the resins in the NH_4^+-form were washed with distilled water, the swelling increased to 90% of its volume in H^+-form; in contrast, when the resins in the H^+-form, after equilibration with acid, were washed with water, 10—20% shrinkage occurred (not shown in Fig. 3). These phenomena cannot be explained fully at present, yet several practical conclusions may be drawn from these results.

First, if the maximum change in volume of a resin in a column should not exceed 25% during a single cycle of operation (which is imperative in order to avoid excessive pressure and void volume variations), the sampling period (during which chelation takes place) at a flow rate of 6 ml min^{-1} should not exceed 50 s for a 0.5 M ammonium acetate buffer, 75 s for a 0.1 M buffer or 100 s for a 0.05 M buffer. Secondly, the column should be packed about 3/4-full with resin in the H^+-form (washed with water) after conversion from the NH_4^+-form (in which state it should be equilibrated with buffer of the same concentration as that used in the ensuing procedure). Packing in the NH_4^+-form would otherwise result in an excessively loose column packing giving rise to large dispersion and degrading the sensitivity. Finally, resin

columns in the NH_4^+-form should never be washed with water, lest excessive pressure develop in the column, causing blockages, leakages or dislodgement of the nylon retaining gauzes. When not in use, the columns should be converted to the H^+-form by normal elution with acid and washed thoroughly with water (see Procedure).

Dual-column system with sequential elution

The preconcentration system described above was designed to increase the overall efficiency of the operation in terms of sensitivity and time economy. The system incorporates almost all features which were proved previously, and the novel dual-column system allows processing of two samples simultaneously during the ion-exchange (sampling) stage and elutes the analytes sequentially by intermittent pumping with two pumps. The concept of a dual-column system was applied earlier in order to increase the efficiency of a flow-injection system [5]. In that system, the columns were processed in alternating mode (i.e., one column was eluted while the other was in the exchange mode), but as the operational cycle of each column consisted of a sampling sequence (during which sample was injected into a sample loop), an ion-exchange stage, and an elution procedure, the elution step being much faster than the others, the gain in time was only moderate, because the rate-determining operations were the sampling and ion-exchange modes. Even when the system was designed so that sampling and elution took place simultaneously in each half system, the sampling frequency was only marginally improved. Elimination of the sample loop and metering of the sample by other means for injection would increase the sampling frequency. The resin column can be considered as a special kind of sample loop in itself, as shown in the designs of Jørgensen and co-workers [4, 7] and Malamas et al. [6] where sample volume was controlled by pumping the sample directly through the column at a certain flow rate for a definite period of time. With some improvements in the valve design, the geometry of the sample zone could be well defined by applying the principles of hydrodynamic injection [8, 9]. The same principle was applied to inject the eluant: by pumping the eluant directly through the column for a given period of time, the geometry of the eluant plug entering the column could be well controlled [4]. These principles were incorporated into the present system, allowing the dual columns to be loaded with samples simultaneously. Of course, the two columns could not be eluted simultaneously, because the two peaks had to be time-resolved. A time delay for one of the columns, obtained by lengthening the line to the detector, did not resolve the peaks sufficiently and there was an undesirable loss in sensitivity, because of mutual dilution of the merging streams of eluates. Therefore, a sequential scheme was adopted: one column was eluted whilst the flow in the other was stopped and after completion of the first elution the process was reversed. This design called for two pumps working intermittently under the control of a dual-channel timer which precisely controlled the different stages of the entire process. The system could be fully automated if the valve is motor-powered and activated by a timer.

In the design of the system, care was also taken to avoid unnecessary aspiration of the eluant (mostly concentrated mineral acids) into the nebulizers, which could be harmful to the instrument. By an ingenious modification in valve design, Jørgensen and co-workers [4, 7] were able to direct water instead of eluant or effluent waste into the nebulizer during the sampling stage and the eluant was recovered for further use. The same principle was adopted in the present design except that, because of the complications associated with the dual-column system, it was not practical to recover the unused eluant. As can be seen in Fig. 2, the water line was not connected with a pump, as precise flow rates were not necessary. A large bottle of distilled water, set at a somewhat higher level than the nebulizer, was simply connected to the valve with tygon tubing and sucked into the nebulizer.

In the present system, another feature which improved efficiency was the elimination of the washing step before elution. This washing step, which was included in most earlier systems, can be done either by the sample carrier stream or by incorporation of a separate washing procedure [3, 5, 6]. The washing step was eliminated by Jørgensen and co-workers in their flow-injection system [4, 7]. The approach has, however, the drawback of leaving a small volume of sample matrix material in the column at the beginning of the next cycle, and this residue is eluted into the nebulizer immediately before the main peak of the analyte. This produces some interference effects when samples with a highly concentrated salt matrix are analyzed; with sea water an inselective absorbance up to 0.03 can be observed at some wavelengths. Thus, for very low contents of metals in highly concentrated salt solutions, background correction would be necessary.

As has been shown earlier, the pH of the samples must be controlled by a buffer. The buffer can be added to the samples immediately prior to injection or it can be merged with the samples as indicated in Fig. 2 by the broken lines which indicate additional streams of 0.5 M ammonium acetate pumped at a rate of 0.3 ml min^{-1}. The results are identical for either approach.

The entire flow-injection system depicted in Fig. 1, excluding the pumps, was miniaturized and constructed as a single module on a compact PVC block (50 X 70 mm X 10 mm). As can be judged from the schematic diagram in Fig. 2, the rotor and stator functions are interchangeable. This means that the columns can either be located on the stator block (as in Figs. 1 and 2) or on top of the rotor. The overall dimensions and connector arrangement are best seen in Fig. 1. Connections of the valve and block were all made by a suitable combination of tygon and silicone rubber tubing, which produced convenient yet reliable joints capable of withstanding the back-pressures created in on-line column systems and also permitted the construction of a more compact system with minimum dispersion.

The results listed in Table 2 were obtained using the system shown in Fig. 1 with a buffer non-confluencing module at a sampling rate of 60 h^{-1} (10-ml samples), the buffer in the samples being adjusted to a level of 0.025 M

TABLE 2

Performance of dual-column flow-injection system with sequential elution/preconcentration and different chelating resins

Resin	Characteristic concentration ($\mu g\,l^{-1}$)				LOQ[a] ($\mu g\,l^{-1}$)				LOD[b] ($\mu g\,l^{-1}$)				R.s.d. (%)				Recovery[c] (%)				Concentration efficiency[d] (fold min^{-1})			
	Cu	Zn	Pb	Cd	Cu	Zn	Pb	Cd	Cu	Zn	Pb	Cd	Cu	Zn	Pb	Cd	Cu	Zn	Pb	Cd	Cu	Zn	Pb	Cd
Chelex-100	0.5	0.12	1.5	0.2	0.2	0.11	2.5	0.2	0.07	0.04	0.8	0.07	2.2	3.2	1.3	1.9	99	92	95	93	88	50	70	60
8-Quinolol	0.6	0.07	0.8	0.13	0.3	0.08	1.4	0.15	0.09	0.03	0.5	0.05	2.3	2.6	2.2	1.9	70	73	101	52	80	87	100	105
122 (weakly acidic)	0.5	0.13	1.0	0.2	0.2	0.12	1.6	0.2	0.07	0.04	0.6	0.07	2.2	1.8	1.2	2.3	97	94	101	44	88	47	83	60

[a]Limit of quantitation (10 σ). [b]Limit of detection based on 99.7% (3 σ) confidence level. [c]From a sea-water matrix with the composition 3.1% NaCl, 1300 mg l^{-1} Mg, 400 mg l^{-1} Ca. [d]Concentration efficiency = [concentration (enrichment) factor] × [sampling frequency (min^{-1})].

ammonium acetate at pH 9.5. The table provides not only an evaluation of the performance of the system, but also a comparison of the behaviour of the different resins (see below).

The concentration efficiencies for the elements studied were significantly higher than in previous designs with the same resin, the improvement being due to the factors discussed above. The concentration efficiency was calculated by multiplying the concentration (enrichment) factor by the sampling frequency per minute. As long as the sample volume was kept within certain limits, so that there was no breakthrough of the analyte, the products were almost constant for a given experimental set-up. The concentration factor was obtained by comparing the peak height of the recording obtained during elution with the response of standard solutions of the same metal ion aspirated continuously directly into the nebulizer at the same flow rate as the eluant; the ratio of the concentrations which gave the same absorption signal is the concentration factor. Figure 4 shows the recording for a series of standard solutions of lead, run by the present system using a 8-quinolinol exchanger and by conventional direct aspiration. The calibration curves are almost identical except that the concentrations of the standard solutions differ by 2 orders of magnitude. The relative sensitivities obtained by f.i.a. at a sampling frequency of 60 h^{-1} were close to those of the graphite furnace obtained with 10-μl samples. The limit of quantitation (LOQ) defined as 10 σ, where σ is the standard deviation of baseline fluctuations, and the limit of detection (LOD), defined as 3 σ, for lead and zinc are illustrated in Fig. 5.

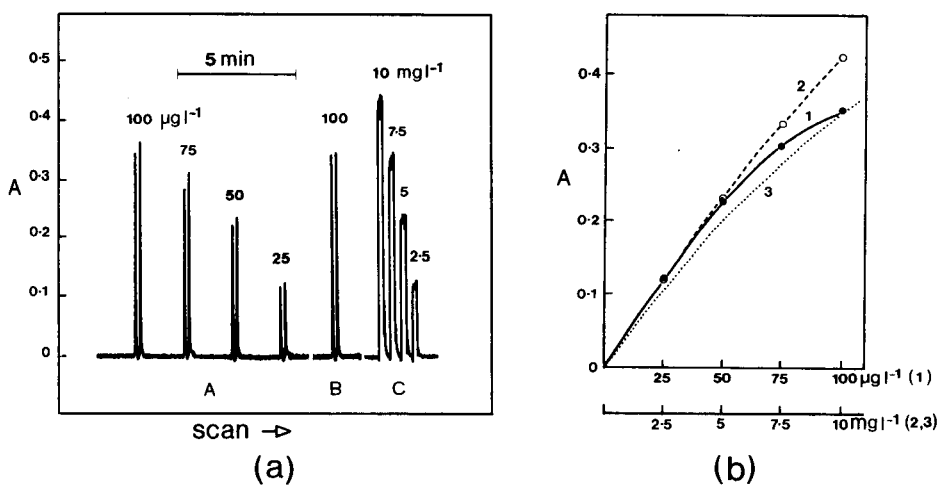

Fig. 4. (a) Recordings of standard lead solutions: A, 25—100 μg l^{-1} lead with the system in Fig. 2; B, a 100 μg l^{-1} lead solution in a matrix simulating sea water under the same conditions as in A but with background correction; C, 2.5—10 mg l^{-1} lead by conventional flame a.a.s. (b) Calibration curves: (1, 2) based on the results from runs A and C, respectively in (a); (3) constructed from data in the Varian-Techtron handbook (1979).

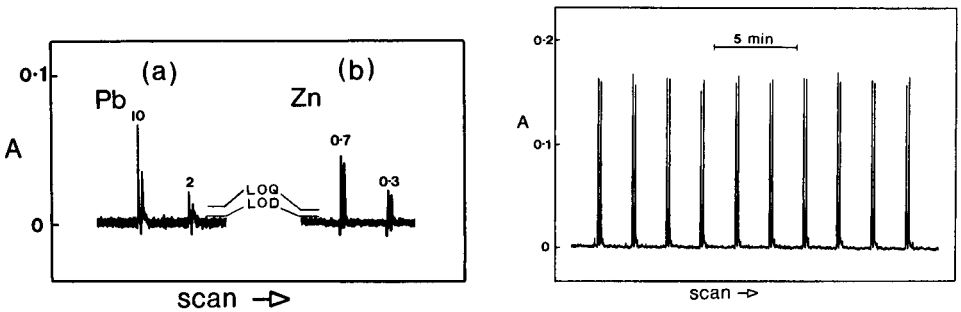

Fig. 5. Recordings of low concentrations of lead (a) and zinc (b) standard solutions with increased amplification to illustrate the limits of quantitation (LOQ) and detection (LOD) of the f.i.a./a.a.s. system. The 10 and 2 $\mu g\ l^{-1}$ lead samples were preconcentrated with an 8-quinolinol column (left peak) and a Chelex-100 column (right peak). The 0.7 and 0.3 $\mu g\ l^{-1}$ zinc samples were preconcentrated with dual Chelex-100 columns.

Fig. 6. Recordings of 10 duplicate runs of a 20 $\mu g\ l^{-1}$ copper standard solution with the system shown in Fig. 2, using confluenced buffer lines and two "identical" Chelex-100 columns. In each pair of peaks, the first peak refers to column A and the second one to column B.

The precision of the system was evaluated by estimating the relative standard deviation of 10 successive determinations from the same column. Figure 6 is a recording of the determination of copper using the buffer confluencing mode of the system incorporating two geometrically identical columns. In this case, the peak heights from the two columns are almost equal, but this is not necessarily so, because peak heights from two individual columns often differ because of small differences in column packings and length of conduits. For routine analysis in which samples are to be analyzed in duplicate, it could be advantageous to use a system with two different column lengths, i.e., different capacities.

Performance of dual-column system with different chelating columns

The overall performance of the flow-injection system depends heavily on the properties of the chelating column. The exchangers used most frequently for preconcentration of heavy metals include the well known Chelex-100 with an iminodiacetate chelating functional group [3, 4], the weakly acidic Amberlite IRC 50 [4], another weakly acidic resin 122 with a salicylic acid functional group [5], and an azo-immobilized (on pore glass) 8-quinolinol exchanger (8-Q) [6].

Chelating exchangers retain selectively heavy metal ions in the presence of alkali and alkaline earth metal ions, which is why they have been used for both batch and on-line preconcentration. Yet the kinetics of the uptake and release of metal ions by the different functional groups are not well described. As in all flow-injection systems, transient signals are obtained from an on-line elution, and differences in the kinetic behaviour of different exchangers would

therefore be expected. In f.i.a., the adsorption of the analytes on the column and the rate of release from it will have more pronounced effects than in a conventional procedure of ion-exchange preconcentration where the entire eluate containing a sample is collected before measurement. In conventional column operation, the recovery of analyte will be the same as long as no breakthrough occurs. Considering that the mean residence time of the sample in the exchange column is very short in the flow-injection sample (1—2 s), the kinetics of the chelating or ion-exchange process will obviously be important. To decide to what extent the differences in concentration efficiency result from the design of the flow system, and how much they reflect the properties of the exchanger used, a comparison of the different exchangers was made with the same flow-injection system. Although this does not eliminate the possibility that a certain resin might be better adapted to a particular design of f.i.a. preconcentration system, such a comparison would definitely yield useful information.

Three types of exchanger, Chelex-100, 8-quinolinol and 122 resin were compared with respect to their concentration efficiency, reproducibility of separation and freedom from interferences. No attempt was made to optimize the conditions individually for each exchanger; the system was operated in all experiments at the same flow rate, column dimensions and pH of the buffer and concentration of eluate. The particle sizes of the exchangers available were different, a factor which certainly affects the rate of uptake and release. Yet the comparison serves the purpose of providing a rough guide to the choice of exchanger.

Table 2 shows that the concentration efficiency varied considerably for different elements using the same exchangers as well as for the same element using different exchangers. Ignoring matrix effects, the 8-quinolinol material almost always had the highest concentration factor. This is probably due to the faster exchange rate of the surface-bound chelating functional groups. The analytes were eluted more readily from the surface, thus being present in a smaller volume of eluate as seen on the scan of cadmium peaks shown in Fig. 7: the half-width of the peak for the column filled with Chelex-100 was 50% wider than that for the 8-quinolinol column. Because of the smaller exchange capacity and comparatively high stability of magnesium 8-quinolinolate (log K_1 = 4.2 [10]), however, the recoveries of most of the heavy metals from a sea-water matrix were not acceptable. The recoveries of the elements decreased roughly in descending order of their stability constants (log K_1 for Cu, Pb, Zn, Cd are 12.2, 9.02, 8.56 and 7.2, respectively [11, 12]). Only lead showed good recovery, while the recovery for copper was low, presumably because of the formation of the ammonium complex in the ammonium acetate buffer. Lower recoveries were not encountered by Malamas et al. [6] in their excellent study of the exchanger, probably because the tap water which they analyzed contains much lower concentrations of alkaline earth metals, particularly magnesium which in sea water has a concentration of 1300 μg ml^{-1}.

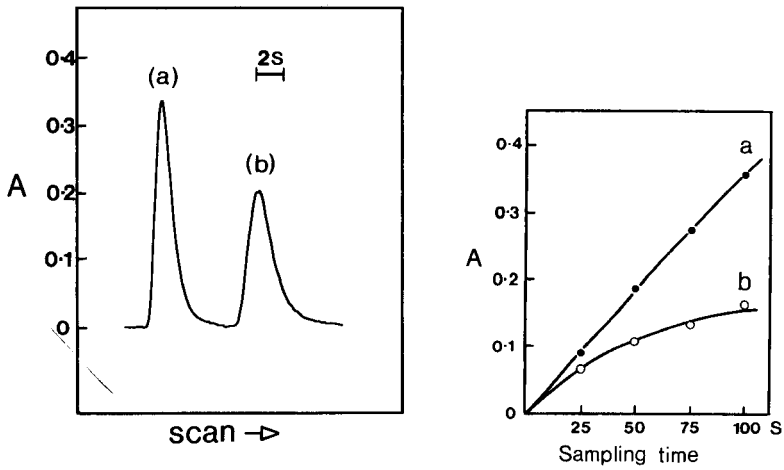

Fig. 7. Rapid-scan elution curves of 10 μg l^{-1} cadmium samples using columns packed with (a) 8-quinolinol on CPG and (b) Chelex-100. The volume of the two columns was identical.

Fig. 8 Signal response for a 10 μg l^{-1} cadmium standard as a function of sampling time (sample volume) using the system depicted in Fig. 2 with 8-quinolinol columns: (a) without matrix constituents; (b) in a simulated sea-water matrix.

Despite the high concentration of alkaline earth metals in the sea-water matrix, good recoveries were obtained for all the metals studied when Chelex-100 resin was used. When the lower stability of the magnesium iminodiacetate complex (log K_1 = 2.94 [13]) and the higher exchange capacity of the column are considered, this is not unexpected. The results obtained with the weakly acidic 122 resin were quite similar to Chelex-100 except for cadmium for which no satisfactory recovery could be obtained in the sea-water matrix. Again the higher stability of the salicylate complex of magnesium (log K_1 = 4.7 [14]) might be the reason for this low recovery. It is, however, interesting to observe that the recovery of heavy metals was considerably better in the present work, at pH 9.5, than when a buffer of pH 5.5 was used for the preconcentration [5].

The lower recoveries described above are thus probably caused by breakthrough of the analytes in the presence of larger concentrations of competing ions. When the standard solution containing the highest cadmium concentration (10 μg l^{-1}) was used to investigate the breakthrough of the column packed with the 8-quinolinol material by increasing the sampling time (and thus the sample volume), there were no signs of breakthrough in the absence of matrix constituents (Fig. 8). The situation was different when the same concentration of cadmium was preconcentrated from a sea-water matrix. Thus, increasing the column capacity by lengthening the column will alleviate this problem to a certain degree, yet back-pressure will be the limiting factor in increasing the column length.

Some general directions as to the choice of chelating or ion exchanger for different applications may be useful. When maximum sensitivity is desired in samples with relatively simple matrix (e.g., tap water or rain water), the 8-quinolinol on CPG will give the best performance, whereas Chelex-100 will give accurate results for a wide range of heavy metals in samples with relatively high content of alkaline earth metals at the expense of 10—40% loss in sensitivity. The weakly acidic 122 resin, not having the troublesome swelling properties of Chelex-100, is considerably easier to handle than Chelex-100, and if cadmium analysis is not required, the 122 resin will be the best choice for samples with higher alkaline earth metal contents. The results in more difficult matrices than sea water, such as those containing high concentrations of iron and aluminium, are difficult to predict. Considerable work is still needed to increase the versatility of the preconcentration system for f.i.a. by detailed studies of chemistries involved.

Comparison of the f.i.a./a.a.s. preconcentration with graphite-furnace a.a.s.

It is worthwhile to compare the proposed f.i.a./a.a.s. technique with the well-established graphite-furnace a.a.s. technique. Some features are compared in Table 3. When the characteristic concentrations and detection limits of the f.i.a./a.a.s. system are compared to those of the graphite-furnace method, the sensitivity of the f.i.a. preconcentration technique is apparently slightly lower. However, the data quoted for graphite-furnace a.a.s. are usually those obtained under optimal conditions and are often irrelevant for routine applications. Characteristic concentrations for both methods will obviously vary depending on the sample volumes used so that practical considerations become very important. In the f.i.a./a.a.s. procedure, very long sampling periods are unlikely to be used routinely; a reasonable sampling frequency of 60 h^{-1} was chosen to estimate the sensitivity and concentration factor.

TABLE 3

Comparison of f.i.a./a.a.s. and graphite-furnace a.a.s.

Characteristic concentration	For f.i.a./a.a.s. at sampling rate of 60 h^{-1}: Cu 0.5, Zn 0.07, Pb 0.8, Cd 0.13 $\mu g\ l^{-1}$. For g.f.a.a.s. with 10-μl sample: Cu 3, Zn 0.1, Pb 2[a], Cd 0.1 $\mu g\ l^{-1}$ [15].
Sample throughput	2—3-fold higher for f.i.a./a.a.s. at comparable sensitivities.
Sample consumption	F.i.a./a.a.s. requires much larger sample volumes.
Precision	Comparable or better for f.i.a./a.a.s.
Spectral interferences from matrix	Much less for f.i.a./a.a.s.
Apparatus	Simpler for f.i.a./a.a.s.
Manipulation	Easier for f.i.a./a.a.s.
Running costs	Lower for f.i.a./a.a.s.
Equipment cost	Much lower for f.i.a./a.a.s.

[a]Wavelength 283.3 nm.

Analogously, the data for the sensitivity of the graphite-furnace method were based on the use of 10-μl samples, which are practical for routine work.

The main drawbacks of the flow-injection preconcentration system in its present form are the need for fairly large sample volumes and the interferences in the exchanger column. The sample volume (10-ml) is not really a limiting factor, except in such areas as clinical and forensic analysis. The sample consumption might be lowered by scaling down the flow system [8], leading to lower sampling and elution rates. However, this in turn demands the construction of a nebulizer for the spectrometer with an uptake rate of <2 ml min^{-1} without loss of sensitivity; ultrasonic nebulization seems a possible route. Chemical interferences are a main obstacle in the development of new methodology for graphite-furnace a.a.s. and such interferences in the preconcentration processes in f.i.a. also pose important and intriguing problems.

Conclusion

The flow-injection a.a.s. system with on-line preconcentration will challenge the position of the graphite-furnace technique, because it yields comparable sensitivity for much lower cost by using simpler apparatus and separation mode. The proposed method offers unusual advantages when matrices with high salt contents (e.g., sea water) are analyzed because the matrix components do not reach the nebulizer.

From the viewpoint of methodology for f.i.a., the present work features, like hydrodynamic injection [8, 9], a novel approach to sample metering and injection of a well-defined zone, by using exact timing in combination with constant pumping rates rather than a loop of a fixed volume.

The future challenge lies in optimization of the parameters on which the selective preconcentration depends: choice and synthesis of column materials, optimization of carrier stream and eluant composition. Atomic absorption and atomic emission methods (including the various modifications of inductively coupled plasma spectrometry), which have systematically been replacing methods based on complex formation (such as spectrophotometry), will also rely on a deeper knowledge of solution chemistry for improved sensitivity and selectivity. Studies of selectivities, capacities and kinetic behaviour of surface-bonded chelating agents, as recently done by Leyden and Wegscheider [16] and Malamas et al. [6], will play a crucial role in further development and application of preconcentration methods for f.i.a.

The authors thank Gillis Johansson of the University of Lund, Sweden, for the gift of the 8-quinolinol exchanger. One of us (F.Z.) is indebted to the Academia Sinica for granting leave of absence and financing his stay at the Technical University of Denmark.

REFERENCES

1 H. M. Kingston, I. L. Barnes, T. J. Brady and T. C. Rains, Anal. Chem., 50 (1978) 2064.
2 L. G. Danielsson, B. Magnussen and K. Zhang, At. Spectrosc., 3 (1982) 39.
3 S. Olsen, L. C. R. Pessenda, J. Růžička and E. H. Hansen, Analyst (London), 108 (1983) 905.
4 S. S. Jørgensen and K. Petersen, Paper presented at 9th Nordic Atomic Spectroscopy and Trace Element Conference, Reykjavik, Iceland, 1983.
5 Z. Fang, S. Xu and S. Zhang, Anal. Chim. Acta, 164 (1984) 41.
6 F. Malamas, M. Bengtsson and G. Johansson, Anal. Chim. Acta, 160 (1984) 1.
7 F. J. Krug, B. F. Reis and S. S. Jørgensen, Proceedings of the Workshop on Locally Produced Laboratory Equipment for Chemical Education, Copenhagen, Denmark, p. 121, 1983.
8 J. Růžička and E. H. Hansen, Anal. Chim. Acta, 161 (1984) 1.
9 J. Růžička and E. H. Hansen, Anal. Chim. Acta, 145 (1983) 1.
10 J. Stary, Yu. A. Zolotov and O. M. Petrukhin, Critical Evaluation of Equilibrium Constants Involving 8-Hydroxyquinoline and Its Metal Chelates, IUPAC Chemical Data Series, No. 24, Pergamon Press, 1979.
11 A. Albert, Biochem. J., 54 (1953) 646.
12 R. Näsänen, Acta Chem. Scand., 6 (1952) 352.
13 L. G. Sillén and A. E. Martell, Stability Constants, Special Publications No. 17, The Chemical Society, London, 1964, p. 427.
14 L. G. Van Uitert and W. C. Fernelius, J. Am. Chem. Soc., 76 (1954) 375.
15 C. W. Fuller, Electrothermal Atomization for Atomic Absorption Spectrometry, The Chemical Society, London, 1977, p. 96.
16 D. E. Leyden and W. Wegscheider, Anal. Chem., 53 (1981) 1059A.

Analytica Chimica Acta, 164 (1984) 41—50
Elsevier Science Publishers B.V., Amsterdam — Printed in The Netherlands

THE DETERMINATION OF TRACE AMOUNTS OF HEAVY METALS IN WATERS BY A FLOW-INJECTION SYSTEM INCLUDING ION-EXCHANGE PRECONCENTRATION AND FLAME ATOMIC ABSORPTION SPECTROMETRIC DETECTION

ZHAOLUN FANG*, SHUKUN XU and SUCHUN ZHANG
Institute of Forestry and Soil Science, Academia Sinica, Shenyang (China)
(Received 20th January 1984)

SUMMARY

The flow-injection system combines on-line ion-exchange preconcentration with atomic absorption spectrometry (a.a.s.) for the determination of traces ($\mu g\ l^{-1}$) of heavy metals in water samples. Miniature columns packed with 60—100 mesh chelating resin (122) with a salicylic acid functional group are used for preconcentration. A multifunctional rotary sampling valve which incorporated two parallel sampling columns allows sampling, exchange, elution and a.a.s. to be achieved sequentially. The increases in sensitivity for nickel, copper, lead and cadmium were 20—28-fold at a sampling rate of 40 h^{-1} with 5-ml samples. Relative standard deviations were 1.5—4.1%. The recoveries of these four metals added to tap, sea and polluted waters were generally satisfactory, except for cadmium in polluted water. The effects of column diameter and elution flow rates on sensitivity are discussed. Possible interferences are described.

Flame atomic absorption spectrometry (a.a.s.) is widely used for the determination of trace metals in environmental samples; although it is much less sensitive than the graphite-furnace technique, it is considerably more efficient. Interferences are usually more severe in the electrothermal method and the extra equipment involved is expensive. Methods of separation and concentration, mainly involving liquid—liquid extraction and ion-exchange, have been devised to allow determinations of trace metals in environmental samples by the flame technique at $\mu g\ l^{-1}$ levels. Preconcentration methods have been reported that are capable of improving the detection limit by one or two orders of magnitude, with the additional advantage of separating the analyte from an interfering matrix [1—3]. However, the procedures tend to be tedious, so that some of the main advantages of flame atomic absorption spectrometry are lost. Attempts have been made, therefore, to automate and speed up the preconcentration process.

Recent publications on flow injection analysis (f.i.a.) have suggested that, besides being a powerful technique in automated chemical analysis, f.i.a. also shows considerable promise in the automation of such pretreatments as liquid—liquid extraction and ion-exchange separation [4]. Recently, Nord

0003-2670/84/$03.00

and Karlberg [5] have reported on sample preconcentration by continuous flow extraction and subsequent measurements by flame a.a.s. in a flow-injection system. A 15—20-fold increase in sensitivity was achieved at a sampling rate of 40 h^{-1} for the metals studied. The application of flow-injection a.a.s. systems to the preconcentration of trace metals with miniature ion-exchange columns has been reported more recently [6, 7]. Olsen et al. [6] determined lead at concentrations as low as 10 $\mu g\ l^{-1}$ and cadmium and zinc down to 1 $\mu g\ l^{-1}$ concentrations. Sampling rates were 30—60 h^{-1}, depending on the extent of preconcentration required. A small column of Chelex-100 resin arranged in an on-line flow-injection system was used for the preconcentration. Jørgensen and Petersen [7] also used a Chelex-100 column on-line, achieving a 3—17-fold enhancement in the a.a.s. measurement of trace metals.

In the present work, a flow-injection system with ion-exchange preconcentration and atomic absorption detection was developed and applied to the determination of trace amounts of heavy metals in some natural waters. A multifunctional rotary valve, incorporating two parallel miniature ion-exchange columns packed with a chelating resin with salicylic acid functional groups, was used for sequential sampling, injection, ion-exchange and elution. A 20—28-fold increase in sensitivity compared to direct aspiration of sample was obtained for nickel, copper, lead and cadmium at a sampling rate of 40 h^{-1} and 40—50-fold enhancements were possible at sampling rates of 20 h^{-1}.

EXPERIMENTAL

Apparatus and reagents

A single-beam Nippon Jarrell-Ash AA-1 MK-II atomic absorption spectrometer with an air—acetylene flame and without background correction was connected to a recorder for the measurements. Instrument settings were as recommended by the manufacturer.

The flow-injection system is outlined in Fig. 1. An eight-channel peristaltic pump (model LDB-1, Second Analytical Instrument Co., Shenyang) was used to propel the samples, carriers and eluant at the flow rates specified in Fig. 1. The valve was a three-layer sandwich type analogous to a commutation injector [8], having three 3:2:3 commutation sections and two parallel sample loops, two eluant loops and two ion-exchange columns arranged on the same rotor. When the rotor was rotated manually at regular intervals, the sampling, ion-exchange and elution processes were done sequentially and alternately on the two columns. Sample loops were made from suitable lengths of 3-mm i.d. glass tubing, coiled and fixed on a board near the valve and connected to the teflon rotor with 0.9-mm i.d. teflon tubing. The eluant loops were made from 2.3-mm i.d. tygon tubing. The volumes of the sample and eluant loops were 5 ml (for 20—30-fold concentration) and 1.5 ml, respectively. The valve was connected to the spectrometer via 10 cm of 0.5-mm i.d. teflon tubing.

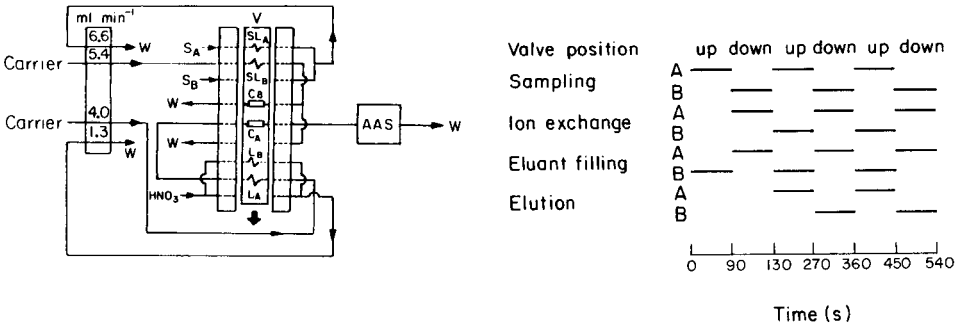

Fig. 1. Flow diagram of the dual-column on-line preconcentration system (a) and the corresponding program for the preconcentration process (b). Subscripts A and B represent channels A and B, respectively. Multifunctional rotary valve (V) parts: S_A, S_B, sample; SL_A, SL_B, sample loop; C_A, C_B, ion-exchange column; L_A, L_B, eluant loop. W, waste. Carrier, 0.1 M ammonium acetate at pH 5.5.

The ion-exchange columns were made from 5-cm sections of tygon tubing (2.5—3 mm i.d.). The ends of the tubes were fitted with 100-mesh nylon screen to retain the resin in the tubes. The screens were kept in place by two short pieces of tygon tubing which were later sealed with a drop of cyclohexanone. With one end fitted with nylon screen, the columns were filled with a slurry of 60—100 mesh ion-exchange resin (resin 122; Institute of Chemical Engineering of Eastern China) which has salicylic acid functional groups on a phenol—formaldehyde copolymer base. The columns were then covered with nylon screen at both ends and connected to the rotor of the valve by short sections of 0.9-mm i.d. teflon tubing. For precise measurements based on duplicate recordings from two different columns, it is important that the geometrical dimensions of the parallel columns be identical.

Working standards of the metals in the ranges 100—400 $\mu g\ l^{-1}$ nickel, 25—100 $\mu g\ l^{-1}$ copper, 100—500 $\mu g\ l^{-1}$ lead and 25—100 $\mu g\ l^{-1}$ cadmium were prepared from 100 mg l^{-1} stock standard solutions; all the solutions were made 0.1 M in ammonium acetate at pH 5.5.

The carrier stream for sample and eluant was 0.1 M ammonium acetate solution with pH adjusted to 5.5. The eluant was 2 M nitric acid.

Procedure

Water samples were acidified on collection with nitric acid to a final concentration of 10^{-3} M nitric acid. A 20-ml aliquot of water sample with 2 drops of methyl orange was neutralized with (1 + 1) ammonia liquor to the yellow colour in a 25-ml volumetric flask, 2 ml of 1 M ammonium acetate at pH 5.5 was added, and the solution was diluted to volume with deionized water. Corrections in the final results were made to compensate for the dilution of the sample.

The manifold of the system is shown in Fig. 1. The system was designed so as to improve efficiency by incorporating two parallel columns. The sample,

carrier and eluant were pumped into their respective lines and the valve was turned manually at 90 s regular intervals (with a 5-ml sample for 20—28-fold concentration). The various stages of the process on the two columns are shown in the program in Fig. 1(b). The first peak of the analyte eluted from the column appeared 185 s after aspiration of the first sample, following two turns of the valve. The next peak was recorded 90 s later after another turn of the valve. Further peaks appeared on every turn of the valve, so that a sampling frequency of 40 h^{-1} could be attained. Figure 2 is a recorder tracing of a series of metal standards processed in duplicate.

When properly used, the lifetime of the columns was estimated to be over 1000 cycles, during which time no appreciable changes in peak heights could be observed. However, if the columns were left in 2 M nitric acid overnight, the ion exchanger might deteriorate to such an extent that it was no longer useful. It is important, therefore, that the columns be thoroughly rinsed with deionized water before the system is shut down.

RESULTS AND DISCUSSION

Design of the flow system

At an earlier stage of the present work, a much simpler flow system was employed. This system incorporated a single column placed after a 2-channel injection valve for sample and nitric acid, and leading directly to the spectrometer. This was much less efficient than the manifold in Fig. 1 and suffered from the defect that the waste stream flowing from the column after the ion-exchange process was directed to the nebulizer of the spectrometer which would tend to be clogged in the analysis of samples having high salt contents (e.g., sea water). It had the advantage, however, of simpler design; because only one column was used, the dimensions of the column were less critical.

The manifold in Fig. 3 is a simplification of the one in Fig. 1. The manipulation and performance were almost identical except that the acid eluant was directly aspirated through the column into the nebulizer without going

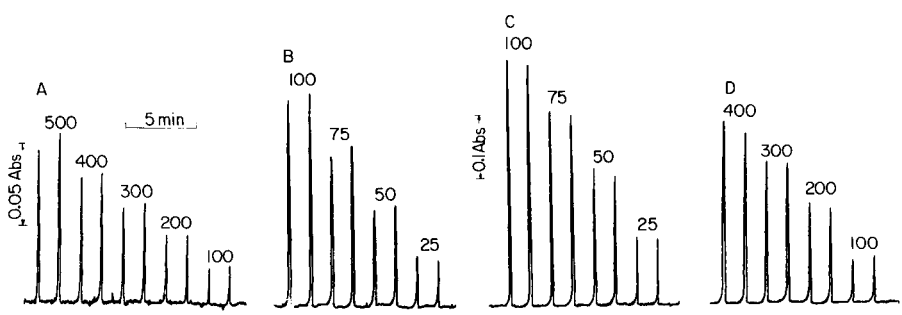

Fig. 2. Recordings of calibration runs: (A) lead; (B) copper; (C) cadmium; (D) nickel standards, with the system in Fig. 1. The numbers on the peaks indicate the concentration in $\mu g\ l^{-1}$.

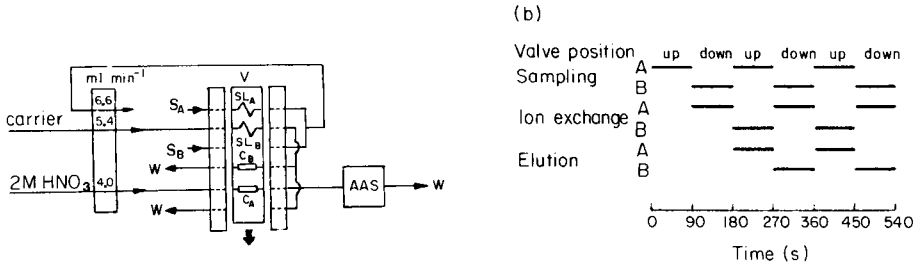

Fig. 3. Flow diagram of a simplified version of the double-column preconcentration system in Fig. 1. Symbols are the same as for Fig. 1.

through an eluant loop. Because of prolonged aspiration of acid into the nebulizer, corrosion problems would arise with certain instruments.

Concurrent and countercurrent elution (relative to the flow direction of the ion-exchange stage) modes were studied for their effects on sensitivity and precision. No significant difference in sensitivity was observed, but the precision was somewhat better for the countercurrent mode with a relative standard deviation of 1.5% for nickel against 2.0% for the concurrent mode.

Optimization of flow rates and column

The elution flow rate was found to be quite critical. Previous reports on the application of flow-injection techniques to a.a.s. have stressed the importance of matching the pumping rate of the flow-injection system to the specified feed rate of the spectrometer for optimum sensitivity and precision [9, 10]. Even air compensation methods have been proposed [10]. The specified feed rates for most commercial instruments are in the range 4—8 ml min^{-1}. The instrument used here had a specified optimum feed rate of 5 ml min^{-1}. However, direct continuous feeding of the eluate into the nebulizer after elution at this flow rate did not yield an optimum peak response, presumably because lack of sufficient time to reach equilibrium during the elution. An investigation of the relationship between elution flow rate and peak height at fixed column dimensions showed that maximum peak height occurred at a lower flow rate (Fig. 4). It should be noted that the different metals have different optimum flow rates, presumably because of the different stabilities of the complexes formed. At lower flow rates of eluant, the analyte has more time for desorption and would be more concentrated in a smaller volume of the final eluate, giving a higher response, if there were no limitations for the optimum feed rate of the spectrometer. The result of these contrary features was an optimum elution flow rate which was lower than the optimum feed rate, and is obviously a compromise. This was further confirmed when the same manifold was connected to an inductively-coupled plasma spectrometer with a nebulizer having a specified feed rate of 2 ml min^{-1}; the optimum elution flow rate occurred at a much lower value of 1—2 ml min^{-1}, with a higher enrichment of the analyte. In contrast to some earlier reports, the difference between the actual and specified feed rates did

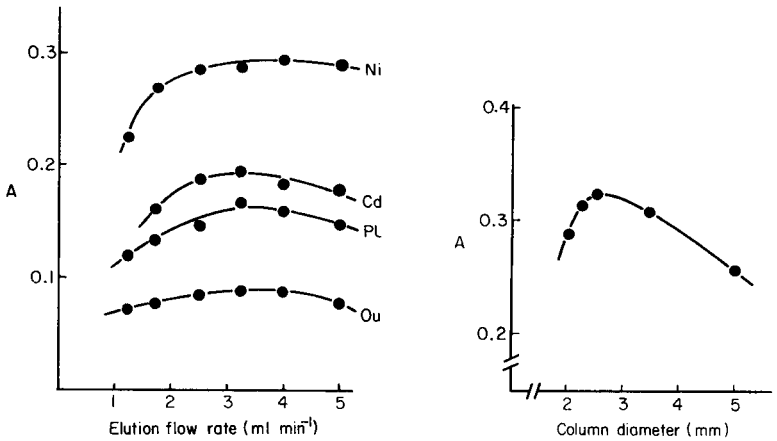

Fig. 4. Relationship between elution flow rates and peak responses of Ni, Cu, Pb, and Cd for the system in Fig. 1. Concentrations were 500, 100, 800 and 100 $\mu g\ l^{-1}$ for Ni, Cu, Pb and Cd, respectively.

Fig. 5. Peak height of nickel as a function of the ion-exchange column diameter for the system in Fig. 1. The column length was 35 mm. Ni concentration, 500 $\mu g\ l^{-1}$.

not affect the precision. Moreover, the precision was not improved by feeding (eluting) at the specified flow rate at the expense of lower sensitivity. Attempts to improve the sensitivity by compensation of the difference between the optimum and specified flow rates, by introducing air at the entrance of the nebulizer as suggested by Yoza et al. [10] were also unsuccessful.

Attempts were made to leach the column at a low flow rate and store the eluate in a loop. The contents were then aspirated with a carrier stream at the specified feed rate of the instrument with the aim of providing optimum flow rates both for the elution and the nebulization and thus of improving the sensitivity. Nord and Karlberg [5] used such an approach successfully in their continuous flow liquid—liquid extraction system. In the present case, however, the sensitivity deteriorated somewhat, possibly because the carrier and eluate plug were all aqueous solutions and dispersion could not be confined to a certain part of the sample zone as Nord and Karlberg did with an organic extractant plug and aqueous carrier. Thus it seemed that the sensitivity gained through using an optimum feed rate could not compensate for the loss of sensitivity through extra dispersion in the system.

The diameter of the ion-exchange column was optimized for fixed column lengths, and fixed exchange and elution flow rates. A column length of 35 mm was chosen so that the back-pressure in the system during operation would be well within the limits tolerable for a low-pressure peristaltic pump. The flow rate chosen for the exchange reaction (5.4 ml min^{-1}) seemed to be the highest possible; higher flow rates led to unacceptable breakthrough of the

analytes because of insufficient interaction with the chelating resin. The peak heights for nickel obtained when different column diameters were used are shown in Fig. 5. The results were similar for the other metals studied, and suggested that column diameter had little effect on the sensitivity in the range 2.2—3.5 mm i.d. Below 2.2 mm, the sensitivity gradually decreased, possibly because of breakthrough resulting from an increase in linear flow rate through the column. Columns with a diameter of over 3.5 mm also yielded lower peaks, presumably owing to dispersion in the larger dead volume of the column, although the recovery was better (99% for a high concentration of 10 mg l^{-1} Ni) than those obtained with thinner columns (85—95%).

It was found at a later stage in this work that even columns with a length of 50 mm would not induce excessive back-pressure to affect the performance of the pump provided that the column diameter was at least 3.5 mm. Thus when high exchange capacity is needed for certain samples (e.g., samples containing large amounts of calcium and magnesium which are partly adsorbed by the resin) longer columns are recommended.

Interferences

Various possible interfering ions often encountered in water samples were tested for their effects on the analyte metals. Iron, Mn, Zn, Ni, Cu, Cd and Pb (2 mg l^{-1}) had no effect on the single metals quantified at concentrations of 10—100 μg l^{-1}. The alkali metals were almost completely separated from the analyte metals in the preconcentration process, and sodium and potassium showed no interference in the determination of any of the analytes studied even at concentrations of a few percent and without resorting to background correction.

The alkaline earth metals posed a more difficult problem. Calcium and magnesium which occur in considerable amounts in many natural waters were partially adsorbed by the resin at pH 5.5 and would eventually be eluted with the analytes. However, 100 μg l^{-1} standard solutions of the analytes containing 1300 mg l^{-1} magnesium and 400 mg l^{-1} calcium, did not show background interferences except for copper, for which there were 46% and 10% enhancements in peak response for magnesium and calcium, respectively. This interference could be removed by rinsing the column with 1 M ammonium acetate (pH 5.5) before elution. This procedure, as reported earlier [3], removes most of the adsorbed calcium and magnesium at the expense of a small loss of the analytes. When 1 M ammonium acetate was examined as carrier stream for the sample to simulate this rinsing process, the results shown in Fig. 6 were obtained. Because of a 20% loss in sensitivity, the rinsing process with 1 M ammonium acetate is not recommended except in extreme cases where the interference is severe and no background corrections can be applied. As a compromise, a more dilute solution of 0.1 M ammonium acetate, which did not degrade the sensitivity but was less effective in rinsing the interferences, was normally used as the carrier.

When this carrier was used, however, large amounts of magnesium and

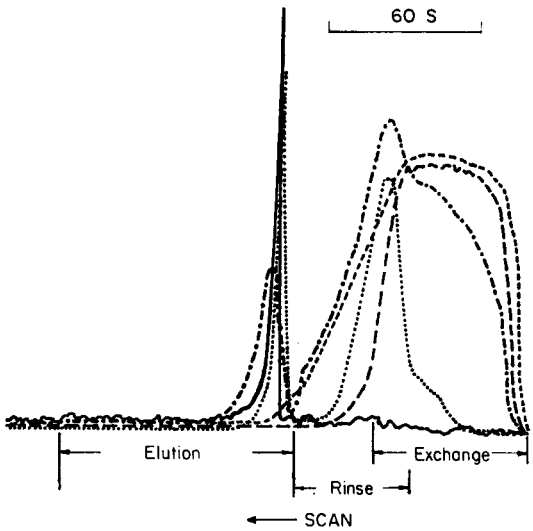

Fig. 6. Absorption signals of K, Na, Ca, Mg and Cu recorded during ion-exchange, rinsing with 1 M ammonium acetate and elution with 2 M nitric acid. Metal ions: (——) Cu; (—·—) Mg; (— — —) K; (· · ·) Na; (· · · ·) Ca. The system in Fig. 1 was used but the effluent from the column during the exchange and rinsing stage was directed to the spectrometer instead of flowing to waste. The concentrations of K, Na, Ca and Mg were 100 mg l^{-1}; Cu concentration was 100 μg l^{-1}. Absorbance scales for each element have been adjusted to ease comparison.

calcium produced severe depressing effects on cadmium and, to a lesser degree, on nickel; this was obviously the result of breakthrough of these analytes because of competition with the alkaline earth metals during the chelation on the small resin column (the column used was 35 mm long with 2.5 mm i.d. for these studies). Increasing the column dimensions, to 50 mm long and 3.5 mm i.d., almost tripled the ion-exchange capacity of the column. As a result, the depressing effect of calcium and magnesium was partially overcome and recoveries of about 75% (compared to 40% with the smaller column) were obtained for nickel added to sea-water samples. The recoveries for cadmium in sea water and other complex matrices were, however, still unsatisfactory and low recoveries (about 25%) were obtained even with the larger column. Hence, the determination of cadmium is possible only in comparatively pure water (e.g., tap water) with the present system (see below). Olsen et al. [6] successfully determined cadmium in sea water, using Chelex 100 to concentrate the metal at pH 9—10. Increasing the pH of the system might also prove beneficial here, because the 122 resin used behaves in much the same way as Chelex 100. Further work on the effects of pH on the recoveries and sensitivity of the analytes are in progress.

Performance of the method

The results obtained for pure solutions using sample volumes of 5 ml are

TABLE 1

Performance of the proposed system

Element	Wavelength (nm)	Concentration factor[a]	Characteristic concentration ($\mu g\ l^{-1}$)	R.s.d.[c] (%)
Ni	232.0	20	7.5	1.5
Cu	324.8	25	6	2.7
Pb	283.3	25	20	4.1
Cd	228.8	28	1	1.6

[a]Sample volume 5 ml; values derived from comparison to the response obtained by direct aspiration. [b]Characteristic concentration is defined as that concentration of the element which gives rise to 0.0044 absorbance unit. [c]For 11 measurements.

TABLE 2

Recoveries of metals added to various water samples[a]

Sample	Recovery (%)			
	Ni	Cu	Pb	Cd
Tap water	91	93	95	91
Sewage water	90	73	108	53
Sewage water	106	90	102	44
Sea water	73	90	88	25
Sea water	75	100	100	25

[a]The samples were spiked with 250 $\mu g\ l^{-1}$ Ni, 20 $\mu g\ l^{-1}$ Cu, 100 $\mu g\ l^{-1}$ Pb, and 20 $\mu g\ l^{-1}$ Cd.

summarized in Table 1. Higher sensitivity could be obtained by increasing the sample volume, but the sampling frequency will be lowered accordingly. Under the recommended conditions, the sampling frequency is 40 h^{-1}.

As shown in Table 2, recovery tests on various types of water samples, done by spiking the samples with known amounts of the metals to be determined, were generally satisfactory. The recovery for cadmium, however, has yet to be improved for sea- and waste waters.

REFERENCES

1 H. M. Kingston, I. L. Barnes, T. J. Brady and T. C. Rains, Anal. Chem., 50 (1978) 2064.
2 T. M. Florence and G. E. Batley, Talanta, 23 (1976) 179.
3 Yang Shide, Fenxi Huaxue, 10 (1982) 543.
4 J. Růžička and E. H. Hansen, Flow Injection Analysis, Wiley Interscience, New York, 1981.
5 L. Nord and B. Karlberg, Anal. Chim. Acta, 145 (1983) 151.
6 S. Olsen, L. C. R. Pessenda, J. Růžička and E. H. Hansen, Analyst (London), 108 (1983) 905.

7 S. S. Jørgensen and K. Petersen, Abstract, 9th Nordic Atomic Spectroscopy and Trace Element Conference, Reykjavik, Iceland, 1983.
8 A. O. Jacintho, E. A. G. Zagatto, H. Bergamin F°, F. J. Krug, B. F. Reis, R. E. Bruns and B. R. Kowalski, Anal. Chim. Acta, 130 (1981) 243.
9 B. D. Mindel and B. Karlberg, Lab. Pract., 30 (1981) 719.
10 N. Yoza, Y. Aoyagi, S. Ohashi and A. Tateda, Anal. Chim. Acta, 111 (1979) 163.

Analytica Chimica Acta, 164 (1984) 51—66
Elsevier Science Publishers B.V., Amsterdam — Printed in The Netherlands

COMPARISON OF ATOMIC FLUORESCENCE POWER EFFICIENCIES FOR THE HELIUM—OXYGEN—ACETYLENE AND AIR—ACETYLENE FLAMES

K. A. SATURDAY[a], A. YUEN and G. M. HIEFTJE*
Department of Chemistry, Indiana University, Bloomington, IN 47405 (U.S.A.)
(Received 26th March 1984)

SUMMARY

Power efficiencies for five elements have been measured for the helium—oxygen—acetylene and air—acetylene flames. The increased power efficiencies found in this study for the helium-diluted flame, coupled with its enhanced atom-formation capabilities, suggest that lower atomic fluorescence detection limits should exist. However, in a comparison study with an air—acetylene flame using identical experimental conditions, a decreased atomic fluorescence signal-to-noise ratio was found for most elements in the helium-diluted flame. This decrease is ascribed to greater background emission noise in the hotter helium-diluted flame and decreased nebulization efficiency caused by the low density of the helium-containing nebulizer gas. A comparison of flame emission detection limits for the two flames confirms the increased sensitivity of the hotter helium—oxygen—acetylene flame, despite its lower nebulization efficiency.

Studies of the physical characteristics [1] and atom-formation properties [2] of the helium—oxygen—acetylene flame have suggested its application to atomic fluorescence spectrometry. The properties of the helium-diluted flame correlate well with those required of an ideal atomic fluorescence flame cell [3, 4]. Among these properties are high desolvation and atomization efficiencies, low background emission, high stability, and low concentrations of quenching species.

The helium—oxygen—acetylene flame was initially studied because of its atom-formation capabilities [5]. In that study, the desolvation rates of individual droplets injected into a flame were measured; it was found that replacing the nitrogen component of an air—acetylene flame with helium doubled the rate of droplet desolvation. Because of this increased rate of desolvation, a greater fraction of sample is available for atomization/excitation and the number of large undesolvated droplets, which can scatter incident radiation, is reduced. A recent study measured the atom-formation efficiency of the helium—oxygen—acetylene flame and showed the flame to possess atom-formation capabilities between those of two commonly-used atom cells, the nitrous oxide—acetylene and air—acetylene flames [2].

---

[a]Current Address: E. I. DuPont De Nemours Co., Inc., Savannah River Laboratory, Aiken, SC 29801, U.S.A.

0003-2670/84/$03.00

The background emission spectrum of the helium—oxygen—acetylene flame is similar to that of the air—acetylene flame [1]. Although the strongest feature in the spectrum of the helium-diluted flame (the OH band at 310 nm) is four times more intense than in the air-sustained flame, neither flame exhibits a background as intense or complex as that of the nitrous oxide—acetylene mixture.

Improvements in burner design have increased the stability of the helium—oxygen—acetylene flame [1, 2]. The first study in which this gas mixture was used showed that the helium-diluted flame could not be safely supported on burners constructed for air—acetylene or nitrous oxide—acetylene combustion [5]. However, simple modifications to existing burners allowed the physical characterization of the flame [2]; further developments in burner design have permitted the flame to be utilized with a commercial nebulization chamber, resulting in safe and reproducible performance [2].

The quenching environment of the helium—oxygen—acetylene flame should be favorable, because helium is the principal flame constituent. Other workers have measured the quenching effects of helium, nitrogen, argon and other species on the atomic fluorescence of several metal atoms in flames [6]. Helium was found to possess a smaller quenching cross-section than nitrogen (0.1 $Å^2$ compared to 6.5 $Å^2$), and was comparable to argon. Because of the low quenching cross-section of helium, an increased fluorescence yield should occur for a helium-containing flame. Verification of this hypothesis is the subject of the present investigation.

Although the characteristics of the helium—oxygen—acetylene flame correlate well with those of the ideal atomic fluorescence atom cell, it has never been used in fluorescence measurements. In the present study, the helium-diluted flame is compared to the air—acetylene flame in its quenching characteristics. Specifically, fluorescence power efficiencies are measured in both flames. It was found that power efficiencies for the helium-diluted flame were greater, but atomic fluorescence signal-to-noise ratios were not greatly improved, because of the decreased nebulization efficiency of the helium-containing nebulization gas and the increased background emission noise of the flame. In contrast, emission measurements exhibit lower detection limits, primarily because of the higher temperature of the helium-sustained flame.

EXPERIMENTAL

Equipment and solutions

Burner. The construction of the capillary burner used has been previously described [2]. However, a component used to support an inert-gas sheath has been added to the burner assembly. The design of this component is similar to one previously described [7] and was constructed from 18-gauge capillary needles (Popper and Sons, New Hyde Park, NY) using the same procedure followed for the burner head construction [2]. The resulting gas-

sheath capillary array fits snugly around the burner head and contains 212 exit ports arranged in four concentric circles to provide sufficient sheathing for the flame.

Instrumental system. A schematic diagram of the optical system used for the determination of fluorescence power efficiencies is shown in Fig. 1; a detailed list of the optical components, detection equipment and experimental conditions is contained in Table 1. In the experimental system, the output of the continuum light source was focused into the center of the flame by lens, L1. Diaphragm D2 formed the limiting aperture for the external optical system, while D1 served to reduce the amount of stray light.

For the measurement of absorption and fluorescence signals, equivalent optical systems were constructed to focus either the continuum source or fluorescence radiation onto the appropriate monochromator entrance slit. Although identical components were used for each of the detection portions of the system, the equivalence of their optical performance could not be assumed. To assess their similarity, the magnification produced by each lens, L2 and L3, was measured. In the absorption portion of the system, the continuum source was focused at the center of the burner, and the sizes of the images produced both at the burner and the monochromator entrance slit were measured. For the fluorescence system, a front-surface mirror was placed at the focal point of L1, in place of the burner, to divert the light beam into the fluorescence portion of the system. Again, the sizes of both images were measured. The image sizes were measured by placing a screen at appropriate positions in the optical system and measuring the size of the images on the screen with calipers. Magnifications computed from the results of these measurements agreed to within 5%, indicating a high degree of similarity in the two optical trains. Any differences in throughput for the two lenses were considered in the calibration of the detector responses described below.

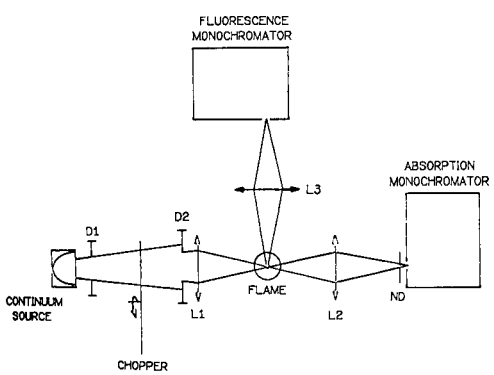

Fig. 1. Schematic diagram of the optical system used for determination of fluorescence power efficiencies. Details concerning the experimental components are in Table 1, and the apparatus is described in the text.

TABLE 1

Experimental components and conditions

Continuum source	300-W xenon arc lamp (Eimac or Cermax) with integral parabolic reflector; powered by a current-regulated power supply (No. VIX-300UV, Varian Eimac Division, San Carlos, CA; now available from ILC Technology, Sunnyvale, CA).
Chopper	480-Hz mechanical chopper (constructed in this laboratory) with associated lamp-phototransistor reference-signal generator.
Optics	L1, F.L. = 10.5 cm; L2 and L3, F.L. = 8.5 cm. All lenses are 3.8-cm diameter quartz. A 0.1% neutral-density filter, N.D. (Melles Griot, Danbury, Conn.) was placed at the entrance of the absorption monochromator. D_1 and D_2 are iris diaphragms (1.25- and 0.90-cm diameter, respectively).
Burner	Capillary burner with an inert gas sheath and interchangeable burner heads for the helium—oxygen—acetylene and air—acetylene mixtures (see text for further details).
Nebulizer	Impingement bead-type premix nebulizer chamber (Model No. 25958) with concentric pneumatic nebulizer (Model No. 20851-01, Instrumentation Laboratories, Inc., Lexington, MA).
Gas handling system	Described previously [1].
Gas flow rates	1.9 l min^{-1} acetylene used throughout. Air—acetylene flame: 10.8 l min^{-1} air with 5.0 l min^{-1} nitrogen sheath. Helium—oxygen—acetylene flame: 8.4 l min^{-1} helium, 2.4 l min^{-1} oxygen with 3.2 l min^{-1} helium sheath.
Monochromators	Absorption: digital step-scanning monochromator (Model EU-700) with associated controller (Model EU-700-32, GCA/McPherson Instrument, Acton, MA). Fluorescence: monochromator with programmable filter attachment (Model EU-700-55, GCA/McPherson Instrument, Acton, MA). Both monochromators are 0.35 m f/6.8 Czerny-Turner mounts with 48 × 48 mm gratings and reciprocal linear dispersion of 20 Å mm^{-1}.
Detectors	Absorption: RCA 1P28 photomultiplier was contained in a Model 50B housing (Pacific Photometric Instruments, Emeryville, CA) powered at —700 V with a high voltage supply (Model EU-42A, Heath Co., Benton Harbor, MI). Fluorescence: An R446 photomultiplier (Hamamatsu Corp., Middlesex, NJ) was contained in a Model 3150 housing (Pacific Photometric Instruments, Emeryville, CA) powered at —1000 V with a high voltage supply (Model 244, Keithley Instruments, Cleveland, OH).

TABLE 1 (continued)

Signal processing	The photocurrent was amplified (Model 427, Keithley Instruments, Cleveland, OH) and converted to a proportional voltage before being processed by a lock-in amplifier (Model 128, Princeton Applied Research Corp., Princeton, NJ).
Readout devices	The resulting signals could be observed with a strip-chart recorder (Model EU-205-11 with Model EU-200-01 potentiometric amplifier and Model EU-200-02 offset module, Heath-Schlumberger, Benton Harbor, MI) or an integrating digital voltmeter (Model 5326B, Hewlett-Packard, Palo Alto, CA).

Solutions. Stock solutions were prepared according to standard methods [8] with reagent-grade chemicals and distilled, deionized water. Successive dilutions yielded solutions in the proper concentration range for this study.

Determination of fluorescence power efficiency

Fluorescence power efficiencies for atoms in flames are equal to the ratio of the fluorescence intensity to the amount of radiation absorbed from the external excitation source [6, 9—13]. For a measurement system based on a monochromator and a continuum source, the following relationship for fluorescence power yields, Y_p, has been derived [9]

$$Y_p = (I_F/\Delta I_A)\,(W_A H_A/W_F H_F)\,(4\pi/\Omega)\,(A_F/A_S)\,(D_F/D_A) \qquad (1)$$

In Eqn. 1, I_F is the measured fluorescence signal; ΔI_A is the difference in signals recorded for the absorption measurement (i.e., the difference between the signals obtained with and without atoms present in the flame) after a correction for the transmission of the neutral density filter was applied; and W_A, H_A, W_F and H_F are the width and height of the entrance slits of the absorption and fluorescence monochromators, respectively. The solid angle of radiation incident on the absorption monochromator is given by Ω, whereas A_F denotes the illuminated area of the flame from which fluorescence is emitted and A_S is the illuminated area at the slit of the absorption monochromator. Corrections for differences in detector response and throughput of the optical system are denoted by D_A and D_F; the quantities $I_F D_F$ and $\Delta I_A D_A$ represent the corrected values of fluorescence and absorption intensity. Values for these parameters are listed in Table 2; their determination is described below.

Evaluation of experimental parameters. The entrance slit height of both monochromators (H_F and H_A) was kept constant at 5 mm. The ratio of the slit widths (W_A/W_F) was approximated by measuring the ratio of the spectral bandpasses of the monochromators at the slit-width settings used in the measurement of power efficiency.

The spectral bandpasses were measured by scanning over a hollow-cathode emission line and measuring the width at the half-peak-intensity point of the wavelength trace. Spectral bandpasses measured by this method agreed,

TABLE 2

Evaluated experimental constants for Eqn. 1

Parameter[a]	Value
H_F,H_A	5 mm
W_A/W_F	5.4
Ω	0.021 sterad
A_F	1.0 cm² air—acetylene flame 1.5 cm² He—O_2—C_2H_2 flame
A_S	0.48 cm²

[a]See text; subscripts A and F denote absorption and fluorescence, respectively.

to within 1%, with the ratio of peak area to peak intensity of the hollow-cathode wavelength scan. The spectral bandpasses of the absorption and fluorescence monochromators were found to be 0.16 and 0.87 nm, respectively, giving an approximate slit width ratio of 5.4. For this approximation to be valid, the reciprocal linear dispersion of the two similar monochromators must be identical, a condition which is probably met. Regardless, selection of the proper conditions for determination of the relative detector response will allow cancellation of this spectral bandpass factor in Eqn. 1 (see Appendix A).

The solid angle of radiation incident on the monochromator, Ω, was calculated as the ratio of the illuminated area of lens L2 to the square of its distance from the absorption monochromator slit. The present system was found to intercept 0.021 steradians of the fluorescence intensity, which is larger than the 0.019 steradian acceptance angle of the monochromator. An assumption made in the derivation of Eqn. 1 requires Ω to be larger than the monochromator acceptance angle; the present instrument meets this condition. The relative error in the solid angle determination is estimated to be 4%.

The area which is illuminated by the continuum source at the entrance slit of the absorption monochromator, A_S, is determined directly. With the Eimac arc lamp, a diffuse circular image of the arc is produced at the monochromator [14]. The 0.48 cm² illuminated area of this image was measured by placing a focussing screen in the plane of the monochromator entrance slits, and measuring the image size either photographically, or visually with calipers. Results of both methods agree to within 5%.

The area of fluorescence in the flame, A_F, can be approximated as the product of the flame width and the height of the image of the excitation source at the center of the flame [9]. The approximation, however, assumes that the light is collimated as it passes through the flame. For the system used in this study, the height of the images remains fairly constant throughout the width of the flame at 1.0 cm ± 0.1 cm. A slight increase in image height is observed near the flame edge. The widths of the sheathed air—

acetylene and helium—oxygen—acetylene flames were measured [2] to be 1.0 ± 0.1 cm and 1.5 ± 0.1 cm, respectively, at a height of 1 cm above the top of the primary reaction zone. Flame widths were determined by measuring the photographic image of a sodium-containing flame. The observation height (1 cm above the primary reaction zone) was selected on the basis of previous studies [2] with the same burner/nebulizer system, which measured the maximum atom concentration for several elements in that region of the flame.

To correct for differences in absorption and fluorescence detector response, the ratio of D_F to D_A was measured rather than the absolute sensitivity of each detector. In the calibration procedure, the responses for both the absorption and fluorescence detectors were measured when the output of a stable continuum source (the Eimac lamp) was directed into each of the monochromators. A front-surface mirror was placed at the focal point of lens L1 instead of the burner as shown in Fig. 1, and served to direct the continuum radiation into the fluorescence monochromator. This mirror was removed for the measurement of the absorption detector response. To avoid overloading the photomultiplier tubes, a 0.1% T neutral-density filter (see Table 1) was placed immediately after lens L1 instead of directly before the absorption monochromator.

The factor D_F/D_A in Eqn. 1 was calculated as the ratio of the responses of the fluorescence and absorption detectors. Separate factors were measured for the relative detector response at each of the wavelengths used in the power efficiency measurements. For each measurement, the monochromator entrance slit height and width were kept constant at the settings listed in Table 2. Appendix A describes in more detail the validity of this method.

Experimental procedure. To evaluate Eqn. 1, both fluorescence and absorption measurements must be made for each element being studied. The ratio of fluorescence intensity to absorbed continuum source radiation was evaluated by recording peak values for both the absorption and fluorescence signals at the wavelength of a particular transition for each element. To obtain these peak values, the monochromators were scanned over the wavelength region of the transition and stopped at the wavelength of maximum absorption or fluorescence. Multiple determinations of the fluorescence and absorption signals were then obtained. For the fluorescence measurements, it was found that no correction for scattered radiation was required.

In order to correct for self-absorption effects in the calculated power efficiency value [6, 12, 13], data were collected over a range of solution concentrations for all elements, and a power efficiency value was calculated for each analyte concentration. These concentration-dependent power efficiency values were then extrapolated to zero concentration to obtain the final reported power efficiencies.

Signal-to-noise studies. To assess the utility of the helium-diluted flame in both emission and fluorescence atomic spectrometry, signal-to-noise ratios

were studied for several elements. For atomic fluorescence, signal-to-noise ratios were measured in the helium–oxygen–acetylene and air–acetylene flames for 10 μg ml^{-1} solutions of six elements. This procedure was selected in order to compare the values for the helium-containing flame with those for the argon–oxygen–acetylene flame obtained with a similar method [4]. For all determinations, a nebulization rate of 2 ml min^{-1} and a 3-s time constant were used. The signal-to-noise ratio for zinc fluorescence was included in this study, although a power efficiency could not be measured for that element because of the low sensitivity of the absorption detector system at the 213.8-nm zinc resonance line.

For atomic emission, detection limits for six elements were determined in both the air–acetylene and helium–oxygen–acetylene flames, using previously described methods [15]. A 100-ms time constant and a 2 ml min^{-1} nebulization rate were used for both flames. No attempt was made to optimize conditions for the best detection limit values.

RESULTS AND DISCUSSION

Power efficiency measurements

Power efficiencies for five elements, obtained in both the air-acetylene and helium–oxygen–acetylene flames, are listed in Table 3. Because resonance transitions were used for all elements, these values also represent the quantum efficiencies for the transitions [16]. The average relative standard deviation for the values is 10%, most of which arises from variation in the fluorescence to absorption intensity ratio, possibly caused by nebulizer drift.

The increases in power efficiency observed here upon substitution of helium for nitrogen are similar to those reported by Jenkins [17] in studies on nitrogen-, helium- and argon-diluted oxygen–hydrogen flames. Ten-fold improvements in power efficiencies were also observed when argon was

TABLE 3

Fluorescence power efficiencies for the air–acetylene and helium–oxygen–acetylene flames

Element	Wavelength (nm)	Neutral density filter transmission (%T)[a]	Concentration range (μg ml^{-1})	Y_p[b]		
				Air–C_2H_2	He–O_2–C_2H_2	Ratio[c]
Fe	248.2	0.0269	100–500	0.31	0.71	2.3
Mg	285.2	0.117	2–30	0.13	0.38	2.9
Cu	324.7	0.170	30–100	0.049	0.14	2.9
Cr	357.9	0.186	300–600	0.061	0.35	5.7
Ca	422.7	0.355	10–75	0.19	0.67	3.5

[a]See Fig. 1. [b]The average relative standard deviation in the fluorescence power efficiencies, Y_p, were ±10%, obtained from three determinations. [c]The power efficiencies in He–O_2–C_2H_2 are ratioed to those in the air–acetylene flame.

substituted for nitrogen in a flame-sheathed hydrogen—oxygen—nitrogen flame [10]. This finding suggests that even further increases in power efficiency might be possible for the helium—oxygen—acetylene flame if a sheath flame were used instead of the inert-gas sheath used in the present study.

In Table 3, power efficiencies for the helium-diluted flame are ratioed to those obtained in the air—acetylene flame. Significantly, the ratio for chromium is higher than that for any other element tested. Johnson and Winefordner [4] noted a similar improvement in signal-to-noise ratio for chromium over that for iron, magnesium and copper when argon—oxygen—acetylene and air—acetylene flames were compared. The findings of the present study suggest that this improvement is caused by an increased fluorescence power efficiency, although an increased atom-formation efficiency (postulated by the previous workers) might also contribute to the improvement.

The increases in fluorescence power efficiency for the helium—oxygen—acetylene flame (cf. Table 3) suggest that sensitivity for different elements might be improved by using this flame. Sensitivity increases can be examined through use of a growth curve. Figure 2 shows growth curves for copper in the air—acetylene and helium—oxygen—acetylene flames. The increased fluorescence produced in the helium-diluted flame can be attributed directly to improved power efficiency, because it is known that free-atom fractions of copper are approximately the same in both flames [2].

In order to illustrate the utility of, and lend credence to, the values of power efficiency in Table 3, the power efficiencies were used to calculate previously unavailable quenching cross-sections between nitrogen and the five elements that were studied. These cross-sections were calculated from the power efficiencies and the computed burnt-gas composition of the air—acetylene and helium—oxygen—acetylene flames. The burnt-gas composition of the air—acetylene flame was described earlier [18, 19] and that for the helium—oxygen—acetylene flame was recently determined and compared with the air—acetylene flame [20]. Both sets of values are listed in Table 4.

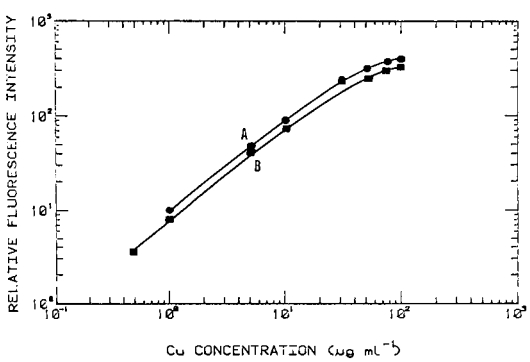

Fig. 2. Fluorescence growth curves for copper (324.7 nm): (A) helium—oxygen—acetylene flame; (B) air—acetylene flame.

TABLE 4

Calculated burnt-gas compositions for the air—C_2H_2 and He—O_2—C_2H_2 flames

Burnt-gas component	Partial pressures (atm.) in different flames			
	He—O_2—C_2H_2[a] 2735 K	Air—C_2H_2[a] 2475 K	Air—C_2H_2[b] 2523 K	Air—C_2H_2[c] 2421 K
N_2	—	0.726	0.73	0.622
He	0.705	—	—	—
CO_2	0.097	0.120	0.12	0.053
H_2O	0.068	0.078	0.07	0.097
CO	0.073	0.055	0.04	0.171
H_2	0.007	0.006	0.00	0.052
O_2	0.024	0.005	0.02	—
OH	0.014	0.005	0.01	0.001
NO	—	0.003	0.01	0.000
H	0.006	0.002	0.00	0.004
O	0.007	0.001	0.00	0.000

[a]From [20]. [b]From [18]. [c]From [19], given as mole-fraction not partial pressure.

For a particular element in a given flame, the power efficiency (Y_p), burnt-gas composition and quenching cross-sections caused by each species (σ_i) are related by

$$Y_p = B/(1 + \tau_0 \sum_i N_i \bar{g}_i \sigma_i) \tag{2}$$

where B is the branching ratio of the transition, τ_0 is its radiative lifetime, i designates the quenching species in the flame (see Table 4), N_i is the number density of i (see Eqn. (3)), $\bar{g}_i$ is the average relative velocity of i (see Eqn. 4) and σ_i is the quenching cross-section of i, defined as πr_i^2 where r_i is the distance between centers of colliding species. The number density is

$$N_i = P_i/kT(1000) \tag{3}$$

in which P_i is the partial pressure of i, k is the Boltzmann constant, and T is flame temperature (K). The average relative velocity is given by

$$\bar{g}_i = (8RT/\pi u_i)^{1/2} \tag{4}$$

in which R is the gas constant and u_i is the reduced mass of quenching species i and the analyte.

In order to calculate the quenching cross-section between nitrogen (σ_{N_2}) and selected elements, three assumptions were made. The first assumption is that the contribution to quenching by He, H_2, OH, O_2, NO, H and O is negligible in both air—acetylene and helium—oxygen—acetylene flames. This assumption is based on the low partial pressure of all these gases except helium, and the low quenching cross-section of monatomic gases. The second assumption is that the quenching cross-sections attributable to carbon dioxide, water and carbon monoxide are collectively equal to $\bar{\sigma}$, where $\bar{\sigma}$ is

defined as the average quenching cross-section weighted for number density. The third assumption is that $\bar{\sigma}$ has the same value in the air—acetylene and helium—oxygen—acetylene flames, despite their temperature difference.

When these three assumptions are applied to Eqn. 2 for the helium—oxygen—acetylene flame, the equation obtained is

$$\bar{\sigma} = [(B/Y_{He}) - 1]/[\tau_0 (n_{CO_2} \bar{g}_{CO_2} + n_{H_2O} \bar{g}_{H_2O} + n_{CO} \bar{g}_{CO})] \quad (5)$$

where Y_{He} is the power efficiency of the particular element in this flame.

Similarly, when the assumptions are applied to Eqn. 2 for the air—acetylene flame,

$$\sigma_{N_2} = \{[(B/Y_{air}) - 1]/\tau_0 - \bar{\sigma} (n_{CO_2} \bar{g}_{CO_2} + n_{H_2O} \bar{g}_{H_2O} + n_{CO} \bar{g}_{CO})\}/n_{N_2} \bar{g}_{N_2} \quad (6)$$

where Y_{air} is the power efficiency of the chosen element in this flame. From Eqn. 5 and the composition and power-efficiency data for the helium—oxygen—acetylene flame, the "average" quenching cross section ($\bar{\sigma}$) of carbon dioxide, water and carbon monoxide was computed for each element. These $\bar{\sigma}$ values were then inserted into Eqn. 6 to produce the nitrogen quenching cross-section (σ_{N_2}) for each element. These cross-sections are listed in Table 5.

The quenching cross-sections of nitrogen for the five elements listed in Table 5 are of the same order of magnitude as those reported for other elements [29]. For copper, a σ_{N_2} value of 19 Å was reported by Bleekrode and Van Benthem [28]. However, their measurement was on copper vapor produced by a small oven containing copper. Presumably, the temperature of this vapor was well below that of the flame used in the present study; it is therefore not unexpected that their value for σ_{N_2} is smaller than the 48 Å^2 obtained here.

Unfortunately, quenching cross-sections between nitrogen and Fe, Mg,

TABLE 5

Calculated quenching cross-sections for five elements in air—C_2H_2 and He—O_2—C_2H_2 flames

Element	B[a]	τ_0[b]	Calculated $\bar{\sigma}$[c] (Å^2)	Calculated σ_{N_2}[d] (Å^2)
Fe (248.3 nm)	0.804 [21]	2.6 [23]	4.5	15
Mg (285.2 nm)	1.00	2.03 [24]	60	55.5
Cu (324.7 nm)	0.985 [22]	7.24 [25]	70	48[e]
Cr (357.9 nm)	1.00	6.51 [26]	25	56
Ca (422.7 nm)	1.00	4.45 [27]	9.3	22

[a] Branching ratio with reference in brackets. [b] Radiative lifetime with reference in brackets. [c] $\bar{\sigma}$ is the number-density-weighted average quenching cross-section. [d] The nitrogen quenching cross-section. [e] A value of 19 has been reported [28].

Cr and Ca have not, to our knowledge, been reported. Nonetheless, the agreement between the values for copper argues for the validity of the power efficiency values calculated here.

Fluorescence intensity measurements

In the measurements represented by Fig. 2, the same nebulizer was used for both the helium—oxygen- and air-fed flames. Unfortunately, the nebulizer was optimized for use of air, and further improvements should be realizable through redesign of the nebulizer. In fact, previous studies have shown that the nebulization efficiency for the present experimental system is 16.5% for an air—acetylene flame, but only 9.9% for the helium—oxygen—acetylene flame [2]. This reduced efficiency results in 40% less sample being introduced into the helium-diluted flame. This fact, coupled with the larger dilution of the atomic species in the increased flame volume of the helium—oxygen—acetylene flame, further underscores the sensitivity of that atom reservoir.

Signal-to-noise comparisons

Despite the increased fluorescence intensity produced by the helium-diluted flame, atomic fluorescence signal-to-noise ratios are no better than those produced by an air-supported flame. Table 6 compares signal-to-noise ratios for the helium—oxygen—acetylene, argon—oxygen—acetylene, and air—acetylene flames. Apparently, an increase in noise and a decrease in nebulization efficiency in the helium-diluted flame outweigh the signal gains. As a result, a poorer signal-to-noise ratio is found for this flame, relative to an air—acetylene flame. The argon—oxygen—acetylene flame of similar inert gas/oxygen ratio exhibits the same type of behavior [4].

The reduced signal-to-noise ratio obtained from the helium—oxygen—acetylene flame (cf. Table 6) can be attributed to increased flame emission which in turn results from the higher flame temperature. Johnson and

TABLE 6

Signal-to-noise ratio comparison between air—C_2H_2, He—O_2—C_2H_2 and Ar—O_2—C_2H_2 flames

Element	$(S/N)^a_{He}/(S/N)_{air}$	$(S/N)_{Ar}/(S/N)^b_{air}$
Zn	0.28	0.71
Fe	0.11	0.60
Mg	0.34	0.55
Cu	0.43	0.40
Cr	0.46	1.4
Ca	1.85	—

[a]Subscripts: He refers to the He—O_2—C_2H_2 flame; air denotes the air—C_2H_2 flame; and Ar indicates the Ar—O_2—C_2H_2 flame. [b]From [4]. The Ar/O_2 ratio for these measurements was similar to the He/O_2 ratio employed in the present work.

Winefordner [4] improved signal-to-noise ratios in the argon—oxygen—acetylene flame by increasing the inert gas/oxygen ratio, which produced a lower flame temperature. Similar results would be expected for the helium-diluted flame, but were not verified here.

Flame emission detection limits

Although the increased temperature of the helium—oxygen—acetylene flame is a detriment to signal-to-noise ratios for fluorescence measurements, it is advantageous in flame emission. Flame emission detection limits, shown in Table 7, verify this expectation. Moreover, the increased fluorescence power efficiency in the helium-fortified flame contributes to the improved emission sensitivity by decreasing the fraction of the excited state atoms that are quenched.

In Tables 6 and 7, calcium is notable as the element for which the detection limit is decreased in both fluorescence and emission measurements. This improved detection can be attributed entirely to the enhanced production of calcium atoms in the helium-diluted flame [2].

The improvements in emission detection limits for the helium-diluted flame listed in Table 5 correspond closely to increases in atomization efficiency by that flame [2]. This atom-formation efficiency is in the general order Ca > Ba > Sr > Cr > Fe > Cu. The same pattern is found in the emission detection limit study, except that iron and chromium are switched in the order, because of increased noise at the wavelength of iron emission selected here.

The foregoing evaluation indicates that the instrumental system used in this study is hardly optimal for exploiting fully the analytical capabilities of the helium—oxygen—acetylene flame. A number of improvements are being investigated in this laboratory. For example, changing the nebulization device to yield equal sample delivery rates for all flame-gas mixtures would allow a clearer appraisal of the helium-diluted flame. In addition, the incorporation of a sheath-flame in place of the inert gas sheath might increase the fluorescence power efficiency. Nevertheless, the enhanced capabilities of the helium—oxygen—acetylene flame demonstrate that further investigation of this atom cell for atomic spectrometry is merited.

TABLE 7

Flame emission detection limits

Element	Wavelength (nm)	Detection limit ($\mu g\ ml^{-1}$)		
		Air—C_2H_2	He—O_2—C_2H_2	Ratio
Cu	324.7	7.21	1.87	3.86
Fe	372.0	22.7	7.74	2.93
Mn	403.1	2.95	1.12	2.63
Ca	422.7	0.85	0.079	10.71
Cr	425.4	4.00	0.91	4.40
Sr	460.7	0.74	0.086	8.62

This work was supported in part by the National Science Foundation through grant CHE 83-14121 and by the Office of Naval Research.

APPENDIX A

Determination of the relative detector response factor for the power efficiency measurements in atomic fluorescence.

In the instrumental system for the measurement of atomic fluorescence power efficiencies, two monochromator/photomultiplier combinations were used to measure the intensity of radiant signals. Reference to the above text shows that one detection combination was used in the measurement of fluorescence emitted by atoms in the flame, whereas the other combination was used to measure energy absorbed by the atom cell. For the calculation of the atomic fluorescence power efficiency, the ratio of fluorescence radiance to absorbed radiance must be known, requiring a knowledge of the relative responses of the detection combinations.

Generally, the response, R, obtained from a detector placed at the exit slit of a monochromator when a continuum source of spectral radiance $B(\lambda)$ in watts cm^{-2} sr^{-1} nm^{-1} is incident upon the entrance slit is given [30] by

$$R = d\,B(\lambda)\,\tau WH\Omega S \tag{A-1}$$

where d is the detector response factor which indicates the output current level per watt of radiant power incident on the device, W and H are the width and height of the monochromator entrance slit in cm; S is the spectral bandpass (in nm) for the selected slit width. The throughput of the monochromator is represented by τ, and the acceptance solid angle of the monochromator is Ω (in steradians). The equation assumes that the source radiation completely fills the monochromator acceptance volume. If any external optics are incorporated into the system, τ will represent the combined throughput of both those optics and the monochromator.

When atomic fluorescence radiation is incident on the monochromator, the resulting detector response is given by

$$I_F = d_F P_F\,\tau_F W_F H_F \Omega_F \tag{A-2}$$

where P_F is the radiance of fluorescence in watts cm^{-2} sr^{-1}. Similarly, an absorption signal can be expressed as

$$\Delta I_A = d_A \Delta P_A \tau_A W_A H_A \Omega_A \tag{A-3}$$

where ΔP_A is the radiance which is absorbed.

In the equation used to calculate fluorescence power efficiencies (Eqn. 1), the term $I_F/\Delta I_A$ appears, representing the ratio of the fluorescence to absorption signals from the photomultiplier. To correct for the response of the detection system, the correction factor D_F/D_A was applied such that

$$(I_F/\Delta I_A)\,(D_F/D_A) = (P_F/\Delta P_A) \tag{A-4}$$

From the above treatment, it can be shown that

$$D_F/D_A = d_A \tau_A W_A H_A \Omega_A / d_F \tau_F W_F H_F \Omega_F \tag{A-5}$$

To evaluate this system response factor, the monochromator and optical system specifications must be measured, in addition to the detector response factors, d_A and d_F.

Rather than evaluate each parameter in Eqn. A-5, the combined effect of all the parameters was determined. The output of a continuum source was directed onto the entrance slits of both the fluorescence and absorption monochromators. The ratio of the detector responses thus measured can be expressed by using Eqn. A-1 to obtain

$$R_F/R_A = d_F\,\tau'_F\,W'_F\,H'_F\,\Omega'_F\,S'_F/d_A\,\tau'_A\,W'_A\,H'_A\,\Omega'_A\,S'_A \quad \text{(A-6)}$$

where the primes designate the quantities used in the calibration procedure rather than the absorption or fluorescence signal detection experiment. If the same experimental conditions are used for both experiments, combination of Eqns. A-5 and A-6 yields

$$D_F/D_A = R_A S_F/R_F S_A \quad \text{(A-7)}$$

The equation for the calculation of the power efficiency (Eqn. 1) then becomes

$$Y_p = (I_F/\Delta I_A)\,(W_A H_A/W_F H_F)\,(4\pi/\Omega)\,(A_F/A_S)\,(R_A S_F/R_F S_A) \quad \text{(A-8)}$$

The spectral slit width, S, is known to be equal to the product of the reciprocal linear dispersion of the monochromator, r, and the slit width, W, thus Eqn. A-8 becomes

$$Y_p = (I_F/\Delta I_A)\,(H_A/H_F)\,(4\pi/\Omega)\,(A_F/A_S)\,(R_A r_F/R_F r_A) \quad \text{(A-9)}$$

Because two similar monochromators were used here, the reciprocal linear dispersions can safely be assumed to be equal. Also, the slit height for both monochromators was the same, leaving Eqn. A-9 as

$$Y_p = (I_F/\Delta I_A)\,(4\pi/\Omega)\,(A_F/A_S)\,(R_A/R_F) \quad \text{(A-10)}$$

REFERENCES

1 K. A. Saturday and G. M. Hieftje, Anal. Chem., 49 (1977) 2015.
2 K. A. Saturday and G. M. Hieftje, Anal. Chem., 52 (1980) 786.
3 R. F. Browner, The Analyst (London), 99 (1974) 617.
4 D. J. Johnson and J. D. Winefordner, Anal. Chem., 48 (1976) 341.
5 N. C. Clampitt and G. M. Hieftje, Anal. Chem., 46 (1974) 382.
6 D. R. Jenkins, Proc. R. Soc., Ser. A., 293 (1966) 493; 303 (1968) 453; 303 (1968) 467; 306 (1968) 413.
7 K. M. Aldous, R. F. Browner, R. M. Dagnall and T. S. West, Anal. Chem., 42 (1970) 939.
8 J. A. Dean and T. C. Rains, in J. A. Dean and T. C. Rains, (Eds.), Flame Emission and Atomic Absorption Spectrometry, Vol. 2, M. Dekker, New York, 1971, Ch. 13.
9 S. J. Pearce, L. de Galan and J. D. Winefordner, Spectrochim. Acta, Part B, 23 (1968) 793.
10 H. P. Hooymayers and C. Th. J. Alkemade, J. Quant. Spectrosc. Radiat. Transfer, 6 (1966) 847.
11 H. P. Hooymayers and G. Nienhuis, J. Quant. Spectrosc. Radiat. Transfer, 8 (1968) 955.
12 H. P. Hooymayers and P. L. Lijnse, J. Quant. Spectrosc. Radiat. Transfer, 9 (1969) 995.
13 P. J. Th. Zeegers and J. D. Winefordner, Spectrochim. Acta, Part B, 26 (1971) 161.
14 R. L. Cochran and G. M. Hieftje, Anal. Chem., 49 (1977) 2040.
15 P. A. St. John, W. J. McCarthy and J. D. Winefordner, Anal. Chem., 39 (1967) 1495.
16 W. J. McCarthy, M. L. Parsons and J. D. Winefordner, Spectrochim. Acta, Part B, 23 (1967) 25.
17 D. R. Jenkins, Spectrochim. Acta, Part B, 25 (1970) 47.
18 A. G. Gaydon and H. G. Wolfhard, Flames, Wiley, New York, 1979.
19 B. V. L'vov, L. P. Kruglikova, L. K. Polzik and D. A. Katskov, J. Anal. Chem. USSR, 30(5) (1975) 715.
20 A. Yuen and G. M. Hieftje, Anal. Chim. Acta, 162 (1984) 403.
21 C. H. Corliss and J. L. Tech, NBS Monograph 108, U.S. Government Printing Office, 1968.
22 P. Hannaford and D. C. McDonald, J. Phys. B., 11(7) (1978) 1177.
23 G. E. Assousa and W. H. Smith, Astrophys. J., 176 (1972) 259.

24 W. W. Smith and A. Gallagher, Phys. Rev., 145(1) (1966) 26.
25 H. Krellmann, E. Siefart and E. Weihreter, J. Phys. B., 8(16) (1975) 2608.
26 H. Bucha, B. Budick, R. J. Goshen and S. Marcus, Phys. Rev., 144(1) (1966) 96.
27 E. Gibbs and P. Hannaford, J. Phys. B., 9(9) (1976) L225.
28 R. Bleekrode and W. Van Benthem, J. Chem. Phys., 51 (1969) 2752.
29 C. Th. Alkemade, Tj. Hollander, W. Snelleman and P. J. Th. Zeegers, Metal Vapours in Flames, Ch. 6, Pergamon Press, New York, 1982.
30 H. T. Betz and G. L. Johnson, in Analytical Emission Spectroscopy, Part 1, Ch. 5, M. Dekker, New York, 1971.

Analytica Chimica Acta, 164 (1984) 67—76
Elsevier Science Publishers B.V., Amsterdam — Printed in The Netherlands

DETERMINATION OF CHROMIUM IN HUMAN SERUM BY ELECTROTHERMAL ATOMIC ABSORPTION SPECTROMETRY

CLAUDE VEILLON*, K. Y. PATTERSON and N. A. BRYDEN

U.S. Department of Agriculture, Beltsville Human Nutrition Research Center, Vitamin and Mineral Nutrition Laboratory, Building 307, Room 215, Beltsville, MD 20705 (U.S.A.)

(Received 5th April 1984)

SUMMARY

An accurate and sensitive method for serum chromium determinations by graphite-furnace atomic absorption spectrometry is described. Samples containing a small amount of magnesium nitrate as an ashing aid/matrix modifier are lyophilized and dry-ashed in silanized quartz tubes; the residue is dissolved in 0.1 M HCl. Because of the very low levels of chromium in serum, strict contamination control measures must be used throughout the procedures for collection, storage, preparation and quantitation. Standard curves are prepared by using a bovine serum pool, which also serves as a quality control measure. The uniform nature of sera obviates the need to use the method of standard additions. The detection limit of the method is about 0.03 ng ml^{-1} Cr and the accuracy of the method is evaluated by comparison with stable-isotope-dilution mass spectrometry.

Chromium has been known to be an essential trace nutrient for many years [1]. It is believed to be involved in glucose metabolism or in the function of the pancreatic hormone insulin. Its role in one type of impaired glucose tolerance was dramatically demonstrated in a supplementation experiment by Jeejeebhoy et al. [2]. Borel and Anderson [3] have extensively reviewed the biochemistry of chromium.

The determination of chromium in biological materials like serum and urine is a formidable task, primarily because of the very low levels present and the large amounts of organic and inorganic matter in the samples. These lead to problems associated with sample contamination and interferences by sample matrix components. Only three techniques have demonstrated sufficient sensitivity for determining chromium in biological fluids below the ng ml^{-1} level. These are graphite-furnace atomic absorption spectrometry (a.a.s.), neutron activation (n.a.a.) and stable isotope dilution mass spectrometry (i.d.m.s.). The most readily accessible and widely used of these, graphite-furnace a.a.s, has contributed most of the literature data on this subject. It is also the technique most susceptible to matrix interference effects.

Prior to 1978, reported values for urinary and serum chromium varied by more than an order of magnitude. Guthrie et al., [4] demonstrated con-

0003-2670/84/$03.00

clusively that graphite-furnace a.a.s. instruments in use up to that time were simply measuring background absorption of urinary components, suggesting that all previously reported urinary chromium values obtained by this method were probably wrong. The problem was insufficient intensity of the deuterium lamp background correctors at the wavelength used to measure chromium. Improved instrumentation with more intense background corrector lamps [5] or wavelength-modulation [6] overcame this problem, and unsupplemented urinary chromium values obtained with adequate instrumentation since that time have stabilized at levels well below 1 ng ml^{-1} and typically below 0.3 ng ml^{-1}.

The situation with reported serum chromium levels was much the same. Determining serum chromium levels is somewhat more difficult in that greater care is necessary in collecting the sample without contamination, and the large amount of organic matter generally precludes placing aliquots directly into the graphite furnace. Using n.a.a. and stringent measures of contamination control and sample preparation, Versieck et al. [7] found a mean serum chromium value of 0.16 ng ml^{-1} with a standard deviation of ± 0.08 ng ml^{-1} for 14 subjects. This was some 1—2 orders of magnitude lower than values previously reported in the literature. Kayne et al. [5] used acid digestion in sealed quartz tubes with ultra-high-purity nitric acid and 30% hydrogen peroxide to prepare serum samples for graphite-furnace a.a.s. Their instrument was modified to increase its background correction capabilities. For eight subjects, they observed a mean serum chromium value of 0.14 ng ml^{-1}, in good agreement with that of Versieck et al. [7].

This paper describes a graphite-furnace a.a.s. method for the determination of chromium in serum on a routine basis; commercially available instrumentation is used. Samples are collected, dried, ashed and dissolved under carefully controlled conditions aimed at minimizing contamination. Values obtained by this method are compared to those obtained by i.d.m.s. [8].

EXPERIMENTAL

Reagents

All water used for rinsing, diluting, etc. was prepared by deionization and contained no detectable chromium. For the i.d.m.s. measurements, chromium was chelated with trifluoroacetylacetone (TFA; 1,1,1-trifluoro-2,4-pentanedione). The commercial product (Alfa Products, Danvers, MA) was purified by low-temperature vacuum distillation in a closed system as shown in Fig. 1. The apparatus was constructed of borosilicate glass and operated in the following way. The threaded teflon plunger of the valve (a) sealed with an O-ring, is removed and crude TFA is placed in reservoir (c). The valve plunger is replaced and the entire system is evacuated through port (b). (It is important to have a cold trap between port (b) and the vacuum pump because some TFA enters the high vacuum line during evacuation of the system.) Valve (a) is then closed and reservoir (f) is submerged partway in a

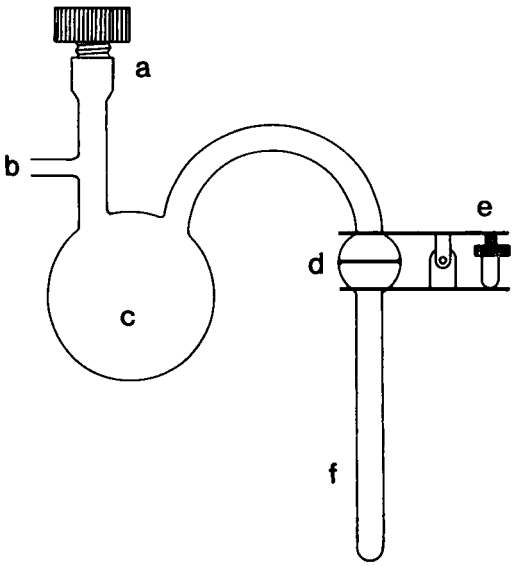

Fig. 1. Schematic diagram of apparatus used to purify TFA by low-temperature vacuum distillation; (a—f) see text.

—60°C bath (Cryocool cc-60, Neslab, Portsmouth, NH) which also serves to cool the cold trap. The TFA then is vacuum-distilled into reservoir (f) while that in reservoir (c) drops in temperature because of evaporation. Before reservoir (c) is empty, the system (i.e., reservoir f) is removed from the cold bath and allowed to warm to room temperature. Clamp (e) is removed and the O-ring-sealed joint (d) is opened to remove the distillate. The product was stored in a polypropylene bottle at —20°C and allowed to warm to room temperature as needed. When TFA was distilled at atmospheric pressure (b.p. 107°C), reagent blanks below 0.2 ng Cr from 0.1 ml of TFA could not be obtained, presumably because of the vapor pressure of $Cr(TFA)_3$ at that temperature. Low-temperature distillation as described above yielded reagent blanks of 0.05 ng Cr. The actual TFA blank contribution is probably much less than this because the 0.05 ng represents the total blank in the i.d.m.s. procedure.

In the i.d.m.s. procedure, 1 M ammonium acetate buffer at pH 5.6 was used to dissolve the ashed sample prior to chelation with TFA. This buffer was prepared in extremely high purity by neutralizing acetic acid prepared by isothermal distillation [9] with ammonia solution prepared from gaseous ammonia and water.

The a.a.s. procedure involved dissolving the ashed samples in 0.1 M HCl which was prepared from more concentrated hydrochloric acid also prepared by isothermal distillation [9]. Magnesium nitrate was used as a matrix modifier/ashing aid and was prepared from high-purity magnesium nitrate (Johnson Matthey Chemicals, Royston, Herts., England). Chromium standard

solutions were prepared from a stock solution prepared by dissolving elemental chromium in hydrochloric acid and subsequent dilution with 0.1 M HCl. For radiotracer studies, ^{51}Cr as chromium(III) chloride (New England Nuclear, Boston, MA) was diluted to the desired count rate with 0.1 M HCl. Quartz tubes used for ashing were silanized with 5% dichlorodimethylsilane (DCDMS; Pierce Chemical, Rockford, IL) in toluene followed by sequential methanol and water rinses.

Instrumentation

Serum chromium determinations were done with a commercially available atomic absorption spectrometer (Model 5000; Perkin-Elmer, Norwalk, CT) which was equipped with a tungsten-halogen lamp for enhanced background correction capabilities at the 357.9-nm chromium line. The instrument was equipped with a graphite furnace (Model HGA 500, Perkin-Elmer), autosampler (Model AS40, Perkin-Elmer) and a strip-chart recorder (Model 56, Perkin-Elmer). All determinations were done with argon as the furnace gas and pyrolytically-coated furnace tubes. Atomization was from the tube wall and calibration was based on peak height. The chromium hollow-cathode lamp (Model 303-6021, Perkin-Elmer) was operated at a current of 25 mA, and the "low" slit height was used at a spectral bandpass of 0.7 nm. The furnace program is shown in Table 1.

Values obtained by graphite-furnace a.a.s. were compared to those obtained by i.d.m.s. The latter utilized a quadrupole mass spectrometer (Model 4000; Finnigan Corp., San Jose, CA) coupled to a gas chromatograph (Model 9610, Finnigan Corp.) and equipped with programmable multiple ion monitoring and a multichannel recorder. The remainder of the g.c./m.s. instrumentation, the procedure, apparatus, and reagents have been described in detail elsewhere [8].

Apparatus

Sera were collected in all-plastic syringes (Safety-Monovette; Sarstedt, Princeton, NJ) which were free of detectable chromium when soaked with water or serum. Needles for venipuncture proved challenging because most are made of stainless steel. Satisfactory needles are the "butterfly" type, a

TABLE 1

Furnace program for serum chromium determinations

Mode	Step	Temperature (°C)	Ramp time (s)	Hold time (s)	Comments
Dry	1	100	15	20	
Dry	2	140	10	20	
Char	3	1350	15	30	Recorder on at 9 s
Atomize	4	2700	0	4	Internal flow 50 ml min^{-1}
Clean	5	2700	1	4	

short, siliconized needle attached to a length of small-bore poly(vinyl chloride) tubing (Minicath; Deseret Medical, Sandy, UT). Apparently the siliconizing process imparts sufficient hydrophobicity to the needle to prevent serum contact with the metallic surface. A single low-chromium serum sample can be repeatedly drawn through several of these needles in succession with no detectable increase in the chromium content.

One feature of the syringes used is that the plunger handle is removable, allowing the samples to be centrifuged without transfer to another container. After centrifugation, the serum was carefully removed with a sterile polystyrene pipette and aliquots were stored in sterile polypropylene tubes (2063; Falcon, Cockeysville, MD) at −20°C.

Samples were ashed in quartz test tubes (10 mm-bore, 100-mm length) fabricated with quartz tubing (Vitreosil; Thermal American Fused Quartz, Montville, NJ). The tubing was first cleaned by soaking in 3% hydrofluoric acid followed by several water rinses and allowed to air-dry prior to fabrication into tubes by standard glass-blowing techniques, taking precautions not to contaminate the surface by touching with bare hands, placing on unclean surfaces, etc. After fabrication, the tubes were again cleaned with the hydrofluoric acid solution and thoroughly rinsed with water. Before use, the tubes were immersed in a 10% nitric acid bath at about 100° C overnight and soaked in this bath at room temperature for one week. All of the following operations were done in a Class-100 clean room. The tubes were thoroughly rinsed with water, drained and dried by lyophilization (see below).

The dry tubes were silanized by filling with 5% (v/v) dichlorodimethylsilane (DCDMS) in toluene. The DCDMS solution was then discarded (not reused) and the tubes were rinsed once with methanol followed by six water rinses. Serum samples (1—2 ml typically) were then weighed into the tubes; magnesium nitrate was added (10 μl of a 0.186 g ml^{-1} solution of $Mg(NO_3)_2 \cdot 6H_2O$ in water per ml of serum). For i.d.m.s. studies, a spike of enriched ^{50}Cr was added at this point. An equal volume of water was used as a blank and was treated in the same manner as the samples. Samples and blanks were then frozen at −20° C prior to lyophilization.

The lyophilization apparatus was of a special design free of stainless steel parts. The main unit consisted of a commercially available corrosion-resistant freeze dryer (Model FD-6-84-VP; FTS Systems, Stone Ridge, NY). The condenser chamber was of polypropylene; the condenser coils were of titanium and were cooled to −84°C by a cascade refrigeration system. An acrylic base plate (25 mm thick) was connected to the condenser chamber via a solvent-welded acrylic tube (several millimeter thick and of appropriate diameter and length to fit the condenser chamber opening). A porcelain desiccator plate with raised legs covered the opening in the base plate to prevent sample containers from blocking the opening. A Viton rubber ring was placed on the base plate as a seal, onto which was inverted a polycarbonate bell jar (5300-1212; Nalge Co., Rochester, NY; Nalge now recom-

mends 5305-1212 in polyetherimide for this service) to form the drying chamber. Tubes with frozen samples were placed in polyethylene racks and dried overnight. The lyophilizer was equipped with a solenoid valve to vent the system to atmospheric pressure through the condenser chamber. To minimize air currents during venting, a flow restrictor consisting of a short length of capillary glass tubing was attached to the intake of the solenoid valve, resulting in a venting time of about 15 min to reach atmospheric pressure. Air vented through the capillary was filtered through a 0.2-μm pore size pleated filter (Gelman Sciences, Ann Arbor, MI).

The quartz tubes containing the dried samples and blanks were placed in groups under inverted quartz beakers resting on flat quartz plates and placed in the furnace for ashing. The muffle furnace (51894; Lindberg, Watertown, WI) has a chamber molded from a light-weight ceramic material of low thermal mass for rapid cooling. More importantly, the heating elements are completely embedded within this material to reduce the possibility of airborne contamination. This was further controlled by operating the furnace completely within a Class-100 clean area. The dried samples were heated at 100°C initially for 1 h, and the temperature was raised 50°C each hour until 250°C was reached. After an hour at 250°C, the furnace controller was set to 480°C for an overnight ash. The furnace was on a timer which shut it off 2—3 h before the workday began, allowing the ashed samples to be removed quickly.

Samples

To investigate the various stages of sample preparation and quantitation, animal serum was endogenously labeled with ^{51}Cr. Adult male CD Sprague-Dawley rats were injected intraperitoneally with 1—2 mCi of ^{51}Cr and their sera were collected after equilibration for several days. Normal rat serum was also labeled with exogenous ^{51}Cr for comparative purposes.

A large pool of bovine serum was collected with particular attention given to minimizing contamination by adventitious trace elements, as described in detail elsewhere [10]. The chromium content of this homogeneous material was carefully characterized by both a.a.s. and i.d.m.s. It also served both as a quality control measure and as a matrix with which to prepare calibration curves for routine determinations of chromium in human sera.

Human blood samples were collected by venipuncture, and the sera were isolated and stored as described above.

Procedures

All manipulations are done in Class-100 clean areas. The numerous details of the procedure are described in the following sections. It is important to note that serious attention must be given to all of these details for successful determinations.

The procedure for chromium in sera by a.a.s. is summarized as follows. Serum samples, typically 1—2 ml, are weighed into the silanized quartz

tubes; magnesium nitrate is added and the samples are frozen at −20°C. Samples are lyophilized overnight and then ashed at a final temperature of 480°C. The ash is dissolved in 0.1 M HCl, 25-μl aliquots are pipetted into the graphite furnace tube, and the furnace program (Table 1) is initiated.

Determinations by i.d.m.s. follow the same general procedure except that a known quantity of enriched ^{50}Cr is added in the first step and the ash is dissolved in ammonium acetate buffer and subsequently chelated with the TFA.

Because of the high degree of uniformity among individual serum samples, the method of standard additions is not required. Instead, calibration curves are prepared from the bovine serum pool to which known amounts of chromium have been added. Because of the rather viscous nature of sera, samples were weighed rather than pipetted for best accuracy and reproducibility. Conversion to volume was made from the specific weight of serum, namely, 1.026 g ml^{-1}, which is the same for both bovine and human sera.

RESULTS AND DISCUSSION

It was reported earlier [11] that a considerable amount of urinary chromium was irreversibly retained in graphite furnace tubes during atomization. This was subsequently shown [12] to be due in part to furnace design and tube material, and is largely overcome by modern instrumentation and pyrolytically-coated graphite furnace tubes. To investigate the same phenomenon for sera, rat serum, endogenously labeled with ^{51}Cr, was taken through the procedure and aliquots were placed in furnace tubes and processed through the furnace program. Tubes were then cut into segments and radioactivity was counted in a γ-spectrometer [11]. The small amount of remaining radioactivity (3—7%) was concentrated in the 2--3 mm near the tube ends.

It was shown earlier [11] that urinary chromium losses began to occur during the "char" cycle of the graphite furnace at temperatures above 1200—1300°C. This was investigated for serum using rat serum endogenously labeled with ^{51}Cr both with and without the magnesium nitrate matrix modifier. Radiolabeled samples were ashed and dissolved, and 25-μl aliquots were placed in individual furnace tubes. The tubes were then heated through steps 1 and 2 of the furnace program (Table 1) to dry the samples. The radioactivity was counted and the tubes were returned to the furnace, and heated to various charring temperatures. Radioactivity was counted again and any chromium losses were calculated. The results are shown in Fig. 2. Losses of serum chromium occur at charring temperatures above about 1200°C, as was the case with urine samples [12]. When magnesium nitrate was added to the samples, losses did not begin until charring temperatures exceeded about 1500°C. The higher charring temperatures possible with the magnesium nitrate modifier enable most of the sample matrix salts which contribute to the background absorption to be removed during the char step.

Next, the dry-ashing procedure in a muffle furnace was investigated. Rat sera both endogenously and exogenously labeled with ^{51}Cr were placed in quartz tubes and radioactivity was counted before and after lyophilization and after dry ashing. No losses of either type of radiotracer were detected in any step. However, when water blanks were investigated in the same manner with carrier-free $^{51}CrCl_3$, a rather serious problem was observed. After lyophilization, all of the tracer remained in the tube, as before. However, when the residue was dissolved in hydrochloric acid after ashing of the tubes at 480°C (muffle furnace), only about 50% of the ^{51}Cr tracer was recovered. The remainder was either bound irreversibly to the quartz tube or physically lost, presumably because of the extremely small amount of chromium in the carrier-free radiotracer. This did not occur when magnesium nitrate was added to the blanks, and only a small amount was lost to the quartz tube when a normal saline solution was used as a blank (Table 2). Silanizing the tubes made no difference in the results, nor would it be expected to, because the DCDMS decomposes before 480°C is reached. The data in Table 2 suggest that when water alone is used as the blank, some of the ^{51}Cr tracer is in contact with the quartz tube surface after lyophilization and binds to, or dissolves in, the quartz irreversibly during ashing at 480°C. The presence of a residue from magnesium nitrate or sodium chloride apparently prevents this. The slightly higher retention in the case of sodium chloride may be due in part to the fact that the tube surface is noticeably etched after ashing (sodium salts are known to attack quartz at high temperatures).

The roles played by silanizing and the magnesium nitrate modifier in preventing both of these problems is illustrated in Table 3. When serum alone is ashed in untreated tubes, a substantial portion of the analyte is irreversibly retained in the quartz. Silanizing the tubes reduces this, and the use of magnesium nitrate reduces it even further. The silanization appears to work in a physical manner, in that the freeze-dried serum separates cleanly from the quartz wall during the initial stages of the ashing procedure. By the time 250°C is reached, the serum has shrunk into a spherical pellet having minimal contact with the quartz tube. This also greatly reduces etching of

TABLE 2

Behavior of $^{51}CrCl_3$ added to blank solutions and processed through dry ashing

Blanks[a]	Recovery (%)[b,c]	Retained in quartz tube wall[c] (%)
H_2O	50	25
$H_2O + Mg(NO_3)_2$	101	0.9
0.9% NaCl	102	2.9

[a]Containing carrier-free $^{51}CrCl_3$. [b]Recovered by equal volume of 0.1 M HCl. [c]Average of 3 trials.

TABLE 3

Behavior of ^{51}Cr in endogenously labeled rat serum processed through dry ashing

Sample	Recovery[a,b] (%)	Retained in quartz tube wall[b] (%)
Serum, no $Mg(NO_3)_2$, untreated tube	92	8
Serum, no $Mg(NO_3)_2$, silanized tube	100	0.8
Serum, + $Mg(NO_3)_2$, silanized tube	101	0.2

[a]Recovered by equal volume of 0.1 M HCl. [b]Average of 3 trials.

the quartz tubes by serum salts. The magnesium nitrate enhances the ashing process as well as permitting higher charring temperature in the graphite furnace.

The bovine serum pool used to prepare calibration graphs also served to monitor instrument performance, standards, or any other factors which might affect accuracy. The chromium content of this homogeneous material was well characterized by the a.a.s. method (using standard additions) and by the i.d.m.s. method. Over a period of several months, 26 a.a.s. determinations gave a mean chromium content of 0.27 ng ml^{-1} (SD = 0.05) and 15 i.d.m.s. determinations had a mean of 0.28 ng ml^{-1} (SD = 0.04). Because the a.a.s. and i.d.m.s. methods used here share a common drying and ashing procedure, they are not independent methods in the strictest sense. However, the results obtained with the rat serum labeled with ^{51}Cr strongly suggest that no analyte is lost during these steps, lending confidence to the accuracy of the results.

The ashed serum matrix causes an enhancement effect on the observed peak heights during atomization. As shown in Fig. 3 standard additions

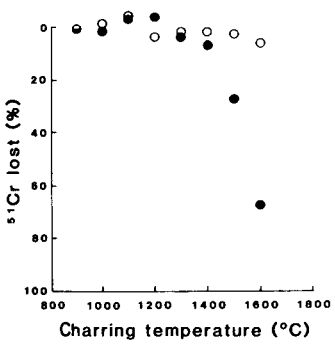

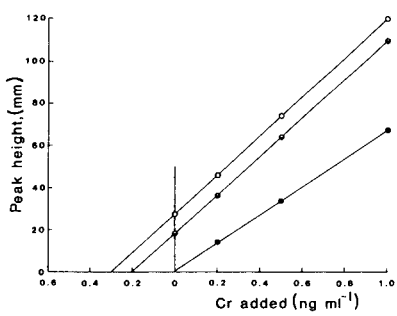

Fig. 2. Loss of ^{51}Cr from endogenously labeled rat serum as a function of charring temperature. Each point represents an individual furnace tube. (•) Serum; (○) serum with magnesium nitrate.

Fig. 3. Calibration graphs: (○) bovine serum; (⊙) human serum; (•) aqueous standards.

plots for serum have a greater slope than aqueous standards. The bovine and human sera have identical slopes, and this was found to be true for about 20 human sera, both individual and pooled, on any given day. Thus, it appears that standard graphs prepared from a bovine serum pool are suitable for chromium determinations in human sera. A human serum pool should serve the same purpose.

In assessing the reproducibility of the method, eight 1-ml aliquots of bovine pool serum were processed in eight individual quartz tubes on the same day. The mean chromium value obtained was 0.27 ng ml^{-1} with a standard deviation of 0.02 ng ml^{-1}. Blanks averaged 0.02 ng ml^{-1}. When eight 25-μl aliquots of a single sample solution were pipetted into the graphite furnace tube and quantified in succession, a mean value for chromium of 0.26 ng ml^{-1} was observed, with a standard deviation of 0.005 ng ml^{-1}.

Serum samples from 15 apparently healthy adults on a normal diet in the Beltsville area were collected and processed. Observed chromium values ranged from <0.05 to 0.29 ng ml^{-1}, with a mean value of 0.11 ng ml^{-1} and a standard deviation of 0.07 ng ml^{-1}. These subjects were part of a larger study on chromium metabolism which is reported elsewhere [13].

With suitable equipment, apparatus, precautions, and sufficient attention to details, serum chromium determinations can be done accurately on a routine basis. Approximately 30—40 determinations can be done daily. Because of the measures taken to prevent contamination, it is possible that this method would be suitable for a number of other trace elements in human serum.

This paper was presented in part at the 10th annual meeting of the Federation of Analytical Chemistry and Spectroscopy Societies, Philadelphia, September 1983. The assistance of J. Versieck in perfecting the dry ashing procedure is gratefully acknowledged.

REFERENCES

1 K. Schwarz and W. Mertz, Arch. Biochem. Biophys., 85 (1959) 292.
2 K. N. Jeejeebhoy, R. C. Chu, E. B. Marliss, G. R. Greenberg and A. Bruce-Robertson, Am. J. Clin. Nutr., 30 (1977) 531.
3 J. S. Borel and R. A. Anderson, in Biochemistry of the Elements, E. Frieden (Ed.), Plenum, New York, Ch. 8, pp. 175—199.
4 B. E. Guthrie, W. R. Wolf and C. Veillon, Anal. Chem., 50 (1978) 1900.
5 F. J. Kayne, G. Komar, H. Laboda and R. E. Vanderlinde, Clin. Chem., 24 (1978) 2151.
6 J. M. Harnly and T. C. O'Haver, Anal. Chem., 49 (1977) 2187.
7 J. Versieck, J. Hoste, F. Barbier, H. Steyaert, J. De Rudder and H. Michels, Clin. Chem., 24 (1978) 303.
8 C. Veillon, W. R. Wolf and B. E. Guthrie, Anal. Chem., 51 (1979) 1022.
9 C. Veillon and D. C. Reamer, Anal. Chem., 53 (1981) 549.
10 C. Veillon, K. Y. Patterson and D. C. Reamer, in Biological Reference Materials, W. Wolf, (Ed.), Wiley, New York, 1984, Ch. 9, pp. 167—177.
11 C. Veillon, B. E. Guthrie and W. R. Wolf, Anal. Chem., 52 (1980) 457.
12 C. Veillon, K. Y. Patterson and N. A. Bryden, Anal. Chim. Acta, 136 (1982) 233.
13 R. A. Anderson, N. A. Bryden and M. M. Polansky, Am. J. Clin. Nutr., (1984), in press.

Analytica Chimica Acta, 164 (1984) 77—82
Elsevier Science Publishers B.V., Amsterdam — Printed in The Netherlands

MOLECULAR EMISSION CAVITY ANALYSIS
Part 27. Indirect Determination of Selenium, Tellurium, Arsenic and Antimony After Extraction as their Diethyldithiocarbamates

AFSANEH SAFAVI[a]

Chemistry Department, University of Birmingham, P.O. Box 363, Birmingham B15 2TT (Great Britain)

ALAN TOWNSHEND*

Chemistry Department, University of Hull, Hull HU6 7RX (Great Britain)

(Received 7th March 1984)

SUMMARY

Measurement of S_2 emission of the diethyldithiocarbamates of As, Sb, Se and Te extracted into tetrachloromethane gives detection limits of 50, 150, 50 and 70 pg (in 5 μl), respectively. Tellurium in the presence of Se, and Sb in the presence of As, can be determined by extraction at pH 9.0. Calibration graphs are linear up to ca. 1 mg l^{-1}.

Sulphur compounds can be determined down to subnanogram levels by molecular emission cavity analysis (m.e.c.a.), based on the generation of S_2 emission in the hydrogen flame environment [1]. Selenium and tellurium similarly generate Se_2 and Te_2 emission [2], but the sensitivity is much less than for S_2, and only $\geqslant$50 ng of selenium and $\geqslant$1 μg of tellurium can be detected [3, 4]. Much lower detection limits (e.g., 7 ng of Se [5]) are obtained by conversion to hydrogen selenide and hydrogen telluride, and transport of the gases to the m.e.c.a. cavity with a stream of nitrogen. Arsenic and antimony can also be determined by m.e.c.a., but again high sensitivity can be achieved only by converting the analytes to volatile species, such as their hydrides [6, 7], for which detection limits were ca. 35 ng of arsenic and 70 ng of antimony [1].

An alternative approach to the determination of Se, Te, As and Sb by m.e.c.a., described in this paper, is to convert them to their dithiocarbamates, and to quantify the extracted ligand by its very sensitive S_2 emission. Such a procedure has already been applied to some metals, giving detection limits of ca. 40 μg l^{-1} [8].

---

[a]Present address: Chemistry Department, College of Arts and Science, University of Shiraz, Shiraz, Iran.

0003-2670/84/$03.00

EXPERIMENTAL

Reagents and apparatus

Doubly distilled water was used throughout. A stock 1000 mg l^{-1} selenium(IV) solution as selenium dioxide was prepared by dissolving 1.4052 g of selenium dioxide (BDH, laboratory reagent) and diluting to 1 l with water. A stock solution of 1000 mg l^{-1} tellurium(IV) as tellurium dioxide was prepared by dissolving 0.1251 g of tellurium dioxide (BDH, laboratory reagent) in 3 ml of 1 M sodium hydroxide, followed by dilution to 100 ml with water. Stock solutions (1000 mg l^{-1}) of arsenic(III) as sodium arsenite (0.3301 g in 250 ml) and antimony(III) as antimony potassium tartrate (0.2669 g in 100 ml) were also prepared. Solutions of lower concentrations were prepared daily by appropriate dilution with water.

A 0.2% (w/v) solution of sodium diethyldithiocarbamate (BDH, AnalaR) was prepared fresh each day. Borate buffer, pH 9.0, was made from 8.5 ml of sodium borate solution (12.4 g of boric acid and 100 ml of 1 M sodium hydroxide diluted to 1 l with water) and 1.5 ml of 0.1 M hydrochloric acid. A 0.1 M disodium-EDTA solution was prepared by dissolving 3.72 g of the solid (BDH, AnalaR) in water and diluting to 100 ml.

A prototype MECA 22 spectrometer (Anacon, Houston, TX) was used in conjunction with an Oxford 3000 potentiometric recorder (Oxford Electronic Instruments, Oxford, Great Britain). A 2.5-mm slit (≡42.5 nm) was employed and stainless steel cavities (3 mm deep × 4 mm diameter) were used.

Calibration procedure

Add exactly 5 ml of 0.0—0.7 mg l^{-1} selenium(IV), tellurium(IV), arsenic(III) or antimony(III) solution, adjusted to pH 2.6 with acetic acid for Se(IV) and As(III), to pH 9.0 for Sb(III), and to pH 9.0 and containing 1.8×10^{-2} M EDTA for Te(IV), to a series of 25-ml volumetric flasks. Add to each, 0.2 ml of 0.2% sodium diethyldithiocarbamate solution, followed by exactly 5 ml of tetrachloromethane, and extract the complex by shaking the mixture for 2 min. Separate the organic phase by passage through a phase-separating paper. Inject 5 μl of the extract into a cool cavity. Evaporate the solvent for 2 min in a stream of air from a cold air blower. Insert the cavity into the flame [H_2 = 3.6 l min^{-1}, air = 3.5 l min^{-1}, N_2 = 5.0 l min^{-1} (4.0 l min^{-1} for arsenic)], and measure the S_2 emission intensity at 384 nm, as a function of time. Continue heating the cavity for a further 30 s after emission has ceased, to clean the cavity, and cool with a cold air blower before injecting the next sample. Measure the peak-height signal. Make three measurements on each extract, and plot the mean peak height vs. concentration.

RESULTS

When a few drops of 0.2% sodium diethyldithiocarbamate were added to a 100 mg l^{-1} selenium(IV) solution as selenium dioxide, a pale yellow precipitate

formed immediately. Formation of the tellurium complex, however, required the addition of acid or EDTA. Tellurium(IV) reacted rapidly with the ligand in solutions acidified with citric, ascorbic or boric acid. In pH 9.0 borate buffer, there was no apparent reaction, but when a few drops of EDTA were subsequently added (without changing the pH), the yellow tellurium complex formed rapidly, as observed by Bode [9]. The mechanism of the effect is not known. The presence of EDTA has the added advantage that it prevents several metal ions (Co^{2+}, Ni^{2+}, Al^{3+}, Zn^{2+}, Cd^{2+}, etc.) from forming extractable diethyldithiocarbamates [9].

The selenium and tellurium chelates were quantitatively extracted into tetrachloromethane at very different pH values (2.6 and 9.0, respectively), again confirming the results of Bode [9]. At these pH values, very little of the excess diethyldithiocarbamate was extracted into the organic phase (Table 1). Thus the S_2 emission from the complexes could be determined by subtracting the very small blank intensities from the total emission signal. Extraction of arsenic(III) and antimony(III), likewise, was maximal at pH 2.6 and 9.0, respectively [9]. Blank extract responses were greatly increased when diethyldithiocarbamate solutions a few days old were used (Table 1), probably arising from carbon disulphide formed by decomposition of the dithiocarbamate.

Optimization of conditions

The effect of EDTA concentration on the emission intensity from tellurium extracts is shown in Fig. 1. The intensity increases linearly with EDTA concentration up to 1.7×10^{-3} M EDTA when the aqueous tellurium concentration was 7.8×10^{-6} M, above which the intensity was constant.

The effects of flame composition on the S_2 emission intensity from the four chelates were similar. Introduction of a small amount of air into the flame depressed the S_2 emission, but larger amounts gave greatly increased intensities, as observed in earlier m.e.c.a. studies [1, 10]. The composition which gave the greatest intensity for all chelates was H_2 = 3.6, air = 3.5 and N_2 = 5.0 l min^{-1} (4.0 l min^{-1} for arsenic). Under these conditions the emissions from the arsenic, antimony and tellurium chelates were essentially all from

TABLE 1

S_2 emission from extracts of Se(IV) and Te(IV) dithiocarbamates

Element	Se (2.5 μg)	Te (5 μg)	As (3.5 μg)	Sb (15 μg)
Intensity (mV)[a]	90 (3)	1.5 (1) 46 (3)[c]	60 (3[b])	75 (0)[b]

[a]Values in parentheses are emissions from blanks. All values are the mean of 3 results. [b]For a dithiocarbamate solution a few days old, the blank is 26 mV for As and 8 mV for Sb. [c]With EDTA added.

S_2, and the peak had a t_m value [1] of 0.5 s. The contribution of Se_2 emission from the selenium chelate was also negligible, although the possibility of SSe emission must not be discounted.

The presence of organic solvents has been reported to suppress S_2 emission in a m.e.c.a. hydrogen flame, especially when the solvent and analyte vapourize in the cavity at the same time, by interfering with the chemiluminescent process [11]. In this instance, tetrachloromethane completely prevented the S_2 emission from all four chelates. However, if the solvent was removed completely from the cavity by gentle evaporation for 2 min in a current of cold air from an air blower, before the cavity was inserted into the flame, intense S_2 emissions were obtained.

Extraction should be done immediately after addition of the diethyldithiocarbamate. Extraction 1 h after chelate formation gave 50% less emission for 0.5 mg l^{-1} selenium and 0.7 mg l^{-1} tellurium; 0.7 mg l^{-1} arsenic gave only 7% of the original signal. Antimony extraction (1 mg l^{-1}) was unaffected. A single extraction was sufficient to achieve quantitative separation of each chelate. A second extraction gave no signal attributable to a dithiocarbamate chelate.

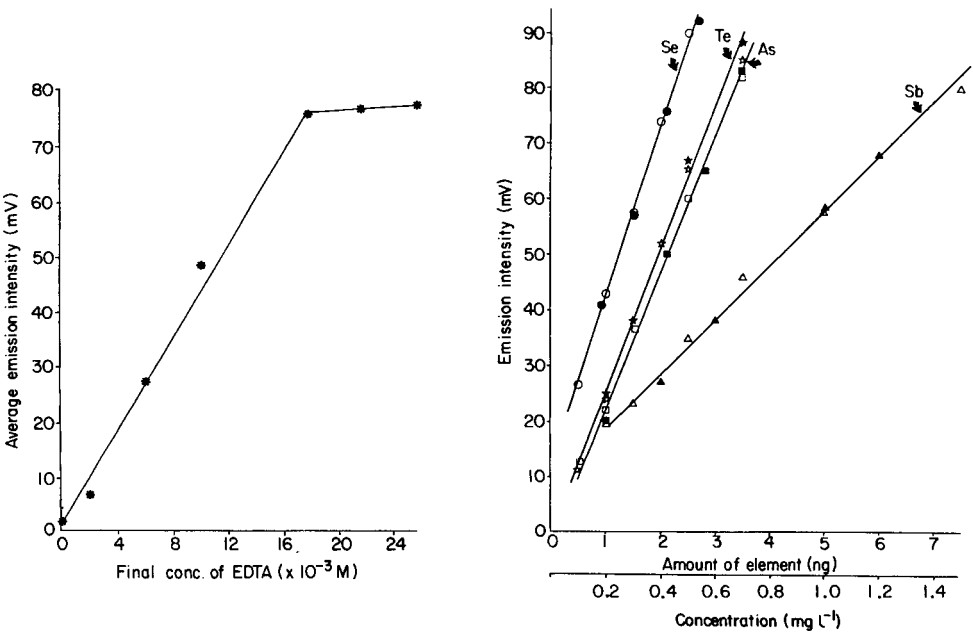

Fig. 1. Effect of concentration of EDTA on S_2 emission intensity obtained from tellurium diethyldithiocarbamate complex. (Recommended flame composition; 1 mg l^{-1} (7.8 × 10^{-6} M) tellurium as TeO_2 in borate buffer, pH 9.0).

Fig. 2. Calibration graphs: (△, ▲) antimony; (□, ■) arsenic; (☆, ★) tellurium; (○, ●) selenium. (Open symbols represent injection of different concentrations in extracts of the same volume; closed symbols represent injection of different volumes of extract of the same concentration.)

The tellurium complex is reported to be very photosensitive, supposedly resulting in the decomposition reaction [9]

$$Te(DDTC)_4 \xrightarrow{h\nu} Te(DDTC)_2 + \text{tetramethylthiuramdisulphide}$$

This is a considerable disadvantage in the spectrophotometric procedure. However, light had no effect on the m.e.c.a. response of this or any of the other chelates, after extraction by the recommended procedure. This may be due to the fact that, once the chelate has been extracted, the total amount of sulphur in the extract is unchanged even if the decomposition reaction occurs. Only a single peak (t_m = 0.5 s) was obtained under all conditions.

Analytical aspects

The calibration graphs obtained for arsenic, antimony, selenium and tellurium were all linear, and very sensitive (Fig. 2). The linearity is unusual for systems based on S_2 emissions, a sigmoidal graph normally being obtained [1] because two sulphur species are involved in the rate-determining step in producing excited S_2 molecules. The linear relationship, also observed previously for metal dithiocarbamates [8], indicates that a different mechanism is operating. For example, S_2 formation may take place intermolecularly from the $-NS_2^-$ moiety in the dithiocarbamate. The precision and detection limit for each element are given in Table 2.

Because selenium and tellurium can be extracted at widely different pH values, determination of tellurium(IV) in the presence of selenium(IV) is possible, by extraction of the former at pH 9.0 [9]. When attempts were made to extract selenium(IV) under the conditions used for tellurium extraction, no S_2 emission was obtained attributable to a selenium chelate. When the weight of selenium was up to 400 times that of tellurium, selenium did not affect the emission intensity from the tellurium chelate. Similarly, up to 400 times (by weight) of arsenic could be tolerated in the determination of 0.5 mg l^{-1} antimony(III). Larger amounts gave increased intensities. The arsenic in the aqueous phase could later be determined by acidifying, and extracting again.

Many metal ions are also extracted as their dithiocarbamates, and would be expected to interfere. This was found to be the case, but addition of EDTA was able to mask the effects of moderate amounts of metal ions. The results for arsenic (Table 3) are typical. In practice, separation of the anionic As, Sb, Te and Se species from metal ions should be relatively easily achieved, for example, by use of an ion-exchange resin [12].

TABLE 2

Precision and detection limits for Se, Te, As and Sb

Element	Se	Te	As	Sb
R.s.d. of m.e.c.a. measurement (%)	2.3	1.7	2.3	3.5
R.s.d. of complete procedure (%)	4.9	3.5	4.1	5.0
Detection limit (pg/5 μl)	50	70	50	150

TABLE 3

Effect of EDTA on metal ion interference on the determination of arsenic (0.3 mg l^{-1})

Metal ion[a]	Effect on intensity (%)			
	1:1 (w/w)		10:1 (w/w)	
	no EDTA	EDTA[b]	no EDTA	EDTA[c]
Cu^{2+}	72	100	100	100
Ni^{2+}	81	0	100	6
Zn^{2+}	94	0	100	0
Cd^{2+}	44	−1	100	−20
Pb^{2+}	13	−8	76	−8
Al^{3+}	37	−1	40	−10

[a]As nitrate. [b]5×10^{-4} M. [c]1×10^{-3} M.

The methods described are very sensitive. The sensitivities are greater than those obtained by direct conventional m.e.c.a. based on Se_2, Te_2, or arsenic or antimony oxide emissions or by a m.e.c.a. volatilization system [1]. The detection limits are all in pg ($\mu g\ l^{-1}$) range.

REFERENCES

1 M. Burguera, S. L. Bogdanski and A. Townshend, CRC Crit. Rev. Anal. Chem., 10 (1980) 185.
2 I. El-Hag, Ph.D. Thesis, University of Birmingham, 1982; I. El-Hag and A. Townshend, Anal. Proc., 20 (1983) 135.
3 R. Belcher, T. Kouimtzis and A. Townshend, Anal. Chim. Acta, 68 (1974) 297.
4 A. Safavi and A. Townshend, Anal. Chim. Acta, 142 (1982) 143.
5 R. Belcher, S. L. Bogdanski, E. Henden and A. Townshend, Anal. Chim. Acta, 113 (1980) 13.
6 R. Belcher, S. L. Bogdanski, S. A. Ghonaim and A. Townshend, Anal. Chim. Acta, 72 (1974) 183.
7 R. Belcher, S. L. Bogdanski, E. Henden and A. Townshend, Anal. Chim. Acta, 92 (1977) 33.
8 I. H. B. Rix, Ph.D. Thesis, University of Birmingham, 1976.
9 H. Bode, Z. Anal. Chem., 144 (1955) 90, 165.
10 R. Belcher, S. L. Bogdanski and A. Townshend, Anal. Chim. Acta, 67 (1973) 1.
11 T. Sugiyama, Y. Suzuki and T. Takeuchi, J. Chromatog. Sci., 11 (1973) 639.
12 I. I. Nazarenko and A. N. Ermakov, Analytical Chemistry of Selenium and Tellurium, Halsted Press, New York, 1972.

Analytica Chimica Acta, 164 (1984) 83—90
Elsevier Science Publishers B.V., Amsterdam — Printed in The Netherlands

PREPARATION OF CONDUCTING ELECTRODES FROM BIOLOGICAL SAMPLES FOR MULTI-ELEMENT TRACE ANALYSIS BY SPARK-SOURCE MASS SPECTROMETRY OR EMISSION SPECTROMETRY

L. VOS and R. VAN GRIEKEN*
Department of Chemistry, University of Antwerp (UIA), B-2610 Wilrijk (Belgium)
(Received 26th April 1984)

SUMMARY

Four decomposition procedures frequently used for biological material (dry ashing, open wet digestion, wet digestion in a teflon bomb and low-temperature ashing) are optimized for the conversion of biological samples to conducting electrodes suitable for multi-element trace determinations by spark-source mass spectrometry or emission spectrometry. The optimized procedures are evaluated with respect to contamination, retention and preconcentration of the trace elements, homogeneity of the electrodes and precision of the final results. Both dry-ashing methods are prone to losses by volatilization; simple dry ashing suffers from contamination problems during electrode preparation. Wet digestion gives better precision; digestion with nitric/sulfuric acids in an open flask is the method of choice for most elements being simpler and giving lower blanks than the bomb method.

Sensitive panoramic analyses of various biological samples can provide valuable information for fundamental studies of biogeochemical pathways and for general biomedical research. Emission spectrometry and spark-source mass spectrometry [1] are particularly useful for these purposes. Both techniques require samples in the form of conducting electrodes.

To prepare suitable electrodes, the biological material must be decomposed first and the residue can then be mixed with a conducting powder (e.g., graphite). Methods of destroying biological materials have been studied extensively [2] but the comparative usefulness of these methods for preparing conducting electrodes has never been thoroughly assessed. Therefore, the characteristics of four frequently used methods (dry ashing, open wet digestion, wet ashing in a teflon bomb, and low-temperature ashing) were optimized and examined in this context, and the optimized procedures for converting biological samples into conducting electrodes were evaluated.

EXPERIMENTAL

Dry ashing

During dry ashing to a temperature at which the organic substances decompose and only the minerals remain, there is a risk of partial or complete

0003-2670/84/$03.00

loss of volatile elements. To establish the maximum permissible ashing temperature, a thermogravimetric curve was recorded for two biological samples, NBS Orchard Leaves and NBS Bovine Liver. Figure 1 shows that the Orchard Leaves decompose at a lower temperature than Bovine Liver. For Orchard Leaves a maximum temperature of 450° C is sufficient whereas 500° C is required for Bovine Liver.

The decomposition can readily be done with a programmable Tecator destruction instrument. A 1-g aliquot of sample (e.g., Orchard Leaves) was placed in the ashing tube and was then ashed for 2 h at 150° C, for 3 h at 250° C, for 7 h at 350° C, and for 12 h at 450° C. The ratio of the weight of the final residue to the weight of the original sample was 0.12 for Orchard Leaves and 0.08 for Bovine Liver.

Conducting electrodes were prepared by mixing the residue with high-purity graphite powder. The mixture was transferred to an agate container with two agate mixing balls, and homogenized with an energetic mixer (Spex, Wig-L-Bug). After homogenization, the resulting powder was compressed into cylindrical electrodes in a perforated polythene cylinder under an axial pressure of 10 tons.

Open wet digestion

During wet decomposition, the sample is decomposed in a mixture of oxidizing acids. Nitric acid is frequently used but not all biological samples are completely decomposed in it and relatively large volumes are required. A mixture of nitric and perchloric acids is very effective, but the boiling point of the latter is very high and unstable perchlorates are formed so that the evaporation of the acid is difficult and implies explosion risks. Finally, a mixture (2 + 1) of nitric acid and sulfuric acid (both Merck, Suprapur) was selected. The sample could be decomposed completely in a relatively small amount of liquid and evaporation of the liquid was rather easy.

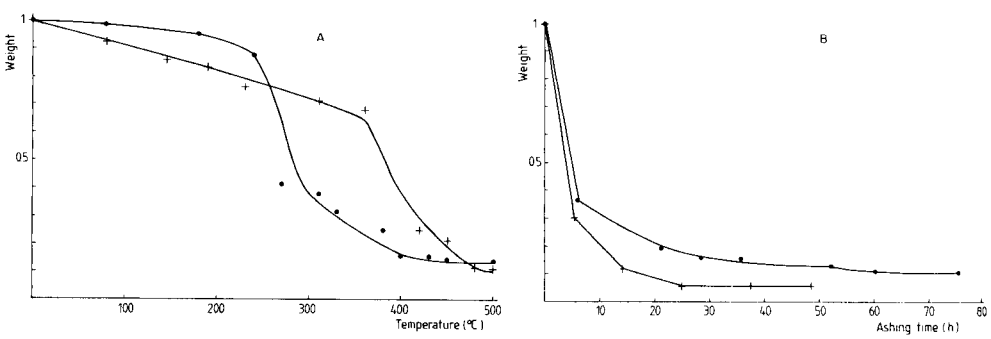

Fig. 1. Weight of the residue from 1 g of biological material as a function of (A) the heating temperature in dry ashing, and (B) the time in low-temperature ashing. Sample: (•) Orchard Leaves; (+) Bovine Liver.

The programmable Tecator instrument was used for the decomposition. After drying, a 1-g sample was transferred to the destruction tubes and 15 ml of the digestion mixture was added, possibly together with an internal standard. A cooling tube was placed on top of the destruction tube for work under reflux conditions. After a night at room temperature, the solution was heated for 4 h at 100° C and finally for 20 h at boiling point (ca. 160° C). After cooling, a clear solution was obtained.

To prepare electrodes, the resulting solution was mixed with graphite powder and evaporated under an i.r. lamp. Any absorption on the wall of the beaker could be neglected compared to the absorption on the graphite because of the much larger surface of the latter. By evaporating slowly, a reasonably homogeneous powder was obtained, but for further improvement the powder was transferred to a polyethene container together with a polyethene ball, and mixed for 30 min in a Wig-L-Bug. The contamination introduced during this mixing procedure was undetectable. The electrodes were compressed from the homogenized graphite powder in the same way as for the dry-ashing procedure.

Wet digestion in a teflon bomb

Decomposition in a sealed teflon vessel under high pressure and temperature is a well-known technique in which volatilization losses are minimal. For subsequent electrode preparation, the digestion liquid must have a low boiling point to allow evaporation onto graphite.

In a series of tests, the optimal sample/acid weight ratio, digestion temperature and digestion time were determined empirically. A mixture of 20 ml of nitric acid (Merck, Suprapur) and 3 ml of hydrogen peroxide (Merck, analytical grade) was necessary to digest 500 mg of botanical matter at 190° C during 12 h. When less acid was used, the resulting solution was clear, but after evaporation onto graphite, greasy electrodes were obtained. This suggests that the biological matter was not completely decomposed but was converted to acid-soluble compounds, as was also observed by Evans and Morrison [3]. To digest animal tissues, only half the amount of the destruction liquid was needed to obtain satisfactory results.

Electrodes were prepared in the same way as after the open wet digestion.

Low-temperature ashing

Low-temperature ashing involves decomposition at low temperatures (100° C) and low pressure, in an excited oxygen plasma. A Tracerlab LTA-300 instrument was used; it has two separate ashing chambers so that two samples (1—2 g) can be ashed simultaneously. The unit was operated under the following experimental conditions: 400-W forward power, 200 ml min^{-1} oxygen flow rate, and a pressure of 2 mm Hg. The samples were regularly mixed, to speed up the ashing, until a constant weight was obtained. A diagram of weight loss versus ashing time for two biological samples is given in Fig. 1B. The final weight loss was 90% for Orchard Leaves and 95% for Bovine Liver.

The residual ash was easily dissolved in diluted (1—2 M) nitric acid (Merck, Suprapur), which allowed for internal standard additions and avoided dry homogenization. The further electrode preparation was the same as for the wet-digestion techniques.

Spectrometric measurements

Both spark-source mass spectrometry (s.s.m.s.) and x-ray emission spectrometry (x.r.s.) were applied to evaluate the procedures for electrode preparation. For s.s.m.s., a JEOL JMS-01-BM-2 instrument was used with photoplate detection. The instrumental parameters and procedure have been described elsewhere [4]. The x.r.s. technique involved secondary target excitation and energy-dispersive detection. The procedure has been described in detail elsewhere [5].

RESULTS AND DISCUSSION

Contamination

To establish the blank levels, each of the four procedures was tested without biological material. The results are presented in Table 1. During dry ashing, the major contamination is introduced during the mixing procedure. The major fraction of the impurities introduced during wet digestion comes from the reagents, especially sulfuric acid and hydrogen peroxide. Except for sulfur, the blank level of most elements in the closed wet-digestion procedure is higher than in the open wet digestion, because of the larger volume of nitric

TABLE 1

Blank levels (expressed as corresponding concentration in the biological sample) for the four techniques of sample preparation

Element	Blank concentration ($\mu g\ g^{-1}$)			
	Dry ashing	Open wet digestion	Wet digestion in bomb	Low-temperature ashing
Na	20	15	17	15
Mg	15	5	10	5
Al	4	1	<1	<1
Si	70	30	20	20
P	2	2	3	<1
S	20	1000	30	10
K	50	48	60	20
Ca	6	4	5	3
Ti	<0.1	<0.1	0.1	<0.1
Cr	<0.1	0.6	0.5	<0.05
Mn	<0.1	0.2	0.3	<0.05
Fe	5.7	4	8	2
Ni	<0.1	0.3	0.5	<0.05
Cu	<0.1	0.5	0.5	<0.05
Zn	3	0.7	1	0.5

acid, and also because the hydrogen peroxide was rather impure. In low-temperature ashing, the contamination is lower, because little acid is needed and no subsequent homogenization in an agate container is necessary.

Retention of the trace elements

The risk of losses of volatile elements is obviously most pronounced during the dry-ashing procedure. These losses have been studied by many authors but their conclusions are sometimes conflicting. Specifically, for dry ashing of Orchard Leaves at 500° C, Nonaka et al. [6] found no losses of Al, Ba, Ca, Ce, Co, Fe, La, Mg, Mn, Na, Sc, Sm, Th, V and Zn; for As, Cu, Cr, Cs, K, Rb and Sb, however, they reported losses ranging between 10 and 60%.

The losses during open wet digestion with nitric and sulfuric acids were studied by Gorsuch [2]. He found no losses of Zn, As, Cu, Co, Ag, Cd, Sb, Cr, Mo and Fe. For Pb, Hg, Se and Sr, the losses were respectively 10%, 6%, 20% and 4%. The losses that might occur during the subsequent evaporation of the digestion liquid with graphite and the influence of the acids used were studied by evaporating a solution containing numerous trace elements directly or in the presence of nitric acid and hydrogen peroxide, or nitric and sulfuric acids. The doped graphite was compressed into pellets and subjected to x.r.f. [5]. The recoveries of the different elements are presented in Table 2. The precision of these measurements is about 5%. Most elements, except Ge, Se and Pb, appear to be retained quantitatively in all cases. The losses of Pb, Se and Ge are less when acid is added but their recoveries remain unsatisfactory for the nitric/sulfuric acid mixture used in the open wet-digestion procedure.

During wet digestion in a teflon bomb, losses are practically impossible. Possible losses during the subsequent evaporation onto graphite can be assessed by inspecting the last column in Table 2.

The losses of trace elements during low-temperature ashing of biological samples have been studied extensively by e.g. Gleit [7], Gleit and Holland [8], Evans and Morrison [3]. They found quantitative recoveries of Sb, As, Cs, Co, Cr, Cu, Fe, Pb, Mo, Mn, Se, Na, Zn, Cd, Ni, Tl, Sn, Sr, Ti and V and minor losses of Au, Hg, Ag, Si and P. When the ash is dissolved in nitric acid and evaporated onto graphite, losses of Ge, Se and Pb can be expected, as is also evident for Table 2.

Preconcentration of the sample

To obtain optimal detection limits, the sample must be preconcentrated as much as possible. To obtain sufficiently conducting electrodes, a graphite/ash weight ratio of 60/40 may not be exceeded; therefore, the sample decomposition has to be as complete as possible.

During dry ashing, the weight loss for Orchard Leaves was 88%. Some 300 mg of sample was needed for a pair of electrodes containing at most 40% of ash. Thus 1 g of biological sample can be converted to a pair of electrodes. The corresponding preconcentration factor defined as the weight ratio of original sample to electrodes, is 3.3.

TABLE 2

Influence of nitric acid, hydrogen peroxide and sulfuric acid on the recovery of trace elements during the evaporation with graphite

Element	Recovery (%)			
	No addition	Addition of HNO_3	Addition of HNO_3 and H_2SO_4	Addition of HNO_3 and H_2O_2
Ti	112	118	118	99
V	109	108	106	107
Cr	108	109	112	110
Mn	103	107	100	103
Fe	113	115	95	(41)
Co	98	108	95	97
Ni	97	98	96	98
Cu	102	102	105	102
Zn	92	94	92	97
Ga	96	95	99	97
Ge	4	75	70	79
As	103	102	95	97
Se	5	11	50	9
Rb	100	98	92	97
Sr	92	91	81	79
Y	95	88	89	88
Cs[a]	103	109	101	104
La[a]	143	137	120	133
Pb[a]	5	43	53	41
Bi[a]	107	100	100	99

[a]These elements were detected by x.r.f. via their *L* x-rays and the results are thus less precise because of spectral overlap and spectrum evaluation problems.

During wet digestion, whether in the open or the closed mode, only 500 mg of biological material can be converted to a pair of electrodes. If more material is evaporated on the same amount of graphite, the electrodes become greasy and exhibit poor mechanical and electrical properties. In this case, the preconcentration factor is 1.7 only.

The most complete decomposition was obtained by low-temperature ashing. The weight loss for Orchard Leaves was 90%, so that the preconcentration factor was 4.0.

Homogeneity of the electrodes

Because during s.s.m.s., for example, only a very small amount of sample is used, the electrodes must be very homogeneous. To test the homogeneity by s.s.m.s., the lower half of four photoplates was exposed with electrodes of the very homogeneous steel alloy NBS SRM-661; the upper half was exposed with electrodes obtained from Orchard Leaves via one of the four preparation procedures. In each case, the six exposures ranged from 0.1 to 10 nC (0.28 mg of graphite is sampled by a 10-nC exposure [9]). After photoplate

evaluation, the precision of the results for the biological samples was compared with that for the steel alloy. It appeared that on average the precision did not differ significantly for any of the four methods. The precision for some alkali and alkaline earth elements was worse in some cases, probably because they crystallize last during the evaporation and may form relatively large crystals that are not homogenized sufficiently.

Precision and accuracy

Three sets of electrodes were made from Orchard Leaves for each of the four preparation procedures, and subjected to s.s.m.s. For the elements that were present at a level at least three times the detection limit, the average results and the relative standard deviations were calculated for each method. The results are listed in Table 3 together with the certified values. The last line of Table 3 shows the average precision. For the two wet-digestion methods, precision was around 14%. For dry ashing and low-temperature ashing, the precision was 19%. Repeated s.s.m.s. with the same electrodes yielded a precision of ca. 12% under the experimental conditions used. The precision of the decomposition techniques is thus 7% and 15% for the wet and dry ashing procedures, respectively. The inferior precision of dry ashing is probably due to variable partial volatilization of the more volatile elements like zinc and lead. During low-temperature ashing, the many manipulations

TABLE 3

Results of triplicate s.s.m.s. determinations of trace elements in Orchard Leaves after the four preparation procedures (the estimated uncertainty is based on triplicate results and includes the measurement uncertainties and the sample treatment variations)

Element	Certified value[a] ($\mu g\ g^{-1}$)	Concentration found ($\mu g\ g^{-1}$)[b]			
		Dry ashing	Open wet digestion	Wet digestion in bomb	Low-temperature ashing
Ti	(20)	22(15)	22(9)	23(10)	17.7(12)
Cr	(2.3)	3.4(15)	3.2(12)	3.0(11)	2.9(18)
Mn	91	54(20)	99(14)	92(18)	90(16)
Fe	300	240(10)	260(8)	310(10)	290(20)
Cu	12	10.6(7)	10.8(7)	12.1(8)	11.3(7)
Zn	25	21(33)	25(17)	27(21)	23(23)
As	14	12.9(17)	14.1(11)	15.3(12)	13.0(18)
Rb	12	9.9(27)	10.8(18)	13.1(19)	11.6(29)
Sr	36	30(20)	33(14)	35(16)	33(18)
Ba	(51)	44(14)	52(16)	45(17)	48(18)
Pb	45	24(31)	37(24)	34(20)	26(28)
Average RSD (%)		20	14	15	18

[a]Tentative values in parentheses. [b]With RSD (%) in parentheses.

that are necessary during the decomposition might have an additional adverse effect.

The average results obtained by s.s.m.s. after the wet digestions agree quite satisfactorily with the certified values. While the data after low-temperature ashing are unacceptably low only for lead, dry ashing gives significantly low results, probably because of losses by volatility in several instances.

This work was partly supported by the Belgian Ministry for Science Policy under grant 80-85/10.

REFERENCES

1 L. Vos, Ph.D. thesis, University of Antwerp, 1984.
2 T. T. Gorsuch, The Destruction of Organic Matter, Pergamon, Oxford, 1970.
3 C. A. Evans and G. H. Morrison, Anal. Chem., 40 (1968) 869.
4 L. Vos and R. Van Grieken, Int. J. Mass Spectrom. Ion Proc., 55 (1983/1984) 233.
5 R. Van Grieken, H. Robberecht, J. Shani, P. Van Dyck and L. Vos, in R. Cesareo (Ed.), X-Ray Fluorescence (XRF and PIXE) in Medicine, Field Educational Italia, Rome, 1982, p. 159.
6 N. Nonaka, H. Higuchi and H. Hamaguchi, Bunseki Kaguku, 30 (1981) 599.
7 G. Gleit, Am. J. Med. Electronics, 2 (1963) 112.
8 G. Gleit and W. Holland, Anal. Chem., 34 (1962) 1454.
9 J. Verlinden, J. Van Puymbroeck and R. Gijbels, Int. J. Mass Spectrom. Ion Phys., 47 (1983) 287.

Analytica Chimica Acta, 164 (1984) 91—101
Elsevier Science Publishers B.V., Amsterdam — Printed in The Netherlands

REAL-TIME THERMAL LENS ABSORPTION MEASUREMENTS WITH APPLICATION TO FLOW-INJECTION SYSTEMS

R. A. LEACH[a] and J. M. HARRIS*
Department of Chemistry, University of Utah, Salt Lake City, UT 84112 (U.S.A.)
(Received 12th June 1984)

SUMMARY

Flow-injection methods are shown to reduce effectively the blank-related uncertainties in trace-level spectrophotometry. When thermal lens detection is used with efficient, real-time data processing, sensitive determinations are possible with response times adequately fast for flow-injection monitoring. Absorbance detection limits of 8.5×10^{-7} in a 1-cm pathlength flow cell were obtained for injections into carbon tetrachloride solvent. Thermal lens detection of iron with 1,10-phenanthroline as reagent produced detection limits of 37 pg of iron in the 100-μl injection volume. The advantages of flow injection for minimizing problems with photochemically unstable analytes in thermal-lens measurements are demonstrated.

Recently developed instrumentation for the measurement of weak optical absorption in solution has produced outstanding improvements in detection limits [1]. Several of these methods are based on the detection of the heat deposited in the sample by the nonradiative relaxation of excited molecules. These calorimetric absorbance methods take advantage of the high optical powers available from lasers to provide increased sensitivity relative to conventional transmittance measurements [2]. Among the calorimetric methods developed which differ primarily according to the technique used to monitor the temperature rise, thermal lens absorption measurements [3] are receiving considerable attention [4—13] because of the simple optical design and absorbance detection limits of the order of 10^{-6} to 10^{-7}.

Unfortunately, the increases in sensitivity which can be obtained with lasers have not always led to improved detection limits in practical applications because of uncertainties in the blank signal which increase in proportion to sensitivity [1]. A significant contribution to the blank uncertainty near the limit of detection is due to manipulation of the ultra-trace level samples prior to detection. Errors caused by sample contamination, loss of analyte, sample carryover, and instrument alignment are all possible when the sample

[a]Present address: E. I. DuPont De Nemours and Co., Pioneering Research Lab, Experimental Station, Wilmington, DE 19898, U.S.A.

0003-2670/84/$03.00

manipulation methods involve conventional laboratory glassware and spectrophotometer cells.

Sample processing in flow-injection systems has been advocated as a means of minimizing the risks associated with sample preparation and transfer to sensitive optical detectors [14, 15]. The advantages of such systems in trace-level determinations arise from the fact that sample processing, including reaction, dilution and sample preconcentration, can be done in an entirely closed, inert manifold prior to detection. In addition, the continuous flow of liquid carrier in the manifold efficiently rinses previous sample injections from the system, reducing carry-over and allowing blank measurements to be made between each sample. Finally, the consumption of costly ultra-pure reagents is also reduced relative to conventional sample handling. Sample-injection volumes of 10—100 μl more closely match the detection volume defined by a focussed laser beam than the 1—3 ml of sample needed in a conventional sample cell.

While flow-injection methods seemingly solve a number of ultra-trace sample handling problems, they impose several restrictions on the optical detector. The response time of the instrument must be adequately short to monitor changing absorbances, while maintaining the photometric precision necessary for low absorbance detectability. In this work, real-time processing of thermal lens data is developed and evaluated with respect to detection of trace-level samples in both aqueous and nonaqueous solvents. In addition, application of the method to the trace-level determination of iron as its 1,10-phenanthroline complex is demonstrated.

THEORY

The development of a thermal lens in an absorbing sample, located beyond the waist of a focussed laser beam, increases the divergence of the transmitted radiation. After the start of illumination, the increasing divergence with time is conveniently monitored by observing the decrease in intensity at the center of the laser beam. For a sample located $3^{1/2} Z_c$ beyond a beam waist of spot size ω_0, where $Z_c = \Pi\omega_0^2/\lambda$, the beam center intensity changes with time according to the following equation [16]

$$I_{bc}(t) = I_{bc}(0)[1 + \theta/(1 + t_c/t) + 0.5\,\theta^2/(1 + t_c/t)^2]^{-1} \quad (1)$$

where $I_{bc}(0)$ is the initial intensity in the absence of the thermal lens, t is the time after the onset of illumination, and θ is proportional to the sample absorbance, given by $\theta = 2.303\,EA$, where E represents the enhancement of the linear portion of the thermal lens response relative to Beer's law [3, 4, 16]: $E = -P(dn/dT)/1.91\,\lambda k$, P being the laser power in Watts, (dn/dT) the variation of refractive index with temperature, k the thermal conductivity, and λ the laser wavelength.

The time constant for formation of the thermal lens, t_c, is given by $t_c = \omega^2\rho C_p/4k$, where ρ is the density, and C_p is the heat capacity of the sample,

and ω is the spot size of the laser beam in the sample. Absorbance information is typically obtained by fitting Eqn. 1 to time-resolved thermal lens data to determine the three independent parameters, θ, $I_{bc}(0)$, and t_c [13]. The advantages of such a multipoint fit relative to a simple two-point, steady-state measurement include increased precision, dynamic range, and data collection rates.

To obtain response times adequate for detection in liquid chromatography, a rapid method for processing thermal lens data was developed which maintained some of the advantages for time-resolved data collection described above while greatly reducing computational times. By rearranging Eqn. 1, an expression linear in θ was obtained

$$\theta(t) = (1 + t_c/t)[(2I_{bc}(0)/I_{bc}(t) - 1)^{1/2} - 1] \quad (2)$$

By fixing t_c at a predetermined value for the solvent used, and assigning $I_{bc}(0)$ to be the first point in the thermal lens transient, the fit was reduced to a single parameter, θ, where all intensity points in time except the first point contribute to the average value $\bar{\theta}$

$$\bar{\theta} = (n-1)^{-1} \sum_{t=1}^{n-1} \theta(t) \quad (3)$$

These simple approximations reduce the time for calculating θ from about 1 min to $\leqslant$250 ms. A source of noise from random fluctuations in $I_{bc}(0)$ was introduced, however, which decreased the resulting precision of the measurement.

The statistical uncertainty in determining $\theta(t)$ was observed to vary with t, being maximized as $t \to 0$. From Eqn. 2, the value of the intensity-dependent factor is small at early time ($t \ll t_c$), because $I_{bc}(t) \approx I_{bc}(0)$, while $\theta(t)$ is obtained by multiplication with the large time constant term. Early in the thermal lens transient, therefore, random intensity fluctuations are magnified and contribute large errors to the value of $\theta(t)$ relative to the errors produced as t approaches t_c. Following a propagation of errors treatment [17], a working functional form of the uncertainty in $\theta(t)$, $\sigma_{\theta(t)}$, may be obtained and used as a weighting function to obtain $\bar{\theta}$ more precisely

$$\sigma^2_{\theta(t)} = [\partial\theta(t)/\partial I(t)]^2 \sigma^2_{I(t)} + [\partial\theta(t)/\partial I(0)]^2 \sigma^2_{I(0)} + [\partial\theta(t)/\partial t_c]^2 \sigma^2_{t_c} \quad (4)$$

where

$$\partial\theta(t)/\partial I(t) = -[I(0)(1 + t_c/t)/I(t)^2][(2I(0)/I(t)) - 1]^{-1/2}$$

$$\partial\theta(t)/\partial I(0) = [(1 + t_c/t)/I(t)][2I(0)/I(t)]^{-1/2}$$

and $\partial\theta(t)/\partial t_c = \{-1 + [(2I(0)/I(t)) - 1]^{-1/2}\}/t$

Near the limit of detection, where θ is small and $I(t)$ is nearly equal to $I(0)$, $\partial\theta(t)/\partial t_c$ is negligible and will therefore not be considered further. Under the same assumption of small θ, the remaining derivatives reduce to

$$\partial\theta(t)/\partial I(t) \approx -\partial\theta(t)/\partial I(0) \approx -(1 + t_c/t)/I(0) \quad (5)$$

Substituting Eqn. 5 into Eqn. 4, the time dependence of the uncertainty in θ is obtained

$$\sigma^2_{\theta(t)} \approx 2(1 + t_c/t)^2 \sigma_I^2/I^2 \quad (6)$$

indicating the expected large errors for small values of t. To reduce the impact of these errors, a weighted average [17] based on Eqn. 6 can be implemented to determine $\bar{\theta}$

$$\bar{\theta} = \sum_{t=1}^{n-1} \theta(t)(1/\sigma^2_{\theta(t)}) \Big/ \sum_{t=1}^{n-1} (1/\sigma^2_{\theta(t)}) \quad (7)$$

Computational time is not increased relative to the conventional average because the weighting function, Eqn. 6, remains constant and requires calculation only once prior to an experiment.

EXPERIMENTAL

Apparatus

The basic thermal lens instrument has been described previously [6, 18]. In this work, either argon ion (Lexel, Model 95) or krypton ion (Coherent, Model 90-K) lasers were used, depending on the wavelength required for a particular determination. The optical configuration, which remained unchanged with the two lasers, comprised a 30.2-cm focal length lens to focus the beam through a 1-cm pathlength flow cell located at approximately $3^{1/2}$ times the confocal distance beyond the beam waist [16]. Beam-center-intensities were measured at a distance of about 4 m beyond the flow cell using a photovoltaic detector (Silicon Detector Corp.; SD-200-12-12-04) with an active area of 5.1-mm diameter.

The fused-silica flow cell used in this work (Starna Cells, Atascadaro, CA, Model 73) was chosen in order to minimize problems from convection [19]. In this design, shown in Fig. 1, the sample flows up vertically through the laser beam, carrying previously heated sample out of the path of the beam. The shallow depth of the rectangular channel, 1 mm, stabilizes the flow profile and reduces dead-volume. Minimal unswept volume exists between the flow-injection manifold and the laser beam, thereby maintaining a high degree of sample integrity under laminar flow conditions.

The flow-injection manifolds used for the evaluation of the thermal lens detector were constructed by using a FIAstar system originally developed by Růžička et al. [20]. For injections of dye solutions, a simple single-stream manifold, as shown in Fig. 2(a), was used while a two-stream manifold designed for chromogenic reactions [15] (Fig. 2b) was used in the determination of iron. In both cases, fluids are pumped by compressed helium regulated above the sealed solvent reservoirs. All transfer lines are 0.5-mm i.d. teflon tubing (Rainin Instruments). Aqueous samples were injected with a valve

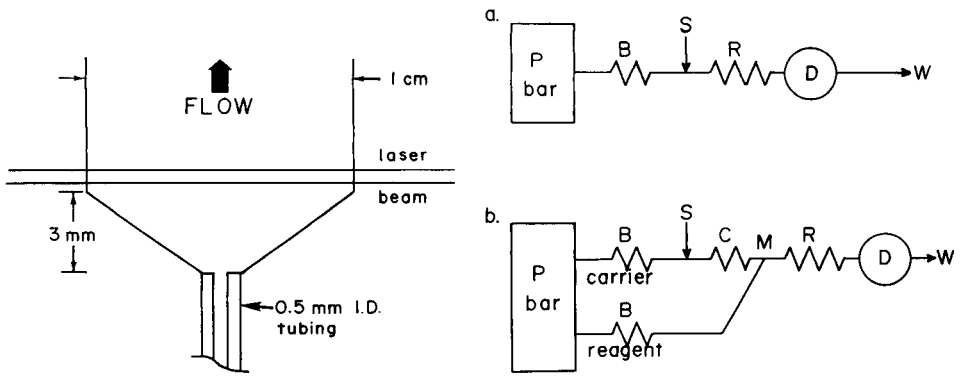

Fig. 1. Flow cell design used. Bulk flow direction perpendicular to the laser beam (not to scale) is indicated by the heavy arrow. Perpendicular to the plane of the page, the depth of the rectangular channel is 1 mm.

Fig. 2. Schematic diagrams of flow-injection manifolds used with thermal lens detection. Fluid streams are pumped with compressed helium at flow rates determined by pressure, P, and the hydrodynamic resistance of braking coils, B. Samples enter the carrier stream at injection valve, S. (a) Single-stream manifold, where a 75-cm coil, R, transfers the sample to the detector, D, and to waste. (b) Two-stream manifold, where sample injections are introduced to the chromogenic reagent at the mixing point M, after passing through a 20-cm delay coil, C.

described previously [20], while organic solutions required an all-teflon rotary value (Rheodyne, Model 50). Sample injection loops were 100 μl in all cases, constructed of tightly coiled 0.5-mm i.d. tubing. Absorbance information was obtained by running repetitive thermal lens experiments at about 2.2 Hz with an 11% illumination duty cycle. Across each thermal lens transient, 100 intensity values were digitized under DMA control (Data Translation, Model DT1761) at a rate of 2 kHz. During the 400 ms between experiments while the sample cooled, $\bar{\theta}$ was calculated for the previous experiment using Eqns. 2 and 7 and a dark signal was digitized and averaged for the following experiment. All calculations were done on an LSI-11-based microcomputer (Terak, Model 8510) running under RT-11 control. After an experimental run, data were smoothed with a 25-point digital filter in order to reduce high-frequency, random fluctuations [21].

Procedures

Performance of thermal lens detection was evaluated using both aqueous and organic carrier streams; and iron was quantified as its 1,10-phenanthroline (1,10-phen) complex in 50:50 methanol/water. Experimental conditions used for these experiments are summarized in Table 1 (also see below). All laboratory-ware was soaked for >1 h in 1:1 sulfuric acid/nitric acid prior to use and then rinsed with deionized water (Sybron/Barnstead Nanopure-3) and methanol (Fisher, Spectrograde).

TABLE 1

Experimental parameters for thermal lens flow-injection systems

Analyte/solvent	Laser power (mW)	Laser wavelength (nm)	Solvent absorbance[a] (10^{-5})	Analyte absorptivity (l mol^{-1} cm^{-1})	Flow rate (ml min^{-1})	D[b]	E[c]
Bromocresol green/ H_2O (2 mM CH_3CO_2Na)	430	647.1	110.0	20010	0.56	1.66	47
Azulene/CCl_4	430	647.1	0.38	173	0.59	1.40	1320
Solvent green 3/ CCl_4	430	647.1	0.38	12780	0.57	1.61	1210
Iron—1,10-phen/ 50:50 methanol/H_2O	500	514.5	22	11100	0.61	3.42	280

[a] 1-cm pathlength. [b] D is the dispersion, defined as $D = C_0/C_{max}$, where C_0 is the original sample concentration, and C_{max} is the concentration at the peak maximum [22]. [c] As defined under Theory.

Bromocresol green in water. The manifold shown in Fig. 2(a) was used. The carrier stream was 2 mM sodium acetate (Fisher) in water, adjusted to pH 9.5 with 1.0 M sodium hydroxide and degassed with helium before use. Standard solutions of bromocresol green (Baker) were prepared by dilution of a 0.672 μM stock solution with the sodium acetate solution in the range 2.7 nM to 0.672 μM. The Kr^+ laser was used.

Azulene and solvent green 3 in carbon tetrachloride. The manifold in Fig. 2(a) was used. The carrier stream was carbon tetrachloride (Fisher Spectrograde), degassed by helium before use. Azulene (Aldrich) standard solutions were made in carbon tetrachloride over the range 14.4 nM to 5.77 μM by dilution of a 0.2886 mM stock solution. Solvent green 3 (Aldrich) standard solutions were made in carbon tetrachloride over the range 0.401 nM to 0.201 μM by dilution of a 2.01 μM stock solution. The Kr^+ laser was used.

Iron—(1,10-phenanthroline [23]. The manifold shown in Fig. 2(b) was used. The carrier stream was 50% (v/v) methanol (Fisher, HPLC grade) and 50% aqueous solution containing 36 mM sodium acetate and 44 mM hydroxyammonium chloride, purified to remove background iron by adsorption onto Amberlite XAD-2 [15, 24]. After mixing, the carrier was degassed with helium. The reagent stream was identical in composition, except for the addition of 1,10-phenanthroline (Aldrich) to give a 0.10 mM reagent solution. Standard iron solutions were prepared over the range of 3.19 μM to 1.6 μM by dilution of a 31.9 μM stock solution of iron(II) ammonium sulfate (MCB, AR grade). The Ar^+ laser was used.

RESULTS AND DISCUSSION

In order to process thermal lens data in real time, one must first determine the time constant, t_c, in advance to provide weighting factors for Eqns. 2 and 6. To allow t_c to be determined under flow-injection conditions, Eqn. 1 was rearranged to a form linear in $1/t$ so that each transient can be processed efficiently and independently

$$[2I(0)/I(t) - 1]^{1/2} = 1/\theta + (t_c/\theta)/t \quad (8)$$

By collecting a number of thermal lens transients across a flow-injected sample and performing a linear least-squares fit of $[2I(0)/I(t) - 1]^{1/2}$ vs. $1/t$ for each transient, t_c was obtained as the ratio of slope/intercept. Typically 40 values of t_c were obtained across a flow-injected peak with the relative standard deviation less than 2%. Values of t_c were independent of θ, for $\theta \leqslant 0.4$, and correlation coefficients for the linear fit were typically $r \geqslant 0.998$.

Real-time processing of thermal lens data was initially characterized by continuously pumping absorbing solutions through the flow cell. When an unweighted average calculated with Eqns. 2 and 3 and the time constants as determined above were used, the uncertainty in evaluating $\theta(t)$ maximized at a time immediately following the shutter opening. In Fig. 3, the expected uncertainty $\sigma_{\theta(t)}$, obtained from Eqn. 6 is plotted vs. time along with experimentally found values of $\sigma_{\theta(t)}$ for $\theta \approx 0.1$. The weighting function as described by Eqn. 6 accurately accounts for the observed uncertainties in $\theta(t)$ for small values of θ.

Substituting Eqn. 6 into Eqn. 7 yields a weighted average which should reduce the effect of these uncertainties on the estimate of $\bar{\theta}$. The improvement in precision relative to a simple average maximizes at about 40% near the limit of detection (Fig. 4). A gradual, logarithmic loss of this improvement is observed as θ increases. This trend is probably due to the assumptions made in deriving the weighting function in Eqn. 5 which do not hold at larger θ. In addition, sources of noise proportional to θ caused by convection [19]

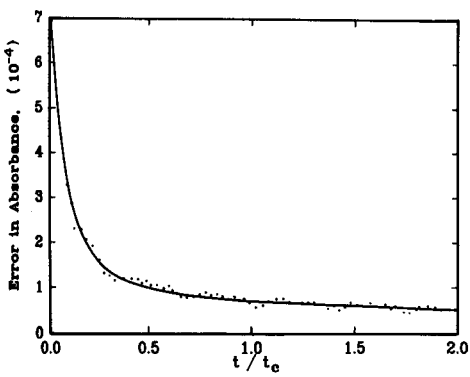

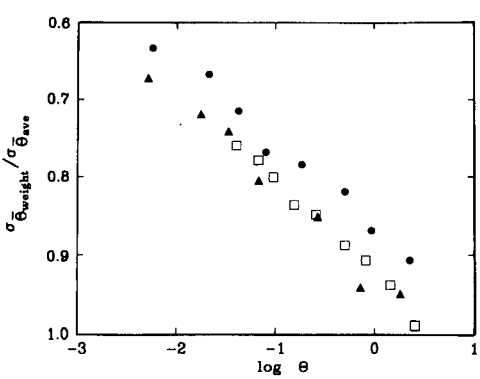

Fig. 3. Standard deviation of measured absorbance vs. time across the thermal lens transient. 100 experiments are averaged for a 2.75×10^{-5} M bromocresol green sample ($A \approx 5.5 \times 10^{-4}$), where t_c = 32 ms. The solid line represents the square root of the weighting function from Eqn. 6, arbitrarily scaled over the same ordinate range as the experimental result.

Fig. 4. Relative precision of weighted estimate relative to a simple average vs. log $\bar{\theta}$: (□) bromocresol green; (●) solvent green 3; (▲) azulene.

or laser power drift are not taken into account by the weighted fit, and may dominate the measurement uncertainty at larger θ.

Detection limits, linear dynamic range, and response time for injected samples were evaluated by constructing calibration graphs over 2.5 or 3 orders of magnitude in sample concentration using aqueous and carbon tetrachloride carrier solutions. The results obtained are summarized in Table 2. Linear correlation coefficients and slopes of log-log plots near 1.0 indicate the linearity of detection response over a wide concentration range. As expected, the detection limit for carbon tetrachloride was superior to that observed for water, because of the more favorable thermo-optical properties and the lower background absorbance of carbon tetrachloride. The responses to triplicate injections of dye solutions are shown in Fig. 5, for aqueous carrier, where the analyte concentration is about 3.3 times the limit of detection, and for carbon tetrachloride carrier with analyte concentration about 18 times the limit of detection. The reproducibility from one injection to the next, in both timing and amplitude of the response, is indicative of the stability of the entire system.

The detection limits of real-time thermal lens monitoring for aqueous samples are smaller by a factor of two at identical flow rates, compared to previous work [26]. This result could be attributed to the greater precision of data analysis, improved flow stability provided by pulse-free pressurized gas pumping, and the use of a flow cell designed to have better laminar flow characteristics. The detection limits for samples in carbon tetrachloride are a factor of 5 lower than results recently reported in static samples [27], indicating the advantages of flow injection for reducing blank-related uncertainties. While an earlier reported thermal lens detection limit in carbon tetrachloride [13] would appear to be superior to these results, that limit was based only on the uncertainty in fitting the thermal lens data transient. Such a limit sets a lower bound on the detection capability but does not account for sample handling and drift contributions to the reproducibility of the blank.

TABLE 2

Flow-injection results with thermal lens detection

Analyte	r^a	Slope[b]	Limits of detection[c]			
			Injected conc. (nM)	Conc. detected (nM)	Absorbance injected (10^{-5})	Absorbance detected (10^{-6})
Bromocresol green[d]	0.9999	0.999	5.5	3.3	11.0	67.0
Azulene[e]	0.9999	1.017	6.4	4.9	0.11	0.85
Solvent green 3[e]	0.9995	1.025	0.18	0.11	0.24	1.4
Iron—1,10-phen[f]	0.9991	0.993	6.4	1.9	7.2	21.0

[a]Correlation coefficient of linear plot. [b]Slope of log—log plot. [c]Defined as 3.29 times the standard deviation of the blank [25], which corresponds to a 95% confidence level. [d]In water (0.2 mM sodium acetate). [e]In carbon tetrachloride. [f]In 50/50 methanol/water.

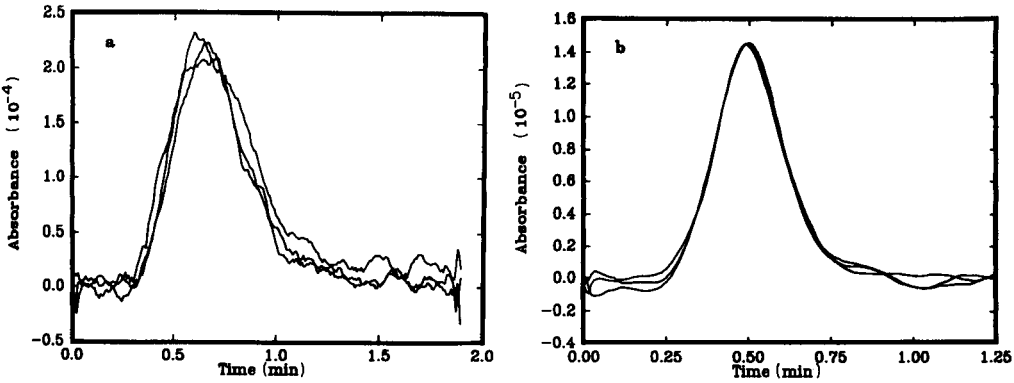

Fig. 5. Detector response to triplicate injections of: (a) bromocresol green in water; (b) azulene in CCl_4.

Quantitative results obtained for a typical spectrophotometric determination, (1,10-phenanthroline) iron(II) in 50:50 methanol/water, are also summarized in Table 2. At the limit of detection, the concentration of iron in the sample injection corresponds to 6.4 nM, or 0.37 ng ml^{-1}. The 100-μl injection volume, therefore, contains about 37 pg of iron. At the flow cell, the iron concentration corresponds to 1.9 nM, or 0.11 ng ml^{-1}. The volume of the beam within the flow cell is only 0.3 μl, therefore, the absorbance measured at the detection limit corresponds to about 34 fg of iron in the beam volume.

A final advantage of flow injection relative to conventional sample handling was observed when a calibration graph was constructed for solvent green in carbon tetrachloride. For static samples, the absorbance decreased with laser radiation exposure, probably because of photodegradation of the analyte during exposure to intense optical power (>1 kW cm^{-2}). The steady loss of sample absorbance was averted by the flowing sample (at 0.57 ml min^{-1}), as shown in Fig. 6 where monitoring of a 2 nM solvent green 3 solution is compared for both flowing and static conditions. The flowing sample shows only slight variation over time, even though a small fraction of absorber is destroyed with each shutter opening. Linearity of the data fit to Eqn. 8 to evaluate t_c was generally poorer ($r \leqslant 0.95$) than with photochemically stable samples because of the changing sample absorbance with time within a single experiment. Even though the time-dependent response was no longer ideal, excellent linearity was obtained for the calibration graph ($r = 0.9995$), with only a 12% decrease in the apparent enhancement.

In summary, flow injection has been shown to be valuable for rapid manipulation of trace-level samples prior to thermal lens detection. Thermal lens detection is generally applicable because both molecular and elemental species can be quantified in either aqueous or organic solvents. Because of the unique solvent dependence of the thermal lens response, which makes

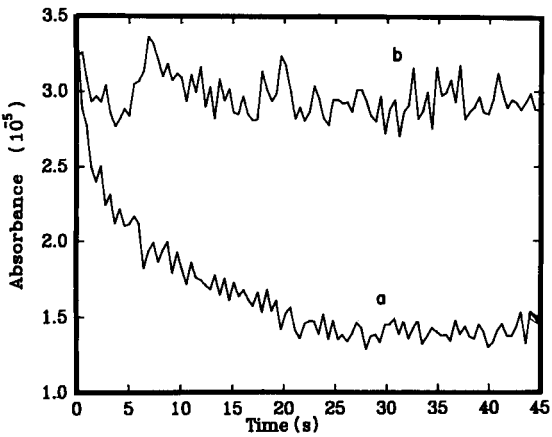

Fig. 6. Sample absorbance vs. time for static (a) and flowing (b) samples. Sample is 4×10^{-9} M solvent green in CCl_4.

nonpolar, organic solvents favorable in terms of sensitivity as well as background absorbance, extraction of analyte into a nonpolar solvent should be considered. Such extraction and phase separations have been routinely incorporated into flow-injection manifolds with excellent results [28].

This work was supported with funds from the National Science Foundation, under Grant CHE82-06898.

REFERENCES

1 T. D. Harris, Anal. Chem., 54 (1982) 741A.
2 C. Hu and J. R. Whinnery, Appl. Opt., 12 (1973) 72.
3 J. M. Harris and N. J. Dovichi, Anal. Chem., 52 (1980) 695A.
4 N. J. Dovichi and J. M. Harris, Anal. Chem., 51 (1979) 728.
5 T. Imasaka, K. Miyaishi and N. Ishibashi, Anal. Chim. Acta, 115 (1980) 407.
6 R. A. Leach and J. M. Harris, J. Chromatogr., 218 (1981) 15.
7 K. Fujiwara, H. Uchiki, F. Shimokoshi, K. Tsunoda, K. Fuwa and T. Kobayashi, Appl. Spectrosc., 36 (1982) 157.
8 K. Miyaishi, T. Imasaka and N. Ishibashi, Anal. Chim. Acta, 124 (1981) 381.
9 C. A. Carter, J. M. Brady and J. M. Harris, Appl. Spectrosc., 36 (1982) 309.
10 C. E. Buffet and M. D. Morris, Anal. Chem., 54 (1982) 1824.
11 K. Fujiwara, W. Lei, H. Uchiki, F. Shimokoshi, K. Fuwa and T. Kobayashi, Anal. Chem., 54 (1982) 2026.
12 C. E. Buffet and M. D. Morris, Anal. Chem., 55 (1983) 376.
13 N. J. Dovichi and J. M. Harris, Anal. Chem., 53 (1981) 106.
14 J. M. Harris, Anal. Chem., 54 (1982) 2337.
15 R. A. Leach, J. Růžička and J. M. Harris, Anal. Chem., 55 (1983) 1669.
16 C. A. Carter and J. M. Harris, Appl. Opt., 23 (1984) 476.
17 P. R. Bevington, Data Reduction and Error Analysis for the Physical Sciences, McGraw-Hill, New York, 1969.
18 N. J. Dovichi and J. M. Harris, Anal. Chem., 52 (1980) 2338.
19 C. E. Buffet and M. D. Morris, Appl. Spectrosc., 37 (1983) 455.

20 J. Růžička, E. H. Hansen and A. U. Ramsing, Anal. Chim. Acta, 134 (1982) 55.
21 A. Savitzky and M. J. E. Golay, Anal. Chem., 36 (1964) 1627.
22 J. Růžička and E. H. Hansen, Flow Injection Analysis, Wiley, New York, 1981.
23 F. Blau, Monatsch. Chem., 19 (1898) 647.
24 R. B. Willis and D. Sangster, Anal. Chem., 48 (1976) 59.
25 L. A. Currie, Anal. Chem., 40 (1968) 586.
26 N. J. Dovichi and J. M. Harris, Anal. Chem., 53 (1981) 689.
27 C. A. Carter and J. M. Harris, Anal. Chem., 56 (1984) 992.
28 B. Karlberg and S. Thelander, Anal. Chim. Acta, 98 (1978) 1.

Analytica Chimica Acta, 164 (1984) 103—109
Elsevier Science Publishers B.V., Amsterdam — Printed in The Netherlands

A COMPARISON OF SPECTROPHOTOMETRIC AND CHEMILUMINESCENCE METHODS FOR THE DETERMINATION OF BLOOD GLUCOSE BY FLOW INJECTION ANALYSIS

P. J. WORSFOLD*
Department of Chemistry, University of Hull, Hull HU6 7RX (Great Britain)
J. FARRELLY and M. S. MATHARU
Department of Chemistry, Sheffield City Polytechnic, Sheffield S1 1WB (Great Britain)
(Received 1st May 1984)

SUMMARY

A flow-injection manifold for the determination of plasma glucose (0—25 mM), incorporating a dialysis unit and a wall-coated enzyme reactor, is described. Spectrophotometric and chemiluminescence methods of detection are compared in terms of precision, accuracy, sample throughput, cost and reliability, and the results obtained from both methods are compared with those obtained from an electrochemical stat analyser.

The feasibility of using flow injection analysis (f.i.a.) for routine applications within a clinical chemistry environment has been illustrated by the number of publications cited in a recent review of the subject by Rocks and Riley [1]. The technique of f.i.a. is simple in concept and application, and with the aid of microcomputer control, would provide the long-term reliability, flexibility and data-handling capability necessary in a clinical chemistry laboratory. It is also economic in terms of capital and running costs, fast, and compatible with essential clinical techniques such as dialysis and reactor tubes (e.g., immobilized enzymes).

One of the most widely reported clinical applications of f.i.a. is the determination of glucose in plasma or serum. Most methods involve the immobilized glucose oxidase (GOD)-catalysed conversion of β-D-glucose and dissolved oxygen to gluconic acid and hydrogen peroxide, whereby β-D-glucose is determined indirectly via a coupled reaction. Early unsegmented continuous-flow procedures included the use of an oxygen electrode [2] and a chemiluminescence reaction with hydrogen peroxide [3]. More recent f.i.a. procedures have included amperometric detection of hydrogen peroxide [4], spectrophotometric detection [5] and chemiluminescence detection using free GOD [6]. At present, however, glucose is generally determined with either a stat analyser (see below) with electrochemical detection for emergency use, or a segmented continuous flow analyser with spectrophotometric detection for routine use. Clearly, the presence of f.i.a. within the

0003-2670/84/$03.00

clinical laboratory, for routine and emergency use has yet to be accomplished. Appropriate commercial systems and further illustrations of the attractions of f.i.a. are therefore required.

This paper describes the use of a manifold for f.i.a., incorporating a dialysis unit and a wall-coated enzyme (GOD) reactor for the determination of plasma glucose. A spectrophotometric method involving the peroxidase-catalysed production of a quinoneimine dye, and a chemiluminescence method involving the iron(III)-catalysed reaction of hydrogen peroxide with luminol, are investigated and their analytical performance is compared with that of a stat analyser incorporating an oxygen electrode.

EXPERIMENTAL

Reagents and samples

Spectrophotometric method. The immobilized enzyme coil (Catalinks, Ames Division, Miles Laboratories) consisted of glucose oxidase (E.C.1.1.3.4) covalently bound to the inner surface of a nylon tube (25 cm long, 1.0 mm i.d.) which was coiled into a cylindrical acrylic exoskeleton. When not in use, the coil was filled with distilled water, capped and stored at 2—8°C. The reagents used were reconstituted with distilled water from kits supplied in conjunction with the coil. Glucose reagent 1 (GR1) contained potassium phosphate (pH 6.5; 0.2 M), disodium-EDTA (12.5 mM), 4-aminophenazone (1.2 mM) and peroxidase (E.C.1.11.1.7; 3000 U l^{-1}). Glucose reagent 2 (GR2) contained potassium phosphate (0.2 M), disodium-EDTA (12.5 mM) and disodium 3,5-dichloro-2-hydroxybenzene sulphonate (HBS, 4.2 mM). Brij-35 was added to GR1 and GR2 (0.3 g l^{-1}) and the reagents were stable for six weeks when stored at 2—8°C. Saline solution (0.18 M) was used as the donor stream for the dialysis unit.

Chemiluminescence method. The immobilized enzyme coil was as described above. Saline solution (0.18 M) was used as the donor stream for the dialysis unit. A solution of phosphate buffer (pH 6.5, 0.2 M) and disodium-EDTA (1.2 mM) was used as the recipient stream for the dialysis unit. The chemiluminescent reagent consisted of a solution of luminol (0.002 M) and sodium carbonate (0.1 M) at pH 11.5 and a solution of potassium hexacyanoferrate(III) (0.025 M).

Standards and samples. D-Glucose standards covering the range 0—25 mM were prepared in saturated benzoic acid solution, at least 24 h before use to ensure attainment of mutarotational equilibrium, and were stored at 2—8°C. Plasma samples in fluoride (glycolysis inhibitor)/oxalate (anticoagulant) tubes were obtained from Doncaster Royal Infirmary (after analysis by an Analox GM6 Stat analyser) and were stored at 2—8°C until required.

Instrumentation and procedures

Spectrophotometric method. The manifold used is shown in Fig. 1. The concurrent donor (saline) and recipient (GR2) streams were pumped at

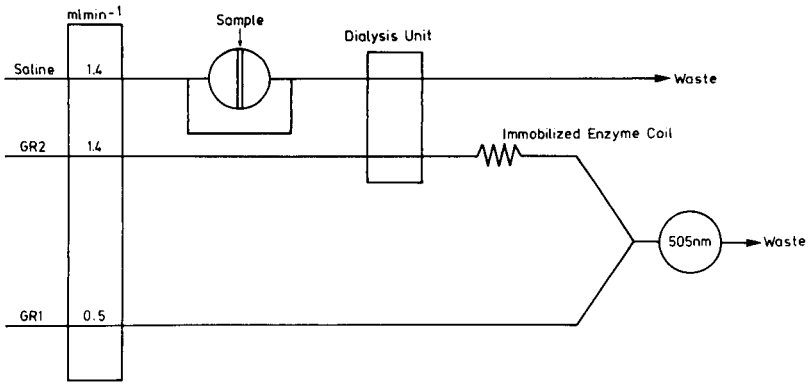

Fig. 1. Manifold for the spectrophotometric determination of plasma glucose. Glucose standards and samples (30 μl) are injected into a buffer stream (GR2) and peroxidase is added downstream (GR1). All tubing is 0.5 mm i.d. Distance from injection valve to dialysis unit, 15 cm; from dialysis unit to immobilized enzyme coil, 15 cm; from coil to confluence point, 15 cm; from confluence point to detector, 35 cm.

1.4 ml min^{-1} and the peroxidase stream (GR1) was pumped at 0.5 ml min^{-1}, using silicone tubing and a peristaltic pump (Ismatec Mini S-840). Polyethylene tubing was used throughout the remainder of the system. Aqueous glucose standards and plasma samples (30 μl) were introduced into the system by means of a rotary PTFE valve, each being injected 5 times. The dialysis unit consisted of two perspex blocks with a triple pass channel machined out of each. The total length of the channel was 240 mm, with a width of 2.0 mm and a depth of 0.3 mm. A preconditioned Cuprophan dialysis membrane (Elkay 170-0406-020) was clamped between the two perspex blocks. The absorbance signal was monitored at 505 nm by using a spectrophotometer (Varian VUV-50) equipped with a flow cell (7.9 μl volume, 10 mm path-length) and a dual analog output. One output signal (1 mV full scale) was fed to a strip-chart recorder (Servograph REC 51) and the other (500 mV for 1.0 absorbance) to a digital multimeter (Hewlett-Packard 3438A, 3½ digit).

Chemiluminescence method. The manifold used is shown in Fig. 2. The concurrent donor (saline) and recipient (phosphate buffer) streams were pumped at 1.0 ml min^{-1} and the luminol and potassium hexacyanoferrate(III) streams at 1.5 ml min^{-1}. The dialysis unit and the sample introduction procedure were as described above. The chemiluminescence signal was monitored by using a modified fluorimeter (Perkin-Elmer 1000). The detection cell consisted of polyethylene tubing (10 cm × 0.5 mm i.d.) tightly coiled and pressed flat against the focussing lens of the photomultiplier tube. Black tape and tubing was used to minimize the amount of stray light reaching the detector. The output signal was obtained directly from the fluorimeter and via a strip-chart recorder.

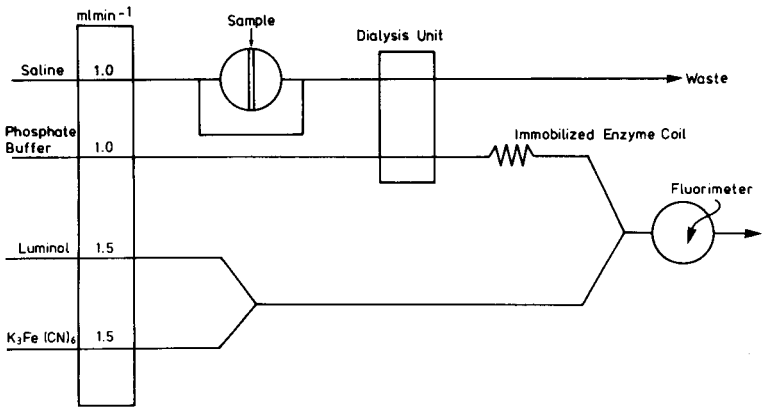

Fig. 2. Manifold for the chemiluminescence determination of plasma glucose. Glucose standards and samples are injected into a buffer stream and luminol/Fe(III) are added downstream. All tubing is 0.5 mm i.d. Distance from injection valve to dialysis unit, 10 cm; from dialysis unit to immobilized enzyme coil, 5 cm; from coil to confluence point, 10 cm; from confluence point to detector, 10 cm).

RESULTS AND DISCUSSION

Spectrophotometric method

The performance of the immobilized GOD coil in a flow-injection manifold without a dialysis unit has been described previously [7]. The results showed that over a wide range of glucose concentrations (0—25 mM) the response was non-linear because of the incomplete conversion of substrate under the stated conditions. The incorporation of a dialysis unit therefore not only removed the protein matrix, and so eliminated viscosity problems in the detector, but also provided a linear response by reducing the amount of substrate reaching the immobilized GOD coil.

Each side of the dialysis unit described above had a surface area of 4.9 cm^2 and a hold-up volume of 150 μl. The flow rates of the donor and recipient streams were matched in order to minimize dispersion within the dialysis unit. By injecting aqueous glucose standards into manifolds with and without the dialysis unit and integrating the resultant peaks the efficiency of transfer was shown to be 13%. Subsequent experiments with whole blood resulted in irreproducible dispersion within both the injection valve and the dialysis unit, because of the high sample viscosity, and therefore all samples were centrifuged and determined as plasma.

Calibration data for aqueous standards (0—25 mM) are given in Table 1. This effectively covers the normal range for plasma glucose (4.2—6.7 mM) [8] as well as hypo- and hyper-glycaemic levels that result from metabolic disorders [8]. The correlation coefficient for the 5 standards (each injected 5 times) was 0.9983 and the relative standard deviations (0.3—2.3%) were adequate for the requirements of the method. A more detailed study over

TABLE 1

Calibration data for the spectrophotometric and chemiluminescence determinations of plasma glucose

Concentration (mM)	Spectrophotometry			Chemiluminescence		
	Mean absorbance[a]	R.s.d. (%)		Mean signal[a,c]	R.s.d. (%)	
		Within batch	Between batch[b]		Within batch	Between batch[d]
5.0	0.0076	1.5	9.4	53	2.2	3.5
10.0	0.0132	2.3	6.6	107	1.4	3.7
15.0	0.0192	0.6	6.1	162	1.3	2.2
20.0	0.0268	1.9	4.3	212	3.9	2.9
25.0	0.0336	0.3	11.3	264	2.2	2.4

[a]All results are means of 5 measurements. [b]Pooled data for 20 measurements over 8 weeks. [c]Relative intensity. [d]Pooled data for 10 measurements over 1 week.

the range 0—10 mM glucose gave similar results. The day-to-day precision was determined by injecting the standards every two weeks for an 8-week period and pooling the results. As can be seen from Table 1, the day-to-day precision ranged from 4.3 to 11.3% and this can be attributed to a small but steady drift over the 8-week period as the activity of the immobilized enzyme coil slowly decreased. However, with a throughput of 75 samples h^{-1} (as compared with a literature value of 60 samples h^{-1} for the Analox GM6 Analyser), recalibration can be done regularly if such accuracy is required. The sample volume injected each time was 30 μl, with less than 100 μl being required in practice for each determination. If even smaller sample volumes are required (e.g., for paediatric work), direct aspiration via a stepping motor-controlled sample probe can be used [9]. The comparative analysis of plasma samples by the above method and by a stat analyser is discussed below.

Chemiluminescence method

Flow injection analysis is excellent for the study of chemiluminescence processes [10] and indeed an enzymatic procedure for glucose with chemiluminescence detection has been reported [6]. The manifold used for the present studies (Fig. 2) incorporates the usual design features of a T-piece for rapid mixing of reagent and sample, a very short mixing coil and a tightly coiled length of tubing serving as the flow cell, but it also incorporates a dialysis unit, which effectively eliminates viscosity effects [6], and an immobilized enzyme coil, which reduces reagent costs. The pH and flow rate of the reagent streams were designed to provide a suitable pH for both the glucose oxidase reaction (pH 6.5) and the luminol reaction (pH 10). Thus the system described above combines the speed and simplicity of f.i.a. with the sensitivity of chemiluminescence and the selectivity and economy of

immobilized enzymes, and would be appropriate for the study of many other enzymatic assays.

Calibration data for aqueous standards (0—25 mM) are given in Table 1. The correlation coefficient for the five standards (each injected 5 times) was excellent (0.9999) and the relative standard deviations (1.3—3.9%) were only slightly higher than those obtained by spectrophotometric detection. Similar results were obtained over the 0—10 mM glucose range. The between-batch precision for ten experiments over a one-week period ranged from 2.2 to 3.7%, which indicates the stability of the system over this time span. A sample throughput of 75 h^{-1} again compares favourably with alternative methods and could be further improved by the design of a more efficient immobilized enzyme reactor (e.g., packed column or single bead string) and dialysis unit. The comparative analysis of plasma samples by the above method and by a stat analyser is discussed below.

Comparison of methods

A random batch of ten plasma samples in fluoride/oxalate containers was analysed by both the spectrophotometric and chemiluminescence methods after analysis by a stat analyser containing an oxygen electrode as the sensor (Analox GM6). The correlations between the results obtained using the oxygen electrode and those obtained from the two flow-injection methods are given in Fig. 3, and can be summarized as follows:

(spectrophotometry) = 1.13 (oxygen electrode) − 1.64; r = 0.972

(chemiluminescence) = 1.13 (oxygen electrode) − 1.19; r = 0.988 where

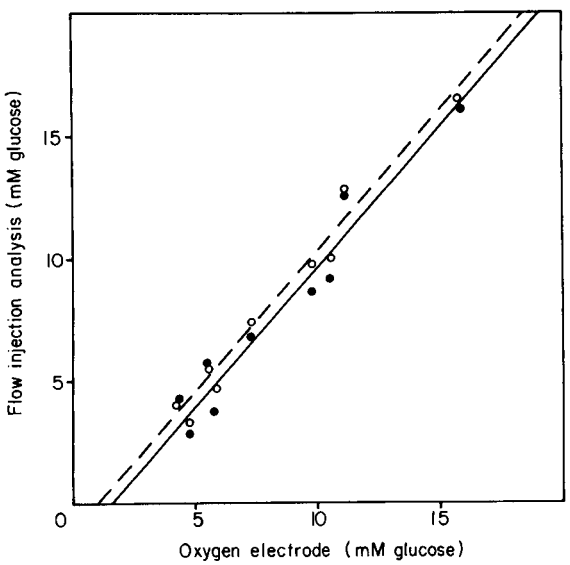

Fig. 3. Correlation of results for plasma glucose between the stat analyser method (oxygen electrode) and (•) the spectrophotometric flow-injection method, (○) the chemiluminescence flow-injection method.

the items in parentheses represent the glucose concentrations in mM obtained by the procedure named.

The correlation coefficients (r) for both methods over the range examined, together with their sample throughputs, indicate that they are both acceptable methods for emergency and small batch applications. A more detailed calibration procedure coupled with the use of control standards should also make either method suitable for routine application. The spectrophotometric method has the advantage of being in routine use with segmented continuous flow systems and therefore the detector, reagents and practical experience are readily available. The chemiluminescence method, however, is very sensitive, does not require the use of a second free enzyme (peroxidase), needs only a photomultiplier and power supply for detection, and has considerable scope for coupling with other peroxide-producing reactions. The use of bioluminescence reagents would extend the sensitivity and application of the technique even further [11].

Conclusions

The efficacy of an on-line dialysis unit and immobilized enzyme coil within a flow-injection manifold is clearly shown by the above results. The use of the spectrophotometric and chemiluminescence detectors further illustrates the versatility of f.i.a. and its suitability for application within a clinical chemistry laboratory. The scope for combining immobilized enzyme technology, chemiluminescence or bioluminescence reactions and f.i.a. is clearly very wide.

The authors are indebted to Ames Division of Miles Laboratories for the provision of Catalinks immobilized glucose-oxidase coils and glucose reagents and to John Leverton of Doncaster Royal Infirmary for the provision of analysed plasma glucose samples.

REFERENCES

1 B. Rocks and C. Riley, Clin. Chem., 28 (1982) 409.
2 H. U. Bergmeyer and A. Hagen, Z. Anal. Chem., 261 (1972) 333.
3 D. T. Bostick and D. M. Hercules, Anal. Chem., 47 (1975) 447.
4 B. Watson, D. N. Stifel and F. E. Semersky, Anal. Chim. Acta, 106 (233) 1979.
5 L. Gorton and L. Ögren, Anal. Chim. Acta, 130 (1981) 45.
6 C. Ridder, E. H. Hansen and J. Růžička, Anal. Lett., 15 (1982) 1751.
7 P. J. Worsfold, Anal. Chim. Acta, 145 (1983) 117.
8 J. F. Zilva and P. R. Pannall, Clinical Chemistry in Diagnosis and Treatment, Lloyd-Luke, London, 1981, pp. 174—211.
9 C. Riley, L. H. Aslett, B. F. Rocks, R. A. Sherwood, J. D. M. Watson and J. Morgon, Clin. Chem., 29 (1983) 332.
10 G. Rule and W. R. Seitz, Clin. Chem., 25 (1979) 1635.
11 L. J. Kricka and T. J. N. Carter (Eds.), Clinical and Biochemical Analysis, Vol. 12, Clinical and Biochemical Luminescence, M. Dekker, New York, 1982.

Analytica Chimica Acta, 164 (1984) 111—118
Elsevier Science Publishers B.V., Amsterdam — Printed in The Netherlands

INVESTIGATION OF THE SURFACE OF A POLYMERIC ADSORBENT WITH PYRENE AS A FLUORESCENCE PROBE

MICHAEL R. RICE and HARVEY S. GOLD*
Department of Chemistry, University of Delaware, Newark, DE 19716 (U.S.A.)
(Received 5th April 1984)

SUMMARY

Pyrene was used as a fluorescence probe to study the surface and pyrene/surface interactions which occur on a polypropylene adsorbent. The surface interaction between this adsorbent and pyrene was found to be very similar to that found for pyrene in hydrocarbon solvents. In contrast to the surfaces of other types of adsorbents, the polypropylene surface presents an energetically homogeneous surface to adsorbing molecules. Consequently, adsorption takes place essentially randomly as opposed to being associated with activated sites.

The photophysical properties of pyrene have led to its use as a fluorescence probe in a variety of applications. The fluorescence emission spectrum of pyrene monomer exhibits unusually detailed vibronic fine structure at room temperature. The relative intensity of each vibronic band has been found to be very sensitive to the microenvironment of the pyrene molecule. These effects of ambience on monomer emission have been studied in detail [1] by observing the variations in the intensity of vibronic bands in a large number of solvents. Dong and Winnik [2] have advocated the use of this feature as a scale for solvent polarity. The sensitivity of the vibronic fine structure of pyrene to its local ambience has been utilized in systems of biochemical interest [3] and in assessing the nature of micellular systems [4].

Because of the rather long excited-state lifetime of pyrene, excimer formation is routine in sufficiently concentrated solutions. Indeed, crystalline pyrene exhibits excimer emission exclusively. Excimer fluorescence occurs as the result of diffusion of an excited-state molecule to within a critical distance of a ground-state molecule [5]. When this occurs, and if the molecules are in the proper spatial orientation, an excited-state dimer (excimer) forms, which may in turn emit photons which are red-shifted relative to the monomer emission. The dimer then dissociates rapidly. Excimer fluorescence is therefore useful for elucidation of the proximity and orientation of neighboring pyrene molecules, especially in the adsorbed state.

Excimer emission observed from polystyrene films doped with pyrene has been found to be caused by ground-state molecular pairs [6]. Similarly,

0003-2670/84/$03.00

ground-state molecular pairs form on silica gel containing adsorbed pyrene [7]; Baüer et al. [7] also inferred that the distribution of active sites on the surface is non-random. The non-random distribution of active sites has been observed via (intramolecular) pyrene excimer emission for the case of molecules chemically bound to silica gel containing a pyrene moiety [8].

In the work cited above, the appearance or absence of excimer emission has been interpreted in various ways in order to explain the nature of the adsorption process. The surfaces investigated were generally heterogeneous with respect to the distribution of the adsorption sites, which maximizes excimer formation because molecules are forced to occupy sites in relatively close proximity. Because the active sites are heterogeneously distributed, so must be the adsorbed molecules. This situation leads to excimer or "excimer-like" fluorescence at surface coverages significantly lower than a statistical monolayer, especially in the case of silica gel.

In the present study, pyrene fluorescence observed from adsorbed-state molecules on polypropylene was investigated. The motivation for this work derived from previous studies which showed that polypropylene is a good adsorbent for the preconcentration of organic molecules present in aqueous solution at trace levels [9]. The nature of the adsorption process and the surface microenvironment of polypropylene is revealed by the fluorescence spectral characteristics of adsorbed pyrene.

EXPERIMENTAL

Polypropylene was obtained from Polysciences (Warington, PA; chromatographic grade, catalog 4342). It was washed with cyclohexane (spectral grade) and tetrahydrofuran (THF; Burdick and Jackson, Muskegon, MI; distilled-in-glass grade) before use. Pyrene was obtained from Aldrich Chemical Company (Milwaukee, WI).

Fluorescence spectra were acquired using a Perkin-Elmer 650-10S spectrofluorimeter equipped with a Hamamatsu R928 extended red-response multi-alkali photomultiplier tube. Fluorescence spectra were acquired at 25°C using a triangular cell.

Pyrene was adsorbed on the polypropylene from THF as previously reported [9], except that samples were not degassed after preparation. Absence of interference from solvent effects on the adsorbed pyrene was validated as described below.

RESULTS AND DISCUSSION

Initially, pyrene was adsorbed on polypropylene from aqueous solution. This procedure proved to be tedious because large volumes of solution were required to achieve high loadings because of the low solubility (6.4×10^{-7} M [10]) of pyrene in water. Consequently, a procedure was developed with THF as the solvent, resulting in considerably more efficient

sample preparation. In order to compare the results obtained with the two methods, use was made of the observation by Kalyanasundaram and Thomas [1] that the ratio of the intensities of the peaks at 383 nm and 372 nm is very sensitive to the microenvironment of the molecule. A comparison of the fluorescence spectra obtained from samples prepared by the two methods is shown in Fig. 1. The fluorescence emission of pyrene dissolved in THF is also shown on this figure. The spectra obtained from samples prepared by the two methods are quantitatively the same, as can be seen from the 383/372-nm ratio, which is 1.68 in each case. This observation indicates that pyrene experiences the same environment regardless of differences in sample preparation technique. If the emission spectrum is examined before complete evaporation of THF, the peak at 372 nm is enhanced relative to the peak at 383 nm, resulting in a smaller value of the 383/372-nm ratio. This is in accord with the findings of Kalyanasundaram and Thomas [1] that polar environments tend to enhance the peak at 372 nm. From these observations, it is clear that adsorption from THF solution results in a sample that is free of artifacts produced by interaction with any residual solvent.

As indicated above, the 383/372-nm ratio and the overall appearance of the emission spectrum are very sensitive to the microenvironment encountered by the molecule. Not surprisingly, the features of the fluorescence spectra shown in Fig. 1 imply an environment much like that found in hydrocarbon solvents. Tables of 383/372-nm ratios published by Kalyanasundaram and Thomas [1] and more recently by Dong and Winnik [2] indicate that the values for hydrocarbons fall within the narrow range 1.65—1.80. Values for pyrene adsorbed on silica gel estimated from the work of Bauer et al. [7] and when present as a dopant in polystyrene [6] are consistent with the values found for pyrene in polar solvents such as water and acetonitrile and in aromatic solvents, respectively. These observations are all in agreement with expectations, and illustrate the utility of using pyrene as a probe of the surface microenvironments which are present on these materials.

The specific surface area of the polypropylene used in these studies was found by BET measurement to be 1 $m^2\ g^{-1}$. In order to derive an estimate of the coverage obtained for a given amount of pyrene adsorbed on a sample, the following calculation was done. A reasonable estimate of the area per molecule of pyrene is 91 $Å^2$ [11]. The total coverage for a given sample is then calculated from the moles adsorbed per gram of polypropylene, assuming that the molecules are adsorbed "flat" (i.e., the molecular plane parallel to the surface). If the assumption of flat adsorption is correct, then the estimate of coverages should be reasonably accurate. The coverage of the sample used to acquire spectrum B in Fig. 1, for example, is approximately 0.5 of the total surface area. Any other assumption regarding orientation of the pyrene molecule on adsorption onto the surface leads to lower apparent surface coverage.

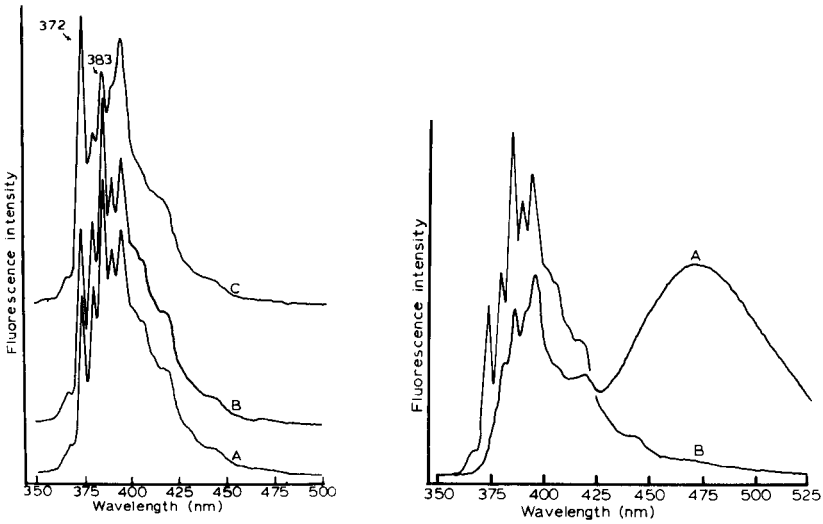

Fig. 1. Molecular fluorescence emission spectra for pyrene: (A) adsorbed on polypropylene from THF solution, 0.2 mg g^{-1} of polypropylene; (B) adsorbed on polypropylene from aqueous solution, 0.2 mg g^{-1} of polypropylene; (C) 1.6 mg l^{-1} pyrene in THF solution. The excitation wavelength was 310 nm in each instance. For clarity, spectra B and C are displaced vertically, and the locations of the 372 and 383 nm peaks are shown.

Fig. 2. Molecular fluorescence emission spectra of pyrene; (A) 2000 mg l^{-1} pyrene in THF; (B) adsorbed-state, 4 mg g^{-1} of polypropylene. The excitation wavelength was 310 nm.

In order to study the effect of higher loadings on the fluorescence spectrum of adsorbed pyrene, samples were prepared containing pyrene in the range from 0.2 mg (curve B, Fig. 1) to 20 mg g^{-1} of polypropylene. Figure 2 shows the emission spectrum (A) obtained from a 2000 mg l^{-1} pyrene solution in THF. There are two points of interest: (1) the intensity of the high-energy vibronic bands is diminished by an inner filter effect; (2) there is a broad, featureless excimer emission centered around 465 nm. The emission spectrum (B) of adsorbed-state pyrene at a loading of 4 mg g^{-1} is also shown in Fig. 2. At this loading, the surface coverage is calculated to be greater than 10 times the surface area of the polypropylene. If the molecules were indeed adsorbing flat as assumed above, then the excimer emission would be expected to be a significant fraction of the total emission because of stacking of molecules on the surface. As can be seen from Fig. 2 (curve B), this is clearly not occurring. On the contrary, the monomer emission is clearly very strong, with little or no excimer emission evident. This provides strong evidence that adsorption is not flat, but occurs in another, perhaps essentially random, orientation.

This behavior of pyrene on polypropylene can be compared to the case of pyrene adsorption on silica gel [7, 12]. Silica gel exhibits excimer fluores-

cence at loadings as low as 3%. This behavior has been ascribed to the heterogeneous dispersion [7] of active sites on the surface of silica gel. This non-random distribution allows pyrene molecules to aggregate and thus form ground-state associations which emit "excimer-like" fluorescence. The lack of excimer fluorescence from pyrene adsorbed on polypropylene in spectrum B (Fig. 2) indicates that an essentially uniform surface is present, across which the pyrene is randomly distributed rather than being associated with some active site as on silica gel. In fact, it is possible that pyrene molecules are able to diffuse into the polypropylene particles, thereby lowering the effective surface concentration, increasing intermolecular separation, and suppressing excimer formation.

No unequivocal excimer fluorescence is observed until the calculated surface coverage reaches 50 times the surface area of the polymer (at a loading of 20 mg g^{-1}). Figure 3 shows the emission spectrum of a sample with this loading; excimer emission is evident in this spectrum, although it is still quite weak. The source of the excimer emission becomes important at this point. Specifically, the emission could arise from ground-state associations as has been found in the cases of polystyrene [6] and silica gel [7], or it could be due to the formation of microcrystals on the surface of the polymer particles. In order to address this issue, the excitation spectra of the various samples were examined.

Figure 4 (spectrum A) is the excitation spectrum of a 1.6 mg l^{-1} pyrene solution in THF. Figure 4 (spectrum B) is the excitation spectrum of the

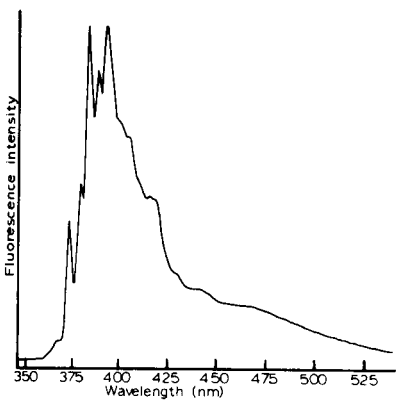

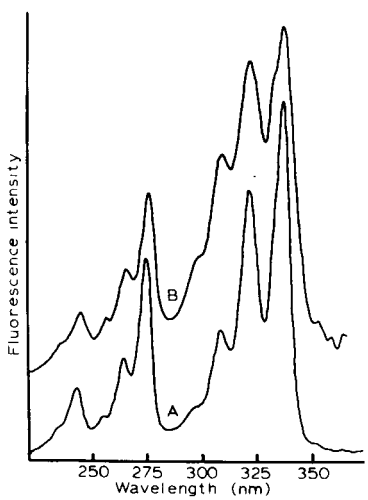

Fig. 3. Molecular fluorescence emission spectrum of adsorbed-state pyrene at a loading of 20 mg g^{-1} of polypropylene. The excitation wavelength was 310 nm.

Fig. 4. Molecular fluorescence excitation spectrum: (A) 1.6 mg l^{-1} pyrene in THF; (B) adsorbed-state pyrene at a loading of 0.2 mg g^{-1} of polypropylene. The emission wavelength was 383 nm. Spectrum B is displaced upwards for clarity.

0.2 mg g^{-1} loading sample of adsorbed pyrene corresponding to the emission spectrum B shown in Fig. 1. The two spectra are clearly identical in terms of the pattern and the position of the vibronic bands. This may be compared to Fig. 5, the excitation spectra of the 20 mg g^{-1} sample of which the emission spectrum is shown in Fig. 3. Figure 5 shows the excitation spectrum (A) of the sample observed at 377 nm (the monomer emission region), while spectrum B is for the same sample observed at 475 nm (the excimer emission region). Spectrum A in Fig. 5 is very similar to the excitation spectrum in dilute solution except that the peaks are broader, resulting in loss of resolution. Overlapping this spectrum is spectrum B, which is that due to the excimer fluorescence. In the region from 289 nm to 345 nm, a plateau is observed which exhibits several peaks. The spectrum then rises to a maximum that does not coincide with the monomer absorption. Initially, this was interpreted as evidence of a ground-state association similar to those observed by earlier workers [6, 7]. However, closer inspection reveals that the peaks in the region from 280 nm to 345 nm are the result of "inverted peaks". The minima in this region correspond to the maxima in the monomer absorption spectrum and may result from absorption of incident radiation by monomer molecules which do not fluoresce at the observation wavelength in the excimer emission region. It is therefore reasonable to conclude that the features in this region are artifacts caused by overlapping absorption and fluorescence emission spectra, and are in fact not real fluorescence transitions in their own right at all. This observation dramatically points out the care that must be exercised when studying systems such as these.

The fluorescence emission and excitation spectra of microcrystalline pyrene are shown in Fig. 6. Comparison of the excitation spectrum A (Fig. 6) with spectrum B in Fig. 5 reveals similarities in the region from 350 nm to 375 nm which is the region least obscured in the adsorbed-state spectrum. The emission spectrum (B, Fig. 6) of the crystalline solid has a broad band which peaks at about 465 nm, in agreement with the excimer peak in the adsorbed-state spectrum. From these observations, it must be concluded that the excimer fluorescence results from the formation of species which are very similar to microcrystalline pyrene. This conclusion is based on the appearance of the excitation spectra acquired from the adsorbed-state sample. If excimer fluorescence resulted from diffusional processes as in solution, there would be no difference among the excitation spectra A and B presented as Fig. 5. If, however, a ground-state association was responsible for the excimer fluorescence, then the excitation spectrum (B, Fig. 5) observed at the excimer emission wavelength would be expected to exhibit differences when compared to the excitation spectrum of crystalline pyrene. This is not observed and the previous conclusion must stand.

Finally, in order to determine whether residual unsaturation of the surface of the polypropylene particles is an important factor affecting the adsorption of pyrene, the following experiment was done. Polypropylene (1 g)

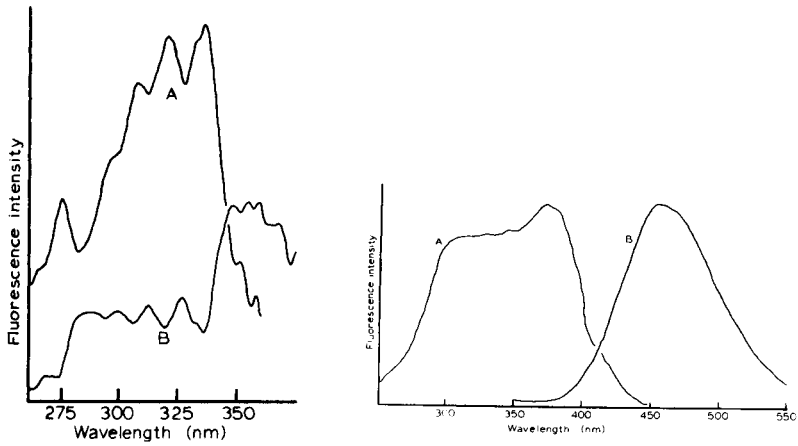

Fig. 5. Molecular fluorescence excitation spectrum of adsorbed-state pyrene at a loading of 20 mg g^{-1} of polypropylene observed with an emission wavelength of (A) 377 nm and (B) 475 nm.

Fig. 6. Molecular fluorescence spectra of pyrene as a microcrystalline solid: (A) excitation spectrum with an emission wavelength of 475 nm; (B) emission spectrum with an excitation wavelength of 318 nm.

was stirred in a solution of 5% (v/v) bromine dissolved in ethanol for 3.5 h in order to brominate any residual unsaturated groups [13]. The polymer was recovered and washed with ethanol and then heated to 35°C in vacuo for 72 h. Pyrene was then adsorbed in the usual manner and the emission spectrum was recorded as described above. No differences were observed when the fluorescence spectrum of this sample (0.2 mg g^{-1}) was compared to the earlier sample (B, Fig. 1). If there is any residual surface unsaturation, it is quite apparent that it is of little importance as a component of the surface microenvironment.

Conclusion

Pyrene can be a valuable tool for assessing the nature of a surface when its fluorescent properties are investigated in the adsorbed state. Polypropylene, which was previously shown to be a good adsorbent for the concentration of trace organic materials from aqueous solution, has been characterized by the pyrene emission and excitation spectra. The surface of the polypropylene used in this study was found to be energetically homogeneous, and there do not appear to be any active surface sites (in contrast to the case of silica gel). Consequently, the adsorbed pyrene is present on the surface in essentially a random distribution. Because a large amount of pyrene can be adsorbed on the surface compared to the measured surface area before excimer fluorescence occurs, pyrene appears to be able to diffuse into the polymer particles to some extent. This would have the effect of lowering the effective surface concentration of pyrene for any given sample.

While diffusion of pyrene into the polypropylene is as yet unproven, the results of recent preliminary controlled thermal-desorption mass spectrometric studies of these samples are consistent with this conclusion. These mass spectral studies show behavior which parallels that observed for systems with incorporated additives and suggest that pyrene on polypropylene is diffused into the bulk rather than being present on the surface. More detailed mass spectrometric studies are presently in progress.

All of the fluorescence observations and the conclusions based thereon are the result of steady-state measurements. A disadvantage is that samples with intrinsically high background fluorescence may not be amenable to this particular fluorescence probe approach. A promising avenue of future research would be time-dependent fluorescence measurements of these systems.

REFERENCES

1 K. Kalyanasundaram and J. K. Thomas, J. Am. Chem. Soc., 99 (1977) 2039.
2 D. C. Dong and M. A. Winnik, Photochem. Photobiol., 35 (1982) 17.
3 P. Lianos, A. K. Mukhopadhyay and S. Georghian, Photochem. Photobiol., 32 (1980) 415.
4 P. Lianos and R. Zana, J. Phys. Chem., 84 (1980) 3339.
5 Th. Forster, Angew. Chem. Int. Ed. Engl., 8 (1969) 333.
6 G. E. Johnson, Macromolecules, 13 (1980) 839.
7 R. K. Bauer, P. de Mayo, W. R. Ware and K. C. Wu, J. Phys. Chem., 86 (1982) 3781.
8 C. H. Lochmüller, A. S. Colburn, M. L. Hunnicutt and J. M. Harris, Anal. Chem., 55 (1983) 1344.
9 M. R. Rice and H. S. Gold, Anal. Chem., 56 (1984) 1436.
10 W. E. May, S. P. Warik and D. H. Freeman, Anal. Chem., 50 (1978) 997.
11 L. D. Snyder, Principles of Adsorption Chromatography. The Separation of Nonionic Organic Compounds, M. Dekker, New York, 1968, p. 200.
12 C. Francis, J. Lin and L. A. Singer, Chem. Phys. Lett., 94 (1983) 162.
13 J. N. Lomonte, Anal. Chem., 34 (1962) 129.

Analytica Chimica Acta, 164 (1984) 119—126
Elsevier Science Publishers B.V., Amsterdam — Printed in The Netherlands

A DIFFERENTIAL PHOTOACOUSTIC MERCURY DETECTOR

J. E. PATTERSON

Chemistry Division, Department of Scientific and Industrial Research, Private Bag, Petone (New Zealand)

(Received 23rd May 1984)

SUMMARY

A sensitive instrument for the detection of mercury is described. The difference in mercury concentration between two identical flow-through silica cells is measured by means of the photoacoustic effect. The cells are illuminated laterally by a 20-W germicidal mercury discharge lamp. A microphone in each cell detects pressure changes produced when mercury vapour absorbs resonance radiation from the lamp and releases the energy to nitrogen flowing in the partially closed cells, as heat derived from quenched fluorescence. A differential microphone connection discriminates against ambient noise and contributes to a detection limit of less than 0.02 ng of mercury with a linear response up to 70 ng. Variables such as gold collector design and heating rate, inlet filters and traps, changes in carrier gas flow, carrier gas composition, lamp operating current and modulation frequency which all affect instrument performance are discussed. Photochemical loss of mercury can be avoided if dry nitrogen, carbon dioxide, or air is used as the carrier gas provided contamination by avid vapours and water is prevented by a calcium oxide trap at the inlet.

Tyndall [1] was the first to observe the photoacoustic effect [2] of gases in 1881. The photoacoustic effect in mercury vapour was first observed by Bell and Tyndall [3] as part of a study of light absorption by gases with chopped sunlight as a source. This may have been molecular absorption in the infrared by traces of diatomic mercury in the saturated vapour. The first observation based on mercury resonance radiation at 253.7 nm was made by Bresler and Ruzin [4] in a cell saturated with mercury vapour illuminated by a mercury discharge lamp. A fall in intensity was observed with time which was restored by removing the illumination for a short period or by the addition of hydrogen to the air and mercury vapour in the cell. The analytical possibilities were not considered. Roe and Cary [5] detected mercury down to 0.05 ng, using a photoacoustic instrument but did not publish their results or a description of apparatus. More recently, a practical instrument was described [6] and some performance data were given.

This paper discusses an improved instrument and the results of experiments conducted to investigate factors influencing its performance. The principal improvement is a twin cell arrangement with microphones connected differentially so as to cancel most ambient noise. This improves the detection limit without requiring lock-in detection of signals. The twin cells may be physically

0003-2670/84/$03.00

connected in series, in parallel, or used singly while the microphones remain connected differentially to cancel external noise. A second improvement is an electrically heated gold-collection system controlled by a solid-state timer. The heating rate and gas flow are optimized so that the total sample fills the cell before any significant proportion exits. This delivers the maximum signal for a given amount of mercury. Signal processing is based on full-wave detection which gives a positive output for mercury in either cell and a positive difference signal for mercury in both cells. A peak detector stores the maximum amplitude of the signal and avoids the need for a chart recorder.

Variables affecting performance which have been investigated include the gold collector design and heating rate, inlet filters and traps, light source current and modulation frequency, and flow rate and composition of the carrier gas.

EXPERIMENTAL

Construction of the instrument is not complicated. A fully housed or a breadboard form of construction may be used according to preference. In either case, attention must be paid to electrical safety and exposure to ultraviolet radiation.

The light source is a Thorn Hytek (15W 92-2013) germicidal lamp, which does not produce ozone; the Philips TUV-15W germicidal lamp should also be suitable. The cells are 450-mm lengths of clear silica tubing (6.7 mm i.d., 0.7 mm wall thickness) each with a side arm 20 mm from one end to accommodate the microphones (Fig. 1). In a recent version, the microphones are accommodated in separate threaded glass T-tubes with plastic caps on two

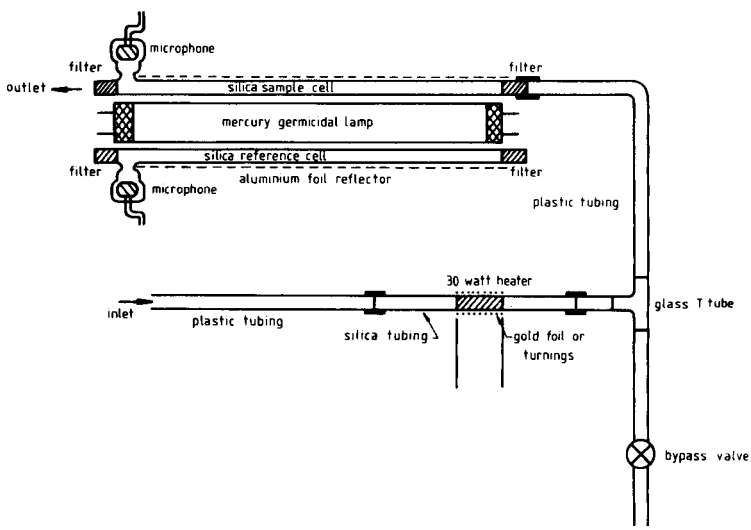

Fig. 1. Basic cell arrangement with one cell acting as a static reference cell.

arms. One arm of the T-tube supports the microphone, another arm has a threaded sealing adaptor for the silica cell and a cellulose filter fills the third. Fittings such as stainless steel Swagelok or plastic equivalents could also be adapted. The cellulose filters sold for "roll-your-own" cigarettes have proven ideal as cell-terminating filters. The cells and light source are wrapped in aluminium foil as previously described [6] with emphasis on electrical safety and minimizing exposure to stray ultraviolet light. Signal amplitudes are approximately doubled when the foil is in place.

The microphones are cheap 9.5-mm diameter electrets with an in-built FET preamplifier. Microphones of larger diameter might give an improved response at the low frequencies (50 Hz) used here. The microphones are mounted so that the diaphragm does not encounter static pressure from the carrier gas. They are mounted inside the cell T-tubes with an air-tight seal made around the leads (Fig. 1). The clearance between the microphone and the inner wall of the T-tube is kept small (about 0.1 mm). To reduce electrical interference from the lamp and nearby wiring, a foil shield connected to an earth potential surrounds the microphones. Acoustic isolation measures required are minimal. The transformer and ballast are rubber-mounted to reduce coupling via the baseplate. The microphone leads are clamped to the baseplate. For measurements at trace levels (<0.1 ng), more stringent isolation may be needed if laboratory acoustic noise levels are high.

The circuit is outlined as a block diagram in Fig. 2. The signal processing consists of several discrete stages. The first four stages comprise a single TL084 Quad FET operational amplifier. The microphones derive power from the circuit via 10 kohm dropping resistors. The twin T-circuit (50 Hz)

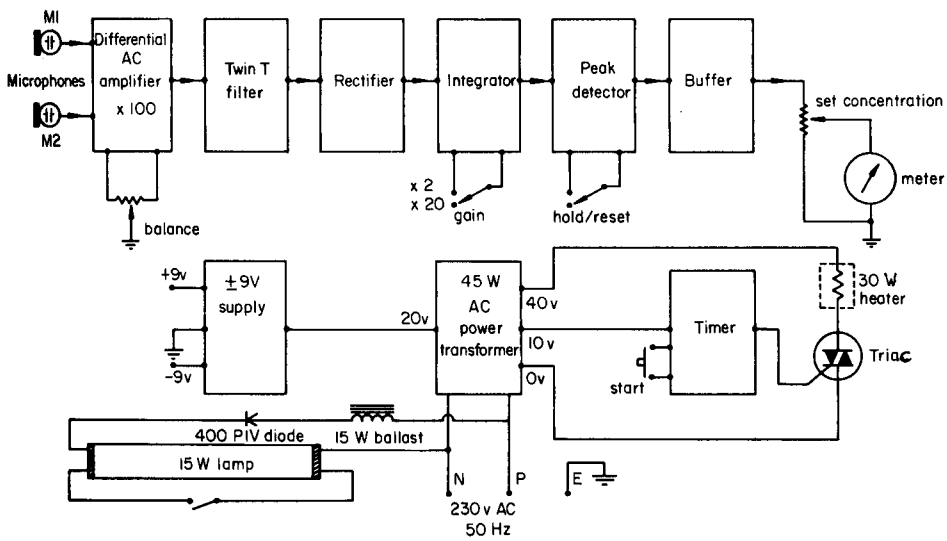

Fig. 2. Electronics block diagram showing signal processing electronics, the gold heater timer, lamp circuitry and power supplies.

has been described previously [6]. Here a 220 kohm resistor is used to broaden the response to take account of short-term shifts in mains frequency. The full-wave precision rectifier is a single amplifier design; the absence of any signal or two input signals of equal amplitude results in no output, whereas any other condition produces a positive output proportional to the difference in the microphone signal amplitudes. The discharging integrator smooths signals and has a gain of 2 or 20 with time constants of 0.4 or 4 s, respectively. For transient signals from heated gold collectors, for example, the higher gain is reduced by about half because of the long time constant of 4 s. The peak detector uses a 741c operational amplifier and a 4.7 μF storage capacitor. The buffer using a TLO81 FET operational amplifier prevents discharge of the storage capacitor. A gain control at the output allows stored readings to be varied, thus simplifying calibration. A digital voltmeter is used for display, reading directly in nanograms. A 555 timer and SC142D triac control the gold collector heater, allowing it to heat for 30 s to release collected mercury. The timer prevents overheating of the gold, thus allowing a fast heating rate to be employed. The lamp is supplied with half-wave rectified power switching at 50 Hz. A thermally operated starter is suitable for starting germicidal lamps on half-wave supplies. Gas discharge starters may give unreliable results.

There are several ways of linking the two photoacoustic cells. If they are connected in tandem, one cell may be used to preview the amplitude of the mercury signal before gold collection. Appropriate gain adjustments may then be made to observe the expected signal. The simplest arrangement is to leave one cell unused as a background reference (Fig. 1). If the mercury levels are high in laboratory air, then the reference cell should be connected in tandem with the outlet of the sample cell to keep it purged with clean nitrogen. Any signals from samples passing into the reference cell will be delayed in time and will have a lower amplitude after dispersion through two filters, and so will not register on the peak detector. This cell arrangement meets most practical requirements and is recommended.

A bypass valve is provided to vent moisture and other contaminants liberated from samples. At the inlet, a calcium oxide trap is used to dry the gas stream and remove any acidic vapours. This is connected in series with a Swinnex membrane filter assembly with a 0.45-μm filter which removes any particulates or aerosols.

An electrically heated gold-collection system is built in. This improved design results in high instantaneous mercury concentrations in the cell, thus shortening the linear range but improving the detection limit. Gold turnings or gold foil strips (about 0.5 g) are carefully packed at the midpoint of a thin-walled silica tube. The gold is placed loosely and then packed in situ so that no gold is rubbed onto unheated portions of the tube. Silica wool or a tube constriction may be used to keep the gold in place. A 30-ohm winding of nichrome wire is wound around the tube centre and held in place by tension produced by coiling the leads which connect the winding to a nearby terminal block.

RESULTS AND DISCUSSION

This design has a mercury detection limit, with gold collection and evolution, of less than 0.02 ng of mercury and a linear range to 70 ng; there is then gradual curvature towards the concentration axis until saturation occurs. For calibration, vapour in equilibrium with liquid mercury at 20° C was transferred by syringe. The detection limit was evaluated using the 20× gain setting on the integrator (Fig. 2) and recording the output on a chart recorder connected across the meter. The peak-to-peak noise amplitude was calibrated by using 50- and 100-μl samples of mercury vapour from vapour in equilibrium with liquid mercury at 0° C. From this information, a detection limit of well under 0.02 ng of mercury was established.

The spectral quality of the radiation source is less critical than in conventional atomic absorption as long as a significant proportion of the output is resonance radiation at 253.7 nm with a stable intensity. Only the absorbed radiation is observed as an acoustic signal. As the lamp current is increased, there is a less than proportional increase in sensitivity (Fig. 3) because of self-absorption and line broadening in the lamp at higher currents. A modulation frequency of 50 Hz derived from half-wave rectification of the lamp power supply is convenient for a.c. mains-operated instruments, and gives a better depth of modulation than that obtained from the full a.c. waveform where the lamp is on twice per cycle. The photoacoustic signal diminishes with an increase in modulation frequency (Fig. 4). Operation at acoustic resonance improves the signal but not by enough to be worthwhile with this particular design; the system would probably become more sensitive to temperature changes and to external acoustic stimulus. A practical instrument exploiting acoustic resonance would, however, be worth investigating. Most mains-based equipment produces more acoustic noise at 100 Hz than at 50 Hz so that the low frequency is quite suitable. The total relaxation time from

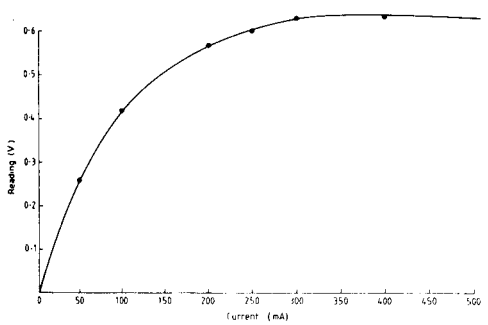

Fig. 3. Response for 22-ng aliquots of mercury vs. lamp current.

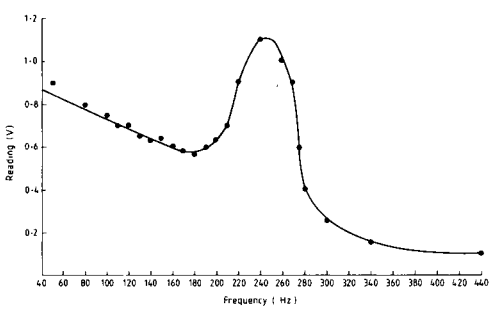

Fig. 4. Response for 22-ng aliquots of mercury vs. frequency of lamp modulation. The instability at low frequencies (40—120 Hz) was caused by the special variable frequency power supply not always re-igniting the lamp.

the atomic excited state through to the appearance of this energy as heat and then sound is responsible for the fall in response at higher frequencies.

There is an optimum gas flow for maximum sensitivity which is also a function of the heating rate for the gold collector. At high flow rates (e.g., 0.6 l min^{-1}), the fastest heating rate (40 V) gives the highest response for a 62-ng standard (Fig. 5) but at a lower flow rate (0.2 l min^{-1}) a lower heating rate provides the highest response. The highest response for a given quantity of mercury will clearly be obtained when all the mercury is in the cell at the same time and is sufficiently diluted to ensure that there is no significant reduction of radiation intensity by the mercury atoms nearest the source. At the fastest heating rate, the mercury vapour is evolved rapidly and occupies only part of the cell, at sufficiently high concentrations to reduce the incident radiation intensity on mercury atoms farther from the source, thus reducing the acoustic signal. However, at concentrations much lower than that produced by the 62-ng standard, the fastest heating rate gives the greatest signal at all flow rates.

The presence of oxygen plus water vapour in the carrier gas can cause a diminished response because the mercury vapour is photo-oxidised by the incident ultraviolet radiation [4]. The absence of either oxygen or water vapour is sufficient to restore the signal to full strength. If the two cells are connected in tandem, then one cell can be used to monitor the losses in the other with a diminished response, because of dispersion of the mercury vapour in the carrier gas after traversing two filters. Further losses observed in the second cell are caused by photochemical reactions with the carrier gas and with impurities. Table 1 shows the responses to 63-ng aliquots of mercury

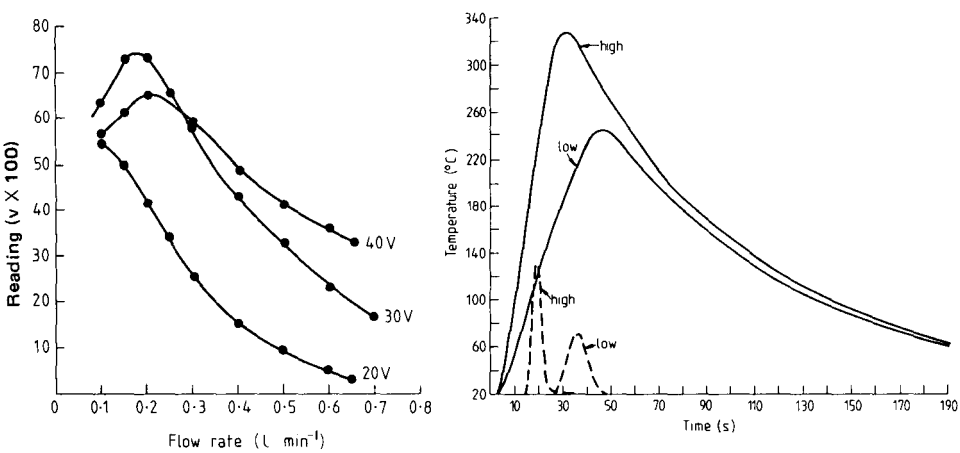

Fig. 5. Response vs. nitrogen flow rate for 62-ng aliquots of mercury released from gold at three different heater voltages.

Fig. 6. Relative signals for 20-ng aliquots of mercury and gold temperature vs. time at two different heating rates. (— temperature, ——— mercury response).

TABLE 1

Responses to 63-ng aliquots of mercury in 20 ml of air

Gas[a]	Response (Cell 1)	Response (Cell 2)	Ratio (1/2)	Gas[a]	Response (Cell 1)	Response (Cell 2)	Ratio (1/2)
Dry N_2	63	40	0.63	Argon	10	5	0.50
Wet N_2	55	27	0.49	Wet argon	53	8	0.15
N_2/CO_2	40	28	0.70	Dry argon	5	2.5	0.50
N_2/ethanol	60	46	0.77	Argon/ethanol	80	55	0.69
N_2/ammonia	94	45	0.48	Argon/CO_2	50	36	0.72
Wet air	26	1	0.04	Dry CO_2	63	43	0.68
Air/ethanol	20	0	0.00				

[a]At 0.25 l min^{-1}.

for different mixtures of gases. Carbon dioxide could be used as carrier gas when inertness is not essential. The reduced response with argon results from the lack of any long-lived collision intermediates required for the quenching of mercury fluorescence as heat. Wet argon gives a good response in the first cell but this is probably a photochemical reaction with water vapour and residual air, as the second cell shows little response. The slight reduction of the signal when moist nitrogen is used as carrier arises from the traces of oxygen present. The enhancement in the second cell, obtained with ethanol present, is probably due to the prevention of oxidation of mercury while ethanol is oxidised. However, in air the ethanol contributes to a complete loss of signal in the second cell, presumably because of the dominance of a mercury photo-oxidation reaction with air which requires water or ethanol to be present. Better quenching of fluorescence by ammonia also results in enhanced signals.

To confirm that the diminished response obtained for some gas mixtures was a photochemical effect, the instrument was connected in series with a conventional 100-mm cold vapour cell on an AA4 atomic absorption spectrometer. Table 2 shows the results for 44-ng aliquots of mercury with air and nitrogen carrier gases. It is clear that if oxygen is absent, mercury is not lost when the light is on. In the other cases, residual oxygen and probably residual moisture cause losses. The "dry" gases were dried with a silica gel trap, which was probably not very effective in reducing the water content to a level comparable to the mercury concentrations. If the photoacoustic cell is considered alone, then even in moist air the signal is identical to that of the dry state despite losses at the cell exits. Long-term operation with moist air causes a gradual loss in sensitivity however, as shown in Table 1. Oxygen-free nitrogen is the recommended carrier gas.

Fumes from a drop of nitric acid placed in the inlet tubing removed the photoacoustic signal and the atomic absorption signal as well. Removal of the acid drop and injection of ammonia fumes restored the signal for mercury. The presence of acid vapours from processes such as tin(II) chloride reduction of mercury in sulphuric acid solution will cause the signal to be greatly diminished. An effective means of removing the acid vapours is to attach to

TABLE 2

Responses to 44-ng aliquots of mercury in 20 ml of air

Photoacoustic readings	Atomic absorbance	Gas mixture (0.25 l min^{-1})	Radiation
44	0.49	"Dry" N_2	on
44	0.28	"Dry" air	on
44	0.29	Moist air	on
0	0.61	"Dry" air	off
50	0.57	O_2-free N_2	on
0	0.60	O_2-free N_2	off

the inlet a short tube filled with several grams of calcium oxide granules; a strip of indicating paper inside the tubing at the instrument inlet changed to the acid colour if the trap was absent whereas no change was noticed with the trap present, even after several hours of operation with a mercury reduction apparatus. Proper venting during sample collection on gold is important, especially if a trap is not used. Traces of moist air introduced with the sample may be in the cell when the gold is heated causing a gradual loss in sensitivity.

The sensitivity to mercury is naturally less for lower heating rates. Figure 6 shows the relative responses for two voltages applied to the heater as well as the change of temperature with time of the gold collector as measured with a thermocouple in contact with the gold at the downstream end with a nitrogen flow rate of 0.2 l min^{-1}.

The photoacoustic mercury detector described here represents only one of many possible configurations and is not a completely optimum design. Some of the more important variables have been discussed; others, such as cell design, remain to be fully investigated. This instrument is extremely sensitive, is linear, preserves its calibration over long periods of time, has a stable zero and is inexpensive to make from readily available parts.

REFERENCES

1 J. Tyndall, Proc. R. Soc. London, 31 (1881) 307.
2 A. G. Bell, Am. J. Sci., 20 (1880) 305.
3 A. G. Bell, Philos. Mag., 11 (1881) 510.
4 P. I. Bresler and B. N. Ruzin, Opt. Spektrosk., 1 (1956) 287.
5 D. K. Roe and R. A. Cary, 175th A.C.S. National Meeting, March 1978; Abstract ANAL. 47.
6 J. E. Patterson, Anal. Chim. Acta, 136 (1982) 321.

Analytica Chimica Acta, 164 (1984) 127—138
Elsevier Science Publishers B.V., Amsterdam — Printed in The Netherlands

DETERMINATION OF AMMONIA IN AIR AND AQUEOUS SAMPLES WITH A GAS-SENSITIVE SEMICONDUCTOR CAPACITOR

F. WINQUIST*, A. SPETZ and I. LUNDSTRÖM

Laboratory of Applied Physics, Linköping Institute of Technology, S-581 83 Linköping (Sweden)

B. DANIELSSON

Department of Pure and Applied Biochemistry, Chemical Centre, University of Lund, S-220 07 Lund (Sweden)

(Received 31st January 1984)

SUMMARY

The properties of a new type of ammonia gas-sensitive semiconductor capacitor are described. The sensor is based on a palladium MOS field-effect capacitor with a thin layer (3 nm) of iridium surrounding the palladium gate. The lower limit of detection for ammonia in air is 1 ppm (0.59 mg kg^{-1}). The analytical characteristics and temperature-dependence of the sensor in measurements of ammonia in air are evaluated. Ammonia in aqueous solutions is determined by the use of a continuous flow system utilizing a gas-permeable membrane in combination with the sensor. The calibration plot of the voltage drop of the capacitor vs. ammonia concentration in 150-μl samples is linear in the concentration range 0.2×10^{-6}—5×10^{-5} M. Ammonia is determined in rain and river water as well as in whole blood and blood serum; 15 samples per hour can be assayed. Analytical recovery studies and the selectivity properties of the system are described and discussed. Finally, the properties of the flow-through system in continuous monitoring are described.

Determinations of ammonia are very important in agriculture, biotechnology and chemical industry. Formation or consumption of ammonia is common in fermentation, thus a sensitive and selective ammonia sensor that can be used for continuous monitoring is especially desirable. In clinical chemistry, a sensitive and simple method for determining of ammonia in whole blood or serum that only requires microliters of samples is valuable. And improved ammonia sensors would simplify the various enzymatic procedures for determining clinically important compounds such as amino acids, creatinine and nucleotide bases [1].

Many methods are known for ammonia determinations. The most commonly used are based on spectrophotometry of the colored species formed with hypochlorite and phenol [2] or with Nessler's reagent. An enzymatic method based on a NADH-coupled reaction has been developed [3], the change in absorbance of NADH being monitored. Other methods are based on potentiometric electrodes, such as the ammonia gas-sensing electrode

0003-2670/84/$03.00

utilizing a gas-permeable membrane in combination with a glass electrode [4]. Also a new polymer membrane-based ammonia-selective sensor has been described [5]. Procedures based on gas-phase molecular absorption [6], fluorimetry [7], etc. have also been reported.

There is a significant demand for small, cheap and selective sensors for ammonia which can be used in continuous measurements. Sensors based on semiconductor technology offer the advantages of miniaturization and direct integration with microelectronics. Ion-selective field effect transistors (ISFET's) have been developed for sodium and ammonium ions [8] as well as for other species [9]. Semiconductor structures with palladium gates are very sensitive detectors for hydrogen and to a smaller extent for gases containing hydrogen atoms, e.g., hydrogen sulphide or ammonia [10]. Recently, it has been shown that the ammonia sensitivity for these devices can be considerably increased if a catalytically active metal (e.g., platinum or iridium) is evaporated in a thin (3 nm), inhomogeneous layer over and outside the palladium gate [11, 12]. The catalytic activity on the surface of these structures in the decomposition reaction of ammonia to nitrogen and hydrogen is thus increased and thereby the ammonia sensitivity. This paper is concerned with a new type of iridium-modified palladium MOS field effect capacitor (Ir/Pd MOS capacitor) with increased sensitivity for ammonia. The properties of the sensor in quantitative measurements of ammonia in air and aqueous solutions, and the determination of ammonium ion in whole blood, blood serum, rain and river water, are described.

EXPERIMENTAL

Chemicals and samples

All reagents were of analytical grade. NADH (grade III), α-ketoglutarate, adenosine diphosphate (ADP; sodium salt, grade III) and L-glutamate dehydrogenase (type III from bovine liver, E.C.1.4.1.3.) were obtained from Sigma Chemical Company. Distilled-deionized water was used throughout.

A stock standard solution (20 mM ammonium ion) was obtained by dissolving 1.320 g of diammonium hydrogenphosphate in 500 ml of water. Working standards were prepared by serial dilution; they were prepared every 3 days and were stored in a refrigerator.

Working buffers used in the continuous flow system were 0.05 M potassium phosphate adjusted to pH 7.7 or 12.7 with potassium hydroxide; these were also prepared every 3 days.

Whole blood samples were taken from three healthy non-fasting volunteers. The serum samples were taken from non-fasting adults and stored at −30° C for several weeks before measurement. Rain, river and tap water was sterile-filtered in order to minimize interferences from biological materials.

Preparation of the sensors and equipment

The Ir/Pd MOS capacitors were made from *p*-type silicon with a thermally grown dry oxide layer (100 nm). Palladium was evaporated through a

1 × 2 mm T-shaped mask on the oxide to a nominal thickness of 200 nm. Iridium was then evaporated through a 1.5 × 2 mm mask over the upper part of the T-shaped palladium gate. The nominal thickness of the iridium film was 3 nm. An aluminum contact was made prior to metallization of the gate (Fig. 1). The prepared Ir/Pd MOS capacitor was mounted on a temperature-controlled sample holder that allowed for measurements in the range 20—200°C. The voltage drop across the capacitor occurring on exposure to ammonia gas was measured with a constant capacitance regulator operating at 25 kHz and recorded with an X-t recorder. The temperature-controlled sample holder and the constant capacitance regulator were built in the laboratory.

The peristaltic pump used was a MicroPerpex (LKB, Bromma, Sweden), and the six-port valve was obtained from Rheodyne. The polytetrafluoroethylene gas-permeable membrane used was SM-33 with pore size 5.0 μm (Sartorius). All gases used were of high purity (quality N48 = 99.998%; Alfax AB, Sweden).

Procedures

Determination of ammonia in air. A carrier gas flow was established by mixing oxygen and nitrogen in a concentration of 20% oxygen in nitrogen by means of manually set flow regulators (Porter Instrumental Model UCD-1000). The total flow rate was 300 ml min^{-1}. The test gas, 1% (v/v) ammonia in argon, is fed through an electronic flow regulator built from a thermal mass flow meter (Brooks Instruments; 5810-21C3 C5B), an electromagnetic valve (Brooks Instruments; 5835-A11C31) and a feedback circuit, and is then injected and mixed with the carrier gas flow. The flow rate of the test gas can be either set manually or controlled by a computer via a D/A converter, and the ammonia concentration in the carrier gas can thereby be set from 1 to 500 ppm (0.59—295 mg kg^{-1}). The carrier gas flow is flushed over the Ir/Pd MOS capacitor by means of a plastic tube mounted very near the surface of the device.

Determination of ammonia in aqueous solutions. The system used for the determination of ammonia in whole blood and serum is shown in Fig. 2. Buffer is continuously pumped through the system at a flow rate of 0.5 ml

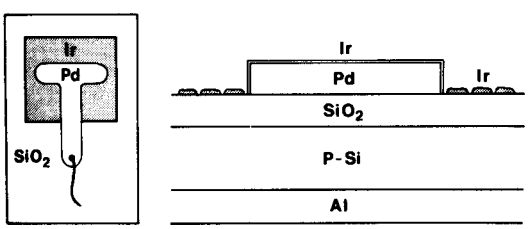

Fig. 1. Left: The Ir/Pd MOS capacitor. The size of the active iridium area is 2.0 × 1.5 mm^2. Right: Schematic cross section of the capacitor.

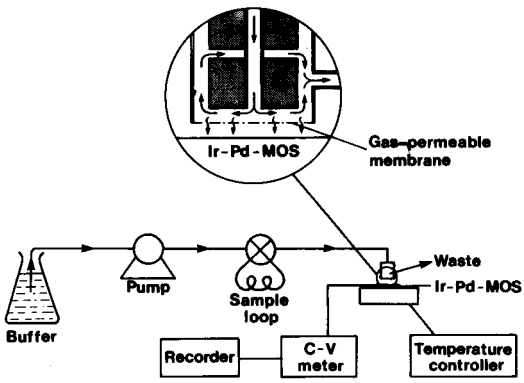

Fig. 2. Schematic diagram of the continuous flow-through system. The enlargement shows the cell with the gas-permeable membrane and the directions of the buffer stream within the cell. For more details, see text.

min^{-1} over a six-port valve with a 150-μl sample loop to the cell with the gas-permeable membrane. The cell was made from a circular teflon rod (diameter 8 mm, length 30 mm) with a 0.5 mm diameter center hole. A circular channel (20 mm deep, i.d. 7.0 mm, o.d. 7.5 mm) was milled around the center hole on one of the plane edges of the rod. The inner channel was connected to the outside of the rod via a 0.5 mm diameter hole. The gas-permeable membrane was attached over the edge of the rod (see Fig. 2).

When buffer solution is introduced in the cell, it flows radially from the center hole to the channel, between the plane edge of the rod and the gas-permeable membrane, and ammonia gas diffuses through the membrane. After the cell, some tubing (0.5 m long, 0.2 mm i.d.) is attached in order to increase the back-pressure. This creates a pressure difference across the gas-permeable membrane, and the amount of ammonia gas that diffuses through the membrane is further increased. The Ir/Pd MOS capacitor is placed 0.3 mm from the membrane. The temperature of the device is set to 35° C. Calibration curves were obtained by introducing 150 μl of standard solutions via the sample loop in the flow stream.

From the whole blood and the thawed specimens of serum, portions of 20 μl were diluted ten-fold with the working buffer (pH 7.7), and 150-μl portions of this dilution were injected in the system. This system, without the sample loop, was also used for the continuous monitoring of ammonium standards in the working buffer (pH 7.7).

For the determination of ammonia in rain, river and tap water, the flow-through system was modified. Water was continuously pumped through the system at a flow rate of 0.45 ml min^{-1}. Working buffer solution (pH 12.7), was continuously pumped at a flow rate of 0.05 ml min^{-1} and mixed with the water flow immediately before the cell with the gas-permeable membrane. The samples were introduced in the aqueous stream via a 150-μl loop in the injection valve.

Enzymatic procedure for ammonia. A method described earlier [3, 13] was followed; α-ketoglutarate was aminated with ammonium ion in the presence of NADH and L-glutamate dehydrogenase (E.C. 1.4.1.3) and the decrease in absorbance at 340 nm caused by substrate consumption provided a measure of the ammonium ion concentration.

For the determination of ammonia in serum and rain water, 0.3 ml of the sample was added to 2.7 ml of reaction solution (0.76 mM α-ketoglutarate, 0.76 mM ADP and 0.24 mM NADH) buffered at pH 7.7. Approximately 30 units of glutamate dehydrogenase were added, and the ammonium ion concentration was calculated from the decrease in absorbance at 340 nm based on data obtained from standard solutions in the same concentration range.

Because of low concentration of ammonia in river or tap water, the sample volume was raised to 2.1 ml which was added to 0.9 ml of the buffered reaction solution (2.28 mM α-ketoglutarate, 2.28 mM ADP and 0.72 mM NADH). The reagent concentrations in this solution were higher so that the final substrate concentration was the same as in the previous measurements. The ammonium ion concentration in these samples was near the lower limit of detection with the enzymatic method. In order to obtain accurate data, the spectrophotometer was connected to an X-t recorder, so that the time lag could be corrected for.

Evaluation of the selectivity properties. In measurements in air, various compounds, at concentrations 50 ppm in air, were flushed over the Ir/Pd MOS field effect capacitor by means of a 100-ml glass syringe. In measurements in aqueous solutions, 150-μl samples of various 50 μM compounds were injected in the flow-through system; the buffer used was 0.05 M potassium phosphate (pH 7.7).

Test for interfering compounds in whole blood and serum samples. The sample (50 μl) was added to 450 μl of working buffer (pH 7.7), containing 2.3 mM of each α-ketoglutarate, ADP and NADH, and 5 units of L-glutamate dehydrogenase. The solution was then incubated for 30 min. After this period, all the ammonium ion available in the sample has been consumed in the enzyme-catalyzed reaction and 150 μl of the solution is injected in the flow-through system. The response from the sensor is then a measure of the amount of interfering compounds.

RESULTS AND DISCUSSION

Measurements of ammonia gas in air

The ammonia sensitivity for an unmodified Pd MOS capacitor is low because of the poor catalytic activity of palladium in the decomposition reaction of ammonia. The catalytic activity and thus the sensitivity were considerably increased by the introduction of a thin (3 nm) metal film of catalytically active iridium over and outside the palladium gate. The metal layer over the surrounding silicon dioxide is not homogeneous; it consists of small, insulated metal islands, as shown in Fig. 1. Probably, the silicon

dioxide acts as a carrier for acid sites, thereby increasing the catalytic activity for ammonia decomposition.

The catalytic decomposition reaction of ammonia is temperature-dependent, thus the sensitivity of the Ir/Pd MOS capacitor is increased as the temperature of the device is raised. Figure 3 shows the response of the sensor to 50 ppm ammonia vs. temperature. In order to optimize the sensitivity, the device is normally operated at 150° C. Higher temperatures will result in an unstable baseline and a shorter life of the device. The ammonia sensitivity at room temperature is decreased but still about 30% of the optimal sensitivity remains, which would suffice for some purposes.

The response of the Ir/Pd MOS capacitor operating at 150° C for various concentrations of ammonia in air is shown in Fig. 4, and a calibration curve thus obtained is shown in Fig. 5. The lowest limit of detection for ammonia gas in air (defined as S/N = 3) was 1 ppm (0.59 mg kg^{-1}). The calibration graph for steady-state values of ammonia is not linear, because of the kinetics of adsorption and desorption of gas to the sensor surface. The coverage of hydrogen atoms, obtained from the dissociated ammonia molecules on the active surface, follows an equation of the form

$$d\theta/dt = C_I P_{NH_3}(1-\theta)^n - C_{II} P_{O_2}^{\alpha} \theta^m \quad (1)$$

where θ is defined as the number of occupied active sites on the surface divided by the number of available sites. The back-reaction when ammonia or hydrogen is oxidized and removed is considered in the second term on the right-hand side of the equation; P_{NH_3} is the partial pressure of ammonia, and P_{O_2} is the partial pressure of oxygen, which is constant; C_I, C_{II}, α, n and m are constants which depend on the rate-limiting reactions on the active surface. At steady state, $d\theta/dt = 0$, thus

$$\theta/(1-\theta)^{m/n} = K_1(P_{NH_3})^{1/m} \quad (2)$$

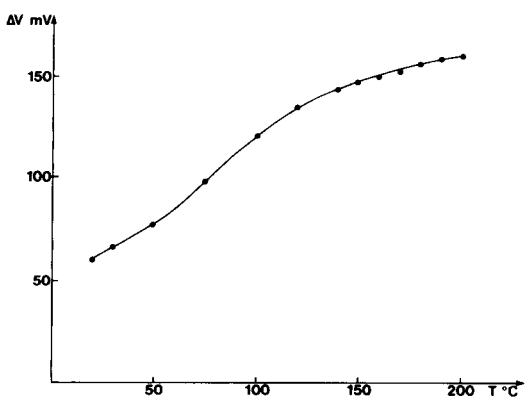

Fig. 3. Temperature-dependence of the sensitivity of the Ir/Pd MOS capacitor. The sensor was subjected to 50 ppm ammonia gas in air at temperatures of 20—200° C, and the steady-state responses of the sensor were monitored.

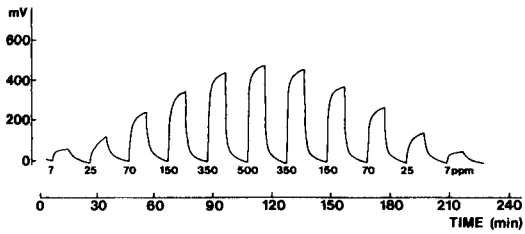

Fig. 4. Typical recording for measurements of ammonia gas in air stream. The ammonia gas pulses were injected in the air stream for 8 min every 20 min. The Ir/Pd MOS capacitor was operated at 150° C.

where K_1 is a constant. For small values of θ, the equation can further be simplified to $\theta = K_1(P_{NH_3})^{1/m}$. If V_{max} is defined as the maximum voltage shift for fully saturated adsorption sites ($\theta = 1$), then the coverage term, θ, is directly related to the ratio between the voltage drop, ΔV, and the maximum voltage shift, V_{max}, by $\theta = \Delta V/V_{max}$. Therefore,

$$\Delta V = K_2(P_{NH_3})^{1/m} \text{ and } \log(\Delta V) = \log K_2 + (1/m)\log P_{NH_3} \quad (3)$$

where K_2 is a constant. The value of m depends on the different decomposition and oxidation reactions that ammonia can undergo on the surface of the Ir/Pd MOS capacitor and the size and thickness of the iridium layer. The values of K_2 and m were obtained by plotting $\log \Delta V$ vs. $\log P_{NH_3}$, and were found to be 24.5 and 1.85, respectively. The plot was linear up to 100 ppm ammonia. Thus, the response of the sensor follows the equation $\Delta V = 24.5(P_{NH_3})^{0.54}$ or $P_{NH_3} = (\Delta V/24.5)^{1.85}$ for $P_{NH_3} < 100$ ppm.

The long-term stability and reproducibility of the Ir/Pd MOS capacitor were evaluated. The mean value of ten successive runs of 100 ppm ammonia was 201.3 mV with RSD = 2.3%. In one experiment, the device was subjected to 250 ppm ammonia 4 times a day during 8 days. The mean value was 408.6 mV ($n = 32$) with RSD = 3.2%. The baseline remained remarkably stable; the mean drift from day to day was 7.3 mV and the overall drift during 8 days was 40 mV.

Measurements of ammonia in aqueous solution

The Ir/Pd MOS capacitor is used for measurements of ammonia gas in air, which is quite suitable for determination of gas produced in fermentors or in environmental analyses. For the determination of ammonium in aqueous solutions, the flow-through system shown in Fig. 2 was used. In this system, ammonia gas is separated from the aqueous solution by means of the gas-permeable membrane. Because ammonia gas is in equilibrium with ammonium ions, ammonium concentration is referred below to the total ammonia nitrogen present, i.e., the sum of the ammonia gas and the ammonium ions.

In order to avoid a high temperature gradient across the air gap between the sensor and the membrane, the temperature of the sensor is set to 35° C.

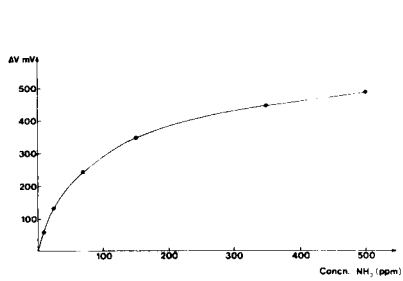

Fig. 5. Calibration curve obtained for steady-state responses of ammonia gas in air. The temperature of the Ir/Pd MOS capacitor was 150° C.

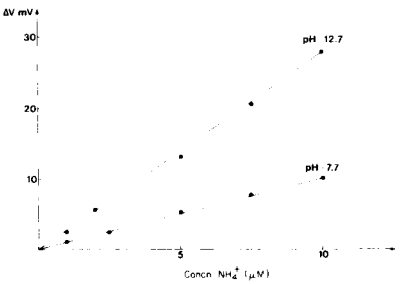

Fig. 6. Calibration graphs obtained from ammonium standards in the flow-through system, operating at pH 12.7 and pH 7.7, respectively. The sample volume injected was 150 μl and the temperature of the Ir/Pd MOS capacitor was 35° C.

The sensitivity of the device is thereby decreased, but the electronic properties of the device are improved. These MOS devices in general are very sensitive to sodium ion contaminations in the oxide layer. These ions can easily travel through the oxide layer at elevated temperatures and induce a drift in the baseline, but at 35° C, the mobility of these ions is negligible. Furthermore, the background noise level of the device is considerably decreased. This means that the decrease in ammonia sensitivity could be well compensated for by increasing the amplification of the signal from the sensor. The temperature of the sensor was set slightly above room temperature to avoid water condensation on the surface of the sensor.

If the Ir/Pd MOS capacitor is exposed to ammonia gas at low concentration during a short time, then $\theta \ll 1$, and the transient equation during ammonia exposure, Eqn. 1 is simplified to $d\theta/dt = C_I P_{NH_3}$, thus

$$\Delta V = K_4 P_{NH_3} \Delta t \tag{4}$$

where K_4 is a constant. The exposure time, Δt, is related to the volume of the sample loop and the flow rate of the system. Thus, a linear relation between ΔV and ammonium concentration can be obtained if a small volume of the sample, containing a low ammonium concentration, is injected in the system. A decreased sample volume will, however, also result in a reduced sensitivity of the system. It was found empirically that a sample volume of 150 μl was small enough to achieve linearity and still large enough to ensure reliable measurements. The flow rate of the system was 0.5 ml min^{-1}, so that a 150-μl sample results in an exposure time, Δt, of 18 s.

In order to estimate the selectivity of the Ir/Pd MOS capacitor, various amines and some other compounds were injected in the flow-through system. The results are presented in Table 1, where a comparison also was made between the selectivity properties in measurements of air and in measurements of aqueous solutions. The selectivity is considerably improved in

TABLE 1

Interferences of various compounds in measurements of air and buffered solutions (pH 7.7) relative to the response for ammonia or ammonium ion

Compound	Relative sensitivity in air (%)	In aqueous solution (%)	Compound	Relative sensitivity in air (%)	In aqueous solution (%)
NH_3[a]	100	100	Ethylenediamine	25	1
Methylamine	70	10	Ethanol	0	0
Ethylamine	30	5	HCl	0	0
Butylamine	5	0	CO_2	0	0
Diethylamine	30	2	CO	2.5	0
Ethanolamine	30	2	H_2	40	60

[a]Ammonium ion for aqueous solution.

aqueous solutions because of the phase-separation stage; probably methylamine and ethylamine are more basic than ammonia and therefore stay in solution at pH 7.7. The other amines have a lower permeability coefficient than that of ammonia.

Calibration graphs obtained from 150-μl ammonium standards at pH 7.7 and pH 12.7 are shown in Fig. 6. The lower limit of detection (defined as S/N = 3) is 0.4 μM at pH 7.7 and 0.2 μM at pH 12.7, and one sample could be processed in less than 4 min. The calibration graphs were linear up to 50 μM. For the determination of ammonium in inorganic samples, pH 12.7 was chosen to ensure complete conversion of ammonium ion to ammonia gas. Several samples, such as tap, river and rain water were measured, and the results are given in Table 2. From the Stångå River, that passes the city of Linköping, two samples were collected. Sample 1 was taken upstream and sample 2 downstream the city. The concentration of ammonium in rain water correlates well with other values reported by Aoki et al. [7] (30×10^{-6} M and 23×10^{-6} M) and Vijan and Wood [6] (29×10^{-6} M).

Also shown in Table 2 are data obtained from the enzymatic method. Because the ammonium concentration in most samples is less than 10 μM, the data obtained from the enzymatic procedure are in the lower limit of detection. A reasonable correlation between the two methods is, however, observed. Precision data were obtained by ten successive determinations of ammonium in a mixture of rain and river water; the mean value was 19.90 μM with RSD = 4.1%.

For the determination of ammonium in whole blood and serum, the pH of the flow-through system was set to 7.7, to avoid ammonia release from labile compounds in the samples. Under alkaline conditions, labile amine groups from glutamine and aspargine are easily hydrolyzed to give ammonia [14]. The ammonium concentration obtained for whole blood and serum samples are presented in Table 3, and for serum samples, these values are compared to those obtained with an enzymatic method. The ammonium concentrations found for fresh whole blood samples are somewhat higher than other values

TABLE 2

Ammonium determinations in various samples at pH 12.7

Sample	NH_4^+ found (μM)	
	Present method[a]	Enzymatic method[b]
Tap (hot)	1.7	2.9
Tap (cold)	0	0
Stångå River 1[c]	1.9	3.0
Stångå River 2[c]	5.4	6.5
Tinner brook[c]	8.8	8.8
Rain water[d]	24.8	20.4

[a]Mean of triplicate determinations. [b]Single measurements; the samples were sterile-filtered before analysis. [c]Collected October 4, 1983. [d]Collected October 11, 1983.

TABLE 3

Ammonium determinations in whole blood and serum samples at pH 7.7, with recovery data

Sample	Ammonium ion concentration (μmol l^{-1})				Recovery (%)
	Found by present method[a]	Found by enzymatic method[b]	Added	Found	
Whole blood samples					
1	69.7[c]	—	0	64.2	10
2	63.2[c]	—	10	74.5	103
3	71.4[c]	—	25	88.2	96
4	97.5[d]	—	50	115.7	103
			75	137.0	97
Blood serum samples					
1	53.2[d]	52.1	0	57.5	—
2	56.0[d]	57.5	5	62.2	94
3	70.3[d]	69.8	10	67.2	97
4	64.7[d]	67.1	25	80.8	93
5	62.0[d]	63.3	50	109.5	104

[a]Means of triplicate determinations. [b]Single measurement. [c]Fresh sample. [d]Frozen sample.

found in the literature [15] (10×10^{-6}—50×10^{-6} M). No correlation study was made because ammonium ion in whole blood samples cannot be determined with the enzymatic method. This shows, however, one of the advantages of the present methods, the ability to measure in colored or turbid samples.

The ammonium concentrations found for the serum samples are larger than other values recently reported [16] (22×10^{-6}—52×10^{-6} M). The

serum samples had been stored at −30° C for several weeks, and the effect of storage often gives rise to elevated ammonia concentrations [16]. The values fit well, however, with those given by the enzymatic method.

The accuracy of the method was evaluated by recovery studies on whole blood and serum samples spiked with known amounts of ammonium. The results are shown in Table 3. The recoveries obtained vary between 93 and 104%. Precision data were obtained from ten successive determinations of ammonia in blood serum. The mean value was 62.0 μM with RSD = 3.7%.

The sample volume taken is 20 μl, and this small sample volume can be of especial value in diagnosis of newborns, where ammonium concentration can be evaluated serially without excessive withdrawal of blood. It is also possible to measure directly in whole blood, which will reduce the analysis time considerably. The ammonium concentration in one sample can be determined in less than 4 min. The influence of possible interfering compounds, such as amines or hydrogen was also investigated for both whole blood and serum. After the incubation step, the ammonium concentrations found were in both cases less than 0.4 μM, thus the selectivity of the system is satisfactory for ammonium determinations in whole blood and serum.

Most analytical procedures used in process control are discontinuous. However, continuous methods are preferable because they reduce the time and cost of sample handling and can give direct information of substrate metabolism. Investigations of the analytical system described above show that it can be very useful in continuous measurements. In one experiment, different ammonium concentrations in aqueous solution were continuously monitored; the recording is shown in Fig. 7. The ammonium concentration in the working buffer (pH 7.7) was changed stepwise and the increasing values correlate very well with the decreasing values. The drift in the baseline was less than 0.5 mV during the experiment.

Conclusion

The new type of ammonia-sensitive sensor based on semiconductor technology is useful. The physics and function of the Ir/Pd MOS capacitor have only been briefly discussed here, a more detailed description is available [11,

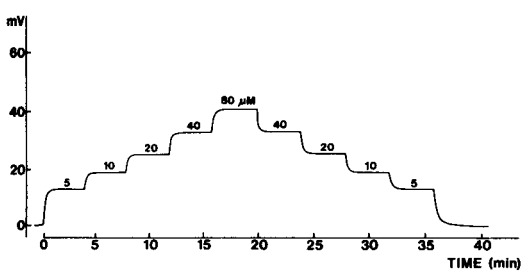

Fig. 7. Recording from continuous monitoring of ammonium concentration in the working buffer (pH 7.7). The ammonium concentration was changed stepwise every 4 min.

12]. The equipment used, including the constant capacitance regulator and the Ir/Pd MOS capacitor, is very simple and cheap to manufacture. An ammonia-sensitive Ir/Pd MOS field effect transistor which would further simplify the necessary equipment and handling is currently being developed.

We thank Ms. Agneta Askendal for making the figures. This work was supported by the National Swedish Board for Technical Development.

REFERENCES

1 See, e.g., P. W. Carr and L. D. Bowers, Immobilized Enzymes in Analytical and Clinical Chemistry, Wiley-Interscience, New York, 1980.
2 J. Crowther and J. Evans, Analyst (London), 105 (1980) 841.
3 B. L. Albert, F. D. Terry and A. J. Milton, J. Appl. Environ. Microbiol., 38 (1979) 212.
4 Orion Research, Analytical Methods Guide, 9th edn., 1978, p. 33.
5 See, e.g., Y. M. Fraticelli and M. E. Meyerhoff, Anal. Chem., 53 (1981) 992.
6 P. N. Vijan and G. R. Wood, Anal. Chem., 53 (1981) 1447.
7 T. Aoki, S. Uemura and M. Munemori, Anal. Chem., 55 (1983) 1620.
8 U. Oesch, S. Caras and J. Janata, Anal. Chem., 53 (1981) 1983.
9 J. Janata and R. J. Huber, in H. Freiser (Ed.), Ion-Selective Electrodes in Analytical Chemistry, Vol. 2, Plenum, New York, 1980, p. 107.
10 I. Lundström, Sensors Actuators, 1 (1981) 403.
11 F. Winquist, A. Spetz, M. Armgarth, C. Nylander and I. Lundström, Appl. Phys. Lett., 43(9) (1983) 839.
12 A. Spetz, F. Winquist, C. Nylander and I. Lundström, Proc. Int. Meet. Chemical Sensors, Kodansha, Fukuoka, Japan, 1983.
13 A. Ishihara, K. Kurahasi and H. Iehara, Clin. Chim. Acta, 41 (1972) 255.
14 See, e.g., H. F. Proeless and B. W. Wright, Clin. Chem., 19 (1973) 1162.
15 I. Oreskes, C. Hirsch and S. Kupfer, Clin. Chim. Acta, 16 (1969) 185.
16 M. Mascini and G. Palleschi, Anal. Chim. Acta, 136 (1982) 69.

Analytica Chimica Acta, 164 (1984) 139—146
Elsevier Science Publishers B.V., Amsterdam — Printed in The Netherlands

SIMULTANEOUS DETERMINATION OF HYPOXANTHINE, INOSINE, INOSINE-5′-PHOSPHATE AND ADENOSINE-5′-PHOSPHATE WITH A MULTIELECTRODE ENZYME SENSOR

ETSUO WATANABE*, SHUNSUKE TOKIMATSU and KENZO TOYAMA

Department of Food Engineering and Technology, Tokyo University of Fisheries, 4-5-7 Konan, Minato-ku, Tokyo 108 (Japan)

ISAO KARUBE, HIDEAKI MATSUOKA and SHUICHI SUZUKI

Research Laboratory of Resource Utilization, Tokyo Institute of Technology, Nagatsuta-cho, Midori-ku, Yokohama 227 (Japan)

(Received 27th February 1984)

SUMMARY

A multielectrode enzyme sensor for the simultaneous determination of adenosine-5′-phosphate (AMP), inosine-5′-phosphate (IMP), inosine (HXR) and hypoxanthine (HX) in fish meat was developed by assembling four enzyme sensors for AMP, IMP, HXR and HX in a flow cell. These compounds were determined from oxygen consumption according to the following reactions:

$$\text{AMP} \xrightarrow{\text{AD}} \text{IMP} \xrightarrow{\text{NT}} \text{HXR} \xrightarrow{\text{NP, } PO_4^{3-}} \text{HX} \xrightarrow{\text{XO, } O_2} \text{Uric acid}$$

where AD is AMP deaminase, NT is 5′-nucleotidase, NP is nucleoside phosphorylase and XO is xanthine oxidase. Enzymes were covalently bound to a membrane prepared from cellulose triacetate, 1,8-diamino-4-aminomethyloctane and glutaraldehyde. Sensors for HX, HXR, IMP and AMP were prepared by attaching membranes of XO, XO—NP, XO—NP—NT, and of XO—NP—NT and AD, respectively, to four oxygen electrodes. Samples extracted from sea bass, bream, flounder, abalone and arkshell were analyzed within 5 min, from the simultaneous response curves of the four electrodes. Results obtained by the multisensor system were in good agreement with those determined by each single electrode.

In the last ten years, many enzyme sensors have been developed by combining immobilized enzymes with electrochemical devices [1—6]. The most advantageous feature of these enzyme sensors is their selectivity, because practical measurements are usually made on mixtures of various compounds. Recently, much attention has been paid to the development of multifunctional enzyme sensors, which would allow components in a sample to be determined without prior separation. For example, the determination of nucleotides in fish meat has been required for the estimation of fish freshness [7]. In previous papers [8—12], enzyme sensors for adenosine-5′-phosphate (AMP), inosine-5′-phosphate (IMP), inosine (HXR) and hypoxanthine (HX) were described and applied to the estimation of freshness in various

fish. However, IMP, HXR and HX had to be determined prior to the determination of AMP. HXR and HX were also determined prior to the IMP determination. Therefore, the experimental procedures were very complicated and time-consuming. In the present paper, the four enzyme electrodes were assembled together in a flow cell. The concentrations of AMP, IMP, HXR and HX were determined from the simultaneous responses of the four electrodes.

EXPERIMENTAL

Materials

The enzymes used were xanthine oxidase (E.C.1.2.3.2. from bovine spleen; Boehringer-Mannheim), nucleoside phosphorylase (E.C.2.4.2.1. from calf spleen), 5′-nucleotidase (E.C.3.1.3.5. from *Crotalus adamanteus* venom) and 5′-adenylic acid deaminase (E.C.3.5.4.6. from rabbit muscle) (all from Sigma Chemicals). Hypoxanthine, inosine, inosine-5′-phosphate and adenosine-5′-phosphate were purchases from Kohjin Co. Dichloromethane, 1,8-diamino-4-aminomethyloctane and cellulose triacetate were obtained from Kokusan Chemical Works, Ashi Kasei Co. and Eastman Kodak, respectively.

Fish and shellfish. Sea bass *Lateolobrax japonicus*, bream *Pagrosomus unicolor* Quoy and Gaimard, flounder *Lepidopsetta bilineata*, abalone *Haliotis discus hannai* and arkshell *Anadara broughttoni* Shrenk were purchased from a local store and stored in ice for up to 2 weeks after instant death. A perchloric acid extract of the flesh of fish or shellfish was prepared as described by Ehira et al. [13].

Construction of multielectrode enzyme sensor

The enzyme electrodes used in the present multielectrode enzyme sensor system were prepared as reported previously [7—10], and contained one of the following membranes: (I) xanthine oxidase (XO) membrane; (II) XO and nucleoside phosphorylase (NP) membrane; (III) XO, NP and 5′-nucleotidase (NT) membrane; (IV) XO, NP and NT membrane and AMP deaminase (AD) membrane. The four enzyme electrodes were inserted in a flow cell as depicted in Fig. 1. The void volume of the flow cell was 0.1 ml. A phosphate buffer solution (0.05 M, pH 7.8) containing cysteine (10^{-4} M) was continuously transferred to the flow cell by a peristaltic pump. The output currents of the oxygen electrodes were recorded simultaneously on a multichannel recorder. The temperature was controlled at 30°C throughout the experiments.

Assay procedure

When the output currents of all electrodes became steady, a known volume (20—50 μl) of sample solution was injected via the injection port into the flowing buffer solution. The enzyme electrode I responded only to HX. The concentration of HX was directly determined from the response

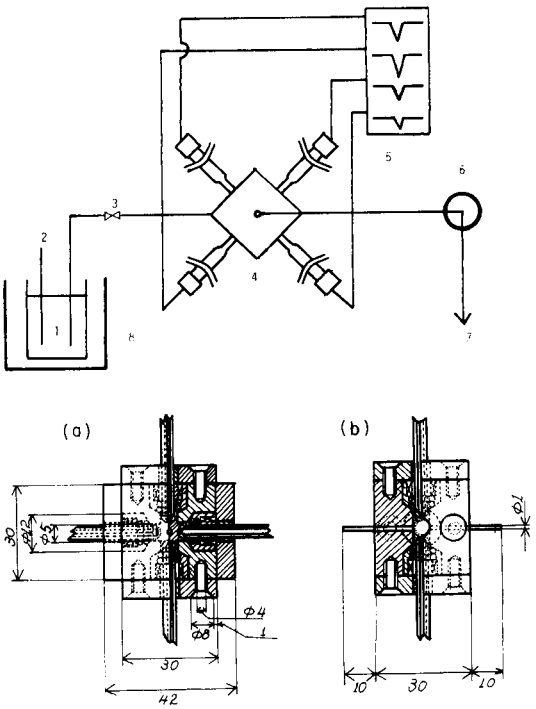

Fig. 1. Schematic diagram of the multielectrode enzyme sensor system for HX, HXR, IMP and AMP determinations: (1) buffer reservoir; (2) air; (3) sample injection port; (4) multielectrode enzyme sensor; (5) recorder; (6) peristaltic pump; (7) waste; (8) incubator; (a) top view; (b) side view of flow cell (dimensions in mm).

(difference between the initial current and the minimum current) of this electrode. Electrode II responded to HX and HXR. Thus the sum of HX and HXR was determined from the response of this electrode. Similarly, the sums of HX, HXR and IMP, and of HX, HXR, IMP and AMP were measured from the responses of electrodes III and IV, respectively. The mathematical treatment is given in the Appendix.

RESULTS AND DISCUSSION

Response of a single enzyme electrode

In order to estimate the influence of oxygen consumption at one electrode on the responses of other electrodes, an enzyme sensor for HX and three oxygen electrodes were inserted into the flow cell. Figure 2 shows typical response curves when a 20-μl aliquot of HX solution (2×10^{-5} M) was injected and transferred at 1 ml min^{-1}. The output current of the HX sensor decreased, reached a minimum and then returned to the initial current within

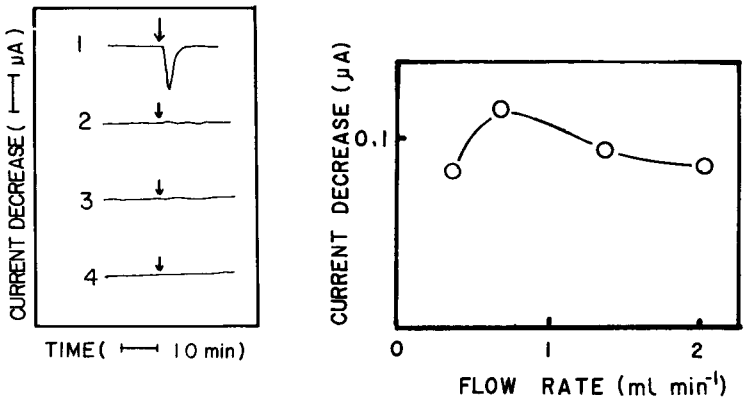

Fig. 2. Mutual influence of sensors on the output currents: (1) HX sensor; (2, 3, 4) oxygen probes. (1 ml min^{-1}, 30°C, pH 7.8, 20-μl sample.)

Fig. 3. Influences of flow rate on output current of HX sensor in the multielectrode enzyme sensor. (pH 7.8, 30°C, 20-μl samples of 2×10^{-5} M HX.)

5 min. However, no appreciable change was observed in the output currents of other three oxygen electrodes. Therefore, the response of an electrode seemed not to be affected by those of other electrodes.

The effects of flow rate and sample volume on the response were investigated using an enzyme sensor for HX as described above (Fig. 2). When 20 μl of 2×10^{-5} M HX solution was injected, the response was 0.1—0.02 μA in the range 0.4—2.0 ml min^{-1}, as shown in Fig. 3. Figure 4 shows the effects of sample volume on the response. The response decreased gradually with increase in sample volume in the range of 5—40 μl. On the basis of these results, the sample volume was fixed at 20 μl in the following experiments.

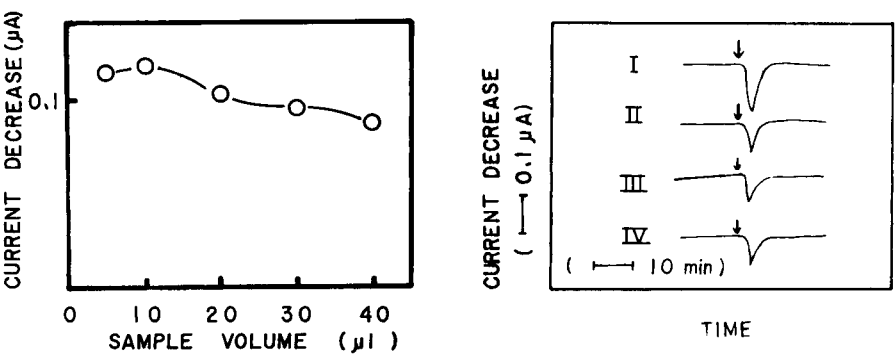

Fig. 4. Influence of sample volume on the output current of the HX sensor in the multielectrode system. (pH 7.8, 30°C, 1 ml min^{-1}.)

Fig. 5. Typical response curves for the multielectrode enzyme sensor: (I) HX; (II) HX + HXR; (III) HX + HXR + IMP; (IV) HX + HXR + IMP + AMP sensors. (pH 7.8, 30°C, 1 ml min^{-1}, 20 μl of 2×10^{-5} M HX; arrows indicate sample injection.)

Simultaneous response of four enzyme sensors

The multielectrode enzyme sensor was composed of enzyme sensors for HX, HXR, IMP and AMP inserted in the flow line. A hypoxanthine solution was injected. Because each sensor incorporates xanthine oxidase, the output currents of the four sensors decreased simultaneously, as shown in Fig. 5. Though the sensor for AMP consisted of two enzyme membranes, no appreciable delay was observed in the response time. Thus the period required to obtain the minimum current was found to be about 5 min after injection of the sample for all sensors.

Determination of the components of coefficient matrix A

Mixtures of HX, HXR, IMP and AMP were applied to the multi-electrode enzyme sensor. The relationships between the responses of the four electrodes and the concentration of each substrate are shown in Fig. 6. Linear relationships were obtained for HX below 2×10^{-3} M, HXR below 5×10^{-3} M and for IMP and AMP below 1.0×10^{-2} M. From these linear relations, each component (k_{ij}) of the coefficient matrix A (see Appendix) was found to be: $k_{11} = 0.15$, $k_{12} = 0$, $k_{13} = 0$, $k_{14} = 0$, $k_{21} = 0.12$, $k_{22} = 0.05$, $k_{23} = 0$, $k_{24} = 0$, $k_{31} = 0.073$, $k_{32} = 0.038$, $k_{33} = 0.0086$, $k_{34} = 0$, $k_{41} = 0.076$, $k_{42} = 0.043$, $k_{43} = 0.0076$ and $k_{44} = 0.004$. Therefore the inverse matrix of A was calculated to be

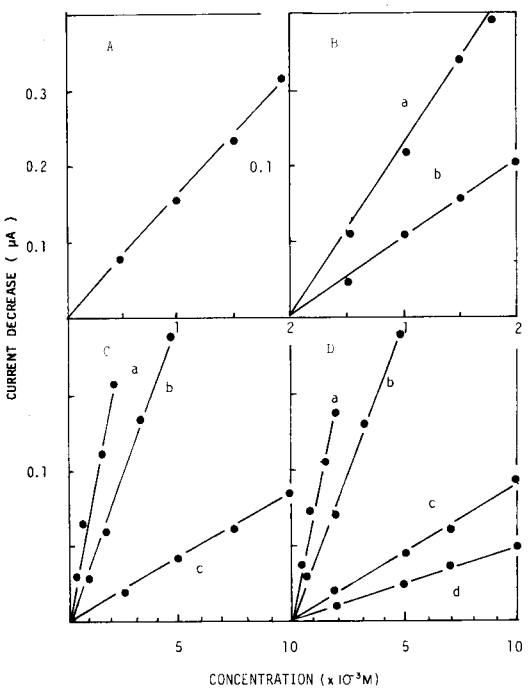

Fig. 6. Calibration graphs for (A) HX, (B) HXR, (C) IMP and (D) AMP. Sensors: (a) HX; (b) HXR; (c) IMP; (d) AMP. (pH 7.8, 30° C, 1 ml min^{-1}.)

$$A^{-1} = \begin{vmatrix} 6.7 & 0 & 0 & 0 \\ -16 & 20 & 0 & 0 \\ 14.1 & -88.4 & 116.3 & 0 \\ 39.9 & -47.1 & -221 & 250 \end{vmatrix}$$

These coefficients were used to calculate the individual concentrations from the responses of the four sensors.

Application to the determination of HX, HXR, IMP and AMP in fish and shellfish

Hypoxanthine, HXR, IMP and AMP concentrations in sea bass, bream, flounder, and abalone were determined by the present multisensor system, and by each sensor for HX, HXR, IMP and AMP, individually. As shown in Table 1, there was usually good agreement between the values determined by both methods. As reported previously [12], HX and HXR accumulated in bream, flounder and sea bass as the storage time in ice increased. In sharp contrast, no HX, HXR or IMP was detected in abalone (1 day storage) or arkshell (12 h storage). In these shellfish, AMP was decomposed rapidly to adenosine. Therefore, the decrease in AMP concentration should be used for freshness evaluation. The multielectrode enzyme sensor allowed the deter-

TABLE 1

Amounts of AMP, IMP. HXR and HX in fish and shellfish flesh (the value in parenthesis is that given by the single sensor)

Sample	Storage time (h)	AMP (μmol g^{-1})	IMP	HXR	HX
Sea bream	12	0.93 (0.54)	9.65 (10.1)	0 (0.06)	0.42 (0.40)
	18	1.04 (1.00)	10.5 (11.0)	0 (0)	0.30 (0.34)
	24	1.43 (1.93)	18.6 (17.8)	0 (0)	0.38 (0.48)
	48	2.55 (1.92)	19.2 (18.1)	0.04 (0.10)	0.43 (0.48)
Flounder	12	1.03 (1.70)	2.06 (2.10)	0.72 (0.86)	0.74 (0.84)
	18	1.25 (1.50)	6.30 (6.91)	0 (0.08)	0.82 (0.78)
	24	0.51 (0.68)	6.20 (6.80)	1.00 (1.00)	1.26 (1.13)
Sea bass	4	1.23 (1.70)	1.63 (1.91)	0.55 (0.60)	0.23 (0.33)
	12	3.31 (3.50)	9.24 (9.30)	1.00 (1.00)	1.21 (1.30)
	24	0.50 (0.49)	8.65 (8.97)	1.26 (1.03)	1.21 (1.26)
Abalone	12	2.8 (2.9)	0 (0)	0 (0)	0 (0)
	24	27.2 (28.0)	0.21 (0.23)	0.32 (0.40)	0.04 (0.10)
	48	8.5 (8.8)	0.16 (0.13)	0.42 (0.48)	0.07 (0.10)
Arkshell	12	4.8 (4.9)	0 (0)	0 (0)	0 (0)
	24	8.0 (8.2)	0.56 (0.60)	0.30 (0.30)	0.10 (0.10)
	48	14.3 (14.7)	0.36 (0.38)	0.12 (0.30)	0.34 (0.38)
	120	0.18 (0.28)	0.58 (0.72)	0.44 (0.40)	0.33 (0.38)

mination of the HX, HXR, IMP and AMP contents of fish or shellfish extracts within 5 min. Further studies are directed towards developing a multifunctional biosensor system which can simultaneously determine HX, HXR and IMP with a single sensor.

APPENDIX

Each sensor can be used in the range of the responses proportional to each concentration of HX, HXR, IMP and AMP, respectively. These relationships can be represented by

$$\begin{Bmatrix} \Delta I_1 \\ \Delta I_2 \\ \Delta I_3 \\ \Delta I_4 \end{Bmatrix} = \begin{vmatrix} k_{11} & k_{12} & k_{13} & k_{14} \\ k_{21} & k_{22} & k_{23} & k_{24} \\ k_{31} & k_{32} & k_{33} & k_{34} \\ k_{41} & k_{42} & k_{43} & k_{44} \end{vmatrix} \begin{Bmatrix} [\mathrm{HX}] \\ [\mathrm{HXR}] \\ [\mathrm{IMP}] \\ [\mathrm{AMP}] \end{Bmatrix} \tag{1}$$

where ΔI_i are the responses of the electrodes, k_{ij} are constants, and [HX], [HXR], [IMP] and [AMP] are the concentrations of each compound. Equation 1 can be rewritten as d = AC, where d is the response vector, A is the coefficient matrix, and C is the concentration vector. Therefore C = A^{-1} d, where A^{-1} is the inverse matrix of A:

$$A^{-1} = \frac{1}{D} \begin{vmatrix} c_{11} & c_{21} & c_{31} & c_{41} \\ c_{12} & c_{22} & c_{32} & c_{42} \\ c_{13} & c_{23} & c_{33} & c_{43} \\ c_{14} & c_{24} & c_{34} & c_{44} \end{vmatrix}$$

and $D = k_{41}c_{41} + k_{42}c_{42} + k_{43}c_{43} + k_{44}c_{44}$, where c_{jk} is the algebraic co-element of k_{jk}, the values being

$$c_{11} = k_{22}k_{33}k_{44} + k_{23}k_{34}k_{42} + k_{24}k_{32}k_{43} - k_{24}k_{33}k_{42} - k_{23}k_{32}k_{44} - k_{22}k_{34}k_{43}$$

$$c_{12} = k_{24}k_{33}k_{41} + k_{21}k_{34}k_{43} + k_{23}k_{31}k_{44} - k_{21}k_{33}k_{44} - k_{24}k_{31}k_{43} - k_{23}k_{34}k_{41}$$

$$c_{13} = k_{21}k_{32}k_{44} + k_{22}k_{34}k_{41} + k_{24}k_{31}k_{42} - k_{24}k_{32}k_{41} - k_{21}k_{34}k_{42} - k_{22}k_{31}k_{44}$$

$$c_{14} = k_{23}k_{32}k_{41} + k_{21}k_{33}k_{42} + k_{22}k_{31}k_{43} - k_{21}k_{32}k_{43} - k_{22}k_{33}k_{41} - k_{23}k_{31}k_{42}$$

$$c_{21} = k_{14}k_{33}k_{42} + k_{12}k_{34}k_{43} + k_{13}k_{32}k_{44} - k_{12}k_{33}k_{44} - k_{14}k_{32}k_{43} - k_{13}k_{34}k_{42}$$

$$c_{22} = k_{11}k_{33}k_{44} + k_{14}k_{31}k_{43} + k_{13}k_{34}k_{41} - k_{14}k_{33}k_{41} - k_{13}k_{31}k_{44} - k_{11}k_{34}k_{43}$$

$$c_{23} = k_{14}k_{32}k_{41} + k_{11}k_{34}k_{42} + k_{12}k_{31}k_{44} - k_{11}k_{32}k_{44} - k_{12}k_{34}k_{41} - k_{14}k_{31}k_{42}$$

$$c_{24} = k_{11}k_{32}k_{43} + k_{13}k_{31}k_{42} + k_{12}k_{33}k_{41} - k_{13}k_{32}k_{41} - k_{12}k_{31}k_{43} - k_{11}k_{33}k_{42}$$

$$c_{31} = k_{12}k_{23}k_{44} + k_{14}k_{22}k_{43} + k_{13}k_{24}k_{42} - k_{14}k_{23}k_{42} - k_{13}k_{22}k_{44} - k_{12}k_{24}k_{43}$$

$$c_{32} = k_{14}k_{23}k_{41} + k_{13}k_{21}k_{44} + k_{11}k_{24}k_{43} - k_{11}k_{23}k_{44} - k_{14}k_{21}k_{43} - k_{13}k_{24}k_{41}$$

$$c_{33} = k_{11}k_{22}k_{44} + k_{14}k_{21}k_{42} + k_{12}k_{24}k_{41} - k_{14}k_{22}k_{41} - k_{11}k_{24}k_{42} - k_{12}k_{21}k_{44}$$

$$c_{34} = k_{13}k_{22}k_{41} + k_{11}k_{23}k_{42} + k_{12}k_{21}k_{43} - k_{11}k_{22}k_{43} - k_{13}k_{21}k_{42} - k_{12}k_{23}k_{41}$$

$$c_{41} = k_{14}k_{23}k_{32} + k_{12}k_{24}k_{33} + k_{13}k_{22}k_{34} - k_{12}k_{23}k_{34} - k_{14}k_{22}k_{33} - k_{13}k_{24}k_{32}$$

$$c_{42} = k_{11}k_{23}k_{34} + k_{13}k_{24}k_{31} + k_{14}k_{21}k_{33} - k_{14}k_{23}k_{31} - k_{13}k_{21}k_{34} - k_{11}k_{24}k_{33}$$

$$c_{43} = k_{14}k_{22}k_{31} + k_{11}k_{24}k_{32} + k_{12}k_{21}k_{34} - k_{11}k_{22}k_{34} - k_{14}k_{21}k_{32} - k_{12}k_{24}k_{31}$$

$$c_{44} = k_{11}k_{22}k_{33} + k_{13}k_{21}k_{32} + k_{12}k_{23}k_{31} - k_{13}k_{22}k_{31} - k_{12}k_{21}k_{33} - k_{11}k_{23}k_{32}$$

Therefore, the concentrations of HX, HXR, IMP and AMP can be estimated from C = A^{-1} d.

REFERENCES

1 S. J. Updike and G. P. Hicks, Nature, 214 (1967) 986.
2 J. A. Burns, Cereal Food World, 21 (1976) 594.
3 D. P. Nikolelis and H. A. Mottola, Anal. Chem., 50 (1978) 1665.
4 M. Kayama, S. Satoh, M. Aizawa and S. Suzuki, Anal. Chim. Acta, 116 (1980) 307.
5 I. Karube, I. Saitoh, Y. Araki and S. Suzuki, Enzyme Microb. Technol., 2 (1980) 117.
6 I. Karube, H. Hara and S. Suzuki, Anal. Chim. Acta, 139 (1982) 127.
7 T. Saito, Y. Arai and M. Matsuyoshi, Bull. Jpn. Soc. Sci. Fish., 24 (1959) 749.
8 E. Watanabe, K. Ando, I. Karube, H. Matsuoka and S. Suzuki, J. Food Sci., 48 (1983) 496.
9 E. Watanabe, K. Toyama, I. Karube, H. Matsuoka and S. Suzuki, Eur. J. Appl. Microbiol. Biotechnol., 19 (1984) 18.
10 E. Watanabe, K. Toyama, I. Karube, H. Matsuoka and S. Suzuki, J. Food Sci., in press.
11 E. Watanabe, T. Ogura, K. Toyama, I. Karube, H. Matsuoka and S. Suzuki, Enzyme Microb. Technol., 6 (1984) 207.
12 I. Karube, H. Matsuoka, S. Suzuki, E. Watanabe and K. Toyama, J. Agric. Food Chem., 32 (1984) 314.
13 S. Ehira, H. Uchiyama, F. Uda and H. Matsumiya, Bull. Jpn. Soc. Sci. Fish., 36 (1970) 491.

Analytica Chimica Acta, 164 (1984) 147—152
Elsevier Science Publishers B.V., Amsterdam — Printed in The Netherlands

FLOW-THROUGH TUBULAR PVC MATRIX MEMBRANE ELECTRODE WITHOUT INNER REFERENCE SOLUTION FOR FLOW INJECTION ANALYSIS

S. ALEGRET, J. ALONSO, J. BARTROLÍ* and J. M. PAULÍS

Departament Química Analítica, Facultat de Ciències, Universitat Autònoma Barcelona, Barcelona (Spain)

J. L. F. C. LIMA and A. A. S. C. MACHADO

Departamento Química, Faculdade de Ciências, Universidade Porto, 4000 Porto (Portugal)

(Received 6th March 1984)

SUMMARY

A simply constructed tubular PVC matrix membrane electrode without inner reference solution suitable for flow injection analysis is described. The nitrate-selective electrode developed allows simple replacement of an exhausted membrane, or change of function with a new sensor membrane. The compact design ensures mechanical stability and the tubular configuration minimizes distortion of the hydrodynamic flow in the detector. Nitrate can be determined in the range 10^{-1}—10^{-5} M, under different flow conditions, with a sampling frequency of about 120 h^{-1}.

The growing demand for analytical methods in industrial, environmental and clinical monitoring has stimulated the development of flow-through techniques such as segmented flow analysis and flow injection analysis (f.i.a.). Among the wide range of detectors used are different types of flow-through electrodes and potentiometric cells [1]. An important feature of these cells is that their geometry can cause much variation in the hydrodynamic conditions of the flow, and so can alter the response obtained from the electrode (stability, reproducibility, response time) [2].

In flow injection analysis, the use of a tubular configuration seems ideal, as the flow characteristics can be kept constant throughout the system. Several tubular potentiometric detectors have been described for f.i.a., including solid-membrane electrodes [3]. In recent years, much effort has been spent on the development of liquid-membrane electrodes, particularly after the introduction by Moody et al. [4] of the non-porous PVC matrix type in which the ion-exchanger and solvent are incorporated. From a mechanical point of view, the inconveniences of these ion-selective electrodes in the construction of flow-through tubular detectors are serious, as the design is excessively complicated by the need to maintain an inner reference solution in contact with the membrane [5, 6]. Some workers have

0003-2670/84/$03.00

replaced the reference solution by solid inner contacts [7, 8]. Lima and Machado [9] suggested the use of an epoxy conductive resin (with a silver base) as a solid inner contact for the construction of liquid membrane electrodes in a PVC matrix. Some reservations had earlier been expressed about this type of electrode [10, 11] because of the apparent absence of reversible thermodynamic processes in the PVC membrane-solid contact interface. The establishment of an inner reference system formed by the solid contact and oxygen has been proposed [12—14]; the oxygen is considered to diffuse from the solution through the PVC membrane until the equilibrium is reached.

This communication describes the construction of a tubular nitrate-selective electrode based on a mobile carrier held in a PVC matrix without inner reference solution, and its behavior in unsegmented continuous flow systems. In previous work [15], this nitrate-selective electrode was evaluated under batch conditions.

EXPERIMENTAL

Apparatus and reagents

Figure 1 is a schematic diagram of the system used to test the flow-through electrodes. The system is composed of a Tecator 5020 Analyzer which has a four-channel (variable loop) automatic injection valve and two peristaltic pumps; the whole is controlled by a microprocessor. The injection valve and the detector are connected by teflon tubing (0.7 mm i.d.). The grounding electrode was a stainless steel tube (0.7 mm i.d.) which was earthed. The potentials were measured at room temperature with a 517 Crison Digilab millivoltmeter connected to a Hitachi Model 56.1002 recorder. A saturated calomel electrode was used as reference.

All the chemicals used were of analytical-reagent grade. The stock solutions of nitrate and the ionic-strength adjustment buffers were prepared with deionized water. The nitrate liquid ion-exchanger was obtained from Orion Research (92-0702). The activating solution (see below) was prepared by adding 0.25 ml of the commercial nitrate liquid ion-exchanger solution to a solution of 0.08 g of PVC in 3 ml of tetrahydrofuran. The epoxy conductive resin was obtained from Epoxy Technology, P.O. Box 567, Billerica, MA 01821, U.S.A.

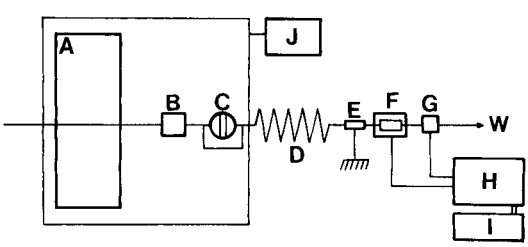

Fig. 1. Schematic flow diagram of the system: A, pump; B, pulse suppressor; C, injection valve; D, mixing coil; E, grounding electrode; F, tubular electrode; G, reference electrode; H, potentiometer; I, recorder; J, microprocessor; W, waste.

Construction of the tubular electrode

The conducting support was prepared by placing the silver epoxy resin inside a cylindrical glass mold (5 mm i.d. × 1.5 cm long) and curing it at 105°C for 2 h. Electric contact was made by winding the inner wire of a shielded cable round the molded cylinder. The whole device was then put into a mold which was filled with liquid perspex. When the liquid perspex polymerized, it covered the conducting support, thus ensuring good electric isolation as well as perfect mechanical stability. Later the cylindrical silver epoxy support was drilled longitudinally with a 1.5-mm diameter drill, and screw threads for assembling the connectors of the tubes of the flow system were machined at the extremes (see Fig. 2).

The activating ion-exchanger was deposited in layers inside the cylinder by pumping the activating solution through the tube (peristaltic pump) and allowing the tetrahydrofuran to evaporate slowly. The inner wall of the cylinder was thus covered with a fine membrane of the sensor suspended in PVC, leaving an inner diameter of ca. 0.7 mm. This technique also makes it easy to replace the membrane when it shows loss of characteristics, or to replace it by a new sensing system. To clean the epoxy support, it is only necessary to pump tetrahydrofuran through it for a few minutes.

Flow system

The tubular nitrate electrode was inserted in the system as shown in Fig. 1. The carrier solution (0.165 M potassium sulfate) was pumped at a flow rate of 2.8 ml min^{-1}. In order to stabilize the baseline, a concentration of 10^{-6} M potassium nitrate was added to the carrier solution. To avoid interference from parasitic currents generated by the peristaltic pumps, a pulse suppressor was used and a grounding electrode was placed immediately before the tubular electrode [16]. With these two attachments in place, the oscillations of the baseline potential were less than 0.1 mV. The parameters, flow rate, injection volume, and the tube length of the flow-injection system, were varied so as to establish their influence on the behavior of the electrode.

RESULTS AND DISCUSSION

Behavior of the tubular electrode

In initial tests, the values of the flow-system parameters upon which dispersion fundamentally depends (injection volume, flow rate and length of tube between injection valve and detector [17]) were varied within the normal range. The injected volume was found to influence dispersion most strongly (Fig. 3). Dispersion values were calculated from the equation [18] $\log D = (H_0 - H^*)/S$, where S is the value of the experimental slope, H_0 is the height of the peak (in mV) obtained by pumping a carrier solution of potassium sulfate with a fixed concentration of nitrate, and H^* is the height of the peak (in mV) obtained by injecting a nitrate solution of the same concentration into a carrier solution of potassium sulfate.

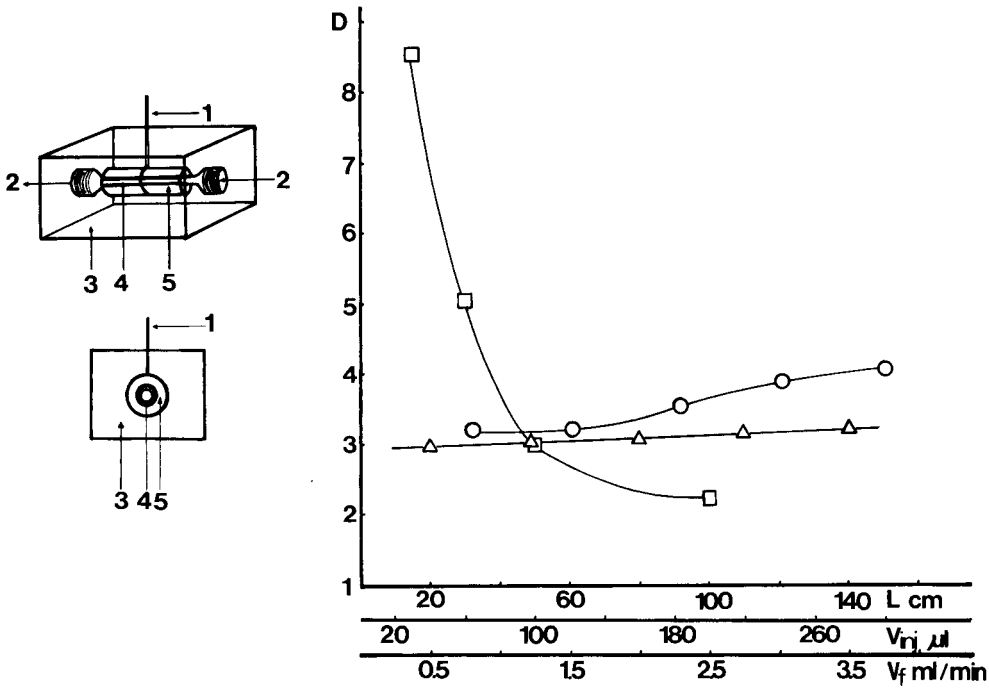

Fig. 2. Tubular flow-through electrode: (1) electric lead; (2) inlet/outlet screws; (3) perspex body; (4) sensor membrane; (5) conductive epoxy.

Fig. 3. Effect of the different flow-system parameters on the dispersion, D. (△) Tube length (V_f = 2.8 ml min^{-1}, V_{inj} = 100 µl); (○) flow rate (L = 90 cm, V_{inj} = 100 µl); (□) injection volume (L = 90 cm, V_f = 2.8 ml min^{-1}). In all cases, the nitrate concentration injected was 5×10^{-3} M.

The upper and lower limits of the near-Nernstian response range varied as a function of dispersion. Under optimal conditions (at high or low dispersion values), these limits were 10^{-1} M and 8×10^{-5} M, respectively. Obviously, it was not possible to obtain these limiting values simultaneously with the same flow parameters. Additional studies showed that it was possible to obtain useful responses to the nitrate concentration in the sub-Nernstian zone by using flow lines involving little or no dispersion. Useful responses could be obtained down to 10^{-5} M nitrate.

The dynamic response of the detector was studied by injecting standard solutions of nitrate prepared with the same background electrolyte concentration as the carrier solution. A system with very low dispersion was used so that the response time depended entirely on the detector [19, 20]. The time was recorded from the beginning of the variation of the baseline potential until it reached 63% and 95% of the steady-state potential. As Table 1 shows, these response times for different concentrations of nitrates are very fast in

TABLE 1

Response time for the tubular nitrate electrode in the flow-injection system

Concentration (M)	Response time (s)		Time for return to baseline (s)
	63%	95%	
10^{-4}	2.8 (±0.2)	7.4 (±0.3)	14.5 (±1)
10^{-3}	1.0 (±0.1)	6.2 (±0.3)	20.0 (±1)
10^{-2}	1.6 (±0.1)	5.3 (±0.2)	25.0 (±1)

the system used. Table 1 also shows the times for return to the baseline measured under the same conditions. The values obtained indicate that viable sample throughputs are around 120 h^{-1}, which is much higher than those obtained with other tubular detectors [3, 6].

Reproducibility was evaluated from repeated injections of 100 μl of 10^{-4}, 10^{-3}, 10^{-2} M solutions of potassium nitrate. The relative standard deviations of the potentials measured for sets of 10 injections were 0.1, 0.56 and 0.44%. In order to confirm the stability of the electrode response, it was tested repeatedly over a long period of time. The electrode maintained a slope of 57—55 mV for one month, after which the slope fell suddenly and the sensor had to be renewed.

A parameter which it was important to establish was the calibration frequency required over a long period of continuous work. The oscillations of the electrode potentials obtained were 1—2 mV/day, which suggests that it is necessary to standardize the electrode daily.

We thank Dr. J. D. R. Thomas (UWIST, Cardiff, Wales), for his valuable comments. Financial support for the exchange of researchers received under a "Portuguese—Spanish Integrated Action" from the respective academic authorities is also gratefully acknowledged.

REFERENCES

1 A. K. Covington, Ion-Selective Electrode Methodology. Vol. 2, CRC Press, FL, 1979, p. 90.
2 P. L. Bailey, Analysis with Ion Selective Electrodes, Heyden, London, 1976, pp. 204—207.
3 W. E. van der Linden and R. Oostervink, Anal. Chim. Acta, 101 (1978) 419.
4 G. J. Moody, R. B. Oke and J. D. R. Thomas, Analyst (London), 95 (1970) 910.
5 A. J. Frend, G. J. Moody, J. D. R. Thomas and B. J. Birch, Analyst (London), 108 (1983) 1357.
6 D. S. Papastathopoulos, E. P. Diamandis and T. P. Hadjiioannou, Anal. Chem., 52 (1980) 2100.
7 M. Trojanowizc, Z. Augustowska, W. Matuszewski, G. Moraczewska and A. Hulanicki, Talanta, 29 (1982) 113.
8 R. W. Cattrall and H. Freiser, Anal. Chem., 43 (1971) 1905.

9 J. L. F. C. Lima and A. A. S. C. Machado, IV Reunião Nacional de Electroquímica, Braga, Portugal, 1983.
10 J. Růžička, E. H. Hansen and J. C. Tjell, Anal. Chim. Acta, 67 (1973) 155.
11 A. K. Covington, CRC Crit. Rev. Anal. Chem., 3 (1974) 355.
12 R. W. Cattrall, D. M. Drew and I. C. Hamilton, Anal. Chim. Acta, 76 (1975) 269.
13 A. Hulanicki and M. Trojanowicz, Anal. Chim. Acta, 87 (1976) 411.
14 J. G. Schindler, G. Stork, H. J. Strüh, W. Schmid, K. D. Karaschinski, Fresenius Z. Anal. Chem., 295 (1979) 248.
15 J. L. F. C. Lima and A. A. S. C. Machado, IV Reunión del Grupo de Electroquímica, RSEQ, Murcia, Spain, 1983.
16 P. van den Winkel, J. Mertens and D. L. Massart, Anal. Chem., 46 (1974) 1765.
17 J. Růžička and E. H. Hansen, Flow Injection Analysis, Wiley, New York, 1981.
18 M. Trojanowicz and W. Matuszewski, Anal. Chim. Acta, 138 (1982) 71.
19 E. Pungor and Y. Umezawa, Anal. Chem., 55 (1983) 1432.
20 A. Haemmerli, J. Janata and H. M. Brown, Anal. Chim. Acta, 144 (1982) 115.

Analytica Chimica Acta, 164 (1984) 153—161
Elsevier Science Publishers B.V., Amsterdam — Printed in The Netherlands

APPLICATION OF ION-EXCHANGE CHROMATOGRAPHY WITH AN ION-SELECTIVE ELECTRODE DETECTOR TO IODINE DETERMINATION IN NATURAL WATERS[a]

EDWARD C. V. BUTLER[b] and ROBERT M. GERSHEY*

Atlantic Research Laboratory, National Research Council of Canada, 1411 Oxford St., Halifax, Nova Scotia, B3H 3Z1 (Canada)

(Received 21st March 1984)

SUMMARY

A system is described which uses a selective electrode for potentiometric detection of anions in natural waters after ion-exchange separation. With an iodide-selective electrode in the flow cell, a linear relationship exists between iodide concentration and potential in the sub-Nernstian range (0—1.0 μM). The limit of detection is 0.015 μM for an injection of 125 μl of sample. For optimum electrode performance, a constant iodide background of about 0.5 μM is required in the column effluent passing through the detector. This background is added uniformly through a short section of hollow-fibre dialysis tubing in a concentric-flow diffusion cell. The detector also responds to other anions which affect the solubility of silver ion. This can be used to advantage if chromatographic separation is sufficient. Preconcentration of iodide in fresh waters on an anion guard cartridge allows determination down to 1 nM concentrations. For sea-water samples, simple chemical pretreatment permits quantitation of different iodine species.

A wide variety of detectors is presently used in ion-exchange chromatography. Individual anions have been quantified by u.v. absorbance, both direct [1, 2] and indirect [3], in addition to electrochemical [4, 5] and refractive index [6] detection. Different detectors connected in series have been used to monitor column effluents for anions as well [7].

For samples with a diversity of anionic constituents, the almost universal response of conductimetric and refractive index detectors can be a disadvantage if chromatographic resolution is inadequate. Electrochemical detectors are more selective, sensitive [8, 9] and flexible.

Most quantitative applications of electrochemistry to liquid chromatography to date have used amperometric or coulometric detection [10—12]. Although there has been frequent use of ion-selective electrodes (i.s.e.'s) as potentiometric detectors in flow injection systems [9, 13, 14], there are few examples of such application to high-performance liquid chromatography (h.p.l.c.) [9].

---

[a]NRCC No. 23604.

[b]Present address: Division of Oceanography, CSIRO Marine Laboratories, G.P.O. Box 1538, Hobart, Tas. 7001, Australia.

0003-2670/84/$03.00

This paper describes the use of an iodide-i.s.e. to measure iodide separated from other anions in fresh waters and sea water by ion-exchange h.p.l.c. For efficient operation of the detector, a background level of iodide is diffused into the column effluent just upstream of the detector. This feature enables on-line preconcentration of iodide on an anion guard cartridge. For sea water, it is advantageous to determine iodide directly and to quantify iodate as the difference between total iodine and iodide. This paper describes the direct determination of iodide in a coastal sea water, and the quantitation of other iodine species after simple chemical pretreatment.

EXPERIMENTAL

Apparatus

The chromatographic system is shown in Fig. 1. It consists of a Beckman single-piston h.p.l.c. pump (Model 110A or 112) with an Autochrom solvent selector, a syringe-loading sample injector (Rheodyne 7125) with a 125-μl sample loop for direct sample introduction, and a combination switching valve (Rheodyne 7000)/loop injection port (Rheodyne 7011) with a guard cartridge (30 mm × 4.6 mm i.d., Brownless AX-GU) in the loop position for sample preconcentration. A presaturator column (200 mm × 5 mm i.d., Brownlee AX-300 bulk phase) was installed between the pump and injection valves. A weakly basic ion-exchange separator column was used (100 mm × 4.6 mm i.d., Brownlee AX-MP cartridge).

The flow cell for the potentiometric detector (Fig. 2) was constructed from a Plexiglas block. An iodide-selective electrode (HNU, ISE-30-53-01) and Ag/AgCl double-junction reference electrode (Chemtrix, RD 1015F) impinged on a 1-mm bore channel. The flow cell had a small volume (6.4 μl). Thus, high linear velocities over the electrode surface and a small boundary layer thickness promoted rapid response at the flow rates used. The reference electrode was in close proximity to the detector electrode to decrease electrical noise in the system. Standard plastic connectors and polyethylene tubing (0.79 mm i.d., 1.6 mm o.d.) were used. Exposed external

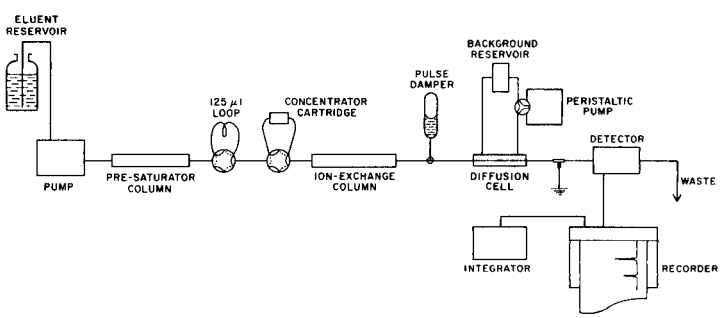

Fig. 1. Schematic diagram of h.p.l.c. system.

surfaces of the unit were painted black, owing to the light sensitivity of the Ag_2S/AgI crystal of the iodide electrode.

A concentric flow diffusion cell to introduce an iodide background into the column effluent (Fig. 3) was fabricated from stainless steel tube fittings (Swagelok, SS-100-R-4-BT and SS-400-3) and 6.4-mm o.d. polyethylene tubing. The diffusion membrane was a 14-mm section of hollow fibre dialysis tubing (Amicon P5-20) connected in-line with 1.6-mm o.d. polyethylene tubing by collars of heat shrinkable plastic. To minimize pressure fluctuations, the external solution (87 ml) was circulated (10 ml min^{-1}) in an enclosed loop by a peristaltic pump (Cole-Parmer, K-7520-10) fitted with two pump heads connected in parallel. Electrical noise from the peristaltic pump was reduced by grounding the eluent stream. The rate of iodide diffusion into the column effluent was very susceptible to pressure fluctuations across the dialysis membrane; small pulsations caused by the h.p.l.c. pump were attenuated by using a sealed 10-ml glass syringe in a dead-end configuration immediately preceding the diffusion cell. Air compressed in the syringe provided the damping action.

Potentials across the detector electrodes were measured by a digital pH/mV meter (Radiometer PHM-63). The meter output was monitored on a strip chart recorder (Honeywell AFB-100A). Peak areas were measured with a single-channel computing integrator (Spectra-Physics Minigrator). For assessment of baseline stability, analog signals from the millivoltmeter were acquired using an Apple II+ computer with an analog-to-digital converter (Interactive Microware).

Supplementary determinations of iodine species in the sea water were done by differential pulse polarography (EG & G Princeton Applied Research Model 174A) with a strip-chart recorder (Heathkit, Model IR-18M).

Reagents

All salts used were of analytical-reagent grade, and solutions were prepared with distilled, deionized water (Millipore, Milli-Q).

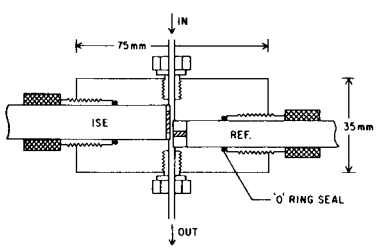

Fig. 2. The i.s.e.-flow cell.

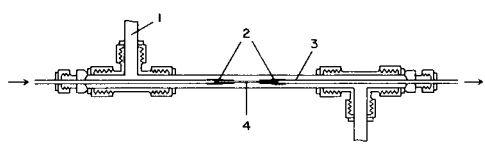

Fig. 3. Concentric-flow diffusion cell: (1) external feed solution; (2) collars from heat-shrink plastic; (3) 1.6 mm o.d. polyethylene tubing transporting eluent; (4) hollow-fibre dialysis tubing.

The eluent was prepared by dissolving 17.0 g of sodium nitrate in deionized water, pipetting in 20 ml of 1 M phosphate buffer (0.5 M NaH_2PO_4, 0.5 M Na_2HPO_4) and diluting to 2 l. The pH of this solution was about 6.7. Before use, it was filtered through a glass fibre filter (Gelman, GF/C), then degassed under vacuum with sonication.

The external solution in the diffusion cell was this eluent supplemented with a small amount of potassium iodide, typically 1×10^{-4} M. Stock standard potassium iodide solution (1×10^{-2} M) was kept refrigerated. Working standard solutions were prepared daily by serial dilution with water or eluent.

Collection and treatment of water samples

Polyethylene bottles (250 ml) were used to take surface waters directly, or in the case of some well-waters, by tap, after thorough flushing of the line. The sea water was sampled by tap from the Aquatron system at Dalhousie University, which is supplied from an intake at 15-m depth in the N.W. Arm of Halifax Harbour, Nova Scotia. All samples were filtered through 0.45-μm membrane filters (Millipore, type HA) within 24 h of collection. The filters were prewashed with deionized water. Filtrates, at natural pH, were stored in the original polyethylene bottles at 4°C in the dark.

Procedure

The eluent is pumped at a flow rate of 1.0—1.2 ml min^{-1} for at least 2 h to equilibrate the system. For direct quantitation, a 125-μl sample aliquot is injected onto the separator column and the iodide concentration is quantified by comparison of the peak height with heights of a range of standards (0.05—1.00 μM).

For enrichment of iodide, a precise volume (2—10 ml) of sample is passed through the concentrator cartridge, manually for <2.0 ml, or with a syringe pump for 2—10 ml. The cartridge is washed with 0.5 ml of deionized water, and then back-flushed with eluent onto the separator column. The iodide concentration is quantified using a calibration curve prepared from similarly preconcentrated standards.

Samples with obvious humic coloration are pretreated by passage through a tetrahydrofuran-activated C-18 Sep-Pak cartridge (Waters Associates).

RESULTS AND DISCUSSION

Performance characteristics

Previous reports indicated that a background level of an electroactive species should be included in the eluent to give a stable electrode potential [13, 14]. We have found that at flow rates of 1.0—1.5 ml min^{-1}, approximately 0.5 μM iodide in the eluent stream was optimal; at background levels greater than this, sensitivity decreased, while for lower iodide concentrations, the benefit of greater sensitivity was outweighed by an increase in response

time and impaired peak resolution. Although it is a simple matter to obtain a constant iodide concentration in the detector stream by adding it to the eluent reservoir, there are disadvantages to this approach. Samples having iodide concentrations less than the background level appear as negative peaks, while those with concentrations near or equal to this level cannot be determined. In-line preconcentration is precluded with the analyte already present in the eluent. The approach used in this study nullifies these problems.

The iodide electrode is influenced by other anions which form insoluble silver salts or that complex silver ion; chloride, bromide, sulfide, cyanide, thiocyanate and thiosulfate all elicited signals from the detector used here. Injection of a standard solution of bromide, iodide, thiocyanate and thiosulfate onto the anion-exchange column produced the chromatogram shown in Fig. 4. The iodide signal was a single positive peak with some tailing.

Each of the "interfering" anions produced a signal similar to the first derivative of a peak having the form of the iodide response. This could be caused by transient response to, first, the leading edge of the interfering anion zone, and then the trailing edge of the zone. Lindner et al. [15] demonstrated exactly the same response when changes in bromide concentration were monitored by a silver iodide membrane electrode. Their system was operated at much higher flow rates to give faster response times which yielded two distinct signals, whereas in the present case there was a coalescence of signals. In a recent theoretical treatment of electrode behaviour based on a solid-state membrane model [16], transient response was predicted for anions for which the bulk electrode membrane shows poor selectivity.

The detector response for different concentrations is shown in Fig. 5. The calibration curves are noticeably curved for concentrations greater than 1.00 μM. Least-squares fits of the linear portion of the calibration curve of peak height as a function of concentration gave a slope of 6.37 mV μM^{-1} (2 s.d. = 0.05), an intercept at —0.02 mV (2 s.d. = 0.03) with a standard error of 0.05 and a correlation coefficient of 0.9996. The linear dependence of potential with concentration at very low analyte levels (sub-Nernstian region) has been well documented by other authors using potentiometric detectors in flow systems [17—19].

The relative standard deviation (r.s.d.) of six separate runs on synthetic solutions containing 0.25 and 2.00 μM iodide were 3.9 and 0.4%, respectively, for peak height, and 4.7 and 1.1% for peak area. The larger concentration is measured with high precision, but one must consider the disadvantage of working outside the linear range of the calibration curve (Fig. 5). In this work, peak heights were routinely used for quantitation, as there was no advantage gained from the use of peak areas. Eight replicate determinations on well-water after preconcentration from a 1-ml sample yielded a mean result of 0.064 μM iodide with r.s.d. 2.4%.

A recovery of 96% was found for preconcentration of iodide on the AX-GU cartridge. This was ascertained by comparing the slope obtained for standard additions of iodide to a well-water sample with a calibration curve

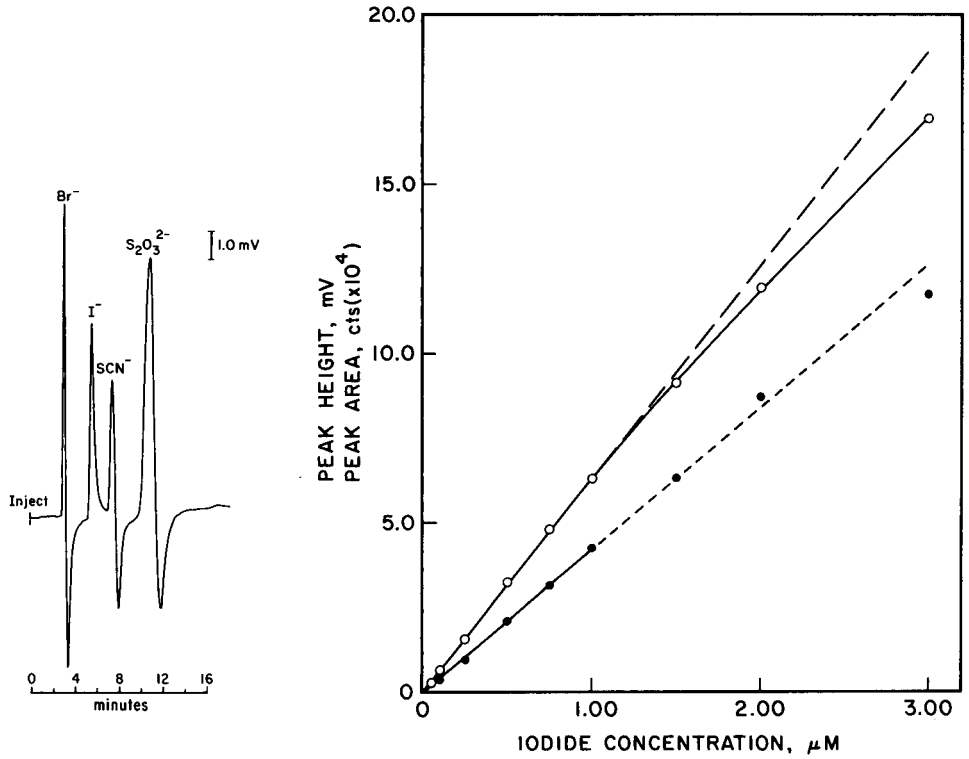

Fig. 4. Chromatographic separation of 250 μM Br^- (3.1 min), 1.0 μM I^- (5.6 min), 150 μM SCN^- (7.4 min), 50 μM $S_2O_3^{2-}$ (10.8 min). Eluent, 0.1 M $NaNO_3$, 0.01 M NaH_2PO_4/Na_2HPO_4; flow rate 1.2 ml min^{-1}; injection volume, 125 μl; temperature, 23 ± 1°C; iodide concentration in external feed solution, 1.0×10^{-4} M.

Fig. 5. Calibration curve for iodide based on peak height (○) and peak area (●) measurements. Flow rate, 1.5 ml min^{-1}; other experimental conditions as for Fig. 4.

for iodide in deionized water. For the same sample, close agreement between direct injection and quantitation after the preconcentration step corroborated the above result, as did the observation that the peak height was directly proportional to the volume (0.5—2.0 ml) of sample preconcentrated.

The limit of detection (taken as twice the standard deviation of the digitized baseline signal over a 1000-s interval) was estimated to be 0.015 μM for direct injection. With preconcentration, this value could be decreased by an order of magnitude.

Iodide in fresh waters

Fresh-water samples were examined first by direct injection; if the iodide concentration was too low for accurate determination, sample volumes of up to 10 ml were preconcentrated before the anions were back-flushed onto the separator column. A typical chromatogram of a well-water sample, after

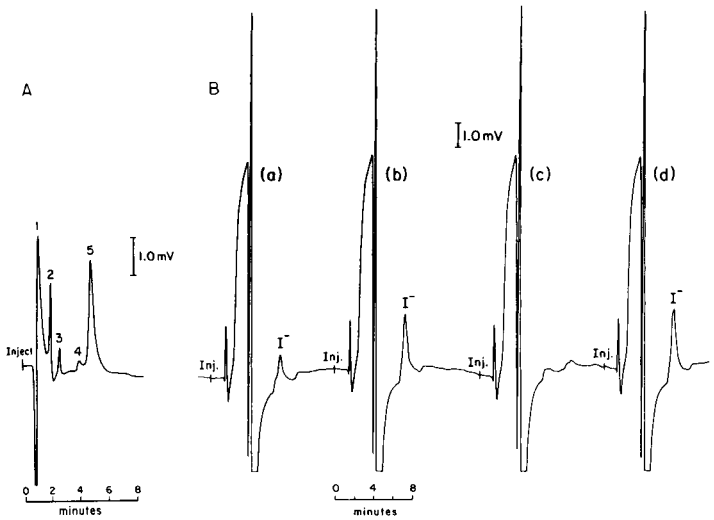

Fig. 6. A, Chromatogram of a well-water sample (conditions as for Fig. 4): (1) solvent front; (2) chloride; (3) bromide; (4) unknown; (5) iodide. B, Chromatograms of a seawater sample (conditions for Fig. 4, except that flow rate was 1.0 ml min^{-1}): (a) untreated, (b) addition of 0.5 M ascorbic acid (100 μl) to deaerated sea water (20 ml); (c) 4-h u.v. irradiation of sea water (50 ml) to which a few drops of 30% H_2O_2 had been added; (d) an aliquot from (c) after treatment (b).

preconcentration, is shown in Fig. 6A. The identity of the other halide peaks was confirmed by preconcentrating an appropriate dilution of a synthetic sample (containing chloride, bromide and iodide) and comparing retention times.

The results obtained for the various fresh-waters fall within reported concentration ranges <0.01—0.40 μM for low mineral ground waters [20, 21]; <0.001—0.14 μM for surface waters [22, 23]. The iodide contents of local tap and river waters were found to be 0.002 μM and 0.004 μM, respectively; 10.0-ml samples were taken for preconcentration.

Iodide in sea water

Iodine in sea water occurs at a concentration of 0.4—0.5 μM, and the iodide fraction ranges from 0 to 0.2 μM, being highest in the surface waters of the euphotic zone. Other iodine species are in insignificant concentrations in seawater.

A protocol to quantify inorganic iodine species in sea water by the present method is: (i) direct determination of iodide, (ii) reduction of iodate to iodide by treatment of the deaerated sample with ascorbic acid, and (iii) quantitation of total iodide to give iodate plus iodide concentration. In preliminary tests with sea water, added iodate was converted quantitatively to iodide by the ascorbic acid reductant. Ultraviolet irradiation of a sample solution oxidizes all iodine species to iodate [24]. After reduction to iodide by ascorbic acid, total dissolved iodine can be determined.

The iodide and iodate concentrations in a sea-water sample (see Fig. 6B) were found to be 0.15 and 0.21 μM, respectively, and organo-iodine was estimated at 0.03 μM, to give a total dissolved iodine concentration of 0.39 μM. Results obtained five months later using differential pulse polarography [24] were 0.22 μM for iodate, 0.41 μM for inorganic iodine, and 0.19 μM iodide (by difference) and 0.43 μM total dissolved iodine.

Chloride and bromide interfere to some extent with this method. The large negative dip preceding the iodide peak (Fig. 6B) resulted from the combined transient response to these two anions. The use of a lower flow rate (1.0 ml min^{-1}) is required to resolve the iodide signal adequately and it is necessary to locate the baseline beneath the iodide peak from a chromatogram of the u.v. photo-oxidized sample before ascorbic acid treatment (see Fig. 6B, C). An additional complication is that preconcentration is not possible with a sea-water sample, or for that matter, any samples with high salt content, because the concentrator cartridge is rapidly overloaded. Given these limitations, the useful range for iodide in sea water is 0.015—1.00 μM.

The authors thank G. K. Morstatt for construction of the flow cell; K. Manson, Amicon Corp., for provision of hollow-fibre dialysis tubing; the Department of Oceanography, Dalhousie University for use of the ultraviolet irradiator; D. Barkhouse, D. J. Embree, E. T. Garside and B. D. Johnson for assistance in collecting water samples; and L. Ramaley, Department of Chemistry, Dalhousie University, for access to the polarographic instrumentation. One of us (E.C.V.B.) acknowledges the receipt of a Visiting Fellowship from the Natural Sciences and Engineering Research Council.

REFERENCES

1 T. Kamiura, Y. Mori and M. Tanaka, Anal. Chim. Acta, 154 (1983) 319.
2 K. J. Stetzenbach and G. M. Thompson, Ground Water, 21 (1983) 36.
3 R. A. Cochrane and D. E. Hillman, J. Chromatogr., 241 (1982) 392.
4 T. Imanari, K. Ogata, S. Tanabe, T. Toida, T. Kawanishi and M. Ichikawa, Chem. Pharm. Bull., 30 (1982) 374.
5 G. S. Pyen and D. E. Erdmann, Anal. Chim. Acta, 149 (1983) 355.
6 P. R. Haddad and A. L. Heckenberg, J. Chromatogr., 252 (1982) 177.
7 B. B. Wheals, J. Chromatogr., 262 (1983) 61.
8 P. T. Kissinger, Anal. Chem., 49 (1977) 447A.
9 K. Brunt, in J. F. Lawrence (Ed.), Trace Analysis, Vol. 1, Academic, New York, 1981, p. 47.
10 R. E. Shoup, Recent Reports on Liquid Chromatography/Electrochemistry, Bioanalytical Systems, West Lafayette, IN, 1982.
11 J. H. Larochelle and D. C. Johnson, Anal. Chem., 50 (1978) 240.
12 J. E. Girard, Anal. Chem., 51 (1979) 836.
13 Zs. Feher, G. Nagy, K. Toth and E. Pungor, Anal. Chim. Acta, 98 (1978) 193.
14 J. Slanina, W. A. Lingerak and F. Bakker, Anal. Chim. Acta, 117 (1980) 91; J. Slanina, F. P. Bakker, P. A. C. Jongejan, L. Van Lampen and J. J. Mols, Anal. Chim. Acta, 130 (1981) 1.

15 E. Lindner, K. Toth and E. Pungor, Anal. Chem., 54 (1982) 202.
16 W. E. Morf, Anal. Chem., 55 (1983) 1165.
17 W. Rohse, G. Roewer, R. Boran and R. Hellmig, Z. Chem., 22 (1982) 226.
18 M. C. Franks and D. L. Pullen, Analyst (London), 99 (1974) 503.
19 M. Trojanowicz and W. Matuszewski, Anal. Chim. Acta, 151 (1983) 77.
20 G. A. Dean, N.Z. J. Sci., 6 (1963) 208.
21 G. L. Feder, U.S. Geol. Surv. Prof. Pap. 954-E, 1979.
22 D. C. Whitehead, J. Appl. Ecol., 16 (1979) 269.
23 D. C. Kocher, Environ. Int., 5 (1981) 15.
24 E. C. V. Butler and J. D. Smith, Deep-Sea Research, 27A (1980) 489.

Analytica Chimica Acta, 164 (1984) 163—170
Elsevier Science Publishers B.V., Amsterdam — Printed in The Netherlands

OPTIMIZATION AND COMPARISON OF FOUR MERCURY WORKING ELECTRODES IN SPECIATION STUDIES BY DIFFERENTIAL-PULSE ANODIC STRIPPING VOLTAMMETRY

CEES J. M. KRAMER*, YU GUO-HUI[a] and JAN C. DUINKER[b]

Netherlands Institute for Sea Research, P.O. Box 59, 1790 AB Den Burg, Texel (The Netherlands)

(Received 2nd April 1984)

SUMMARY

Four types of working electrodes are compared with respect to sensitivity, resolution, peak width and suitability for copper speciation studies by differential-pulse anodic stripping voltammetry. The hanging mercury drop electrode, two rotating mercury film electrodes with in-situ and pre-formed films and a stationary mercury film electrode with a vibrationally induced jet-stream are examined. The last electrode appears to be the most useful system with the highest sensitivity. Conditions for mercury film formation must be optimized for each individual electrochemical system in order to avoid erroneous conclusions from standard addition procedures and apparent complexation capacity measurements.

The different species of an element in sea-water solution must be distinguished for understanding distribution patterns, geochemical cycles, bioavailability and toxic effects in the marine environment. Differential-pulse anodic stripping voltammetry (d.p.a.s.v.) has sufficient sensitivity to allow direct measurements of very low concentrations of some trace metals in natural waters; it also allows the distinction and determination of different species with none or only minor sample pretreatment, provided that sampling, storage and sample treatment have been done appropriately.

The mercury working electrodes commonly used consist of either a mercury drop, such as the hanging mercury drop electrode (Kemula type; HMDE) and the static mercury drop electrode (SMDE) [1] or a mercury film (MFE) on an electroactive support like glassy carbon (GC) or gold. The mercury film can be applied to the GC surface prior to or during the voltammetric measurement. In the former procedure (pre-formed MFE) the mercury solution is replaced by the sample. The second method (in-situ MFE) [2] requires a spike of Hg^{2+} ions to the sample; mercury and analytes are then codeposited. In all cases, the analyte has to be transported from the bulk

Present addresses: [a]Second Institute of Oceanography, National Bureau of Oceanography, Hangzhou, Peoples Republic of China. [b]Institut für Meereskunde, Universität Kiel, Düsternbrookerweg 20, D-2300 Kiel, Federal Republic of Germany.

0003-2670/84/$03.00

solution to the mercury/water interface. Various transport mechanisms are used. Different forms of rotating electrodes with correspondingly different stirring properties were proposed by Opekar and Beran [3]. Commercially available rotating (RMFE) or stationary (SMFE) film electrodes usually have a flat surface with straight sides. A new transport design was presented by Magjer and Branica [4], who claimed that more efficient transport towards the electrode surface and decreased thickness of the effective diffusion layer resulted from the action of a vibrator and the presence of a conically shaped hole in a disc below the stationary film electrode (jet-stream mercury film electrode, JMFE). Certain advantages and disadvantages associated with the various electrode types are summarized in Table 1.

In previous reports, these types of electrode have been discussed individually or only two types have been compared [2, 4—7]. In this paper, the characteristics of four electrode types (HMDE, RMFE pre-formed, RMFE in-situ and JMFE pre-formed) are compared with respect to their suitability in the determination of very low concentrations, in distinguishing between different (copper) species, and in measuring the apparent complexation capacity of natural waters for copper. The accuracy and precision of the results obtained with these electrodes in d.p.a.s.v. depend on sensitivity, peak half-width, peak potential (compared to the potential window available) and calibration. These properties may be affected by film thickness, pH and

TABLE 1

Comparison of mercury drop and film electrodes

	MDE	MFE
Types	HMDE, SMDE	RMFE, JMFE; pre-formed or in situ
Electrode form	Hg drop	Tiny drops on carrier surface
Electroactive area	Small	Large
Variation of area	Easy, with drop size	Difficult
Mercury	New drop for each measurement	Many measurements with same film possible
Time necessary for uniform distribution of M in Hg	Long	Short
Stripping process	Slow, broad peaks	Fast, sharp peaks
Resolution and precision	Acceptable	Good
Use at moderately high Me concentrations	Good	Variable
Electrode movement	No	Possible
Sample transport	Magnetic stirring, flow-through cell	Rotation of electrode, jet stream by vibrator, flow-through cell, magnetic stirring
Suitable for speciation studies	Yes	In situ, no; pre-formed, yes

the nature and concentration of organic matter. It was found that for each individual electrochemical system, it was advisable to examine the effects of these parameters and to optimize them rather than take working conditions straight from the literature.

EXPERIMENTAL

A PAR model 174 Polarographic Analyzer was used with a model 315 automated electroanalysis controller (E.G. & G./PARC). For d.p.a.s.v., the modulation amplitude was 25 mV, drop time 0.5 s, and scan rate 5 mV s^{-1}. Conditioning and deposition potentials were 0 and −900 mV, respectively. The conditioning time for the film electrodes was 1.5 min; no conditioning was used for the HMDE. The deposition time was 180 s, unless stated otherwise. When the Kemula-type HMDE (Metrohm, E-410) was used, the sample was stirred with a teflon-covered bar driven by a synchronous motor (Metrohm, E-405). The home-made RMFE (6 mm diameter; GCA grade, Tokai) was rotated by a synchronous motor at 1500 rpm (Dunkel Motoren, ITT), designed as described by Sipos et al. [8]. The transport of solution to the JMFE (6 mm diameter, GCA Tokai) was achieved by a vibrating disc with a conical hole, placed below the electrode surface. Vibration frequency was 50 Hz [4].

All GC electrodes were polished to a mirror-like finish with 6- and 3-μm diamond paste (Hyprez, Engis) and 1-, 0.3- and 0.05-μm aluminium oxide (Buehler) successively, until satisfactory baseline characteristics were obtained. A platinum coil was used as counter electrode; again, a clean electrode was essential to avoid problems with non-linear response [9] or poorly shaped voltammograms and abrasive powder or an electrochemical procedure [10] were used. A Ag/AgCl (saturated KCl) (Metrohm) reference electrode was used. The HMDE and RMFEs were fitted in a silanized glass polarographic cell (25 ml, Metrohm); the JMFE was placed in a perspex housing containing a FEP teflon cell (100 ml).

The pH was measured and controlled with a pH-stat, consisting of a pH meter (Metrohm, E-632) and Impulsomat (Metrohm, E-473), connected to a solenoid valve (Bürkert, type 117A), releasing carbon dioxide to the sample solution as required. This procedure helps to maintain existing equilibria in sea-water (essential in speciation studies) in contrast to the use of buffers. Bulk sea water (35.2‰ salinity) was filtered through a 0.45-μm acid-washed Sartorius membrane filter, and stored in darkness at 4°C in high pressure polythene. A mercury arc tube (medium pressure, 1000 W, Hanovia) surrounded by quartz tubes at 6-cm distance was used for destruction of organic matter during 10 h, after addition of 0.5 ml of nitric acid and 0.03 ml of 30% hydrogen peroxide to 60 ml of sample [11]. Evaporation was prevented by water cooling.

Merck Suprapur chemicals were used, except for carbon dioxide (lecture bottle, Baker), hydrogen peroxide (Perhydrol, Merck) and standard metal

stock solutions (Dilut-it, Baker). The mercury stock solution (8×10^{-4} M) was prepared by dissolving mercury in nitric acid. Twice-distilled water from quartz was used. All operations were done in a laminar-flow clean bench.

RESULTS AND DISCUSSION

Comparison of working electrodes

The behaviour of the various working electrodes with respect to the copper peak was studied using u.v.-irradiated seawater, which had been spiked with 0.3×10^{-6} mol dm^{-3} Cu^{2+} (HMDE) or 9.4×10^{-8} mol dm^{-3} Cu^{2+} (MFEs). For d.p.a.s.v., 3.0-min deposition times at pH 2.9 were used. Characteristic voltammograms are given in Fig. 1 for the different electrodes tested. Quantitative aspects are summarized in Table 2. The peak with the HMDE (—110 mV) is broad and not ideally separated from the mercury oxidation wave; the sensitivity is about two orders of magnitude lower than that with the film electrodes. Clearly, there are important differences in performance between the different types of film electrodes. Several authors have previously studied the sensitivity, resolution and reproducibility of peaks at film electrodes, but it is difficult to compare their results because of differences in experimental conditions. As was observed by Florence [2], the pre-formed RMFE is less sensitive and had broader peaks than the in-situ RMFE; this was confirmed here. The pre-formed JMFE has by far the highest sensitivity; the peak potential (—250 mV at the RMFE) is shifted to values around —290 mV and

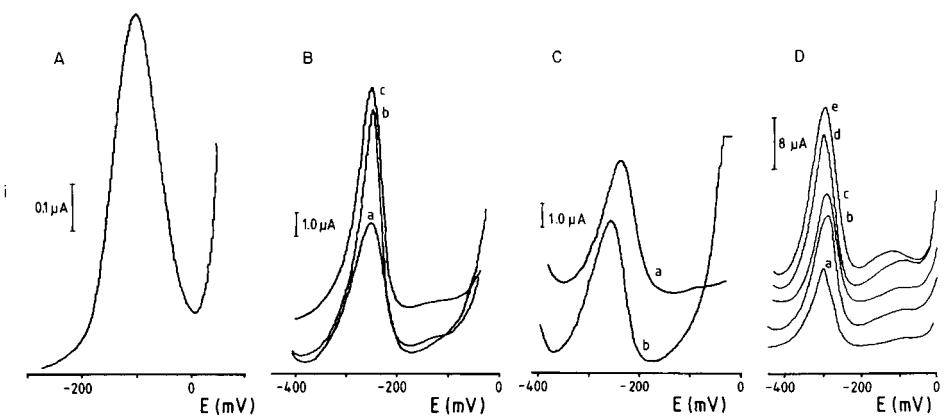

Fig. 1. Typical voltammograms of a u.v.-irradiated sea-water sample at pH 2.9. (A) Spiked with 0.3×10^{-6} M Cu^{2+} at HMDE. (B) spiked with 9.4×10^{-8} M Cu^{2+} at RMFE; film formation in situ with different mercury concentrations: (a) 8×10^{-5} M; (b) 4×10^{-5} M; (c) 2×10^{-5} M. (C) Spiked with 9.4×10^{-8} M Cu^{2+} at pre-formed RMFE; film formed from 8×10^{-5} M Hg^{2+} with deposition time: (a) 15 min; (b) 30 min. (D) Spiked with 9.4×10^{-8} M Cu^{2+} at pre-formed JMFE; film formed from 2×10^{-5} M Hg^{2+} with deposition time: (a) 5; (b) 10; (c) 15; (d) 20; (e) 30 min.

TABLE 2

Sensitivity, peak potential (E_p) and peak width ($w_{1/2}$) for copper ion at different electrodes under different conditions of film preparation. Optimal conditions for the different film electrodes are asterisked

Electrode	Hg^{2+} conc. (M)	Film t_{dep} (min)	E_p (mV)	$w_{1/2}$ (mV)	Sensitivity[a] ($A\ M^{-1}$)
HMDE	—	—	−110	90	2
RMFE	2×10^{-5}	—	−260	50	89
(in-situ)	4×10^{-5}	—	−260	45	108*
	8×10^{-5}	—	−250	70	51
RMFE	8×10^{-5}	15	−270	70	57*
(pre-formed)	8×10^{-5}	30	−260	70	57
JMFE	8×10^{-5}	5	−295	64	236
(pre-formed)	8×10^{-5}	10	−289	69	255*
	8×10^{-5}	15	−289	69	242

[a]6 mm diameter GC electrode; 3-min deposition time.

the other characteristics compare favourably with those of the pre-formed RMFE. An in-situ JMFE might have even further improved characteristics compared to the pre-formed version (analogously to the situation with the RMFEs). This may be important for total concentration determinations but it is irrelevant for speciation studies, as the addition of Hg^{2+} ions to the sample solution will change existing equilibria. In such studies, only the HMDE and pre-formed film electrodes should be used. The JMFE is the obvious choice on the basis of sensitivity.

Optimum film conditions

Theoretically, uniform distribution of deposited metal in a film is considerably faster in a thin than in a thick mercury layer. Moreover, diffusion through the layer and stripping out into the solution is faster in a thin layer [12]. Higher metal concentration in a film amalgam should result in higher sensitivity and lower resolution. Sharper peaks are expected to result from thinner films [13]. The present findings support this in general. Thick mercury films resulting from increased mercury concentrations in solution or from longer mercury deposition times gave poorer resolution and decreased sensitivity. At first sight, reduction of film thickness would seem ideal for increasing resolution and sensitivity, but these properties actually decrease below critical values of film thickness.

In addition, an important effect of film properties on calibration characteristics was observed. Figure 2 illustrates that perfectly linear behaviour can be

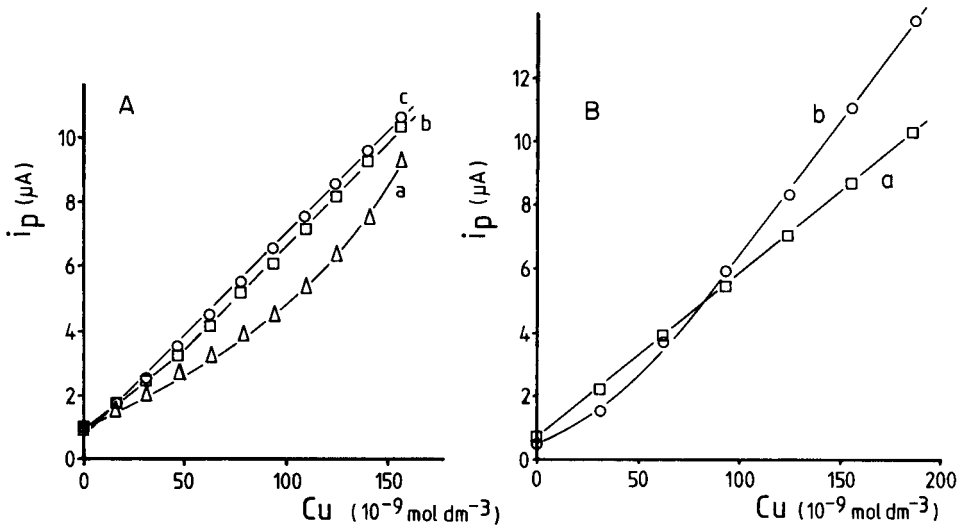

Fig. 2. Calibration curves for copper in a u.v.-irradiated sea water sample: (A) at a RMFE formed in situ (conditions as in Fig. 1B); (B) at a pre-formed RMFE (conditions as in Fig. 1C).

obtained with both in-situ and pre-formed film electrodes, but film thickness is obviously a critical factor. Accordingly, it is essential, for each individual electrochemical set-up, to establish the experimental conditions that optimize sensitivity, resolution and calibration characteristics (see below). Another important effect of variations in film properties was the shift of the mercury oxidation wave to more negative potentials, which could obscure the second copper peak around —150 mV and also affect the baseline.

The response of the three types of film electrodes was tested under a range of experimental conditions, involving different combinations of Hg^{2+} concentration in solution (2—8 × 10^{-5} M) and film formation time (5—30 min). The variations of the copper peak potential (the resolution from the oxidation wave), the peak half-width and the sensitivity for copper were studied in relation to variations in experimental conditions. The findings for the JMFE are summarized in Table 3 and Fig. 1D. Optimum conditions imply maximum separation from the mercury oxidation wave (E_p minimal), minimum peak half-width and maximum sensitivity. Table 3 shows that for a given Hg^{2+} concentration, there is a particular deposition time which satisfies these requirements simultaneously. The optimum deposition time decreases with increasing mercury concentration. It is also observed that optimum values of the properties remained essentially unchanged.

Optimum conditions should be determined for each experimental arrangement. Ideally, this would involve an experimental scheme such as that represented in Table 3, resulting in a wide range of parameter values. As sensitivity is usually the most critical factor, the maximum value can then be selected.

TABLE 3

Copper peak potential (E_p), peak width ($w_{1/2}$) and sensitivity related to different mercury concentrations[a] and film deposition times (pre-formed JMFE, sea water + 95 × 10^{-9} M Cu^{2+}, t_{dep} = 3 min, optimal values are underlined)

Film	E_p (mV)			$w_{1/2}$ (mV)			Sensitivity (A M^{-1})		
t_{dep} (min)	I	II	III	I	II	III	I	II	III
5	−285	−288	<u>−295</u>	67	<u>64</u>	<u>64</u>	140	140	236
10	−288	<u>−293</u>	−289	69	72	69	191	185	<u>255</u>
15	−288	−288	−289	67	72	69	178	<u>229</u>	242
20	<u>−293</u>	−288	−268	<u>64</u>	75	67	<u>255</u>	210	229
30	−288	−275	−268	77	72	69	<u>274</u>	185	217

[a]Mercury ion concentrations are indicated by I (= 2 × 10^{-5} M), II (= 4 × 10^{-5} M) and III (= 8 × 10^{-5} M).

For routine analyses, it may be sufficient to select one particular Hg^{2+} concentration; the range of film deposition times should then cover the optimum time for that concentration. Similar experiments were done for the pre-formed and in-situ RMFEs. The effects of different mercury concentrations in the in-situ RMFE and different film deposition times in the pre-formed RMFE are shown in Table 2 and in Fig. 1B, C. Thick mercury films resulting from high mercury concentration (Fig. 1B) or long film deposition times (Fig. 1C) result in poor resolution and decreased sensitivity. Under optimum conditions, maximum separation between the copper and mercury peaks is obtained and the conditioning potential which should lie between the copper and mercury oxidation peak potentials can then be selected easily. Under non-optimum conditions, inappropriate selection often results in irreproducible results.

A small extra copper peak (sometimes two peaks) was observed at a potential more positive than the copper oxidation peak, under the optimum film conditions. The extra peak is usually attributed to different oxidation states [14] or differently binding energy of the metal with the mercury monolayer [12]. It has been indicated [15] that the extra copper peaks depend on the deposition potential and are minimal at the potential applied here (−900 mV).

Non-linear calibration

The response of the RMFE systems to Cu^{2+} additions was tested for different properties of the film. The results are given in Fig. 2. Linear calibration curves were obtained only with the optimum film conditions. A similar procedure, based on standard copper additions, was used to determine the apparent copper complexation capacity of natural waters [16]. The shape of curves (a) in Fig. 2A and (b) in Fig. 2B would suggest that the present samples contained dissolved organic matter, able to bind ionic copper in non-labile complexes even though the samples were u.v.-irradiated and did not contain

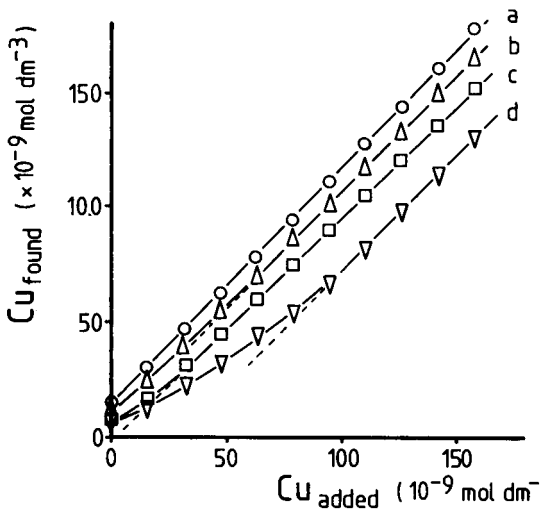

Fig. 3. Calibration plots for copper added to sea-water samples after different digestion procedures (pre-formed RMFE): (a) u.v. irradiation (after addition of nitric acid and hydrogen peroxide); (b) boiling with nitric acid; (c) pH 2.9 (addition of HCl); (d) natural pH (no digestion).

such complexing material. Figure 3 shows calibration plots for copper in sea water after different treatments. The ultraviolet irradiation seems to be fully effective in destroying material that may complex copper, as indicated by Batley and Florence [11]. Thus, the selection of optimum conditions is essential not only for apparent complexation capacity measurements but for correct concentration determinations by standard addition techniques.

The authors thank Dr. M. Branica (Zagreb, Yugoslavia) for supplying the JMFE system.

REFERENCES

1 H. Schmidtpott, Laborpraxis, 4 (1980) 28.
2 T. M. Florence, J. Electroanal. Chem., 27 (1970) 273.
3 F. Opekar and P. Beran, J. Electroanal. Chem., 69 (1976) 1.
4 T. Magjer and M. Branica, Croat. Chem. Acta, 49 (1977) L1.
5 G. E. Batley and T. M. Florence, J. Electroanal. Chem., 55 (1974) 23.
6 G. E. Batley and T. M. Florence, J. Electroanal. Chem., 72 (1976) 121.
7 W. Lund and D. Onshus, Anal. Chim. Acta, 86 (1976) 109.
8 L. Sipos, T. Magjer and M. Branica, Croat. Chem. Acta, 46 (1974) 35.
9 C. J. M. Kramer, Yu Guo-hui and J. C. Duinker, Fresenius Z. Anal. Chem., 317 (1984) 383.
10 R. C. Koile and D. C. Johnson, Anal. Chem., 51 (1979) 741.
11 G. E. Batley and T. M. Florence, Anal. Lett., 9 (1976) 379.
12 F. Vydra, K. Stulik and E. Julakova, Electrochemical Stripping Analysis, Ellis Horwood, Chichester, 1976, p. 283.
13 W. T. de Vries, J. Electroanal. Chem., 9 (1965) 448.
14 M. J. Pinchin and J. Newham, Anal. Chim. Acta, 90 (1977) 91.
15 M. Plavsic, D. Krznaric and M. Branica, Mar. Chem., 11 (1982) 17.
16 J. C. Duinker and C. J. M. Kramer, Mar. Chem., 5 (1977) 207.

Analytica Chimica Acta, 164 (1984) 171—180
Elsevier Science Publishers B.V., Amsterdam — Printed in The Netherlands

DETERMINATION OF PROMETHAZINE BY ANODIC DIFFERENTIAL-PULSE VOLTAMMETRY

R. I. BAXTER and G. SVEHLA*

Department of Analytical Chemistry, The Queen's University, Belfast BT9 5AG, Northern Ireland (United Kingdom)

B. KERR and A. D. WOOLFSON

Department of Pharmacy, The Queen's University, Belfast, Northern Ireland (United Kingdom)

(Received 26th April 1984)

SUMMARY

A differential-pulse voltammetric method is described for the determination of promethazine hydrochloride. The method is based on the anodic oxidation of promethazine on a glassy carbon electrode at +0.64 V vs. SCE in Prideaux buffer of pH 2.3. The reversibility of the oxidation was tested by cyclic voltammetry; the electrode process is quasi-reversible. From the results of microcoulometric experiments and a study of acid—base equilibria, a mechanism for the electrochemical oxidation is presented. The method is applied to determine promethazine hydrochloride in pharmaceutical formulations. Calibrations are linear over the 0.1—1 and 1—5 mg/50 cm^3 ranges.

Antihistamines are an important group of drugs in the treatment of allergic reactions. Their action is thought to be due to the release of histamine, whose effect they block, probably by competitive occupation of histamine receptor sites. One widely used antihistamine drug is promethazine hydrochloride, *N*-(2-dimethylamino-n-propyl)phenothiazine hydrochloride. Numerous chromatographic, spectrophotometric and mass spectrometric procedures for its determination exist, but they are relatively slow and thus affected by oxidative degradation in aqueous environments [1]. There is therefore a need for a rapid assay procedure for promethazine, for which differential-pulse voltammetry (d.p.v.) seemed an obvious choice.

While the literature on chromatographic and spectrophotometric determinations of antihistamines is enormous (pre-1975 [2] and post-1975 [3] contributions have been reviewed), there are few electroanalytical methods. Among these, non-aqueous conductometric [4, 5] and two-phase potentiometric [6] titrations are suitable for higher concentrations, while liquid-membrane ion-selective electrodes have been developed for diphenhydramine [7] and chlorphenyramine [8], which are both diphenylmethane derivatives. Some of these compounds, like chlorphenyramine [8], can be determined by cathodic polarography in strongly acidic aqueous solutions at the

dropping mercury electrode. Chemical oxidation, followed by cathodic polarography have been suggested for the determination of diphenhydramine [9], phenothiazine [10] and 7-phenothiazine derivatives in non-aqueous media [11]. Bromination of phenothiazine derivatives, including promethazine, can also be followed by cathodic polarography [12].

A number of *N*-substituted phenothiazine derivatives can be determined by controlled-potential coulometry, based on anodic oxidation at +0.25 V (vs. SCE) [13]. Merkle and Discher [13] used anodic voltammetry to determine the optimum potentials for the oxidation. It was established that in strongly acidic medium (6 M sulphuric acid), a one-electron oxidation takes place with the stabilization of a free radical; at lower acid concentration (0.5 M sulphuric acid), this radical spontaneously disproportionates to form the original phenothiazine and the corresponding sulphoxide.

In the present paper, details are given for the determination of promethazine by an anodic pulse voltammetric method, with a glassy carbon electrode. The analytical optimization study was supplemented by controlled-potential microcoulometry and cyclic voltammetry to elucidate the electrode processes involved.

EXPERIMENTAL

Reagents and chemicals

A pharmacopoeial sample of promethazine hydrochloride was kindly supplied by May and Baker (Dagenham, Essex). Fresh solutions were made up daily and were kept in the dark to avoid photochemical degradation [1].

All measurements were made in Prideaux buffers, prepared by adding different volumes of 1 M potassium hydroxide to 25 cm^3 of stock solution containing a mixture of acetic, *ortho*phosphoric and boric acids; their total molarity was 0.08. A suitable volume of 2 M potassium chloride was always added before the mixture was diluted to 100 cm^3, so that the buffer of the desired pH had always the same ionic strength of 0.5 M. The composition of each buffer was taken from the literature [14]. Analytical grade reagents were used throughout.

Aluminium oxide (BDH; highly pure for polishing) containing α-Al_2O_3 with a particle size of 0.3 μm was used to polish the glassy carbon electrode between measurements.

Deaeration was done by bubbling oxygen-free nitrogen through the solution.

Apparatus

A Tacussel PRG5 polarograph and electrode assembly, combined with a Hewlett-Packard HP 7035-B *x-y* recorder was used for all the d.p.v. measurements. A three-electrode cell was used throughout, consisting of a Metrohm EA-276/2 glassy carbon working electrode, a platinum wire auxiliary electrode and a saturated calomel reference electrode. The latter two were

supplied with the Tacussel instrument. By optimization experiments, the best operating conditions were found to be: 50 mV pulse amplitude, with a pulse width of 48 ms and a sampling period ("window") of 8 ms. Unless otherwise stated, voltammograms were recorded with a mean scan rate of 10 mV s^{-1} between 0 and +2 V limits (vs. SCE). Usual current sensitivities were between 2.5 and 50 μA, but these were adjusted according to the nature of the experiment.

Some of the calibration graphs were obtained with a Metrohm E-506 polarograph using the same settings as described above. This instrument was used for the assay experiments on Phensedyl and Phenergan samples.

The same electrode system was used in the coulometric experiments. A home-made cell was used; it consisted of two vertical tubes (75 mm high and 32 mm in diameter) which were connected at the bottom by a horizontal glass tube (40 mm long, 12 mm in diameter), in the middle of which a No. 4 glass frit was sealed. The test solution was placed together with the indicator and reference electrodes in one arm, while pure buffer was placed together with the auxiliary electrode in the other arm. The levels of the solutions in the two arms were exactly matched to avoid liquid flow caused by hydrostatic pressure differences. Magnetic stirring was applied when necessary. The electrodes were connected to the input terminals of a Metrohm Coulostat E-524, which was operated in the constant potential ("E const") mode. The coulostat was coupled to the Metrohm E-525 integrator.

For cyclic voltammetry, an instrument was built in the Department of Chemistry to a specification taken from the literature [15] but with a wider range of functions. The instrument consists of a potentiostat (polarograph) unit, linked to a Hewlett-Packard HP-3310B function generator and a 1201B 100-mV dual trace oscilloscope. To obtain cyclic voltammograms, either the Hewlett-Packard 7035B *x-y* recorder was used (with lower sweep rates), or the voltammograms were displayed on a storage oscilloscope and photographed. The electrode system was identical to that used in the d.p.v. and coulometric experiments.

A Radiometer P26 pH meter was used with Metrohm glass and saturated calomel electrodes.

Procedures

Electrochemical methods. For the d.p.v. experiments, 20—50 cm^3 of buffer were added to the cell, followed by the appropriate amount of stock promethazine solution, and the solutions were deaerated for 5 min before measurements.

For the coulometric experiments, 20 cm^3 of test solution was placed into the cell described earlier, and, after deaeration, first a differential-pulse (d.p.) voltammogram was recorded. Then stirring was started and electrolysis was done at the peak potential value for about an hour, which meant an approximately 10% conversion. Longer electrolysis times were not attempted to avoid the blockage of electrode surfaces by deposition of

materials. During this time, a cushion of nitrogen was maintained above the solution to avoid atmospheric oxidation. After this, a new d.p. voltammogram was recorded (without stirring). From the numbers of microequivalents, displayed on the digital readout of the integrator, the number of electrons was calculated from Faraday's Law. The glassy carbon electrode surface had to be cleaned very thoroughly after these electrolyses by using aluminium oxide powder on a wetted Metrohm polishing cloth. Similar cleaning procedures were followed before d.p.v. and cyclic voltammetric experiments.

Cyclic voltammetry was done in the same cell as the d.p.v. experiments, with a wide range of sweep rates and concentrations. Peak height and potential was evaluated from each voltammogram, and the reversibility of the process was assessed from the data.

Determination of promethazine. Dissolve or dilute a sample, which contains 100 μg to 5 mg of active ingredient, with a pH 2.3 buffer and make up the solution to 50 cm^3. Deaerate and obtain a voltammogram between 0 and +1 V, using the glassy carbon working electrode. As indicated above, satisfactory instrumental parameters were 10 mV s^{-1} scan rate, 50 mV pulse amplitude, 48 ms pulse duration and 8 ms sampling period. Older types or worn glassy carbon electrodes tend to acquire static electricity during the cleaning process, resulting in an unusually high blank current (baseline); this can be overcome by scanning the potential range 2—3 times before recording the voltammogram. Evaluate results from a calibration graph obtained with standard promethazine hydrochloride solutions. It is advisable to use separate calibration graphs for the 0.1—1 mg/50 cm^3 and the 1—5 mg/50 cm^3 ranges with current sensitivities of 5 and 10 μA/full scale, respectively.

RESULTS AND DISCUSSION

Differential-pulse voltammetry

The d.p.v. behaviour of promethazine was investigated over a wide pH range. This not only allowed optimization of the pH for the analytical procedure, but also enabled conclusions to be drawn on the acid—base characteristics of the compound, and through this on the mechanism of the electrochemical reaction. Measurements were made over the pH range 2.3—11.3, covering the whole range as evenly as possible. No attempts were made to go outside this range, as previous experience has shown that the glassy carbon electrode does not work reversibly after it has been exposed to strongly acidic solutions and promethazine precipitates from very alkaline solutions. At all the pH values investigated, one well-defined peak was observed (Fig. 1) accompanied by one or more smaller peaks, which in general were poorly resolved. At pH 2.3 (Fig. 1a), the major peak appears at 0.64 V (vs. SCE) for anodic pulses, but at 0.68 V for cathodic pulses. The peak heights are almost equal. This, and the fact that the separation of the

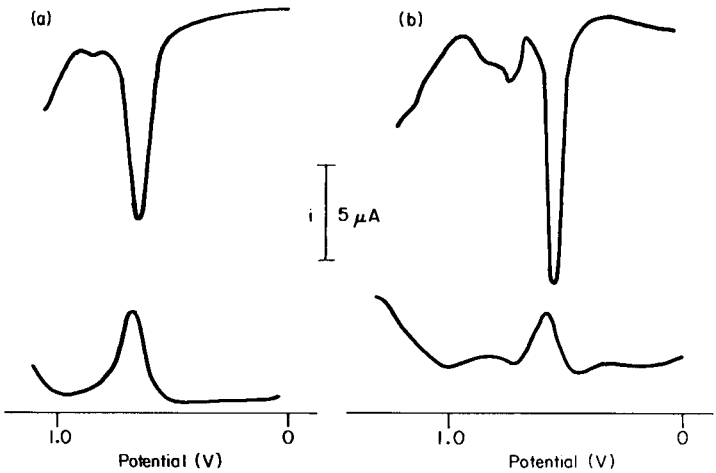

Fig. 1. Differential pulse polarographic traces obtained with 7.4×10^{-5} M solutions of promethazine hydrochloride at (a) pH 2.3 and (b) pH 5.8. (Further details in text.)

peak (ca. 40 mV) is close to the pulse amplitude (50 mV) indicates that the oxidation is almost reversible and that the products do not block the active surface of the electrode. Repeated experiments indeed showed that results at this pH are more reproducible than at higher values; for this reason, pH 2.3 is recommended for quantitative work. The smaller peak at this pH occurs at 0.80 V with anodic pulses; when the direction of the pulse is reversed, this peak becomes insignificant. At pH 5.8 (Fig. 1b), the major peak increases with the anodic pulse and so does the minor one; a shoulder appears beside the peak. With cathodic pulses, the major peak decreases, though a minor peak also occurs. Further data (Table 1) indicate that the electrode process is at best quasi-reversible over all the pH range investigated. Ratios of peak currents were always above 2, even when the peak separation equalled the theoretical value for full reversibility (50 mV). Cyclic voltammetry confirmed this conclusion.

TABLE 1

Variation of various voltammetric characteristics with pH[a]

pH	2.3	2.5	3.2	4.3	5.8	6.3	7.3	9.0	10.35	11.3
E_p^a(V)	0.640	0.610	0.600	0.580	0.532	0.528	0.490	0.460	0.420	0.420
E_p^c(V)	0.680	0.660	0.650	0.620	0.590	0.550	0.530	0.480	0.460	0.460
i_p^a(μA)	10.38	14.50	11.88	11.38	14.50	12.88	11.75	15.00	12.63	11.50
i_p^c(μA)	4.87	5.25	3.75	3.87	3.50	3.50	3.50	2.88	2.50	6.25
i_p^c/i_p^a	2.13	2.76	3.17	2.94	4.14	3.68	3.36	5.21	5.05	1.84
$E_p^a - E_p^c$(mV)	40	50	50	40	42	22	40	20	40	40

[a]For a 7.4×10^{-5} M promethazine hydrochloride solution.

where $E^{0''} = E^{0'} - (0.059/2) \log K$. Thus the peak potential decreases linearly with pH, the slope equalling 29.5 mV/pH. From the data of Fig. 4, the constants can be evaluated as $E^{0'} = 0.424$ V, $E^{0''} = 0.710$ V and $K = 2 \times 10^{-10}$ ($pK = 9.76$); the pK value equals the pH of the break-point on the graph. Accordingly, in acidic medium, the oxidation follows the scheme $HR^+ \rightarrow O^{2+} + H^+ + 2e^-$, while in alkaline solutions the deprotonated species is involved: $R \rightarrow O^{2+} + 2e^-$. The full chemical mechanism is given in Fig. 5, R being the promethazine base, and HR^+ the promethazine hydrochloride (I). In acidic media, I is oxidized to the dication (II) by a two-electron/one proton reaction. The dication (II) is stabilized by resonance, the other limiting structure having the free charge on the C-2 atom. Some authors [17] believe that the two electrons are taken up in two separate steps (with a monocation intermediate stabilized through resonance with three limiting structures); none of the present experimental results have indicated this, however. The electrode reaction is then followed by a purely chemical stabilization reaction, in which the sulphoxide (III) is formed. In alkaline media (pH > 9.76), the promethazine base reacts without the release of the proton, to form the dication (II) again.

Determination of promethazine by d.p.v.

For the determination of promethazine in promethazine hydrochloride, in Phensedyl and in Phenergan by the procedure outlined in the Experimental section, the calibration graph for the 0.1—1 mg/50 cm^3 range was linear, with a correlation coefficient of 0.998. The lowest determinable concentration [18] was 82 μg/50 cm^3. A set of voltammograms illustrating the variation of peak height with concentration is given in Fig. 6.

Results for the Phensedyl and Phenergan preparations are shown in Table 2. These preparations (originating from May and Baker) were diluted fifty-fold with the buffer for voltammetry. Each result in Table 2 refers to a

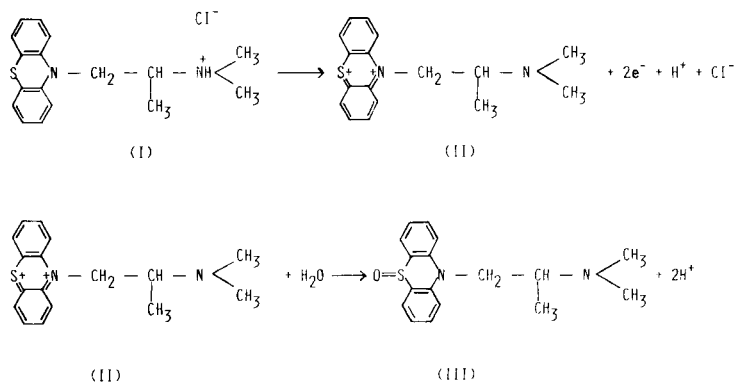

Fig. 5. Electrochemical oxidation path of promethazine hydrochloride, followed by chemical stabilization through hydrolysis.

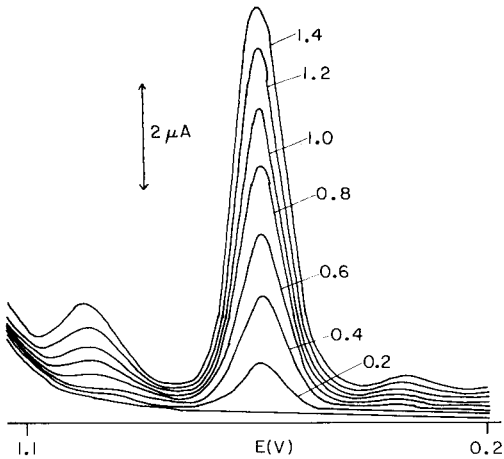

Fig. 6. Differential-pulse voltammograms obtained with promethazine hydrochloride solutions; the numbers on the curves are concentrations (mg/50 cm^3).

TABLE 2

Determination of promethazine hydrochloride in Phensedyl and Phenergan samples

Sample	Promethazine HCl content (mg/5 cm^3)	
	Specification	Found
Phensedyl cough linctus[a]	3.6	3.25, 3.29, 3.29, 3.33, 3.21
Phenergan compound expectorant linctus[b]	5.0	3.79, 4.70, 4.33, 3.71, 3.67, 4.25, 4.00

[a]Other components are 9.0 mg codeine phosphate and 7.2 mg of ephedrine hydrochloride per 5 cm^3. [b]Other components are 45 mg of potassium guaiacol sulphonate, 65 mg of citric acid and 0.01 cm^3 Ipecacuana liquid extract (BP) per 5 cm^3.

different diluted sample. No attempt was made to determine the promethazine content by another, independent method; the results are reproducible (especially for phensedyl) and are close to the makers' specification. The fact that results are consistently lower than those specifications illustrates the fact that promethazine decomposes in solution.

The pulse voltammetric procedure is eminently suitable for studies of the decomposition of promethazine in aqueous solution. As this phenomenon is of great clinical and pharmaceutical interest, a detailed study has been made; the results will be reported in a separate publication.

R.I.B. and B.K. acknowledge postgraduate grants received from the Department of Education, Government of Northern Ireland.

REFERENCES

1 B. J. Meakin, J. Stevens and D. J. G. Davies, J. Pharm. Pharmacol., 30 (1978) 75.
2 B. Kerr, M.Sc. Project Report, Queen's University, Belfast, 1981.
3 C. D. Taylor; M.Sc. Project Report, Queen's University, Belfast, 1981.
4 S. Haque, Z. Blagojevic and K. Nikolic, Acta Pharm. Jugosl., 17 (1967) 123.
5 K. Nikolic and Z. Cupric, Acta Pharm. Jugosl., 21 (1971) 159.
6 P. A. Johansson and R. Gustavic, Acta Pharm. Suec., 13 (1976) 407.
7 K. Kina, N. Maekawa and N. Ishibashi, Bull. Chem. Soc. Japan, 46 (1973) 2772.
8 E. Jacobsen and K. Høgberg, Anal. Chim. Acta, 71 (1974) 157.
9 H. Hoffmann, Arch. Pharm., Ber. Deut. Pharm. Ges., 305 (1972) 254.
10 A. G. DuMortier and G. J. Patriarche, Z. Anal. Chem., 264 (1973) 153.
11 I. Nemec, N. Sulcova and K. Waiser, Cesk. Farm., 28 (1979) 59.
12 M. M. Ellaithy, Indian J. Pharm. Sci., 42 (1980) 41.
13 F. H. Merkle and C. A. Discher, Anal. Chem., 36 (1964) 1639.
14 C. Jordan. Microchem. J., 25 (1980) 492.
15 R. Bezman and P. S. McKinney, Anal. Chem., 41 (1969) 1560.
16 A. J. Bard and L. R. Faulkner, Electrochemical Methods: Fundamentals and Applications, Wiley, New York, 1980, pp. 221, 259.
17 L. G. Chatten, R. A. Locock and R. D. Krause, J. Pharm. Sci., 60 (1971) 588.
18 K. Doerffel, Statistik in der Analytischen Chemie, VEB Deutscher Verlag für Grundstoffindustrie, Leipzig, 1966, p. 177.

Analytica Chimica Acta, 164 (1984) 181—194
Elsevier Science Publishers B.V., Amsterdam — Printed in The Netherlands

ASSESSMENT OF DIFFERENTIAL-PULSE ADSORPTION VOLTAMMETRY FOR THE SIMULTANEOUS DETERMINATION OF NICKEL AND COBALT IN BIOLOGICAL MATERIALS

S. B. ADELOJU and A. M. BOND*

Division of Chemical and Physical Sciences, Deakin University, Waurn Ponds, Victoria 3217 (Australia)

M. H. BRIGGS

Division of Biological and Health Sciences, Deakin University, Waurn Ponds, Victoria 3217 (Australia)

(Received 5th June 1984)

SUMMARY

An assessment of the voltammetric method based on chelate adsorption at the hanging mercury drop electrode is described for the simultaneous determination of nickel and cobalt in biological materials. The interfacial accumulation of the elements as metal dimethylglyoximates during the adsorption step, and the use of differential-pulse voltammetry during the reduction step, provide substantial gains in the sensitivity of their voltammetric responses. The decomposition of the sample material by direct dry ashing provides a blank-free approach for the accurate determination of the elements. Application of the method to the available certified biological reference materials for cobalt and nickel was successful. The limits of detection obtained under the conditions of this study were 0.01 $\mu g\ g^{-1}$ and 0.02 $\mu g\ g^{-1}$ for cobalt and nickel, respectively, in bovine liver.

Cobalt and nickel belong to the class of elements considered to be essential for man, plants and animals [1]. Cobalt serves its paramount, established function as a component of vitamin B_{12} [2, 3] while nickel has recently been found to be essential for a number of metabolic processes [4—7]. Although both of these elements are required only in minute quantities for maintaining normal health, a lower or higher concentration of either of them, relative to the physiological optimal level, may in course of time lead to toxicity or deficiency states resulting in impairment or abnormalities in health [2, 4—11]. Concern about the significance and toxicity of these elements has therefore encouraged the development of numerous analytical techniques for their determination in various matrices [12—20]. However, the natural levels of these elements in biological materials still remain largely uncertain, possibly because of the lack of precise and accurate methods for their determination [2].

The electroanalytical techniques employed to date for the determination of cobalt and nickel include d.c. polarography (d.c.p.), differential-pulse

0003-2670/84/$03.00

polarography (d.p.p.) and stripping voltammetry (s.v.). However, owing to the extreme irreversibility of the electrode processes for these elements in non-complexing media [21—23], it is quite difficult to achieve adequate detection limits by these techniques for their determination at the rather low concentrations at which they are often present in most biological materials. Several workers [18—20, 24—27] have therefore resorted to the use of complexing agent/media to achieve better limits of detection for cobalt and nickel by these techniques. One of the first most substantial increases in sensitivity achieved by such chelate or complex adsorption at a mercury electrode was reported by Komarek [28] who used dimethylglyoxime ($DMGH_2$) to obtain 4—5-fold enhancement of the polarographic wave of cobalt. Similar approaches have since been employed to determine nickel and palladium (as dimethylglyoximates) by d.c.p. and d.p.p. [20, 29, 30]. The best limit of detection obtainable by these polarographic techniques is 1—2 ng ml^{-1} [20]. However, the use of the dropping mercury electrode (DME) with these techniques does not allow full analytical exploitation of the sensitization possible with chelate adsorption. The use of stationary electrodes enables increased surface concentrations of the chelates to be achieved and hence improves the detection limits obtainable for these elements. Consequently, Golimowski et al. [19] used a hanging mercury drop electrode (HMDE) with the technique of adsorption voltammetry to exploit fully the analytical utility of adsorbed chelate sensitization; they determined trace amounts of nickel in wine by this approach. Pihlar et al. [18] further explored the $DMGH_2$-sensitized adsorption voltammetry, achieving a detection limit of 1 pg ml^{-1} in aqueous solution, and used this approach in both d.c. and d.p. modes to determine nickel in selected biological materials.

The formation of cobalt and nickel dimethylglyoximates under similar pH and other solution conditions suggests that the simultaneous determination of both elements by the chelate adsorption voltammetric method may be possible and in the last few years a great deal of work has been reported on this subject [19, 31—36]. In the present study, an assessment of a method for the simultaneous determination of cobalt and nickel in biological materials by $DMGH_2$-sensitized differential-pulse adsorption voltammetry (d.p.a.v.) is reported. In particular, conditions required for the determination of varying concentration ratios of these elements in various biological materials are considered.

EXPERIMENTAL

Reagents and standard solutions

All acids and ammonia solution used were Aristar grade (B.D.H. Chemicals) while other reagents were of analytical-grade purity. Ammonia/ammonium chloride (4 M) buffer solution was prepared by mixing appropriate amounts of hydrochloric acid (4 M) and ammonia solution (8 M). Dimethylglyoxime (0.1 M) was prepared by dissolving an appropriate amount of the reagent

(≥98%; Ajax Univar, Sydney, Australia) in 96% ethanol. Stock solutions (1 g l^{-1}) of cobalt(II) and nickel(II) ions were prepared by dissolving their chloride salts in 0.1 M hydrochloric acid and storing in pre-washed polyethylene bottles. The required standards were prepared daily by appropriate dilution of the stock solution with the desired buffer concentration. Distilled-deionized water was obtained by passing distilled water through a Barnstead Sybron Nanopure water purification system (Barnstead Sybron Corporation, Boston, MA) to which a Millipore Organex-Q cartridge was attached to remove remaining trace organics after the initial purification. This water was used in all sample and solution preparations.

Instrumentation and glassware

Voltammograms were recorded with an EG & G Princeton Applied Research microprocessor-controlled polarographic analyzer (PAR Model 384) equipped with a PAR Model 303 static mercury drop electrode and a PAR Model 305 stirrer. The electrode compartment consisted of a hanging mercury drop electrode (HMDE), silver—silver chloride (saturated KCl) and a platinum wire as working, reference and auxiliary electrodes, respectively. Cobalt and nickel chelates were accumulated onto the mercury electrode at a fast stirring rate with a medium-size drop with a surface area of 0.015 cm^2.

All solutions were deoxygenated with highly purified nitrogen at the start of each determination for 15 min and a flow of nitrogen was maintained over the solution to prevent oxygen interference during the measurements. Standard solutions of cobalt and nickel were added to the polarographic cell from fixed-volume Socorex micropipettes with disposable tips. The solution was deoxygenated for 30 s after each standard addition.

All glassware and polyethylene bottles were soaked in 2 M nitric acid for at least seven days, washed three times with distilled-deionized water, soaked in distilled-deionized water and finally soaked in 0.1 M hydrochloric acid until ready for use.

Biological standard reference materials

Bowen's Kale was obtained from H.J. Bowen (Department of Chemistry, Reading University, Whiteknights Park, Reading, Berks., England). Bovine Liver, Orchard Leaves and Oyster Tissue were obtained from the U.S. Bureau of Standards (Washington, DC). All materials were treated as recommended by the suppliers.

Procedures

Sample decomposition. Accurately weigh 0.5 g of sample into a pre-cleaned silica dish and heat gently on a hot plate at medium rate to volatilize as much as possible moisture and organic matter. Spread out the sample, from time to time, with a pre-cleaned silica rod to accelerate drying. When the sample is fairly dried (30—60 min), transfer the dish to a temperature-controlled muffle furnace set to 450°C. Leave in the furnace for 8 h (or if preferred

overnight) to complete decomposition. Remove from furnace, leave to cool and add 3 ml of 6 M hydrochloric acid. Warm on a hot plate at medium rate to dissolve the sample ash and to extract elements from any insoluble residue. Transfer quantitatively to a 10-ml volumetric flask by washing the dish with distilled-deionized water and mix thoroughly to ensure homogeneity.

Voltammetric determinations. Pipette 1 ml of the sample solution into a 10-ml (or 25-ml for Oyster Tissue or 50-ml for Orchard Leaves) volumetric flask, add 0.5 ml (or 1.25 ml) of ammonia buffer solution plus 25 μl (or 100 μl) of 0.1 M dimethylglyoxime and make up to volume with distilled-deionized water. Mix thoroughly and transfer an aliquot (5—10 ml) into the polarographic cell. Deoxygenate and determine nickel and cobalt simultaneously by adsorption voltammetry under the following conditions: operating mode, differential pulse; adsorption potential, —0.8 V vs. Ag/AgCl (saturated KCl); scan rate, —4 mV s^{-1}; duration between pulses, 0.5 s; modulation amplitude, —50 mV; adsorption time, 15—225 s (stirred); equilibration period 15 s (unstirred). The amount of cobalt and nickel present in the sample is quantified by the standard addition method using the d.p.a.v. peaks which appear at about —1.15 V and —1.03 V vs. Ag/AgCl, respectively. Two standard additions were found to be adequate for accurate results.

Working area. This work was undertaken in clean air conditions controlled at a temperature of 22.5 ± 0.5° C. All sample preparations were done in a class-100 clean room while the analytical measurements were done in a class-1000 clean room. Both of these laboratories form part of the Deakin University Trace Analysis Unit.

RESULTS AND DISCUSSION

Factors influencing the utilization of differential pulse adsorption voltammetry for the accurate simultaneous determination of cobalt and nickel

Concentration ratio and dependence on adsorption time. The simultaneous determination of cobalt and nickel by the chelate adsorption voltammetric method requires careful consideration of the possible concentration ratios at which the elements may be present in real samples. The ratio of these elements varies tremendously in biological materials, ranging from 1:1 to 1:20 (and vice versa) or perhaps even more. Such diverse concentration ratios can significantly influence the required sensitization of cobalt and nickel responses with any chelating or complexing agent if the two elements are to be determined simultaneously in a particular sample. Hence, detailed investigation of the factors resulting in such enhancement of the electrode processes are required [18, 20].

Figure 1 illustrates the influence of the total adsorption time (including equilibration time) on the d.p.a.v. peaks of cobalt and nickel at varying concentration ratios. These voltammograms show that the chelate adsorption approach provides a substantially greater increase in sensitivity for cobalt

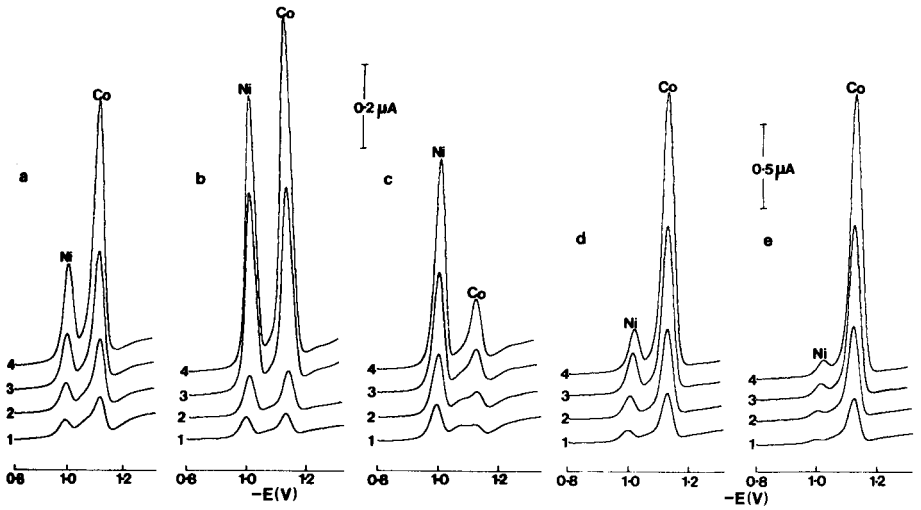

Fig. 1. Dependence of nickel and cobalt d.p.a.v. peaks on adsorption time and concentration ratios: (a) 1 μg Ni l^{-1} and 1 μg Co l^{-1}; (b) 4 μg Ni l^{-1} and 2 μg Co l^{-1}; (c) 2 μg Ni l^{-1} and 0.2 μg Co l^{-1}; (d) 2 μg Ni l^{-1} and 5 μg Co l^{-1}; (e) 0.4 μg Ni l^{-1} and 4 μg Co l^{-1}. All 0.1 M NH_3/NH_4Cl, 8 × 10^{-4} M $DMGH_2$. Adsorption time: (1) 30 s; (2) 60 s; (3) 120 s; (4) 240 s (including 15 s equilibration time).

than for nickel with increasing adsorption time. Thus adequate resolution of the d.p.a.v. peaks is very dependent upon the adsorption time used. For all biological samples examined, the use of an adsorption time of 240 s gave adequate resolution for both cobalt and nickel peaks. The substantial increase in sensitivity obtained with this adsorption time for cobalt, particularly at the high Ni:Co ratio (Fig. 1b and c), is quite significant for the determination of these elements in biological materials where such a concentration ratio is often encountered. The data in Fig.1 also imply that the simultaneous determination of both elements at higher Ni:Co concentration ratios than those examined may be possible by use of even longer adsorption times. In summary, the adsorption time required for this simultaneous determination will depend on the concentration ratio at which they are present in any given sample.

Influence of buffer concentration. The precision and accuracy of the chelate adsorption voltammetric approach for simultaneous determination of both elements will be significantly dependent on the difference in their peak potentials. Substantial error in the results obtained can easily be caused by overlapping peaks. The main factor influencing the peak position and hence the peak-to-peak separation for nickel and cobalt is the chosen buffer concentration [18, 20]. Figure 2 shows the influence of various buffer concentrations; the cobalt peak becomes well separated from the nickel peak as the buffer concentration is increased. The results in Table 1 show that at a buffer concentration greater than 0.01 M, the peak potential for nickel becomes

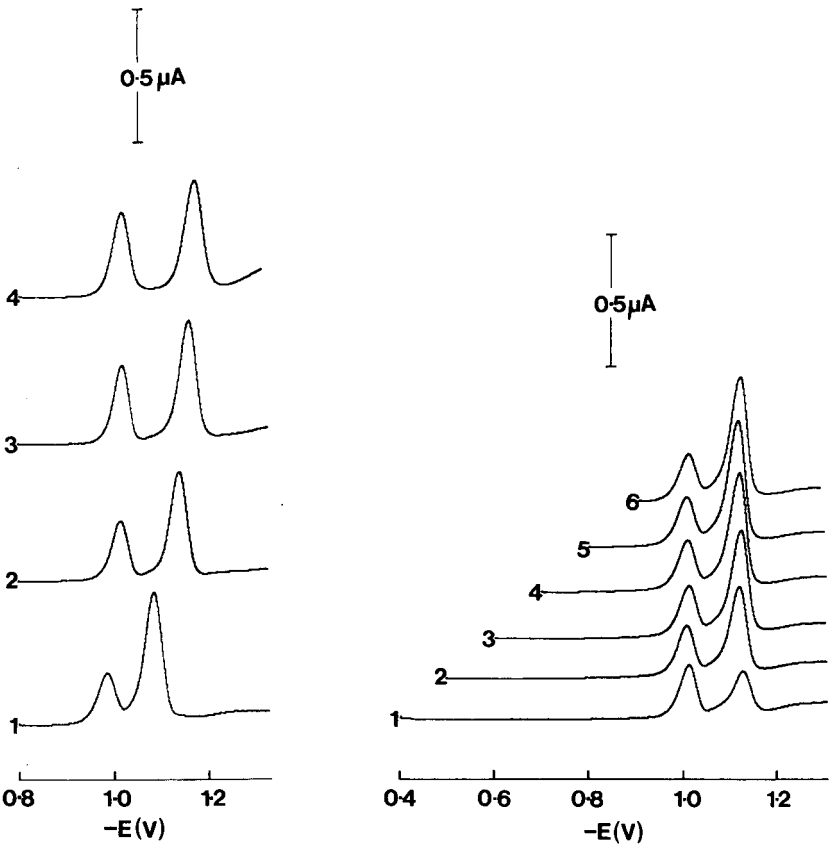

Fig. 2. Influence of buffer concentration on nickel and cobalt d.p.a.v. peaks: (1) 0.01 M; (2) 0.1 M; (3) 0.5 M; (4) 1.0 M NH_3/NH_4Cl. Adsorption time, 240 s (including 15 s equilibration time); 4×10^{-4} M $DMGH_2$; 1 μg Ni l^{-1} and 1 μg Co l^{-1}.

Fig. 3. Dependence of nickel and cobalt d.p.a.v. peaks on adsorption potential (E_a): (1) —0.4 V; (2) —0.5 V; (3) —0.6 V; (4) —0.7 V; (5) —0.8 V; (6) —0.9 V. Adsorption time, 180 s (including 15 s equilibration time); 8×10^{-4} M $DMGH_2$; 0.1 M NH_3/NH_4Cl.

independent of the buffer concentration whereas the value obtained for cobalt changes considerably for all buffer concentrations. The largest separation between the cobalt and nickel peaks was obtained in 1 M buffer solution.

The peak currents per unit concentration, unlike peak potentials, did not follow any well defined trend with variation in the buffer concentration (Table 1). The increase in the nickel peak currents with increasing buffer concentration has been examined in detail by Flora and Nieboer [20].

TABLE 1

Influence of buffer concentration on the peak currents and peak potentials of cobalt and nickel[a]

$[NH_3/NH_4Cl]$ (M)	i_p(Co) (nA)	E_p(Co) (±0.002) V	i_p(Ni) (nA)	E_p(Ni) (±0.002) V	$E_p(Co) - E_p(Ni)$ (±2) mV
0.01	484 ± 1	−1.092	163 ± 2	−0.992	−100
0.10	418 ± 2	−1.146	225 ± 1	−1.022	−124
0.50	460 ± 4	−1.166	300 ± 4	−1.024	−142
1.00	415 ± 4	−1.178	289 ± 5	−1.022	−156

[a]Error is mean deviation, $n = 3$. Conditions as for Fig. 2.

The main criterion used in selection of an adequate buffer concentration is the precision of the results obtained for simultaneous determination of both cobalt and nickel. From the data in Table 1 the best reproducibilities for these elements were obtained in buffer concentrations <0.5 M. The considerably decreased peak current obtained for nickel in 0.01 M buffer solution makes concentrations less than this unsuitable for the simultaneous determination of ultra-trace amounts of both elements. The recommended buffer concentration for the simultaneous determination of cobalt and nickel at the trace and ultra-trace levels is therefore in the range 0.1—0.5 M.

Dependence on the concentration of dimethylglyoxime. The concentration of dimethylglyoxime used is also of paramount importance in obtaining accurate results for cobalt and nickel [20] when determined simultaneously. The cobalt peak increased substantially with increasing $DMGH_2$ concentration while the nickel peak decreased slightly as the concentration of the chelating agent increased and the separation between the cobalt and nickel peaks decreased as the $DMGH_2$ concentration increased (Table 2). Clearly, the optimal $DMGH_2$ concentration for simultaneous determination of the two elements, with respect to sensitivity lies between 1×10^{-4} M and 4×10^{-4} M. However, depending on the relative concentration of the two elements in real samples, the $DMGH_2$ concentration may be altered to values

TABLE 2

Influence of dimethylglyoxime concentration on the peak currents and peak potentials of cobalt and nickel[a]

$[DMGH_2]$ (M)	i_p(Co) (nA)	E_p(Co) (±0.002 V)	i_p(Ni) (nA)	E_p(Ni) (±0.002 V)	$E_p(Co) - E_p(Ni)$ (±2 mV)
2×10^{-5}	146 ± 2	−1.144	240 ± 3	−1.014	−130
1×10^{-4}	319 ± 3	−1.148	237 ± 1	−1.022	−126
4×10^{-4}	418 ± 2	−1.146	225 ± 1	−1.022	−124
8×10^{-4}	536 ± 3	−1.130	200 ± 1	−1.016	−114

[a]Error is mean deviation, $n = 3$. Conditions: 0.1 M NH_3/NH_4Cl, otherwise as for Fig. 2.

above or below this range to permit adequate detection and determination of both elements simultaneously.

Choice of adsorption potential. The selection of an appropriate adsorption potential, E_a, is also critical for the accurate simultaneous determination of cobalt and nickel in biological materials at varying concentration ratios. The sensitivity obtained and the speed of operation can be greatly influenced by the choice of adsorption potential [18]. Figure 3 shows that the sensitivity obtained for cobalt increased as E_a becomes more negative while the nickel peak decreased slightly. The largest peak current was obtained for cobalt at −0.8 V, beyond which no further increase was observed. The increased enhancement of the cobalt d.p.a.v. peak when this deposition potential (−0.8 V) is used can be valuable for the simultaneous determination of both elements in biological samples because the concentration ratio (Ni:Co) in these materials is often high. This adsorption potential was therefore used for all further work. Traces of other metal ions commonly present in biological materials such as copper and zinc may be deposited at this accumulation potential. However, because the d.p.a.v. potential scan is done in the negative rather than positive direction as is the case with anodic stripping voltammetry and owing to the selectivity of the chelate adsorption for cobalt and nickel, little or no interference will be experienced unless excessively large amounts of a particular element are present. For example, zinc(II) ions give an additional peak close to that of cobalt and may cause interference if present in large amounts [32].

Scan-rate and pulse-height dependences. Scan rates between 1 and 4 mV s^{-1} gave adequate resolution for both cobalt and nickel peaks and also maintained sufficient sensitivity for their determination (Fig. 4). Scan rates exceeding 4 mV s^{-1} gave distorted and drawn-out peaks, because of instrumental artifacts with the instrument used. A scan rate of 4 mV s^{-1} was therefore chosen as the best compromise between resolution, sensitivity and speed of routine operation. This scan rate gave linear responses for increasing concentrations of cobalt and nickel.

The cobalt peak current increased linearly with modulation amplitude (pulse height) over the range of −5 to −100 mV at the scan rate of 4 mV s^{-1}. Generally, the peak potentials shifted to more positive values with increasing amplitude. The separation between the cobalt and nickel peaks was superior at the smaller amplitudes as expected. The use of a pulse amplitude of −50 mV gave sufficient sensitivity and adequate peak separation for simultaneous determinations and is recommended for routine work.

Application to biological materials

The adequate utilization of the established conditions for the simultaneous determination of cobalt and nickel in biological materials requires an efficient decomposition method involving minimal use of reagents to reduce the danger of contamination. Direct dry ashing, which requires no reagent except for the minimal amount of acid used for dissolution of the sample ash, was

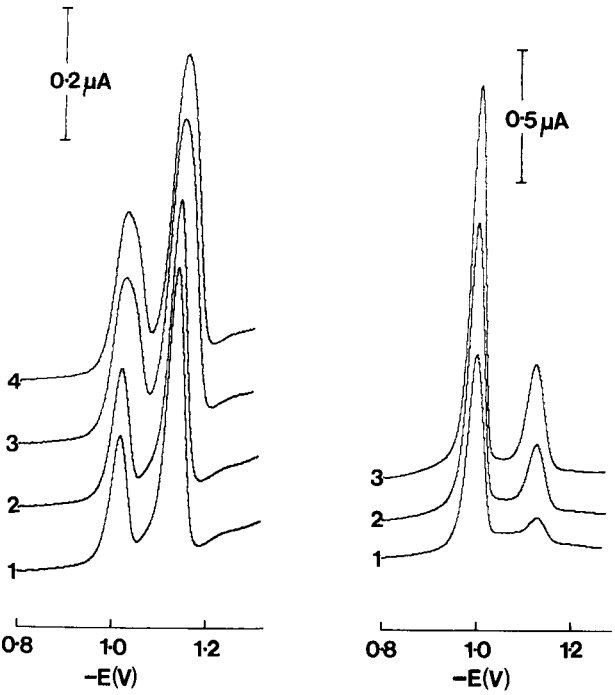

Fig. 4. Influence of scan rate on the resolution of the nickel and cobalt peaks: (1) —2 mV s^{-1}; (2) —4 mV s^{-1}; (3) —6 mV s^{-1}; (4) —8 mV s^{-1}. Other conditions as in Fig. 3.

Fig. 5. Simultaneous determination of nickel and cobalt in Bowen's Kale by the standard addition method. Standards added: (1) 0; (2) 2.5 μg Ni l^{-1} + 0.5 μg Co l^{-1}; (3) 5 μg Ni l^{-1} + 1 μg Co l^{-1}. Adsorption time 240 s (including 15 s equilibration time).

first tested for the simultaneous determination of cobalt and nickel in biological materials by a recovery study. The results in Table 3 show acceptably good agreement between the values obtained by the d.p.a.v. approach and the certified value for cobalt in the Bowen's Kale sample. Based on the mean values, the recoveries of cobalt and nickel by the dry-ashing method are 96—102% and 99—101%, respectively. Gorsuch [37, 38] has previously shown that full recoveries of both elements can be obtained by dry ashing at temperatures $<500°C$.

The results in Table 4 indicate that direct dry ashing is adequate for the simultaneous determination of cobalt and nickel in a wide range of biological materials by the d.p.a.v. approach. Careful consideration of other factors such as the sample ash dilution volume and the required $DMGH_2$ concentration is, however, necessary in obtaining the most accurate results. Figure 5 shows that the simultaneous determination of cobalt and nickel in Bowen's Kale can easily be made by using the proposed conditions. The use of lower $DMGH_2$ concentrations gave non-linear responses and inadequate precision

TABLE 3

Recoveries of cobalt and nickel in Bowen's Kale by the direct dry-ashing method

Co added (ng)	Total Co found (ng)	Actual Co in sample ($ng\ g^{-1}$)	Ni added (ng)	Total Ni found (ng)	Actual Ni in sample ($ng\ g^{-1}$)
0	66	66	0	1050	1050
25	90	65	250	1297	1047
50	114	64	500	1539	1039
100	168	68	1000	2043	1043
Mean[a]		66 ± 1	Mean[a]		1045 ± 4
Certified value[b]	60 ± 10 ng g^{-1}		Certified value	None	

[a]Error is mean deviation. [b]Error is standard deviation for results obtained by various instrumental techniques.

for both elements. Attempts to use the same dilution volume and $DMGH_2$ concentration as those used for Bowen's Kale for the oyster tissue sample were unsuccessful. However, dilution of the sample ash to a large volume and the use of higher concentration of $DMGH_2$ allowed simultaneous determination of cobalt and nickel in this sample. Figure 6 shows that the accurate determination of these elements in the oyster tissue also depends on the adsorption time used. Adequately linear responses were obtained for cobalt and nickel by the standard addition method with a total adsorption time of 120 s (Fig. 6a) and a $DMGH_2$ concentration of 4×10^{-4} M. The results in Table 4 show that this approach provided precise and accurate results for nickel, and precise results for cobalt in the Oyster Tissue sample. The use of a longer adsorption time of 240 s (Fig. 6b) gave non-linear responses for both elements. The appearance of an additional peak at −1.21 V which decreased in height with the addition of the standard reflects the complex

TABLE 4

Concentrations of cobalt and nickel found in some biological standard reference materials by differential-pulse adsorption voltammetry

Reference material	Cobalt ($\mu g\ g^{-1}$)		Nickel ($\mu g\ g^{-1}$)	
	Found[a]	Certified[b]	Found[a]	Certified[b]
Bowen's Kale	0.066 ± 0.001	0.06 ± 0.01	1.045 ± 0.004	None
Bovine Liver	0.143 ± 0.005	None	0.219 ± 0.008	None
Orchard Leaves	0.107 ± 0.003	None	1.33 ± 0.07	1.3 ± 0.2
Oyster Tissue	0.22 ± 0.03	None	1.05 ± 0.02	1.03 ± 0.19

[a]Error is mean deviation (n = 3 or 4). [b]Error is standard deviation for results obtained by various instrumental techniques.

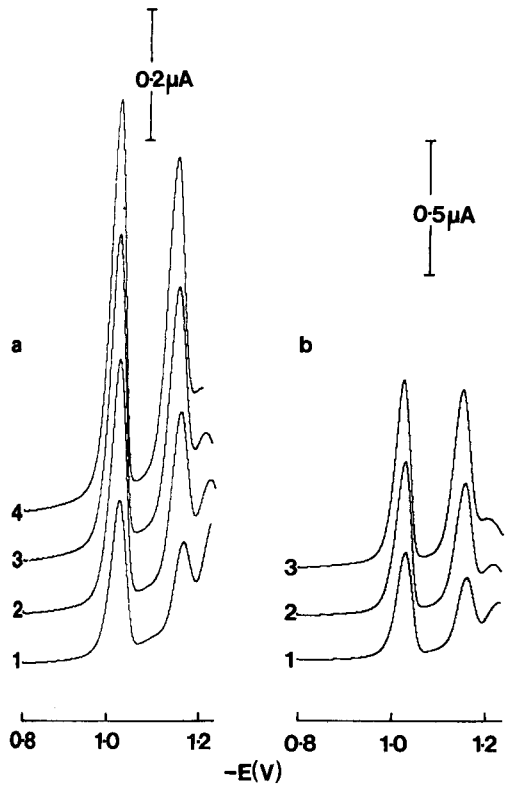

Fig. 6. Simultaneous determination of nickel and cobalt in Oyster Tissue by the standard addition method. Standards added: (1) 0; (2) 1 μg Ni l^{-1} + 0.5 μg Co l^{-1}; (3) 2 μg Ni l^{-1} + 1 μg Co l^{-1}; (4) 3 μg Ni l^{-1} + 1.5 μg Co l^{-1}. Adsorption time (including 15 s equilibration time): (a) 120 s; (b) 240 s.

nature of the oyster tissue sample. The additional peak is probably due to zinc [32, 39] which is present in this sample at a relatively high concentration.

The simultaneous determination of cobalt and nickel in the Orchard Leaves by the d.p.a.v. approach also required substantial dilution and lower $DMGH_2$ concentration. Figure 7 and the results in Table 4 show that accurate determination of these elements in the sample was readily made by dilution to 500 ml and with only 1×10^{-4} M $DMGH_2$. Dilution to lower volumes and use of higher concentration of $DMGH_2$ as well as the use of shorter adsorption times did not provide adequately linear responses for cobalt and nickel. Interestingly however, the substantial dilution used for the Orchard Leaves is also useful for the determination of these elements in the other samples at $DMGH_2$ concentrations in the range 1×10^{-4}—4×10^{-4} M. Owing to the relatively low concentration of cobalt in Bowen's Kale, it is preferable not to dilute this sample ash beyond 250 ml. It is therefore

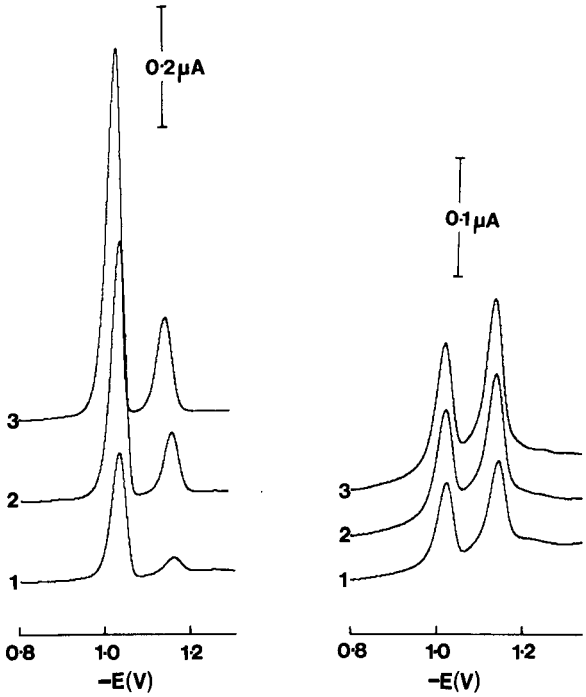

Fig. 7. Simultaneous determination of nickel and cobalt in Orchard Leaves by the standard addition method. Standards added: (1) 0; (2) 1.25 μg Ni l^{-1} + 0.25 μg Co l^{-1}; (3) 2.5 μg Ni l^{-1} + 0.50 μg Co l^{-1}. Adsorption time 240 s (including 15 s equilibration time).

Fig. 8. Simultaneous determination of nickel and cobalt in Bovine Liver by the standard addition method. Standards added: (1) 0; (2) 0.05 μg Ni l^{-1} + 0.05 μg Co l^{-1}; (3) 0.10 μg Ni l^{-1} + 0.10 μg Co l^{-1}. Other conditions as in Fig. 7.

reasonable to conclude that the simultaneous determination of both elements can be done accurately for all samples containing $\geqslant 0.1$ μg g^{-1} cobalt in the presence of higher concentrations of nickel by dilution of the sample ash to 500 ml and use of $DMGH_2$ concentration between 1×10^{-4} and 4×10^{-4} M. Figure 8 confirms that this approach is useful for the simultaneous determination of cobalt and nickel in Bovine Liver. This method should therefore also be applicable to other sample materials.

Conclusion

The d.p.a.v. method based on the formation of nickel and cobalt dimethylglyoximates provides a simple and suitable approach for the simultaneous determination of both elements in biological materials. Careful consideration of the required dilution and $DMGH_2$ may be needed for samples different from those considered above. The direct dry-ashing procedure provides a blank-free approach; under the conditions used, no blank

levels for either cobalt or nickel could be detected with an adsorption time of 240 s and $DMGH_2$ concentrations between 1×10^{-4} and 4×10^{-4} M. The limits of detection established for simultaneous determination of cobalt and nickel in Bovine Liver under the prescribed conditions were 0.01 $\mu g\ g^{-1}$ and 0.02 $\mu g\ g^{-1}$ respectively (signal-to-background 2:1). Lower detection limits may be achieved either by increasing the adsorption time or by increasing the $DMGH_2$ concentration. The detection limits established above are adequate for most biological materials.

REFERENCES

1 E. J. Underwood, Trace Elements in Human and Animal Nutrition, 4th edn., Academic Press, New York, 1977.
2 J. Versieck and R. Cornelis, Anal. Chim. Acta, 116 (1980) 217.
3 B. T. Golding and P. J. Sellar, Educ. Chem., 11 (1983) 204.
4 F. H. Nielsen and D. A. Ollerich, Fed. Proc. Fed. Am. Soc. Exp. Biol., 33 (1974) 1767.
5 A. Schnegg and M. Kirchgessner, Z. Tierphysiol., 36 (1975) 63.
6 F. W. Sunderman, S. Nomoto, R. Morang, M. W. Nechay, C. M. Burke and S. W. Nielsen, J. Nutr., 102 (1972) 259.
7 M. Kirchgessner and A. Schnegg, Nutr. Metabol., 23 (1979) 62.
8 M. Kirchgessner, in J. O. Nriagu (Ed.), Nickel in the Environment, Wiley, New York, 1980, pp. 635—652.
9 L. Friberg, G. M. Nordberg and V. B. Vouk (Eds.), Handbook on Toxicology of Metals, Elsevier/North Holland Biomed. Press, Amsterdam, 1979.
10 T. D. Luckey and B. Venugopal, Metal Toxicity in Mammals, Vols. 1 and 2, Plenum Press, New York, 1977.
11 G. Rubanyi, I. Birtalan, A. Gergely and A. G. B. Kovach, Am. J. Obstet. Gynecol., 143 (1982) 167.
12 M. Stoeppler, in J. O. Nriagu (Ed.), Nickel in the Environment, Wiley, New York, 1980, pp. 663—721.
13 R. G. Smith and H. L. Windom, Anal. Chim. Acta, 113 (1980) 39.
14 F. F. Cantwell, J. S. Nielsen and E. Hrudey, Anal. Chem., 54 (1982) 1498.
15 D. Rosales and J. M. Cano-Paron, Analyst (London), 107 (1982) 385.
16 R. M. Pearson and H. J. Siem, Anal. Chem., 49 (1977) 580.
17 C. K. Bhaskare and S. Devi, Talanta, 25 (1978) 544.
18 B. Pihlar, P. Valenta and H. W. Nürnberg, Fresenius Z. Anal. Chem., 307 (1981) 337.
19 J. Golimowski, H. W. Nürnberg and P. Valenta, Lebensmittelchem. Gerichtl. Chem., 34 (1980) 116.
20 C. J. Flora and E. Nieboer, Anal. Chem., 52 (1980) 1013.
21 J. Dandoy and L. Gierst, J. Electroanal. Chem., 2 (1961) 116.
22 H. Grubitsch and J. Schukoff, Fresenius Z. Anal. Chem., 253 (1971) 201.
23 D. R. Crow and M. E. Rose, Electrochim. Acta, 24 (1979) 41.
24 J. J. Lingane and H. Kerlinger, Ind. Eng. Chem., Anal. Ed., 13 (1942) 77.
25 C. Pekker, M. Herlem and J. Badoz-Lambling, Fresenius Z. Anal. Chem., 224 (1967) 302.
26 H. Sawamoto, J. Electroanal. Chem., 113 (1980) 301.
27 P. R. Stout and J. Levy, Coll. Czech. Chem. Commun., 10 (1938) 136.
28 K. Komarek, Coll. Czech. Chem. Commun., 12 (1947) 399.
29 T. Fujinaga and B. K. Puri, Ind. J. Chem., 14A (1976) 72.
30 M. I. Abdullah and L. G. Royle, Anal. Chim. Acta, 58 (1972) 283.
31 L. Mart, H. Rützel, P. Khlare, L. Sipos, U. Platzek, P. Valenta and H. W. Nürnberg, Sci. Tot. Environ., 26 (1982) 1.

32 A. Meyer and R. Neeb, Fresenius Z. Anal. Chem., 315 (1983) 118.
33 P. Ostapczuk, P. Valenta, M. Stoeppler and H. W. Nürnberg, in S. S. Brown and J. Savory (Eds.), Chemical Toxicology and Clinical Chemistry of Metals, Academic Press, New York, 1983, pp. 61—64.
34 L. Mart, Tellus, 35B (1983) 131.
35 P. Ostapczuk, M. Goedda, M. Stoeppler and H. W. Nürnberg, Fresenius Z. Anal. Chem., 317 (1983) 252.
36 H. W. Nürnberg, P. Valenta, V. D. Nguyen, M. Goedde and E. Urano de Carvalho, Fresenius Z. Anal. Chem., 317 (1984) 314.
37 T. T. Gorsuch, Analyst (London), 84 (1959) 135.
38 T. T. Gorsuch, The Destruction of Organic Matter, 1st edn., Pergamon Press, Oxford, 1970.
39 S. Marchidan, J. Vartires, I. Tanase and N. D. Totir, Rev. Roum. Chim., 28 (1983) 275.

Analytica Chimica Acta, 164 (1984) 195—207
Elsevier Science Publishers B.V., Amsterdam — Printed in The Netherlands

DETERMINATION OF COPPER IN SEA WATER BY CATHODIC STRIPPING VOLTAMMETRY OF COMPLEXES WITH CATECHOL

CONSTANT M. G. VAN DEN BERG

Department of Oceanography, University of Liverpool, Liverpool, L69 3BX (Great Britain)

(Received 13th May 1983)

SUMMARY

A reduction current is obtained when an aqueous solution of copper and catechol is subjected to differential-pulse cathodic stripping voltammetry (d.p.c.s.v.) because of the reduction of copper(II)—catechol complex ions which adsorb onto the hanging mercury drop electrode (HMDE). The most likely form of the adsorbed complex ions is CuL_2^{2-} (L being catechol). A.c. polarographic measurements showed that these complex ions adsorb more strongly onto the drop than free catechol ions. Monolayer adsorption density is obtained at 2.1×10^{-10} molecules/cm^2, equivalent to a surface area of 78 Å^2 complex ion, which agrees well with the molecular surface area calculated from the bond lengths. Analytically useful currents are obtained at very low metal concentrations, such as in uncontaminated sea water. The possible interference by other trace metals, major cations, and organic complexing ligands is investigated. Competition for copper ions by natural organic complexing ligands is evident at low concentrations of catechol. Analysis of the dissolved copper concentration in sea water by d.p.c.s.v. at the HMDE (at neutral pH) compares favourably with the d.p.a.s.v. technique at a rotating disk electrode (at low pH) because of the shorter collection period and greater sensitivity.

Voltammetric techniques have become established as sensitive and reproducible means to determine metal concentrations in natural water samples. Especially differential-pulse anodic stripping voltammetry (d.p.a.s.v.) has become popular because of its application to the determination of both total and labile metal concentrations, and therefore its usefulness in studies of metal speciation in natural water samples [1—5]. There are many metals, however, which cannot be determined by a.s.v., for instance because the standard reduction potential to the elemental state is at a more negative value than can be reached in aqueous media. Sometimes such metals can be determined conveniently by cathodic stripping voltammetry, c.s.v., the reverse of the previous technique. Preconcentration then sometimes takes the form of adsorption of surface-active metal complex ions onto the electrode. Thus the concentration of cobalt in aqueous solution can be determined by the addition of 2-nitrosonaphthol or diethyldithiocarbamate, and of nickel by using dimethylglyoxime (DMG) [6, 7]. Variants of c.s.v. have been used to determine selenium [8], iron [9] and sulfide [10], and penicillins by means of their adsorbed complex ions of copper [11].

0003-2670/84/$03.00

In preliminary work [12], it was shown that a reduction current appeared when a solution of catechol and copper of natural pH was subjected to c.s.v. at a hanging mercury drop electrode (HMDE), preceded by collection with open circuit. In the present work, the composition of the adsorbed film is investigated as well as the conditions which optimize the formation of this film. Complex adsorption is measured by using a.c. polarography and c.s.v., and the maximum adsorption density is calculated. Possible interference by surface-active organic material in sea water and by organic complexing ligands are investigated.

EXPERIMENTAL

Equipment and reagents

In most polarographic experiments, a PAR 174A polarograph was used with a PAR 303 static mercury drop electrode (SMDE) as either HMDE or DME. The surface area of the HMDE was 2.83 mm^2. The clock in the polarograph was altered in order to increase the pulse rate to 10 s^{-1} and 5 s^{-1}. A home-made water-jacketed experimental cell, which held 50—60 ml, was used for some experiments; its lid had an aperture for the electrode block of the SMDE and an additional hole for the pH electrode. A modular Bruker E-310 polarograph was used for a.c. polarography, and a Metrohm 628-10 rotating disk electrode (surface area 7.1 mm^2) for comparative d.p.a.s.v. analyses. The reference electrode of the SMDE was saturated KCl, AgCl/Ag. The pH was measured with a Radiometer PHM-64 research pH meter with a combined pH/calomel reference electrode, calibrated for the free hydrogen ion scale with a solution of 0.01 M HCl in 0.69 M NaCl. In several experiments, the solution was buffered at pH 7.7 by making it 0.005—0.01 M with respect to a (*N*-2-hydroxyethylpiperazine-*N'*-2-ethanesulphonic acid) buffer stock solution containing 1 M HEPES and 0.5 M ammonia (Aristar). Metal contamination in this buffer solution was removed by shaking the solution for 1 h with 10^{-4} M manganese dioxide followed by filtration through a 0.45-μm membrane filter [13].

The sea water used in these experiments was unfiltered surface water of the South Atlantic, collected during a cruise with R.R.S. Discovery in April 1982 and stored frozen. All experimental work was done in a clean-room supplied with a slight overpressure of filtered air. All normal precautions were taken to prevent contamination of the samples with trace metals by soaking containers and pipettes in acid and by using equipment dedicated to this project.

Distilled water was produced by a double quartz distillation unit. Some distilled and sea-water samples were u.v.-irradiated for 3 h in quartz tubes containing 80 ml of liquid, by a 1-kW lamp. A stock solution of 0.1 M catechol was prepared freshly every day and oxygen was removed by purging with argon to prevent its oxidation to the corresponding *o*-quinone. Triple-distilled mercury was used (Oakes Eddon & Co., Liverpool). Standard metal solutions were prepared from BDH atomic absorption standards.

Procedures for c.s.v.

The sample (10 ml) was pipetted into the cell, the pH was adjusted to 7.7 by the addition of 100 μl of HEPES buffer, and the sample was purged with argon. Catechol solution (100 μl) was added, giving a final concentration of 10^{-3} M, the stirrer was started, the potentiostat was switched on at −1 V, and a fresh mercury drop was made, which indicated the start of the period of collection. After a collection period of between 1 and 3 min, the stirrer was stopped, 10 s later the potential was switched to −0.05 V, and after 20 s the c.s.v. scan was initiated. Scanning parameters were: differential pulse mode, pulse rate 10 s^{-1}, scan rate 10 mV s^{-1}, pulse amplitude 25 mV. The sensitivity was poorer with slower pulse rates or with linear sweep voltammetry.

In some experiments, adsorptive collection was done with open circuit. The potential of the HMDE in such conditions is 0.05 V in sea water, and 0.035 V in 0.01 M KNO_3 (measured against the Ag/AgCl reference electrode).

RESULTS

Cathodic stripping voltammetry in presence of catechol

A well-defined peak becomes apparent at −0.2 V when a solution is subjected to d.p.c.s.v. after catechol has been added. Examples of such scans are given in Fig. 1. These results were obtained in 50 ml of sea water which also contained 5 × 10^{-9} M copper(II) and 0.008 M HEPES; HEPES has only weak metal binding capacity [14] and no effect on the copper collection efficiency was observed when HEPES was present at concentrations around 0.01 M. The collection time was 3 min with open circuit. The peak at

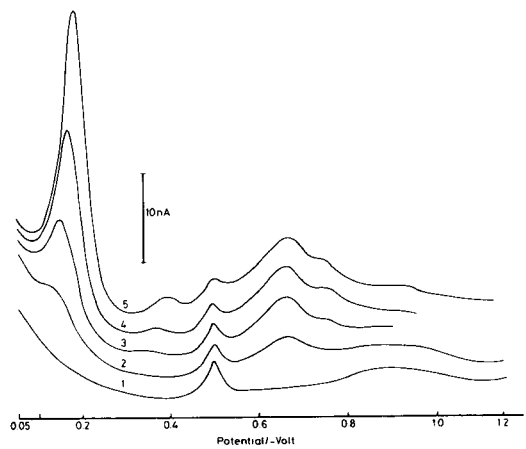

Fig. 1. D.p.c.s.v. in presence of catechol for sea water with 5 × 10^{-9} M Cu^{2+} added. Catechol concentrations: (1) 2 × 10^{-6} M; (2) 1.6 × 10^{-5} M; (3) 3.6 × 10^{-5} M; (4) 7.6 × 10^{-5} M; (5) 1.8 × 10^{-6} M. For details, see text.

—0.2 V increased with the catechol concentrations. Additions of metal ions showed that this peak was due to copper(II). Apparently, copper—catechol complex ions are adsorbed as a film onto the electrode surface, giving rise to a large reduction current when the potential is scanned in the negative direction. This peak is not caused by the reduction of catechol but by that of the metal ion, as the peak height is related to the copper concentration and the reduction potential corresponds to that of copper (shifted in negative direction). Other peaks are apparent when the scan is continued to more negative potentials. It was ascertained by standard additions that those peaks (scan 5, Fig. 1) are related to the reduction of adsorbed complex ions of iron at —0.4 V, uranium at —0.5 V, vanadium at —0.68 V and antimony at —0.73 V. The lead peak, which is present at —0.5 V in absence of catechol, is masked in presence of catechol.

Composition of the adsorbed film of metal—catechol complexes

In Fig. 2(a) the d.p.c.s.v. reduction current of 10^{-8} M copper is plotted as a function of the catechol concentration in sea water and distilled water of pH 7.7 (the collection time was 3 min at —0.05 V, pulse rate 2 s^{-1} and scan rate 5 mV s^{-1}). It was found that the peak current increased exponentially with the catechol concentration until a maximum was reached.

Further information about the type of complexes that adsorb can be obtained from Fig. 2(b) which shows the species distribution of CuL and CuL_2 complexes calculated as a function of the catechol (L) concentration.

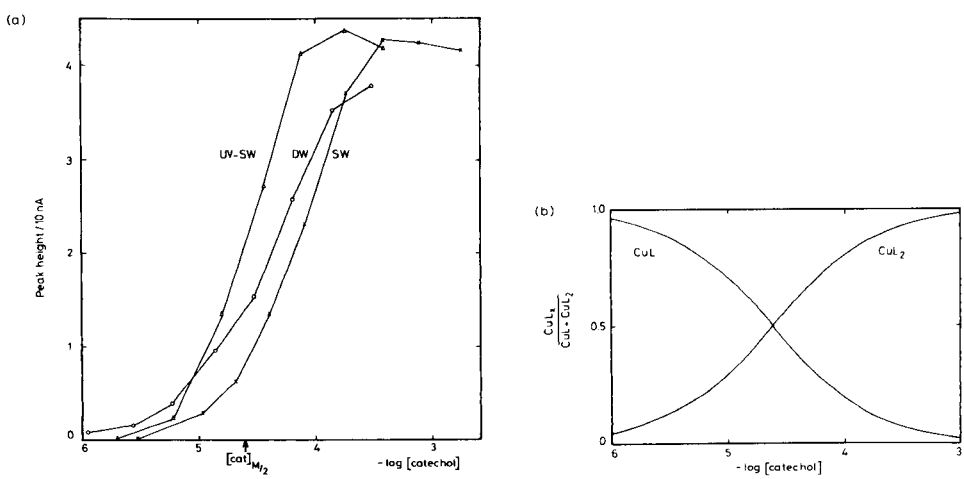

Fig. 2. (a) The reduction current (peak height) from d.p.c.s.v. of copper(II) in sea water (SW), u.v.-irradiated sea water (UV-SW) and in distilled water (DW), as a function of the catechol concentration; $[cat]_{M/2}$ is that catechol concentration which produces 50% of the maximum peak height, and is indicated for UV-SW. (b) Calculated distribution of CuL and CuL_2 (L being catechol) complex ions as a function of the catechol concentration in sea water.

Values for the conditional stability constants, K'_{CuL} and β'_{CuL_2}, were calculated from stability constants given in Martell and Smith [15], using the Davies equation to correct the values to an ionic strength of 0.7. Comparison of Fig. 2(a) and (b) shows that the exponential increase in the copper–catechol reduction current in u.v.-irradiated sea water corresponds to a similar increase in the importance of the CuL_2 fraction. This suggests that the copper reduction peak is due to adsorption of CuL_2 complex ions. The charge on the HMDE is positive at potentials positive of the electrocapillary maximum, which is located at a potential of −0.56 V vs. NCE [16] in chloride solutions similar to sea water. Adsorption of the CuL_2^{2-} complex ion is therefore aided by coulombic attraction at potentials positive of about −0.5 V.

D.c. polarographic experiments

Complex adsorption was studied by d.c. polarography at the DME. The current was sampled, with a drop rate of 2 s^{-1} and a scan rate of 2 mV s^{-1}, in sea water and in 0.01 M KNO_3 containing 3×10^{-6} M Cu(II), 0.0075 M HEPES buffer, and various concentrations of catechol. It was found that the half-wave potentials shifted strongly in the negative direction in both media, indicating that Cu(II) and not Cu(I) is complexed. Adsorption of the complex caused the wave to become steeper, and the diffusion-limited current increased: in sea water by 13% (3×10^{-4} M catechol) or 122% (7×10^{-4} M catechol), and in 0.01 M KNO_3 by 54% (1.2×10^{-5} M catechol) or 37% (10^{-4} M catechol). The increase in sea water is greater than in the potassium nitrate electrolyte because the apparent reduction wave in sea water without catechol is caused by the single electron reduction step of Cu(II) to Cu(I) [17, 18] as a result of chloride complexation of Cu(I). A similar increase of the diffusion-limited current was observed for Ge(IV), Sn(IV), As(V) and Sb(V) when catechol was added to the solution [19].

Plots of log $[i/(i_d - i)]$ as functions of the applied potential (Fig. 3) show the increase in the steepness of the wave, and its shift in the negative direction when catechol is added to the solution. The reciprocal slope was found to be 44 mV in sea water without catechol, giving an apparent value for n of 1.3, which is indicative of the irreversible nature of the reduction of Cu(I) in chloride media. A slope of 29 mV was obtained in 0.01 M KNO_3, corresponding to the reversible 2-electron reduction of Cu(II) in this medium. In presence of catechol, the following values for the reciprocal slope were obtained: in 0.01 M KNO_3, 33.4 mV with 1.2×10^{-5} M catechol, and 19.4 mV with 10^{-4} M catechol; and in sea water, 19.3 mV with 3×10^{-4} M catechol, and 19.8 mV with 7×10^{-4} M catechol. The magnitude of the shift of the half-wave potentials in the negative direction was larger than can be calculated from the stability of the complex ions, which may have been caused by adsorption stabilization [20].

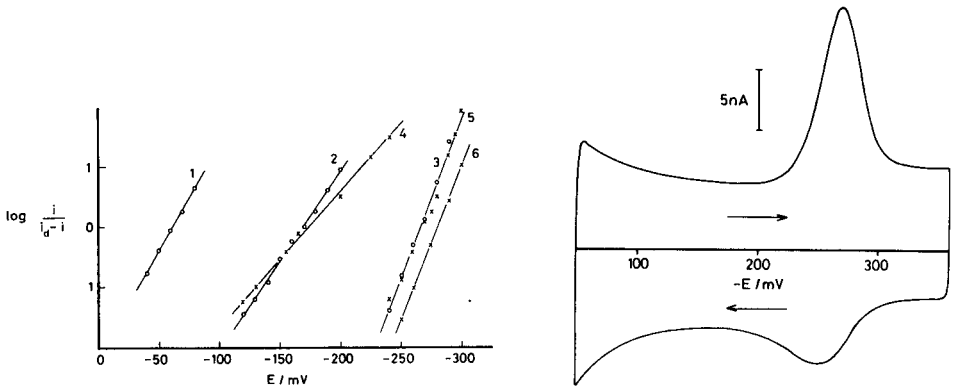

Fig. 3. Plots of log $[i/(i_d - i)]$ as functions of E. D.c. polarography of (○) 0.01 M KNO_3 and (×) sea water, both containing 3×10^{-6} M copper and catechol, at pH 7.8. Catechol concentrations: 0 (curves 1 and 4), 1.2×10^{-5} M (2), 10^{-4} M (3), 3×10^{-4} M (5), and 7×10^{-4} M (6).

Fig. 4. Cyclic voltammetry of copper—catechol complex ions adsorbed onto the HMDE, in presence of 5×10^{-4} M catechol and 10^{-6} M copper in sea water; scan rate 50 mV s^{-1}.

Cyclic voltammetry

These experiments were done with the HMDE, and the scans were preceded by a collection period of 1 min at low (2×10^{-8} M) concentrations of copper. Each scan was started at −0.05 V, and scan rates of 20, 50, 100 and 200 mV s^{-1} were applied. All solutions contained 5×10^{-4} M catechol, 0.0075 M HEPES and either 2×10^{-8} or 3×10^{-6} M copper. An example of a cyclic voltammetric scan is given in Fig. 4. Cathodic (reduction) peak potentials were found to shift in the negative direction with increasing scan rates, while anodic peak potentials shifted in the positive direction at low metal concentration and in the negative direction at high metal concentration. The magnitudes of these shifts (with scan rates from 20 to 200 mV s^{-1}) were −22 mV for the cathodic, and +5 mV for the anodic peak potentials at low metal concentrations, and respectively −42 mV and −30 mV at high metal concentrations. These shifts indicate a small degree of irreversibility at high scan rates. The difference, ΔE_p, of the peak potentials of the cathodic and anodic waves was found to increase with the scan rate (from 20 mV s^{-1} to 200 mV s^{-1}) from 33 to 55 mV at high, and from 35 to 62 mV at low copper concentrations. The difference in the peak potentials is caused by diffusion of the reduced metal into the electrode, away from the surface, before it can be re-oxidized. Both the anodic and cathodic currents diminished (at low copper concentration) when the scans were repeated rapidly with the same drop. Complete recovery occurred when the potential was held for 15—30 s at −0.05 V before the scan was repeated, thus allowing amalgamated metal to become re-oxidized and return to the adsorbed film.

A.c. polarographic experiments

The capacitance of the double layer is suppressed as a result of displacement of electrolyte ions by adsorption of organic molecules. Suppression of the capacitance was measured by a.c. polarography with the HMDE in order to investigate whether free or complexed catechol ions, or both, adsorb. The capacitance was measured after collection (similar to Cosovic and Vojvodic [21]) at −0.5 and at −0.05 V. The pH of the solution (u.v.-irradiated 0.02 M NaCl) was fixed at pH 7.5 with phosphate buffer as it was found that HEPES buffer caused capacitance suppression. An a.c. frequency of 170 Hz was used, with a wave amplitude of 10 mV and a scan rate of 5 mV s^{-1}. It was found that addition of catechol caused partial suppression of the capacitance, but this suppression was increased strongly by addition of 10^{-7} M copper: by 25% after collection at −0.5 V and by 200% after collection at −0.05 V. These results indicate that there is adsorption of free catechol ions onto the drop, but the metal-complex ions adsorb more strongly, especially when collection takes place at a potential anodic of the electrocapillary maximum.

Adsorption density of metal–catechol complex ions onto the mercury drop

The amount of metal–catechol complex ions that adsorb onto the electrode was calculated from the reduction current (in coulombs) as measured from the surface area under the peak produced by a linear potential scan. The maximum adsorption density was obtained by increasing the metal concentration until nearly constant peak currents were obtained, after a constant collection period of 3 min at −0.05 V, and a scan rate of 50 mV s^{-1} (see Fig. 5). The solutions (sea water and 0.01 M KNO_3) contained 5×10^{-4} M catechol and were buffered at pH 7.8 with HEPES. The data were

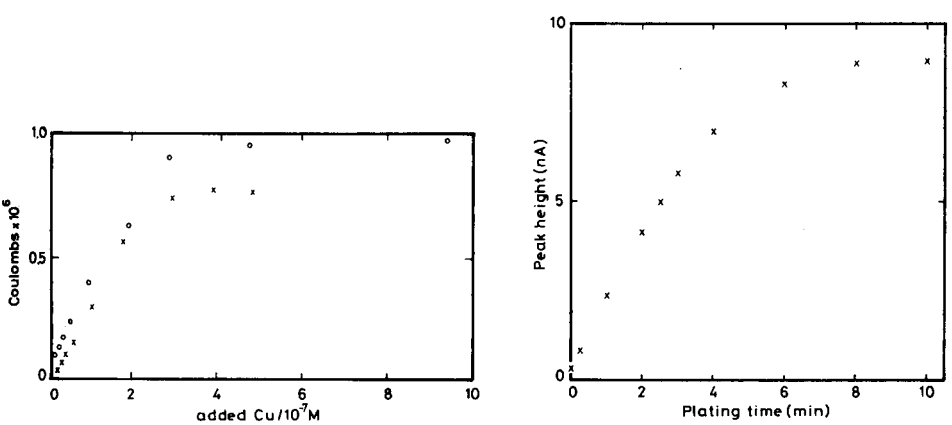

Fig. 5. Determination of the maximum adsorption capacity of copper–catechol complex ions onto the HMDE: (×) in sea water; (○) in 0.01 M KNO_3.

Fig. 6. The d.p.c.s.v. reduction current (peak height) of 5×10^{-9} M copper in sea water as a function of the collection period.

fitted by least-squares regression to the following linearized form [22] of the Langmuir equation

$$C_M/i_r = C_M/i_m + 1/(Bi_m)$$

where C_M is the dissolved metal concentration, i_m is the current maximum, which, it is implicitly assumed, is obtained at monolayer coverage, and B is a constant, which is related to the free energy of adsorption.

The dissolved metal concentration was approximately equal to the total metal concentration, as the amount of metal that adsorbed was negligible. Plots of the data as C_M/i_r as a function of C_M were linear, and values for i_m were calculated from the reciprocal slope: a value of 1.16×10^{-6} C was obtained in 0.01 M KNO_3, and of 0.80×10^{-6} C in sea water. The density of metal complex ions, Γ_m, adsorbed per cm^2 of drop area, was calculated from the current from $\Gamma_m = i_m/nFA$) (where A is the surface area of the drop), giving maximum adsorption densities of $\Gamma_m = 2.12 \times 10^{-10}$ molecules cm^{-2} in 0.01 M KNO_3, and 1.5×10^{-10} molecules cm^{-2} in sea water. The smaller surface coverage in sea water may have been caused by competition for surface area by complex ions of uranium, iron and vanadium which were present in trace amounts in the sample. The surface area occupied by each copper(catechol)$_2$ complex ion at monolayer coverage amounts to 78 $Å^2$ in 0.01 M KNO_3, which agrees well with the calculated surface area of 68 $Å^2$ which is occupied by a complex ion of that type [23] adsorbed flat onto the drop surface.

Effects of the collection time and variation of pH

The peak current of the copper—catechol complex ions is plotted as a function of the collection time (with open circuit) in Fig. 6. The solution consisted of 50 ml of sea water, with 8×10^{-9} M copper(II) added, and containing 0.008 M HEPES and 8×10^{-5} M catechol. Each scan was started at −0.050 V. The peak current increased almost linearly at short plating periods up to about 4 min, after which the peak current levelled off. The drop was still not saturated with complex ions of copper, as much larger currents were obtained at higher concentrations. It is therefore possible that after prolonged collection periods an increasing area of the drop is covered by complex ions of other metals present in sea water. For instance, the maximum reduction current was reduced by about 10% by addition of 5×10^{-8} M Fe(III) to the solution.

The peak current was also measured as a function of the pH after a collection period of 3 min at −0.15 V in 0.01 M KCl containing 8×10^{-4} M catechol and 10^{-8} M copper (Fig. 7). It was found that the peak potential shifted about 0.04 V/pH unit in the negative direction with increasing pH, which reflects the increasing stability of the copper—catechol complexes. The peak height doubled when the pH was increased from 6 to 8.

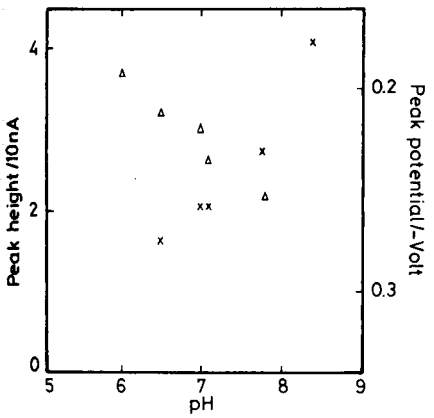

Fig. 7. Effect of the solution pH on the d.p.c.s.v. peak height and potential of the copper—catechol complex ion: (△) potentials; (×) peak heights.

Interferences

Natural organic material with surface-active and electroactive properties, and inorganic anions forming mercury(I) salts, could interfere by covering the HMDE with a possibly inactivating layer. Such effects were tested by d.p.c.s.v. measurements in sea water in absence of catechol, as shown in Fig. 8. Scan 1 was obtained after a 3 min collection (open circuit), the pulse rate was 2 s^{-1}, and the scan rate 5 mV s^{-1}. Two organic peaks appeared to be present, at −0.25 and −1.1 V, which increased with the collection time (scan 2). Both peaks were removed by u.v. irradiation of the sample. A small peak at −0.5 V was caused by lead present as contamination in the triple-distilled mercury. This peak was masked by the reduction current of uranium when catechol was added to the solution (Fig. 1). A broad peak at −1 V was produced by the reduction of dissolved iodate. The height of this peak was not dependent on the collection time. Scans 3 and 4 show the effect of standard additions of iodate. A peak of iodide was apparent only in freshly u.v.-irradiated seawater: u.v.-irradiation apparently causes reduction of dissolved iodate to iodide. The effect of additions of iodide is shown in scans 5 and 6. This peak could be eliminated by using a collection potential of −0.1 V or more negative. The reduction peak of iodide has been used before to determine its concentration in acidified media [24]. Evidently, iodide can be readily determined also at the natural pH of sea water, which may be more advantageous if one wants to prevent its spontaneous oxidation at low pH.

Competition by natural organic complexing ligands. Complexing ligands can reduce the magnitude of the copper—catechol signal by competing for free Cu^{2+} with the catechol ions. Inorganic complexing ligands such as OH^-, CO_3^{2-} and Cl^- are present at constant levels in natural water samples, and these ligands contribute to the activity coefficient, α_{Cu}, of dissolved inorganic copper(II). The fraction of copper that is present in inorganic

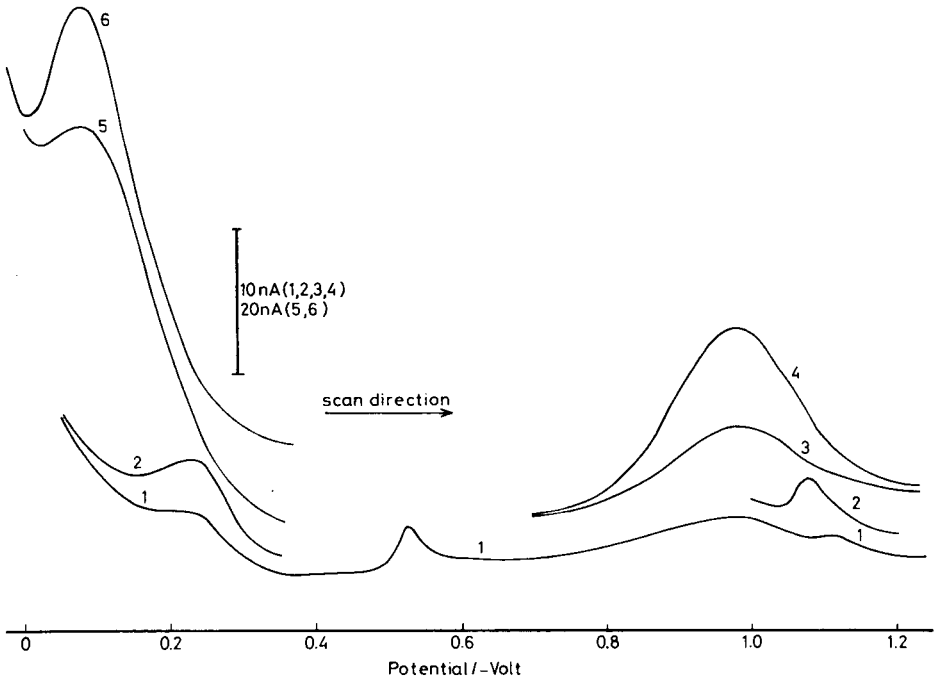

Fig. 8. D.p.c.s.v. of Atlantic sea water at pH 8.2 in absence of catechol. Curves: (1) 3 min collection; (2) 6 min collection; (3) 3 min collection after addition of 8×10^{-7} M IO_3^-; (4) 3 min collection after addition of 2.4×10^{-6} M IO_3^-; (5) 6 min collection after addition of 3.3×10^{-7} M I^-; (6) 6 min collection after addition of 6.67×10^{-7} M I^-.

complexes is negligible at catechol concentrations greater than 10^{-5} M, because in sea water the value for α_{Cu} is about 30 [25], whereas the α-coefficient for copper—catechol is 180 at a catechol concentration of 10^{-5} M. Any reduction in the copper—catechol peak by inorganic complexation reactions can be automatically corrected for by using the standard addition technique.

However, natural water samples are known to contain variable, small amounts of strong organic complexing ligands with conditional stability constants possibly similar to that of EDTA for Cu^{2+} in sea water [25, 26]. The kinetics of formation of such complexes in sea water can be very slow as a result of exchange reactions with Ca^{2+} and Mg^{2+} [27] so that standard additions to such a sample would provide a measure of the labile copper fraction which can be extracted from its organic complexes at a given concentration of catechol. Such effects were tested by measuring the peak current of the dissolved copper concentration (2.3×10^{-9} M) in sea water as a function of the catechol concentration before and after u.v.-irradiation (Fig. 2a). It was found that the value for $[cat]_{M/2}$ was shifted to 7×10^{-5} M from 2.5×10^{-5} M catechol as a result of ligand competition by dissolved

natural organic compounds. The maximum peak height was obtained at about 4×10^{-4} M catechol, when all copper complexes with the natural organic ligands had dissociated.

In a further experiment, the apparent copper concentration of sea water was determined by standard metal additions at three concentrations of catechol: 8×10^{-5} M catechol gave $7.8 \pm 1.8 \times 10^{-10}$ M copper, 3×10^{-4} M catechol gave $1.3 \pm 0.3 \times 10^{-9}$ M copper, and 8.3×10^{-4} M catechol gave $2.3 \pm 0.6 \times 10^{-9}$ M copper. Interference by natural organic complexing ligands can therefore be overcome by using a high catechol concentration (8×10^{-4} M), or by u.v.-irradiation.

The ligand competition between dissolved organic material in sea water and added catechol could be of interest in the study of metal—organic interactions in natural waters. The degree of competition can be precisely defined by means of the known stability constants of the copper—catechol complexes. Investigations into this application are presently undertaken in this laboratory.

Competition by other metal ions. The ions of other metals such as lead, zinc, iron, uranium and vanadium also produce reduction peaks, but the sensitivity of c.s.v. for these metals is less than for copper, either because weaker complexes are formed with catechol, or because the configuration of the complexes is less favourable for adsorption. Their reduction potentials are well separated from that of copper. Complex ions of these and other metals can compete with copper for surface area on the drop if they are present in relatively high concentrations. The sensitivity for copper therefore needs to be checked by standard additions. There is some complexation of catechol by calcium and magnesium ions in sea water, but the effect on the conditional stability constant is negligible compared with that caused by hydrogen ions. The plot of the peak current against the catechol concentration in distilled water in Fig. 2(a) produced a value for $[\text{cat}]_{M/2}$ of 6.3×10^{-5} M catechol, which is higher than in u.v.-irradiated sea water. A lower value would be expected if competition by major cations were significant.

Determination of dissolved copper in sea water

A concentration of 8×10^{-4} M catechol was selected to determine the copper concentration in unfiltered sea water, and the results were compared with those obtained by d.p.a.s.v. at a rotating disc electrode (RDE) preplated with a mercury film. The d.p.c.s.v. was done with 0.008 M HEPES (pH 7.8) in the solution, a collection period of 3 min, and the same scan parameters as before. The results of a d.p.c.s.v. analysis of a sample from the South Atlantic and of two standard additions of 1.67×10^{-9} and of 3.33×10^{-9} M copper are shown in Fig. 9(a). The initial copper concentration in the sample ($2.3 \pm 0.6 \times 10^{-9}$ M) was calculated from these and two more standard additions by linear extrapolation. This result was checked by d.p.a.s.v. measurement of the same sample at pH 2, as shown in Fig. 9(b).

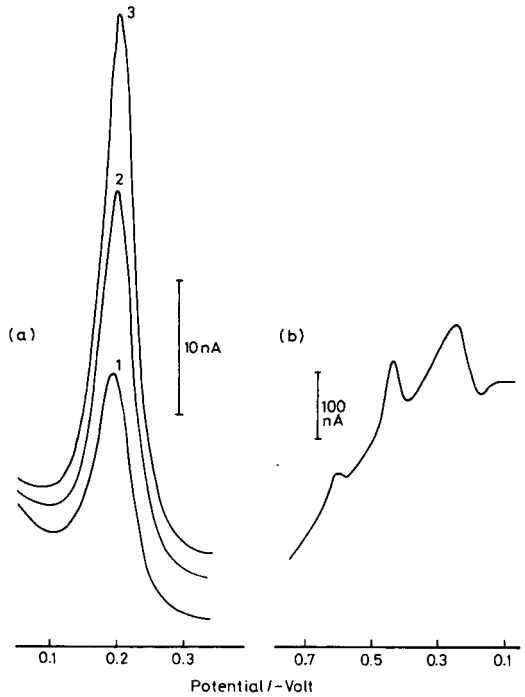

Fig. 9. (a) Determination of copper in Atlantic sea water by d.p.c.s.v. at the HMDE. Curves: (1) sea water; (2) $+1.67 \times 10^{-9}$ M copper; (3) $+3.33 \times 10^{-9}$ M copper. (b) Determination of copper in Atlantic sea water adjusted to pH 2 by d.p.a.s.v. at the RDE.

The peaks of Cd (—0.6 V), Pb (—0.45 V) and Cu (—0.3 V) are visible. Comparison shows that the actual peak current is much larger for the d.p.a.s.v. measurement, because of the long plating time (20 min) and the larger surface area of the RDE, but the sensitivity of the measurement is less because of the greater capacitance current and the strongly sloping baseline. A much longer plating time is therefore needed in order to produce a useful peak. The a.s.v. measurements after standard additions were done with reduced plating times [28]. There were no systematic differences between the apparent initial copper concentrations as determined by d.p.a.s.v. and by d.p.c.s.v. at catechol concentrations of $\geqslant 8 \times 10^{-4}$ M and greater, but smaller copper concentrations were obtained by d.p.c.s.v. at lower catechol concentrations as a result of competition by natural organic complexing ligands (see above).

Improved sensitivity and a scan without the peaks from Fe, U and V, can be obtained by using a negative collection potential at —1.05 V. The d.p.c.s.v. scan is then started 20 s after switching the potential to —0.05 V. The peak height is further increased by using a faster pulse rate ($10\ s^{-1}$) and scan rate ($10\ mV\ s^{-1}$) [12]. The detection limit in these conditions is 6×10^{-11} M copper after a 3-min collection (calculated from 3× the standard

deviation (10 degrees of freedom) of the determination of 2×10^{-10} M copper in distilled water in presence of 5×10^{-4} M catechol).

REFERENCES

1 G. Gillain, G. Duyckaerts and A. Disteche, Anal. Chim. Acta, 106 (1979) 23.
2 S. R. Piotrowicz, M. Springer-Young, J. A. Puig and M. J. Spencer, Anal. Chem., 54 (1983) 1367.
3 J. C. Duinker and C. J. M. Kramer, Mar. Chem., 5 (1977) 207.
4 J. R. Hasle and M. I. Abdullah, Mar. Chem., 10 (1981) 487.
5 S. K. Nilsen and W. Lund, Mar. Chem., 11 (1982) 223.
6 Kh. Z. Brainina, Stripping Voltammetry in Chemical Analysis, Wiley, New York, 1974.
7 B. Pihlar, P. Valenta and H. W. Nürnberg, Fresenius Z. Anal. Chem., 307 (1981) 337.
8 G. Jarzabek and Z. Kublik, Anal. Chim. Acta, 143 (1982) 121.
9 J. A. Cox and M. Majda, Anal. Chim. Acta, 118 (1980) 271.
10 K. Shimizu and R. A. Osteryoung, Anal. Chem., 53 (1981) 584.
11 U. Forsman, Anal. Chim. Acta, 146 (1983) 71.
12 C. M. G. van den Berg, Anal. Lett., (1984) in press.
13 C. M. G. van den Berg, Mar. Chem., 11 (1982) 323.
14 N. E. Good, G. D. Winget, W. Winter, T. N. Connolly, S. Izawa and R. M. M. Singh, Biochem., 5 (1966) 467.
15 A. E. Martell and R. M. Smith, Critical Stability Constants, Vol. 3, Plenum Press, New York, 1977.
16 J. Heyrovsky and J. Kuta, Principles of Polarography, Academic Press, London, 1966.
17 M. J. Pinchin, Anal. Chim. Acta, 90 (1977) 91.
18 M. Odier and V. Plichon, Anal. Chim. Acta, 55 (1971) 209.
19 C. McCrory-Joy and J. M. Rosamilia, Anal. Chim. Acta, 142 (1982), 231.
20 A. J. Bard and L. R. Faulkner, Electrochemical Methods, Wiley, New York, 1980.
21 B. Cosovic and V. Vojvodic, Limnol. Oceangr., 27 (1982) 361.
22 C. M. G. van den Berg, Mar. Chem., 11 (1982) 307.
23 A. F. Wells, Structural Inorganic Chemistry, 4th edn., Clarendon Press, Oxford, 1975.
24 G. Colovos, G. S. Wilson and J. L. Moyers, Anal. Chem., 46 (1974) 1045.
25 C. M. G. van den Berg, Mar. Chem., 14 (1984) 201.
26 K. Hirose, Y. Dokiya and Y. Sugimura, Mar. Chem., 11 (1982) 343.
27 B. Raspor, H. W. Nürnberg, P. Valenta and M. Branica, J. Electroanal. Chem., 115 (1980) 293.
28 L. Mart, H. W. Nürnberg and P. Valenta, Fresenius Z. Anal. Chem., 300 (1980) 350.

Analytica Chimica Acta, 164 (1984) 209—222
Elsevier Science Publishers B.V., Amsterdam — Printed in The Netherlands

DETERMINATION OF URANIUM(VI) IN SEA WATER BY CATHODIC STRIPPING VOLTAMMETRY OF COMPLEXES WITH CATECHOL

CONSTANT M. G. VAN DEN BERG* and ZI QIANG HUANG[a]

Department of Oceanography, University of Liverpool, Liverpool, L69 3BX (Great Britain)

(Received 20th January 1984)

SUMMARY

Polarographic (d.c.) measurements showed that complex ions of uranium(VI) with catechol adsorb on the dropping mercury electrode. This effect is used to determine uranium(VI) directly in sea water. Optimal conditions include pH 6.8, 2×10^{-5} M catechol, and a collection potential between −0.1 and −0.4 V (vs. Ag/AgCl) at a hanging mercury drop electrode. The cathodic scan is made with the linear-scan or differential-pulse mode (d.p.c.s.v.). The detection limit with the d.p.c.s.v. mode is 3×10^{-10} M after a collection period of 2.5 min. Between pH 6 and 8, the peak height increases with pH and with catechol concentration up to 5×10^{-5} M. There is linear relationship between the collection time and the measured peak height until the drop surface becomes saturated. With a collection period of 3 min, the reduction current increases linearly with the metal concentration up to about 5×10^{-8} M U(VI). The maximum adsorption capacity of the mercury drop is 4.4×10^{-10} mol cm^2; each complex ion then occupies 0.38 nm^2, equivalent to the size of about one catechol molecule. Interference by high concentrations of Fe(III) is overcome by selectively adsorbing U(VI) at a collection potential near the reduction potential of Fe(III). Organic surfactants reduce the peak height for uranium by up to 75% at unnaturally high concentrations only (4 mg l^{-1} Triton X-100). Competition by high concentrations of Cu(II) for space on the surface of the drop is eliminated by addition of EDTA.

The geographical distribution of uranium is of interest because the element is used in the production of energy in nuclear reactors. It is of geochemical interest because it belongs to the actinide group, the geochemical pathways of which have not been studied as rigorously as those of some of the transition metals (e.g., copper, lead, zinc and cadmium). The stable oxidation state is uranium(VI) in oxygenated waters, and its predominant form is the uranyl ion which is complexed by carbonate in carbonate-bearing waters [1]. Uranium(VI) occurs in sea water therefore as an anion, and has a very long residence time of $2—4 \times 10^6$ years [2]. The metal behaves as a well-mixed element with an average concentration of 3.3 μg l^{-1} (1.4×10^{-8} M) in sea water of 35‰ salinity [2].

Several techniques have been developed for the determination of U(VI) in

[a]Permanent address: Third Institute of Oceanography, The National Bureau of Oceanography, Xiamen, China.

0003-2670/84/$03.00

water including α-spectrometry [2], neutron activation [3], spectrophotometry [4], molecular fluorescence spectrometry [5], complexiметric titration [6], pulse polarography [7], and gas chromatography [8]. These techniques are presently not sufficiently sensitive for the direct determination of U(VI) in sea water, so that a pre-concentration stage is necessary, which may be liquid—liquid extraction, or sorption on activated carbon or chelating resins [2—8]. The measurement is then further complicated by the necessity to add a radio-tracer of uranium to check the recovery of the pre-concentration step.

It would obviously be useful to be able to determine the concentration of U(VI) directly in the sample. Recently, a variant of the technique of cathodic stripping voltammetry (c.s.v.) was developed for the determination of copper(II) ions in sea water [9, 10]. This method involves measurement of the reduction current of the complex ions of copper with catechol (probably CuL_2^{2-}) which are adsorbed strongly onto the hanging mercury drop electrode (HMDE). In this paper, this technique is applied to the determination of U(VI). Catechol is a suitable complexing agent because of the great stability of its complex ions with UO_2^{2+} (see below). Recently, uranium(VI) was determined by cathodic stripping voltammetry (c.s.v.) [11]; a reduction peak was obtained when uranyl ions were stripped after deposition on a glassy carbon electrode which had tri-n-octylphosphine oxide adsorbed on its surface. This method is not sufficiently sensitive to be used with sea water as even after 45 min for plating a poorly reproducible broad peak was obtained on the shoulder of the background current. The method described below is about two orders of magnitude more sensitive after a plating period of only 3 min. While this paper was in preparation, Lam et al. [12] described the determination of uranium by a similar technique. As will be shown, this technique did not employ the optimal analytical conditions, and therefore could not be applied to determine uranium in sea water without pre-concentration.

EXPERIMENTAL

Reagents, equipment and samples

A 0.005 M stock solution of U(VI) was prepared by dissolving spectroscopic grade (99.999%) U_3O_8 (Johnson Matthey Chemicals) in a minimum amount of concentrated nitric acid (Aristar; BDH Chemicals), and dilution with distilled water. Most of the equipment and chemicals were the same as those used for the determination of copper [9]. A stock solution of 0.1 M catechol was prepared freshly every day. Buffer solutions were prepared with 1 M HEPES (*N*-2-hydroxyethylpiperazine-*N'*-2-ethanesulphonic acid) and 0.5 M NaOH, or 1 M PIPES (piperazine-*N*,*N'*-bis-2-ethanesulphonic acid, monosodium salt) and 0.5 M NaOH.

Sea water was collected from the Irish Sea (from the surface) and stored in 50-l polyethylene containers. The water was filtered through 0.45-μm

filters and then analyzed. Some of the sample was stored acidified. The salinity of the sample was 33‰.

Procedure

The determination of about 10^{-8} M U(VI) was done as follows. The sample (10 ml) was pipetted into the electrochemical cell and adjusted to pH 6.7—8.0 by adding HEPES or PIPES buffer. Oxygen was removed by purging with an inert gas (purified nitrogen or argon), and catechol was added to give a concentration of 2×10^{-3} M. A new mercury drop was extruded, the potentiostat was switched on and the stirrer was started (i.e., start of the collection period). The collection potential was —0.3 V, unless it was necessary to discriminate against high concentrations of iron(III) ($>10^{-8}$ M), in which case it was necessary to measure at pH 6.8 and set the potentiostat at —0.4 V (about 0.15 V on the positive side of the U(VI) reduction potential, and about 0.04 V negative of the Fe(III) reduction potential). The stirrer was stopped after a suitable definite period (usually between 1 and 4 min depending on the metal concentration), and the potentiostat was switched to —0.3 V after a rest period of 15 s; 10 s later the scan was recorded using either the differential pulse (d.p.c.s.v.) or linear sweep (l.s.c.s.v.) mode. The measurement was repeated after a standard addition of 10^{-8} M U(VI). The peak current/U(VI) concentration relationship was linear at concentrations up to about 5×10^{-8} M U(VI) for a collection period of 3 min, so that standard additions should be below this level. Linearity to higher uranium concentrations can be obtained with shorter collection times.

RESULTS

Polarography of uranium(VI) in sea water

Only a single peak is produced when a solution of U(VI) in sea water (pH 3) is subjected to differential pulse polarography (d.p.p.) at the dropping mercury electrode (DME) (Fig. 1). This peak corresponds to the reduction of U(VI) to U(V) [13]; the half-wave potential, $E_{1/2}$, for the further reduction of U(V) to U(IV) and U(III) is at —0.9 V (vs. SCE) [13, 14], but this wave is not generated at high chloride concentrations when the DME is used. The plot of log $(i/i_d - i)$ as a function of applied potential, for d.c. polarography in the solution at pH 3, was found to be a straight line with a reciprocal slope of 58 mV, confirming that the reduction of U(VI) is a reversible one-electron process, with $E_{1/2} = -0.163$ V (vs. Ag/AgCl). At higher pH values, between 4 and 6, the peak at —0.16 V becomes much smaller (at pH 7 it disappears completely), and a second peak appears at —0.55 V at pH 5.9 (curve 2, Fig. 1) because of hydrolysis of the UO_2^{2+} ion [13]. Addition of catechol to this solution causes the formation of a maximum at —0.67 V (curve 3, Fig. 1), as a result of adsorption of complexes of catechol with the uranyl ion or its hydrolysis products. Reduction potentials U(VI)/U(V) or similar uranyl complexes have been reported before, e.g., at —0.59 V (with

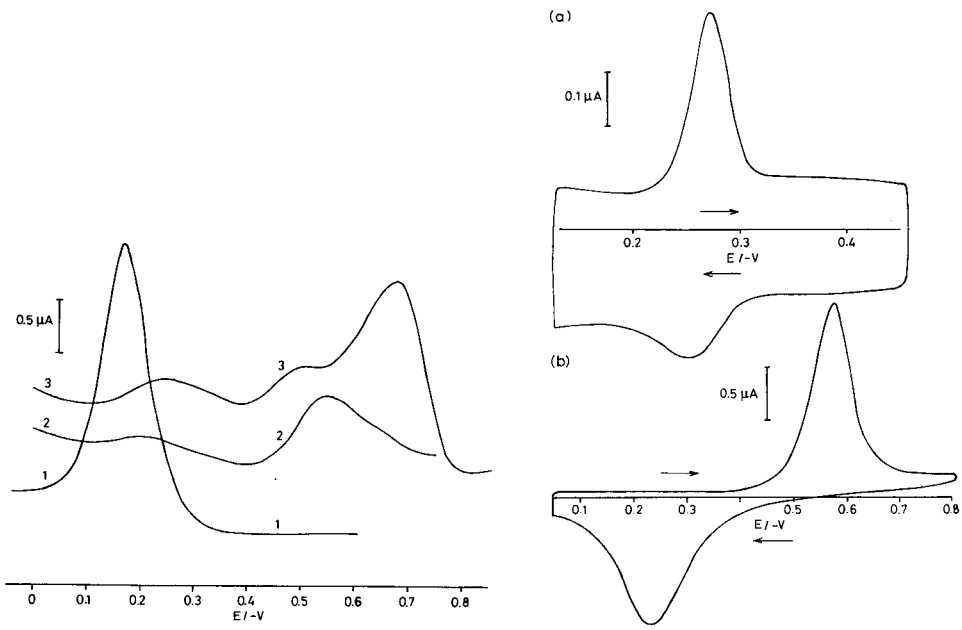

Fig. 1. Differential pulse polarography of 9×10^{-5} M U(VI) in sea water. Curves: (1) pH 3; (2) pH 5.9; (3) pH 5.9 in presence of 2×10^{-4} M catechol.

Fig. 2. Cyclic voltammetry of 9×10^{-5} M U(VI) in sea water: (a) at pH 2.8; (b) at pH 7.5 in presence of 10^{-3} M catechol. Scan rate 50 mV s^{-1}.

8-hydroxy-6-methylquinol) and at −0.39 V (with 5-hydroxyquinazoline) vs. NHE [15]. The present result for uranyl ion in presence of catechol is quite different from that of Lam et al. [12] who only observed a single peak at −0.25 V (Ag/AgCl) at pH 4.6 when catechol was present. They did not find an adsorption maximum, possibly because they used an acetate pH buffer, which forms complexes with uranium in competition with catechol.

The reduction of the complex ions of U(VI) with catechol is irreversible; Fig. 2 shows the cyclic voltammetric scans for sea water (to which 9×10^{-5} M U(VI) had been added) at pH 2.8 (Fig. 2a), and at pH 7.5 in presence of 10^{-3} M catechol (Fig. 2b). The cathodic peak potential is at −0.58 V in the presence of catechol, whereas the anodic peak potential is at −0.24 V. It appears therefore that U(V) is oxidized initially to UO_2^{2+}.

These measurements were done with rather high concentrations of U(VI). However, the reduction current at a HMDE can be increased for low concentrations of U(VI) if the measurement is preceded by a collection period during which the catechol complex is adsorbed onto the electrode. Attention was therefore devoted to optimizing the conditions for the determination of uranium in sea water. Complex ions of catechol with iron(III) and vanadium(V) were found to have reduction potentials near that of uranium(VI). Possible interferences by these metals were also investigated.

Effect of the catechol concentration

The reduction current of 7×10^{-8} M U(VI) in sea water was measured by linear-sweep c.s.v. in the presence of various concentrations of catechol at pH 6.9, using a collection time of 1 min (with magnetic stirring) at a potential of −0.1 V. Each scan was started 15 s after stopping the stirrer. The experiment was repeated with sea water from which carbonate had been removed at pH 3 by purging with argon. The results are presented in Fig. 3(a); sizeable currents were found even at low concentrations (10^{-5} M) of catechol in absence of carbonate ions. However, the peak height increased as the catechol concentration increased (particularly at $>2 \times 10^{-4}$ M) until a maximum was reached at 0.005 M.

The peak shape changed with increasing catechol concentration and at about 10^{-4} M catechol a second peak appeared, initially as a shoulder on the negative side of the first. This second peak shifted to about 75 mV more negative than the first and attained a height of ca. 30% of the main peak with 5×10^{-4} M catechol. At higher catechol concentrations, the height of the second peak diminished while that of the first increased further. The second peak probably represented stripping of a metal-catechol complex species that was adsorbed by the electrode more strongly than the first. Plots of the peak heights of the two peaks as a function of the uranium concentration were parallel to each other.

Earlier experiments with a.c. polarography [9] showed that catechol is adsorbed on the HMDE but that adsorption is much greater in the presence of metal ions. Uranium adsorption therefore probably reflects the species distribution of complexes with catechol in solution. This distribution as a

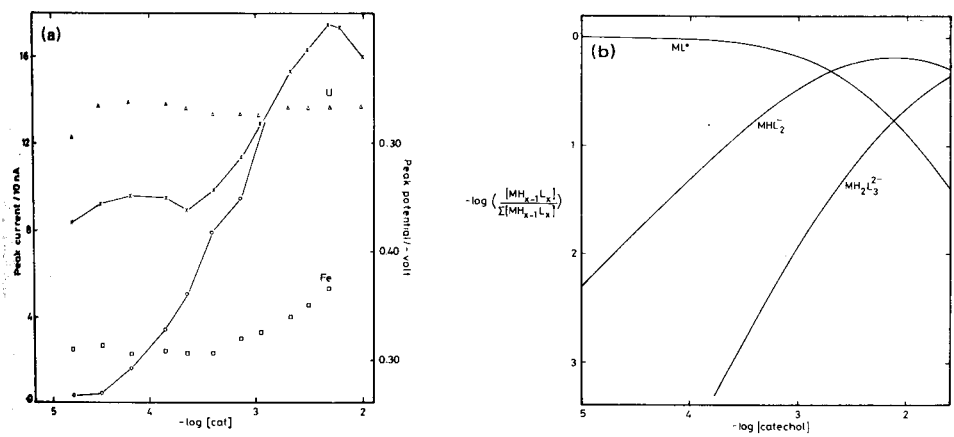

Fig. 3(a) Peak currents and potentials as a function of the catechol concentration in sea water. Conditions: l.s.c.s.v., 50 mV s^{-1}, 1 min collection at −0.1 V, pH 6.9, 0.008 M PIPES buffer, 7×10^{-8} M U(VI), 7×10^{-8} M Fe(III). (—) Peak currents; (×) after removal of carbonate; (○) untreated sea water; (□) peak potentials of Fe(III); (△) peak potentials of U(VI). (b) The distribution of U(VI)/catechol complex ions as a function of the catechol concentration, in sea water of pH 6.9; M = UO_2^{2+}, L = catechol^{2-}.

function of the catechol concentration is shown in Fig. 3(b); the stability constants used for the calculation are listed in Table 1. Maximum peak current is obtained when the UHL_2^- complex ion predominates, which suggests that this ion adsorbs preferentially. However, the large current obtained at lower catechol concentrations indicates that the neutral UL complex also adsorbs. Adsorption is strongly decreased by the presence of carbonate ions at catechol concentrations less than 10^{-3} M, as a result of ligand competition. The α-coefficient of uranium complexation by carbonate in sea water of pH 6.9 is 3×10^4 (from the stability constants in Table 1, using an ion-pairing model [20]) which is the same as that of 10^{-3} M catechol. Thus, the competing effect of carbonate will be negligible at higher concentrations of catechol.

The peak potential of uranium (Fig. 3a) showed little variation with the catechol concentration, which suggests that complex ions are also formed with the reduction product, U(V). These complex ions also adsorb onto the electrode to some extent, causing a large oxidation current during cyclic scanning. Adsorption of U(V) complex ions is much weaker, however, as a much smaller current was obtained following collection at potentials more negative than the reduction potential of U(VI) in this solution (see below).

The peak of 7×10^{-8} M Fe(III) in the same solution shifted to more negative potentials, towards that of U(VI) as the catechol concentration increased (Fig. 3a). However, its peak height was only 10—15% of that of 7×10^{-8} M uranium.

Effect of the collection potential

The reduction current of 7×10^{-8} M uranium was measured by linear-scan c.s.v., in sea water of pH 6.8, in presence of 2×10^{-3} M catechol, after a collection period of 1 min at various potentials. The scan was always started from —0.3 V. The peak height diminished considerably when collection potentials more negative than —0.4 V were selected (Fig. 4). This effect is caused by reduction of the adsorbed complex ions at potentials near, or more negative than, the reduction potential (—0.54 V) of U(VI) in this medium. The electrostatic contribution to the adsorption of the negatively

TABLE 1

Stability constants for complexation of U(VI) and catechol in solutions with an ionic strength of 0.7 M ($M^{2+} = UO_2^{2+}$, L = catechol)

Reaction	log K^*	Ref.	Reaction	log K^*	Ref.
$M^{2+} + H_2O = MOH^+ + H^+$	—5.2	16	$LH^- = L^{2-} + H^+$	—12.99	19
$M^{2+} + H_2O = MOH^+ + H^+$	—5.8	17	$LH_2 = LH^- + H^+$	—9.19	19
$2M^{2+} + 2H_2O = M_2(OH)_2^{2+} + 2H^+$	—6.1	17	$M^{2+} + L^{2-} = ML$	15.8	19
$3M^{2+} + 5H_2O = M_3(OH)_5^+ + 5H^+$	—16.9	17	$M^{2+} + HL^- = MHL^+$	6.2	19
$M^{2+} + CO_3^{2-} = MCO_3$	10.1	2	$ML + HL^- = MHL_2^-$	4.9	19
$M^{2+} + 2CO_3^{2-} = M(CO_3)_2^{2-}$	16.02	18	$MHL_2^- + HL^- = MH_2L_3^{2-}$	3.7	19

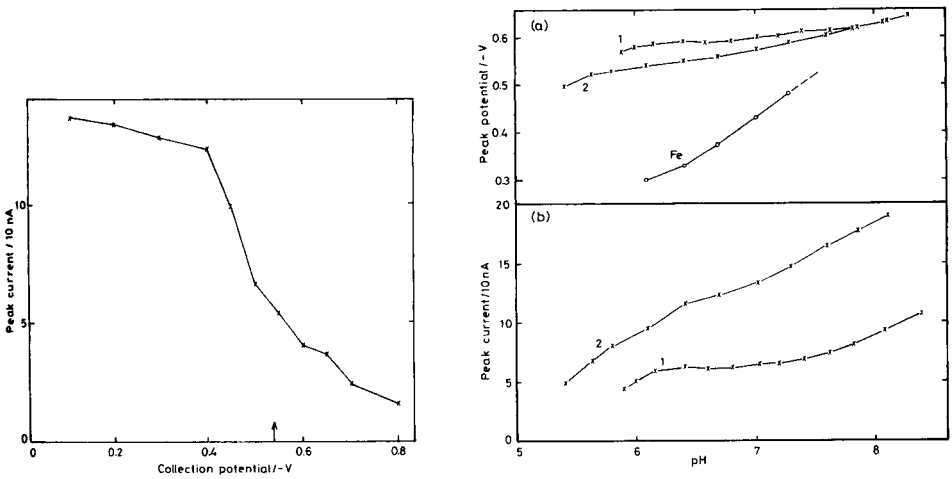

Fig. 4. Peak current of uranium as a function of the collection potential. Conditions: sea water, 7×10^{-8} M U(VI) added, 0.008 M PIPES, 1 min collection, linear-scan c.s.v., 50 mV s^{-1}. The peak potential is indicated on the x-axis.

Fig. 5. The effect of pH on (a) the peak potential and (b) the peak current for U(VI) in sea water with 3.3×10^{-8} M U(VI) added, containing (1) 8.3×10^{-5} M and (2) 2×10^{-3} M catechol. The peak potentials for 5×10^{-8} M Fe(III) in solution (2) are indicated by "Fe". Conditions: linear-scan c.s.v., 50 mV s^{-1}, 1 min collection at −0.1 V, 15 s rest, scan at 50 mV s^{-1}.

charged metal complex ions diminishes at potentials more negative than −0.52 V (the electrocapillary maximum in this solution [21]); this may also reduce the collection efficiency in this potential region.

The reduction peak from 7×10^{-8} M Fe(III) disappeared completely at collection potentials more negative than about −0.4 V. This potential can therefore be used to discriminate against moderate concentrations of this metal.

Effect of pH

The pH of the solution affects the U(VI) determination because of changes in the distribution of the complex ions with catechol. The reduction current and potential of the U(VI)-catechol complexes were therefore determined by linear-scan c.s.v. in sea water as a function of pH, with two concentrations of catechol (8.3×10^{-5} M or 2×10^{-3} M catechol). The pH was varied by adding dilute hydrochloric acid or sodium hydroxide. The reduction current increased strongly with the pH (Fig. 5a): the peak height at pH 8 is twice that at pH 6 with 2×10^{-3} M catechol, and 1.8 times that with 8×10^{-5} M catechol. The peak potential becomes more negative as the pH increases (Fig. 5b), shifting 90 mV between pH 6 and pH 8 in 2×10^{-3} M catechol, and 50 mV in 8×10^{-5} M catechol. This shift is small compared to the peak shift for iron(III), which amounts to −0.3 V over the same pH

range: at pH 7.3 the iron reduction peak is present on the shoulder of the uranium peak, and the two peaks become indistinguishable at pH > 7.6.

Effect of collection time

Adsorption of complex ions of uranium with catechol onto the HMDE was measured as a function of the collection period, at two concentrations of uranium (10^{-8} M and 10^{-7} M) in presence of 6×10^{-8} M iron. Measuring conditions were 2×10^{-3} M catechol, in sea water at pH 6.8, a collection potential (E_{col}) of −0.10 V, and linear-scan c.s.v. (50 mV s^{-1}). The peak height increased linearly with the collection time, presumably until the drop surface was nearly saturated. The plot was linear up to a collection time of about 10 min for 1.3×10^{-8} M U(VI), but up to only 1 min for 1.1×10^{-7} M U(VI). The reduction current of 6×10^{-8} M Fe(III), in presence of 1.3×10^{-8} M U(VI) first increased up to a collection time of about 5 min, and then decreased, presumably because the drop was largely covered by the more strongly adsorbed U(VI) complexes.

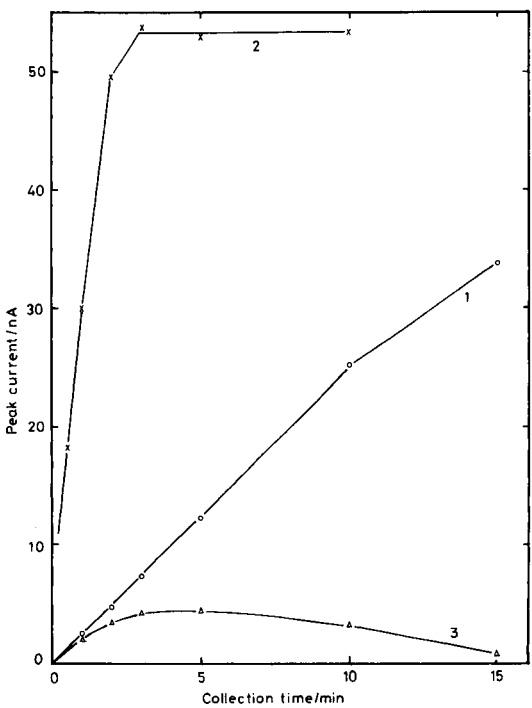

Fig. 6. The reduction current of U(VI) in sea water containing 2×10^{-3} M catechol, as a function of the collection time. Conditions: linear-scan c.s.v., 50 mV s^{-1}, $E_{col} = -0.1$ V. Curves: (1) 1.3×10^{-8} M U(VI); (2) 1.1×10^{-7} M U(VI); (3) peak height of Fe(III).

Effect of surface area of the drop

The final peak current can be maximized by selecting a large drop size, because there are no dilution effects arising from amalgam formation. The relationship between the measured reduction current and the calculated surface area of the drop, which was varied by using a micrometer-type HMDE, was found to be linear for surface areas of 1.5—4 mm^2. In these tests, the collection time was 3 min. For optimal sensitivity, the drop size should be as large as is consistent with drop stability.

Maximum adsorption density of the HMDE

The peak current/uranium concentration relationship is linear up to a concentration of about 5×10^{-8} M U(VI) with a collection time of 3 min, in sea water containing 2×10^{-3} M catechol and at pH 6.85. The increase in the peak current becomes less at higher metal concentrations and a maximum is reached when the drop surface is covered completely with complex ions. The maximum adsorption capacity of complex ions onto the HMDE was evaluated from the area of the stripping peaks obtained by linear-scan c.s.v. after a collection time of 3 min. The data were fitted to a linear version of the Langmuir equation [9]. The same value for the maximum charge, 42 $\mu C\ cm^{-2}$, was obtained, after collection at —0.05, —0.25, and —0.45 V (the contribution of the second peak to this charge was about 10%). This is equivalent to an adsorbed layer of 4.4×10^{-10} mol cm^{-2}, in which each complex ion occupies 0.38 nm^2. This area is half that occupied by each adsorbed CuL_2^{2-} complex ion (L being catechol) [9], and is equivalent to the surface area occupied by a single catechol ion (calculated area of 0.34 nm^2 [9]). This result suggests that either only the UL complex adsorbs, or that only half of each UHL_2^- ion adsorbs, while the second catechol group points away from the surface.

Values for log B in the Langmuir equation were 7.56 (collection potential —0.05 V), 7.54 (—0.25 V) and 7.26 (—0.45). These values have no absolute meaning [9] but are given for purposes of comparison. They indicate a decrease in the adsorption energy as the potential becomes more negative (nearer the electrocapillary maximum), a finding similar to that obtained for copper [9].

Interferences

The c.s.v. determinations of uranium are affected by adsorption of complex ions of other metals if their reduction potentials are close to that of U(VI), or if there is competition for surface area. It was found that of a number of metals tested [Bi(III), Fe(III), Sn(III), Cd(II), Zn(II), Sb(V), V(V), Pb(II) and Cu(II)], only Pb(II), Fe(III) and V(V) produced peaks near that of U(VI). The peak given by V(V) is about 0.2 V more negative than that for uranium, while the Fe(III) peak is nearer depending on pH and catechol concentration, and precedes the uranium peak. At pH 6.8, in 2×10^{-3} M catechol, the Fe(III) peak is 0.16 V more positive than the uranium

peak. Interference by Fe(III) is eliminated by using a collection potential of −0.35 V, with only a small loss of sensitivity for uranium. The Pb(II) peak is very close to that of U(VI), but appears only at concentrations exceeding 10^{-7} M Pb, much greater than those in unpolluted natural waters (10^{-9}—10^{-8} M). This peak can be masked by making the solution 10^{-3} M with respect to EDTA (this also masks the copper peak).

Competition for space on the surface of the mercury drop was tested by adding 10^{-7} M of the above ions to the solution. It was found that the uranium concentration could be determined readily by using the standard addition technique, but that the sensitivity was suppressed by about 10% by some strongly adsorbing metals (Cu and V) in the presence of catechol.

The effect of competition from organic complexing ligands was tested by addition of EDTA to the solution. There was no decrease in the current from catechol complex ions of U(VI) when up to 2×10^{-3} M EDTA was present in sea water containing either 5×10^{-4} M or 2×10^{-3} M catechol. The copper peak (10^{-8} M) disappeared at about 2×10^{-4} and 10^{-3} M EDTA, respectively, at these catechol concentrations while the iron and vanadium peaks were not affected. Ligand competition by carbonate was described above, and is negligible in the presence of 2×10^{-3} M catechol.

Natural organic surfactants present in sea water could interfere by covering the surface of the mercury drop and so blocking further adsorption of catechol complexes. This effect was tested by adding a non-ionic surfactant, Triton X-100, to u.v.-irradiated sea water. This surfactant has been used before as a model compound to characterize natural organic surfactants, and some coastal waters have been shown to contain surfactants equivalent to 0.01—0.5 mg l^{-1} Triton [22]. At pH 6.9 in presence of 10^{-4} M catechol, no decrease in peak current was observed until about 0.3 mg l^{-1} Triton X-100 was present. However, the peak height diminished strongly at higher surfactant concentrations to about 10% of the initial peak with 1.5 mg l^{-1} Triton and 4% with 2.5 mg l^{-1}. In presence of 2×10^{-3} M catechol, the effect of the added surfactant was much reduced: no effect was found up to 0.4 mg l^{-1} Triton X-100, above which the peak height decreased, 25% of the initial response being attained with 4 mg l^{-1} Triton. The peaks were reproducible when the surfactant was present, so that the metal concentration could be determined by using standard additions. Usually, it was found that the sensitivity in untreated, stored Irish Sea water was 5—10% less than after u.v.-irradiation. It is not, however, advisable to remove natural organic material by means of u.v.-irradiation, as checks revealed that this removed 70—80% of the dissolved U(VI) at pH 7 but rather less when the sample was first acidified to pH 2.3; the effect may be caused by photochemical reduction of U(VI).

Determination of uranium in sea water

In view of the above findings, a pH value of 6.8—7 (PIPES buffer) and a concentration of 2×10^{-3} M catechol were selected for the determination of

uranium in sea water. The voltammograms for determinations of sea water containing 3.3×10^{-9} M uranium (the metal concentration had been reduced to this level by u.v.-irradiation) by linear-scan c.s.v. are shown in Fig. 7(a). Scans 2 and 3 included a standard addition of 5×10^{-9} M U(VI). Good resolution was obtained for the peaks of Fe(III) (−0.43 V), U(VI) (−0.58 V) and V(V) (−0.73 V). The iron peak was eliminated by collection at −0.4 V (curve 3), which also caused a small reduction in sensitivity for uranium. The relative standard deviation (RSD) of the determination of 3×10^{-9} M uranium under these conditions was 7%, because of variability of the slope of the base line. The second peak of uranium was small and masked by the vanadium peak.

Better results were obtained by using d.p.c.s.v. The voltammograms obtained for untreated Atlantic water [9] are shown in Fig. 7(b). The base

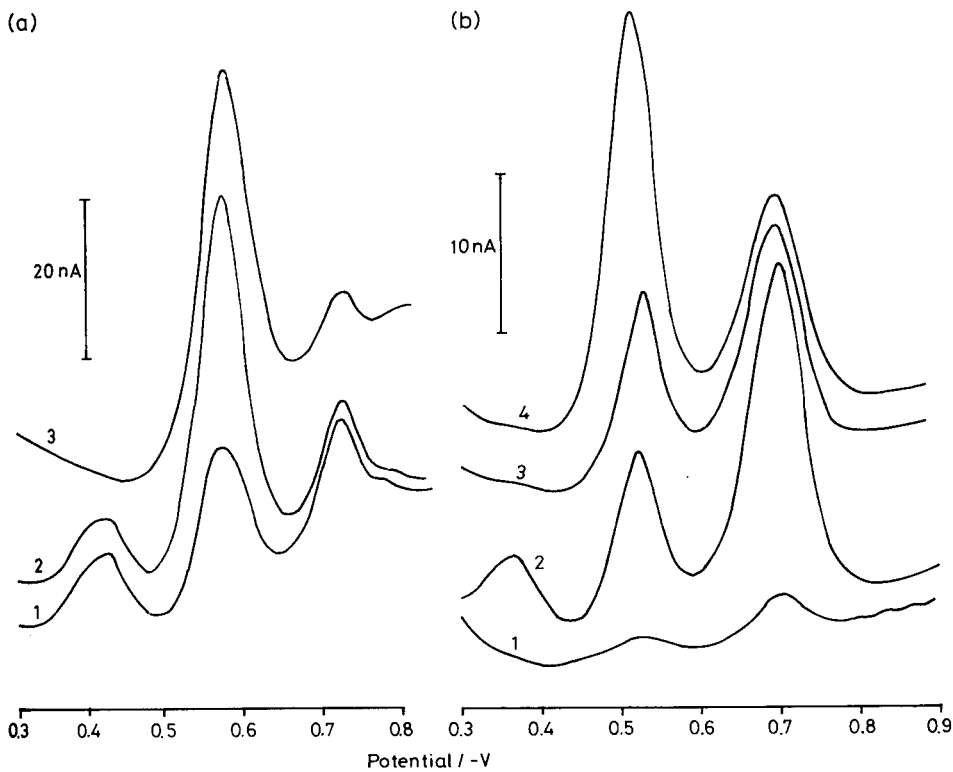

Fig. 7. Determination of uranium in sea water at pH 6.85 (0.008 M PIPES and 2×10^{-3} M catechol). (a) Linear-scan c.s.v. (50 mV s^{-1}, 2.5 min collection at −0.3 V, u.v.-irradiated sea water). Curves: (1) 3.3×10^{-9} M U, 2×10^{-8} M Fe and 3×10^{-8} M V; (2) as (1) but 8.3×10^{-9} M U; (3) as (2) but collection at −0.4 V and scanning from −0.3 V. (b) D.p.c.s.v. (10 mV s^{-1}, pulse rate 10 s^{-1}, pulse amplitude 25 mV, 2 min collection; Atlantic sea water containing 1.4×10^{-8} M U, 1.5×10^{-8} M Fe, 3×10^{-8} M V). Curves: (1) $E_{col} = -1.0$ V; (2) $E_{col} = -0.1$ V; (3) $E_{col} = -0.3$ V; (4) as (3) with standard addition of 1.7×10^{-8} M U.

line is less curved and more reproducible than when linear-scan c.s.v. was used. Scan 1 was preceded by a 2-min collection at −1 V and shows the shape of the base line. Small peaks of uranium and vanadium were still obtained because some complex ions adsorbed during the d.p. scan, and because a small amount of the reduced metal ions may form complex ions with catechol and adsorb. Scan 2 was preceded by collection at −0.1 V, scans 3 and 4 at −0.3 V. Scan 4 contains a standard addition of 1.7×10^{-8} M U(VI). As a result of the irreversibility of the reduction of the uranium-catechol complex ions, the vanadium peak height was increased more strongly than the uranium peak by the differential pulse modulation: comparison of scans 3 in Fig. 7(a) and (b) shows that the vanadium peak is increased by a factor of about 5 relative to that of uranium by switching to the differential-pulse mode. Nevertheless, uranium can be determined precisely in untreated sea water by d.p.c.s.v., because the peak potential for vanadium is well separated from that of uranium. Concentrations of 1.35×10^{-8} M and 1.32×10^{-8} M uranium were found for samples of Atlantic and Irish Sea water, which are in excellent agreement with reported values [3]. Samples which had been stored after acidification gave the same results as those which had not been acidified. The detection limit (three times the relative standard deviation [23]) was calculated from the d.p.c.s.v. determination of 3.3×10^{-9} M uranium in u.v.-irradiated sea water. A relative standard deviation of 3% was observed (10 degrees of freedom), giving a detection limit of 3×10^{-10} M uranium after a collection period of 2.5 min at −0.3 V. The relative standard deviation for the determination of 1.3×10^{-8} M uranium by d.p.c.s.v. in untreated sea water was 1.5% after 2.5 min collection. The limit of detection could be reduced by using a longer collection period. At low uranium concentrations, the uranium peak increases linearly with collection time (Fig. 6) whereas the iron peak diminishes (because of less efficient adsorption) so that resolution can be improved by collection for a longer time (e.g., 15 min which would give a detection limit of $<10^{-10}$ M). The sensitivity of these determinations in 0.01 M KCl electrolyte was the same as in sea water.

DISCUSSION

Polarography of uranium(VI) at pH 3, with the DME, shows that U(VI) is reduced reversibly to U(V) with a half-wave potential of −0.163 V (versus Ag/AgCl). This wave becomes smaller with increasing pH and a second wave appears at about −0.55 V at pH 5.9. Addition of catechol causes the formation of an adsorption maximum at −0.67 V. The wave at −0.55 V is caused by the irreversible reduction of hydrolyzed U(VI) ions, and that at −0.67 V is caused by adsorption of catechol complex ions with U(VI). The calculated half-wave potential for the latter wave is −0.43 V (calculated for 2×10^{-3} M catechol, pH 6.8). The further shift towards more negative potential is caused by adsorption stabilization of the U(VI)-catechol

complex [21]. Reduction of this complex is irreversible as demonstrated by cyclic voltammetry (Fig. 2): the cathodic and anodic peak potentials are at −0.58 V and −0.24 V, respectively. Complex ions of U(VI) are reduced to U(V), which is oxidized initially to the free uranyl ion, followed by relatively slow complex re-formation. It is likely that U(V) also forms complex ions with the abundantly available catechol ions as the peak potential varies only slightly with changes in the catechol concentration (the variation is much less than that for copper or iron). These complex ions are also adsorbed, though more weakly than those of U(VI); the oxidation current of cyclic scans is almost as large as the reduction current (i.e., there is very little diffusion away from the surface) and a small but significant reduction peak is obtained also when a collection potential on the negative side of the reduction potential of U(VI) is maintained (at −1 V).

In electrolytes of neutral pH containing low concentrations (10^{-9}—10^{-8} M) of U(VI), with 10^{-3} M catechol present, adsorption of the uranium complex ions depended linearly on collection time until the surface was nearly saturated (Fig. 6), on the surface area of the drop, and on the uranium concentration (until surface saturation). Adsorption also increased with the catechol concentration until a maximum was reached at 5×10^{-3} M. This maximum coincides with the predominance of complex ions of the UHL_2^- type, which suggests that this ion is adsorbed on the drop, in a similar manner to the CuL_2^{2-} complex ion. However, the surface area occupied by each complex ion at surface saturation is equivalent to that of a single catechol molecule, which indicates either that only the UL complex adsorbs, or that only one ligand of the UHL_2^- complex is adsorbed at the drop surface.

At pH values between 6.8 and 7.0, in presence of 2×10^{-3} M catechol, the peaks of U(VI) and Fe(III) are well separated, and uranium can be determined directly in sea water. The detection limit under those conditions by d.p.c.s.v., is 3×10^{-10} M using a collection period of only 2.5 min. These limits are approximately doubled if the linear-scan mode is used.

The above results are quite different from those obtained recently by Lam et al. [12] who were unable to determine uranium directly in sea water, probably because their experiments were done at low pH (pH 4) and at low concentrations (5×10^{-6} M) of catechol.

The authors are grateful for discussions with Professor J. P. Riley, and for his comments on the manuscript.

REFERENCES

1 D. Langmuir, Geochim. Cosmochim. Acta, 42 (1978) 547.
2 T.-L. Ku, K. G. Knaus and G. G. Mathieu, Deep-Sea Res., 24 (1977) 1005.
3 J. Holzbecher and D. E. Ryan, Anal. Chim. Acta, 119 (1980) 405.
4 T. M. Florence and Y. Farrer, Anal. Chem., 35 (1963) 1613.
5 W. C. Li, D. M. Victor and C. L. Chakrabarti, Anal. Chem., 52 (1980) 520.
6 S. F. Marsh, M. R. Betts and J. E. Rein, Anal. Chim. Acta, 119 (1980) 401.

7 G. W. C. Milner, J. D. Wilson, G. A. Barnett and A. A. Smales, J. Electroanal. Chem., 2 (1961) 25.
8 R. F. Sieck, J. J. Richard, K. Iverson and C. V. Banks, Anal. Chem., 43 (1971) 913.
9 C. M. G. van den Berg, Anal. Chim. Acta, 165 (1984) 000.
10 C. M. G. van den Berg, Anal. Lett., (1984), in press.
11 K.-H. Lubert, M. Schnurrbusch and A. Thomas, Anal. Chim. Acta, 144 (1982) 123.
12 N. K. Lam, R. Kalvoda and M. Kopanica, Anal. Chim. Acta, 154 (1983) 79.
13 I. M. Kolthof and J. J. Lingane, Polarography, Vol. 2, Interscience, New York, 1952.
14 L. Sipos, Lj. Jeftic and M. Branica, Electroanal. Chem. Interface Electrochem., 32 (1971) 35.
15 M. S. Antelman, The Encyclopedia of Chemical Electrode Potentials, Plenum Press, New York, 1982.
16 G. Dongarra and D. Langmuir, Geochim. Cosmochim. Acta, 44 (1980) 1747.
17 C. F. Baes, Jr., and R. E. Mesmer, The Hydrolysis of Cations, Wiley, New York, 1976.
18 C. Tsymbal, Nucl. Sci. Abstr., 23 (1969); abstr. 49767.
19 A. E. Martell and R. M. Smith, Critical Stability Constants, Vol. 3, Plenum Press, London, 1977.
20 C. M. G. van den Berg, Mar. Chem., 14 (1984) 201.
21 J. Heyrovsky and J. Kůta, Principles of Polarography, Academic Press, London, 1966.
22 B. Cosovic and V. Vojvodic, Limnol. Oceanogr., 27 (1982) 361.
23 J. D. H. Strickland and T. R. Parsons, A Practical Handbook of Seawater Analysis, Fish. Res. Board Can., Bull. 167, 2nd edn., Ottawa, 1977.

Analytica Chimica Acta, 164 (1984) 223—232
Elsevier Science Publishers B.V., Amsterdam — Printed in The Netherlands

PREPARATION OF METAL DITHIOCARBAMATE COMPLEXES FOR CHROMATOGRAPHIC SEPARATION AND MULTI-ELEMENT DETERMINATIONS

A. M. BOND* and G. G. WALLACE[a]
Division of Chemical and Physical Sciences, Deakin University, Victoria 3217 (Australia)
(Received 19th April 1984)

SUMMARY

Metal-dithiocarbamate complexes are amenable to separation by chromatography and subsequent detection by atomic absorption spectrometry, u.v.-visible spectrophotometry or electroanalytical methods. Three methods of complex formation are investigated for pyrrolidinedithiocarbamate and diethyldithiocarbamate: direct formation in a solvent suitable for subsequent chromatographic separation; liquid—liquid extraction and removal of co-extracted ligand to minimize possible interferences observed with some detection methods; and precolumn formation in which the complex is deposited onto a Sep-Pak cartridge and then eluted in a solvent suitable for chromatography. Each of the methods is examined with respect to simplicity of operation, concentration factors and amenability to combination with liquid chromatography. Generally, precolumn formation of the complex is to be preferred. These methods are successfully applied to determinations of copper, nickel, cobalt, lead, mercury, cadmium, selenium, chromium(III) and chromium(VI) at the $\mu g\ l^{-1}$ level.

The dithiocarbamate ligand has been used in the field of analytical chemistry for many years [1—3]. The ability of this ligand to form neutral complexes with a wide range of metals which are then extractable into organic media has led to its widespread use in liquid—liquid extractions. Such procedures have generally been employed as a sample clean-up or preconcentration step prior to metal determination by atomic absorption spectrometry [4—6] or spectrophotometry [7—9], etc.

In previous work in these laboratories, the dithiocarbamate ligand was used as a complexing agent to enable metals to be determined by reversed-phase high performance liquid chromatography (h.p.l.c.) with electrochemical (e.c.), and/or ultraviolet (u.v.) spectrophotometric detection [10, 11]. Two methods of dithiocarbamate formation were considered. In one, the chelate was formed in situ by inclusion of the dithiocarbamate ligand in the chromatographic solvent; the aqueous metal sample was injected and the complex formed within the chromatographic system. In the other, "external" method, the aqueous metal sample was added to a solution of the chroma-

[a]Present address: Chemistry Department, University College Cork, Cork, Ireland.

0003-2670/84/$03.00

tographic solvent containing excess of ligand prior to injection of the sample into the chromatographic system.

"In-situ" formation is by far the more convenient method for sample analysis but is limited to metals which form (stable) complexes rapidly in solution. "External" formation, as described previously [10] was suitable for determinations of nickel, copper, cobalt, chromium(III) and chromium-(VI). However, as is described below, the preparation of other (Pb, Hg, Cd and Se) dithiocarbamate complexes is not suitable with this approach and other methods of "external" complex formation have been investigated. These are liquid—liquid extraction, as has been described by other workers [4—6, 12] and precolumn formation. A marked improvement in detection levels is observed, particularly when the latter method of complex formation is employed. The advantages of the various complex formation methods should apply equally well to other analytical measuring techniques. The relative merits of each preparation mode are discussed in detail and the optimum method for multi-element analysis by h.p.l.c./e.c./u.v. is shown to depend on the concentration(s) of the metal(s) to be determined.

EXPERIMENTAL

Reagents and standard solutions

All chemicals used were of analytical-grade purity unless otherwise stated. All organic solvents were of liquid-chromatographic grade (Waters Associates, Milford, Massachusetts). Acetate buffer was prepared in the conventional manner. Dithiocarbamate salts (Ajax Chemicals) were recrystallized twice from ethanol before use (see Discussion).

Metal stock solutions were prepared by dissolving nitrate salts of copper-(II), nickel(II), cobalt(II), lead(II), cadmium(II) and chromium(III), and potassium dichromate or selenium dioxide in distilled-deionized water.

The chromatographic solvent was 70% acetonitrile/30% acetate buffer (0.02 M pH 5.5)/0.01 M sodium nitrate unless otherwise stated.

Instrumentation

The liquid chromatographic-based system employed has been described in detail elsewhere [10, 11]. A Model 6000A solvent delivery system (Waters Associates) was used in conjunction with a Model U6K universal injector. A Model 450 variable-wavelength detector (Waters) was used for spectrophotometric detection. Two separator columns were considered: (i) C_{18} μBondapak (30 cm long, 3.9 mm i.d.) from Waters; (ii) C_{18} Spherisorb (25 cm long, 4.6 mm i.d.) from Altex. The ion-exchange guard column (3 cm long, 3.9 mm i.d.) was packed with Amberlite CG400 anion-exchange resin.

The electrochemical detector used was a Model TL-5 (Bioanalytical Systems). A glassy carbon working electrode, platinum auxiliary and Ag/AgCl (3 M NaCl) reference electrodes were employed. The potentiostat was a Model LC4 (Bioanalytical Systems).

A modified liquid–liquid extraction vessel (Fig. 1) was used, to provide ready access to the organic layer for direct injection into the l.c. system. "Sep-Pak" cartridges containing C_{18} μBondapak material were obtained from Waters Associates.

RESULTS AND DISCUSSION

Two of the more commonly employed dithiocarbamate ligands, pyrrolidine-dithiocarbamate (I; PDC) and diethyldithiocarbamate (II; DDC) were considered.

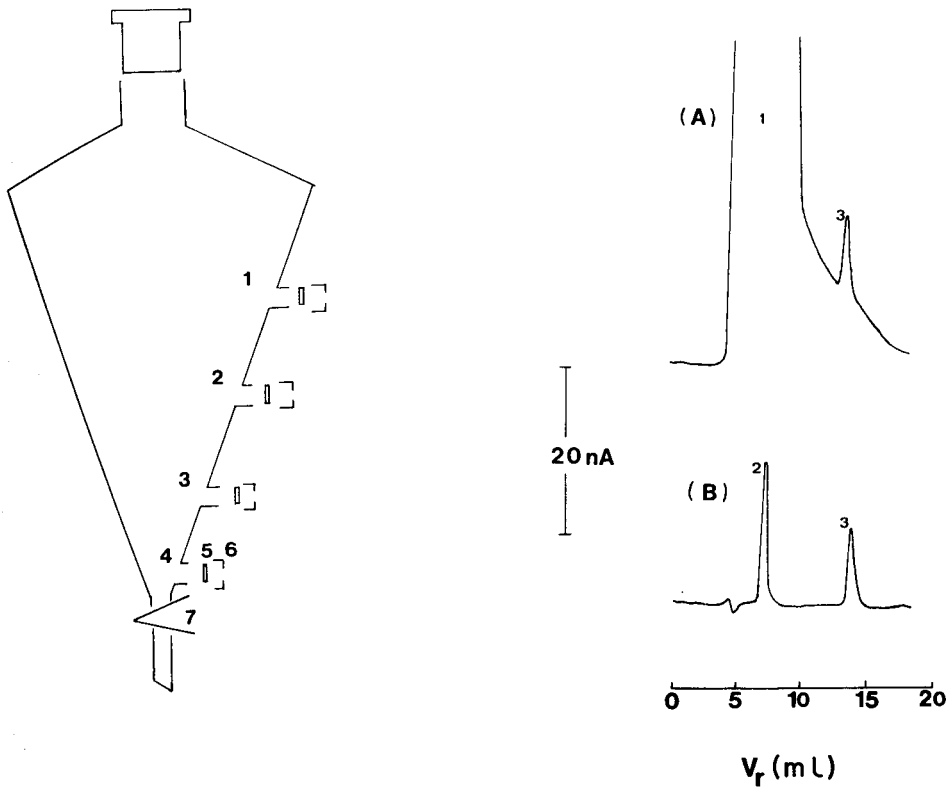

Fig. 1. Modified extraction vessel allowing syringe access to different levels: 1, 2, 3, 4, syringe ports; 5, teflon-backed rubber septum; 6, screw cap with syringe inlet; 7, tap.

Fig. 2. Determination of cobalt (10 ng) using "external" complex formation with 10^{-3} M PDC. Chromatograms obtained (A) without the ion-exchange guard column and (B) with the guard column. Responses: (1) PDC; (2) thiuram disulfide; (3) $Co(PDC)_3$. Experimental conditions: injection volume, 10 μl; C_{18} μBondapak column; solvent flow rate, 1.3 ml min^{-1}; detection, d.c. amperometry (E_{app} = +1.20 V vs. Ag/AgCl) at glassy carbon (BAS cell).

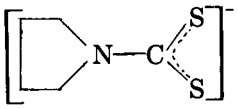

(I)

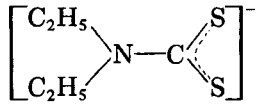

(II)

In order to evaluate the feasibility of the three "external" complex preparation methods (formation in the chromatographic solvent, liquid–liquid extraction and precolumn formation), eight metals, with chromium in two oxidation states, were considered. They were copper(II), nickel(II), cobalt(II), chromium(III), chromium(VI), lead(II), cadmium(II), mercury-(II) and selenium(IV).

Direct formation in the chromatographic solvent

In principle, samples may be added directly to the chromatographic solvent (containing the dithiocarbamate ligand) and then injected onto the column [10]. This method is referred to as "external" complex formation in the chromatographic solvent. The major disadvantage reported [10] was the inherent dilution factor involved (e.g., factor of 2 to 5). Furthermore, complications were encountered at the detection stages (u.v. or e.c.). These complications were due to the presence of a response from the large excess of dithiocarbamate at the solvent front (Fig. 2A). This problem can be overcome by removal of excess of ligand from the sample on an ion-exchange guard column which is inserted into the l.c. system prior to the separation stage (Fig. 2B). Detection limits achieved with this type of preparation are detailed in Table 1. This method of preparation was successful for determinations of copper, nickel, cobalt, chromium(III) and chromium(VI) as dithiocarbamate complexes. No interelement effects were observed.

With extension of this method to include the determination of lead, cadmium, mercury and selenium, further problems were encountered. The low solubility of cadmium and mercury dithiocarbamates in the partially aqueous chromatographic solvent caused problems. These complexes precipitated at relatively low levels, rendering standards cloudy immediately after addition of the metal. Furthermore, the instability of the lead dithiocarbamate complex in this partially aqueous media caused difficulties. Monitoring of the electrochemical oxidation response associated with the lead complex with time indicated a decrease in concentration of the complex; a response from the free ligand oxidation was also observed. The prior preparation of selenium dithiocarbamates in the chromatographic solvent where excess of ligand was present caused a problem. The yellow solution observed upon addition of selenium(IV) turned red within a few minutes and finally a red precipitate (selenium metal) was obtained. This is similar to results reported by Foss [13] on the decomposition of tellurium dithiocarbamates.

Therefore, the preparation of metal-dithiocarbamate standards/samples in the chromatographic solvent (externally) is only suitable for Cu(II), Ni(II),

TABLE 1

Detection limits (pg) for determination of metals as dithiocarbamate complexes with different methods of sample preparation

Metal	Detection limits[a] (pg)					
	"External" formation in chromatographic solvent[b,c]		Liquid—liquid extraction[c]		Pre-column formation[c]	
	E.c.[d]	U.v.[e]	E.c.[d]	U.v.[e]	E.c.[d]	U.v.[e]
Copper	200	1000	10	50	4	20
Nickel	120	1000	6	50	2	20
Cobalt	500	500	25	25	10	10
Chromium(III)	100	100	10	5	2	2
Chromium(VI)	40	100	4	5	1	2
Lead	—[f]	—[f]	25	50	10	20
Cadmium	—[f]	—[f]	5	5	2	2
Mercury	—[f]	—[f]	20	50	8	20
Selenium	—[f]	—[f]	5[g]	5[g]	2[g]	2[g]

[a]Detection limit taken as the amount of metal required to give a signal to noise ratio = 2. Injection volume 10 μl. [b]Results were similar for either PDC or DDC at the 5×10^{-4} M level. [c]Procedure detailed in text. [d]D.c. amperometry (E_{app} = +1.20 V vs. Ag/AgCl). [e]U.v. detection at 254 nm. [f]Method not applicable. [g]With the DDC ligand only.

Co(II), Cr(III) and Cr(VI) provided that a dilution factor is acceptable. If other metals [Hg(II), Pb(II), Cd(II), Se(IV)] are to be determined or if a dilution factor is not acceptable, alternative methods of complex formation must be considered.

Liquid—liquid extraction

In an attempt to overcome the above problems, a procedure based on liquid—liquid extraction as described in the literature, was devised. The procedure used was as follows unless otherwise stated. The sample was first buffered to pH 4 with 1 M acetate buffer, 5% (w/v) sodium nitrate was added to the buffer solution to break down colloids which can form in the presence of excess of ligand [14], and 1 ml of aqueous 1% (w/v) dithiocarbamate solution was added to the sample which was then mechanically agitated for 3 min. The extraction solvent (carbon tetrachloride, chloroform, or dichloromethane) was then added, and the mixture was agitated for a further 3 min and left to separate for 5 min. Finally, an aliquot from the organic layer was injected into the liquid chromatographic system.

When this procedure was used, two major sources of impurities produced chromatographic peaks in blank extractions. Trace metal impurities were troublesome. It was found necessary to purify the aqueous 1% (w/v) dithiocarbamate solution by extracting twice with chloroform or dichloromethane (10 ml per 100 ml of 1% (w/v) dithiocarbamate solution). Purification of the acetate buffer solution by addition of aqueous 1% (w/v) dithiocarbamate

(1 ml per 100 ml of buffer) and extracting twice with dichloromethane (10 ml per 100 ml of buffer) was also necessary. Care should be taken in the choice of extraction solvent as it has been found [15] that the trace element content varies widely from solvent to solvent and indeed from one manufacturer to the other. The use of l.c.-grade solvents has proven suitable in that after the purification steps outlined above the level of metallic impurities was below the detection levels (ca. 0.1 + 01.0 $\mu g\ l^{-1}$) achieved by the methods of determination described in this and previous work [10, 11].

Other responses present in the chromatograms of blank injections arose from the breakdown of the dithiocarbamate ligand

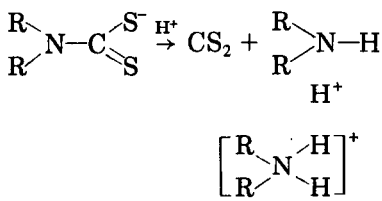

The amine produced in this reaction gave a response in both the electrochemical (d.c. amperometry, E_{app} = +1.20 V vs. Ag/AgCl) and spectrophotometric (λ = 254 nm) detection stages. Monitoring of this response with time indicated that the rate of decomposition of the ligand (rate of formation of the amine) increased with decreasing pH and increasing dielectric constant of the extraction solvent. This rate of decomposition was shown to be less for the PDC ligand than the DDC ligand. However, it was possible to use either ligand provided that the pH of the acetate buffer was >4. Extraction of the metal dithiocarbamates into dichloromethane resulted in negligible interference from the decomposition products provided that the factors detailed in the above extraction procedure were adhered to. This method proved suitable for extraction of all metals under consideration (Table 1) except for chromium(III) and chromium(VI).

The extraction of chromium(III) and chromium(VI) as dithiocarbamate complexes is limited by the rate of formation of the $Cr(DTC)_3$ complex. It was found necessary to allow at least three hours for the formation reaction to proceed before addition of the extraction solvent. Extraction of the complexes was then completed within five minutes. Unlike other metals where a twenty-fold concentration factor was possible, chromium(III) and chromium(VI) could only be extracted with a ten-fold concentration factor before extraction efficiency decreased.

As well as the concentration factors available with the liquid—liquid extraction approach, there are other advantages. The solubility problems, previously encountered with the mercury and cadmium dithiocarbamates are overcome because the complexes are extracted into a relatively non-polar organic media. The problem with instability of the lead complex is also overcome because the complex is much more stable in the organic media than the partially aqueous chromatographic solvent. The stability of the

selenium dithiocarbamate complex is also much improved with this procedure, wherein it is extracted into an organic media where a relatively small excess of ligand is present. However, sufficient stability for selenium determination is only observed if the DDC rather than the PDC ligand is employed.

When this extraction procedure was used, it was found convenient to include the ion-exchange guard column in the system for two reasons. Firstly, some ligand is transferred to the organic phase during the extraction and this is effectively removed using the ion-exchange guard column. The second function of the ion-exchange guard column is novel; it allows injection of samples in dichloromethane directly on to the reversed-phase separator column. This procedure (injection in a solvent stronger than the chromatographic solvent) generally results in premature elution and bad tailing of peaks [16]. These problems were also observed in this work if the ion-exchange guard was not included in the system (Fig. 3B) but were overcome with inclusion of the guard column (Fig. 3C), presumably because the dichloromethane injected is retained to some degree on the ion-exchange resin. However, the metal dithiocarbamate complex passes through unretained and is therefore eluted onto the separator column in the chromatographic solvent.

With the inclusion of the ion-exchange guard column, the liquid—liquid extraction procedure could be used directly for preconcentration and determination of all nine metals. The only interelement effect observed was when mercury was determined in the presence of selenium using the PDC ligand [17]. This, along with the fact that the $Se(PDC)_2$ complex is less stable than $Se(DDC)_2$ led to the use of the DDC ligand for multi-element determinations (Fig. 4). Similar approaches to multi-element determinations based on liquid—liquid extraction have been examined [18—20] but without electrochemical detection and not for as wide a range of elements.

Precolumn formation

Precolumn formation involves deposition of the complex from a suitable solvent (deposition solvent) onto a small column (Sep-Pak) packed with a stationary phase which is capable of retaining the species of interest.

The procedure involves reaction of the metal with the dithiocarbamate ligand in much the same way as in the initial stages of the liquid—liquid extraction method. (As noted before, complex formation was rapid except in the case of chromium where reaction times of 2—3 h were required.) However, the complex is not then extracted into an organic solvent but deposited onto a short column (Sep-Pak) containing silica-based C_{18} material. The complex is then eluted with a relatively non-polar organic solvent such as dichloromethane. In this way, all of the advantages gained by presenting the complex in an organic media (as in liquid—liquid extraction) are again obtained. A further advantage is that higher concentration factors are achievable. For all metals considered, a fifty-fold concentration factor was obtained with a precision of ±10% (Table 1). This was true even for formation of

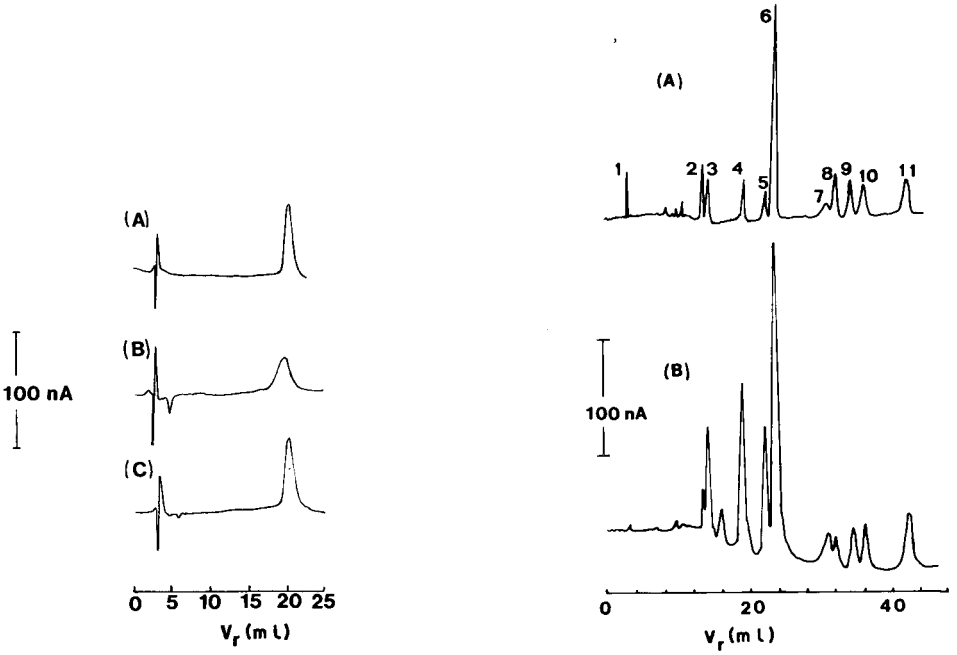

Fig. 3. Effect of solvent on chromatogram for injection of 10 μl of copper (63 ng) as $Cu(DDC)_2$: (A) acetonitrile, similar results with or without ion-exchange guard column; (B) dichloromethane without guard column; (C) dichloromethane with guard column. Experimental conditions: C_{18} μBondapak column; solvent flow rate, 2 ml min^{-1}; detection, d.c. amperometry (E_{app} = +1.00 V vs. Ag/AgCl) at glassy carbon (BAS cell).

Fig. 4. Multi-element determinations by the liquid—liquid extraction method from a single injection. Peaks: (1) solvent front (DDC); (2) 9.5 ng cadmium; (3) thiuram disulfide; (4) 25.0 ng chromium(VI); (5) 68.6 ng lead; (6) 51.2 ng nickel; (7) 43.8 ng selenium(IV); (8) 24.4 ng cobalt; (9) 23.0 ng chromium(III); (10) 21.9 ng copper; (11) 67.2 ng mercury. Experimental conditions: C_{18} Spherisorb column; chromatographic solvent, 50% acetonitrile/20% methanol; solvent flow rate, 2 ml min^{-1}; liquid—liquid extraction with DDC ligand and dichloromethane as the solvent; injection volume, 10 μl. (A) Spectrophotometric detection (254 nm); (B) d.c. amperometry (E_{app} = +1.20 V vs. Ag/AgCl) at glassy carbon (BAS cell).

chromium(III) and chromium(VI) dithiocarbamates, indicating that the extraction efficiency and not the formation of the chromium dithiocarbamates limited the extraction method.

The increased concentration factors are presumably due to the fact that during the elution stage the effective volume of the phase from which the metal complex is being separated is decreased. In liquid—liquid extraction this volume (V_1) may be of the order of 200 ml whereas in precolumn preparation it is equal to the volume of the stationary phase in the short column which is much less (ca. 1 ml). The relationship between the mole

fraction (x) extracted and other parameters is given by

$$x = K_D V_2/(V_1 + K_D V_2)$$

where x is the mole fraction of solute in the organic phase, K_D the distribution coefficient, V_1 the volume of aqueous (stationary) phase, and V_2 the volume of organic phase.

A further advantage of the precolumn preparation is that it is much more practical to use with small volumes of sample. For example, complete elution of the metal dithiocarbamates can be achieved with 0.5 ml of dichloromethane. The only interelement effect observed when this approach was applied was the interference between the mercury and selenium complexes (see above) when the PDC ligand was used.

It was found necessary to remove metallic impurities (low mg l^{-1} levels of Ni, Cu and Pb) from the C_{18} Sep-Pak cartridges before their use. Flushing with 5 ml of aqueous 1% (w/v) PDC solution followed by 10 ml of dichloromethane was found suitable. A more limited study [21] using pre-column complex formation has been described for cobalt, copper and nickel.

Conclusions

Three methods of dithiocarbamate complex formation have been investigated and their relative merits discussed. Although "external" formation in the chromatographic solvent is the simplest procedure, it is not suitable for multi-element determinations of all the eight metals considered. Liquid—liquid extraction is recommended for determination of all eight metals, with chromium in two oxidation states, and it has the advantage of simplifying sample clean-up and/or preconcentration stage. Precolumn preparation offers similar advantages to liquid—liquid extraction but has the added ability to concentrate samples even further than the liquid—liquid extraction approach.

This project was supported by Research Grants provided by the Ordnance Factory, Maribyrnong, Victoria, Australia and the Australian Research Grants Scheme.

REFERENCES

1 M. Delepine, Bull. Soc. Chim. Fr., 3 (1908) 652.
2 E. E. Reid, Organic Chemistry of Bivalent Sulfur, Vol. 4, Chemical Publishing Co., New York, 1962.
3 G. D. Thorn and R. A. Ludwig, The Dithiocarbamates and Related Compounds, Elsevier, New York, 1962.
4 K. W. Bruland, R. P. Franks, G. A. Knauer and J. H. Martin, Anal. Chim. Acta, 105 (1979) 233.
5 J. D. Kinrade and J. C. Van Loon, Anal. Chem., 46 (1974) 1894.
6 J. M. Lo, J. C. Yu, F. I. Hutchison and C. M. Wal, Anal. Chem., 54 (1982) 2536.
7 T. Takada, Y. Okabe and K. Nakano, Bull. Chem. Soc. Jpn., 54 (1981) 3589.
8 G. R. Desai and J. Paul, Microchem. J., 22 (1977) 176.

9 H. Yoshida, M. Yamamoto and S. Hikime, Jap. Anal. (Bunseki Kagaku), 11 (1962) 197.
10 A. M. Bond and G. G. Wallace, Anal. Chem., 53 (1981) 1209; 54 (1982) 1706.
11 A. M. Bond and G. G. Wallace, Anal. Chem., 55 (1983) 718.
12 A. Hulanicki, Talanta, 14 (1967) 1371.
13 O. Foss, Acta Chem. Scand., 3 (1949) 1385.
14 V. Sedivec and J. Flek, Coll. Czech. Chem. Commun., 29 (1964) 1310.
15 F. S. Jacobs, V. Ekambaram and R. H. Filby, Anal. Chem., 54 (1982) 1240.
16 C. Wu and J. J. Wittick, Anal. Chim. Acta, 79 (1975) 308.
17 A. M. Bond and G. G. Wallace, J. Liquid Chromatogr., 6 (1983) 1799.
18 G. Drasch, L. V. Meyer and G. Kauert, Fresenius Z. Anal. Chem., 311 (1982) 571, 695.
19 G. Drasch, G. Kauert and L. V. Meyer, in P. Bratter and P. Schramel (Eds.), Analytical Chemistry in Medicine and Biology, Walter de Gruyter & Co., Berlin, New York, Vol. 2, 1983.
20 E. B. Edward-Inatimi, J. Chromatogr., 256 (1983) 253.
21 N. Häring and K. Ballschmiter, Talanta, 27 (1980) 873.

Analytica Chimica Acta, 164 (1984) 233—249
Elsevier Science Publishers B.V., Amsterdam — Printed in The Netherlands

EXTRACTION BASED ON THE FLOW-INJECTION PRINCIPLE
Part 6. Film formation and dispersion in liquid—liquid segmented flow extraction systems

LAGE NORD

Department of Analytical Chemistry, Royal Institute of Technology, S-100 44 Stockholm (Sweden)

BO KARLBERG*

Bifok AB, Box 124, S-191 22 Sollentuna (Sweden)

(Received 20th April 1984)

SUMMARY

The dispersion mechanism in flow-injection extraction systems has been investigated. The phase with the highest affinity for the tubing material forms a thin film on the wall (e.g., 0.055 mm in a 0.7-mm i.d. PTFE tube with pentanol/water at a flow velocity of 11 cm s^{-1}). The film thickness increases linearly with increasing flow velocity and can be related to the viscosity/interfacial tension ratio in such a way that a low ratio indicates a thin film. The analyte is extracted into the film and into the adjacent segments. The film is stationary relative to the moving segments and this results in a backward transport of analyte molecules giving rise to dispersion. The thicker the film, the larger the dispersion. By decreasing the tube diameter and the flow velocity, lower dispersion results. Minimum dispersion is obtained for systems in which the phase carrying the analyte does not form the film.

Liquid—liquid solvent extraction procedures have been reported for continuous-flow systems for some time, only recently have extraction systems based on the principles of flow injection analysis (f.i.a.) appeared in the literature [1]. In this adaptation, aqueous samples are injected into an aqueous carrier stream which is merged and mixed with an aqueous reagent stream. The resultant aqueous stream is then segmented with an organic reagent stream. The analyte is then extracted in a coiled reaction tube, separated, and sensed by a flow-through detection system. In simple applications, a single-line aqueous stream serves as both the reagent and carrier stream.

Numerous applications of flow-injection extractions have been developed and reported [2—18]. The technique has been adopted in many laboratories although the theory for the extraction mechanism does not exist. Classical principles of f.i.a. are readily applied to the portions of the system not involved in the extraction process, namely the aqueous phase prior to segmentation and the organic phase after phase separation.

0003-2670/84/$03.00

The principle of f.i.a. is best summarized as (a) sample injection after the pump, (b) reproducible timing, and (c) controlled dispersion. Reproducible timing and controlled dispersion still prevail in the integrated extraction section, i.e., phase segmentation to phase separation, although the origin and mechanism of the dispersion process in the extraction coil have not yet been adequately described. The introduction of air or segments of evaporated organic phase into f.i.a. extraction systems will, as in single-phase systems, totally disrupt the f.i.a. cornerstones of reproducible timing (because of the compressibility of the gaseous compounds) and controlled dispersion (because of the distortion of the concentration gradient of the injected sample). Consequently, an ice bath was introduced in early experiments to prevent solvent evaporation [1, 4]. It was later found that evaporation could also be prevented by applying back-pressure after the extraction coil [6].

Objections have been raised as to whether there is really a particular branch of continuous flow extraction that could be claimed to be based on f.i.a. principles [19]. The three f.i.a. cornerstones aforementioned are, however, valid for, and present in, the extraction systems cited. While most of the factors governing dispersion in single-phase flow-injection systems are well known and carefully described [20], very little is known about the dispersion process in two-phase flow-injection systems. In practical situations, it is sufficient to know that the dispersion phenomena can be reproduced from sample to sample and from sample to standard solutions. However, in the development of new applications, it is unsatisfactory that knowledge of the factors that influence the dispersion process is so limited. The object of this paper is to justify or discredit some of the speculations appearing in the literature about two-phase flow-injection systems and to add new, valuable information about the dispersion process in an extraction coil.

Peak broadening in flow-injection systems

Peak broadening occurs as a consequence of the physical dispersion processes which act on the injected sample plug. The origin of dispersion in unsegmented systems has been comprehensively discussed. There are two important practical consequences to peak broadening: dilution of the original sample as it is transported through the system to the detector (decreased sensitivity) and reduction in the maximum sampling frequency. In order to estimate sample plug dilution, Hansen et al. [21] introduced the dispersion coefficient D defined by C^0/C where C^0 is the original concentration of the injected sample and C represents a particular concentration on the output gradient curve; C usually represents the maximum detected value, C^{max}, because the peak-height evaluation is most commonly used [20].

While the dispersion coefficient, D, is a widely accepted and useful quantity, there is no corresponding entity which reflects the influence of peak broadening on the sampling frequency in f.i.a. The sampling frequency is, of course, strongly dependent on the level of carry-over that can be accepted

over the entire operating concentration range. In practical situations, this means that the "worst case" situation (strongest sample concentration peak followed by weakest sample concentration peak) governs the sampling frequency. The quantification is then straightforward: 3600 is divided by the peak width expressed in seconds measured for the strongest concentration peak at the carry-over level. This level should be defined for the minimum concentration peak.

From the above discussion, it follows that peak broadening is a fundamental consideration in successful application work based on f.i.a. Usually, peak broadening is characterized by the calculated variance, σ^2, or standard deviation, σ, of a peak. The standard deviation can be expressed in length units (σ_l), in time units (σ_t), in volume units (σ_v) and, for segmented systems, in the number of segments (σ_s). The dispersion coefficient, D, is directly proportional to σ_v while the sampling frequency is inversely proportional to σ_t. The relationship between σ_t and σ_v is $\sigma_t = \sigma_v/Q$, where Q is the volumetric flow rate. When the volumetric flow rate is kept constant, the relative changes in dilution and sampling frequency can be based on either σ_t or σ_v. On changing the flow rate, predictions about the degree of dilution must be based on σ_v and the sampling frequency on σ_t. A great advantage to using variances in expressing peak broadening in subdivisions of the total system, is their additivity, i.e., individual contributions to the overall peak broadening can easily be calculated and compared.

EXPERIMENTAL

Extraction system for f.i.a.

A conventional extraction system for f.i.a. was used [22] (see Fig. 1). The pump was a Bifok FIA 08 unit (Sollentuna, Sweden) and the flow injection analyzer was a Bifok FIA-05 equipped with a six-port valve, L-100-1. The injected volumes were in the range 25—50 μl.

Three different types of segmentors were used: (a) a modified A8 fitting [1] to produce large individual segments; (b) a Bifok segmentor [22] by which the segment size can be varied from 2 to 15 mm; (c) a modified T-fitting to produce small segments (the outlet was enlarged).

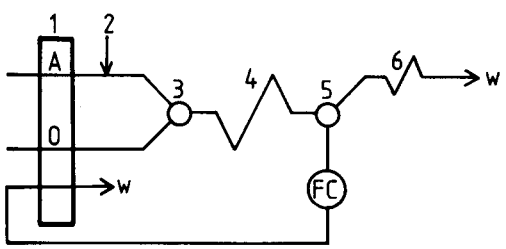

Fig. 1. Manifold for extraction in f.i.a.: peristaltic pump (1), sample injector (2), segmentor (3), extraction coil (4), phase separator (5), flow cell (FC), restrictor (6) and waste (W). A is the aqueous phase and O the organic phase.

The extraction coil materials were PTFE, polyethylene, steel and glass. Various lengths and inner diameters were tested. Two types of separators were employed: the T-separator working on the principle of phase density and material affinity differences [1] and the membrane separator [9].

The spectrophotometric detector (Perkin-Elmer, model LC-55) was equipped with an 8-μl h.p.l.c. steel cell. The length of the restrictor in Fig. 1 was varied to give a sufficient overpressure so that evaporation of the organic solvent could be prevented.

The organic solvents, pentanol and chloroform, were of analytical grade and used without further purification. Bromocresol green (BCG) and caffeine were used as model extractants for the pentanol/water and chloroform/water extraction systems respectively. The composition of the aqueous carrier was, in each case, identical with the extracted solution except that the extractant itself was omitted. In this way, the pH and the ionic strength could be kept constant across the entire sample zone. Changes in the volumetric dispersion were estimated using peak-height values.

System for intraphase dispersion experiments

A special system was constructed in order to investigate the dispersion process which occurred in a segmented stream. The aim was to study the carry-over per se between segments of the same phase. The system was essentially the same as that in Fig. 1. The injection and detection techniques differed. Dye was introduced into a single segment by means of a syringe

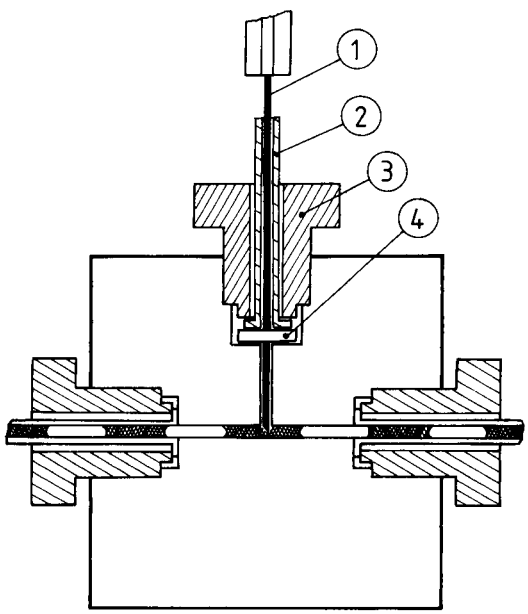

Fig. 2. Septum injector for injection into a single segment: syringe needle (1), PTFE guide tube for needle (2), connector (3), and PTFE-coated silicone rubber septum (4).

(Fig. 2). A PTFE tube placed perpendicularly to the light path in the spectrophotometric detector replaced the ordinary flow cell. This arrangement made it possible to measure the absorbance in both phases without separation. Similar detector arrangements have been described by Cockshott [23] and Snyder and Adler [24].

Nonextractive conditions had to be chosen. For example, a BCG/pentanol sample solution was introduced into a single pentanol segment when the dispersion in this phase was studied. The flow was then started and the sample travelled within the segmented stream through the tube under examination. The total variance was measured. By omitting the tube studied, the "reference" variance was obtained, thereby making it possible to calculate the variance originating in the tube itself.

Figure 3 is a photographic reproduction of a recorder tracing. The evaluation principle for the peak width, W, is indicated. In separate experiments it was found that the peak width, W, was independent of injected volumes in the range 1—10 μl (coil length 1 m, i.d. 0.7 mm, linear flow velocity 3.8 cm s^{-1}).

For Gaussian peaks, $W/4$ is the standard deviation, σ. However, peaks in

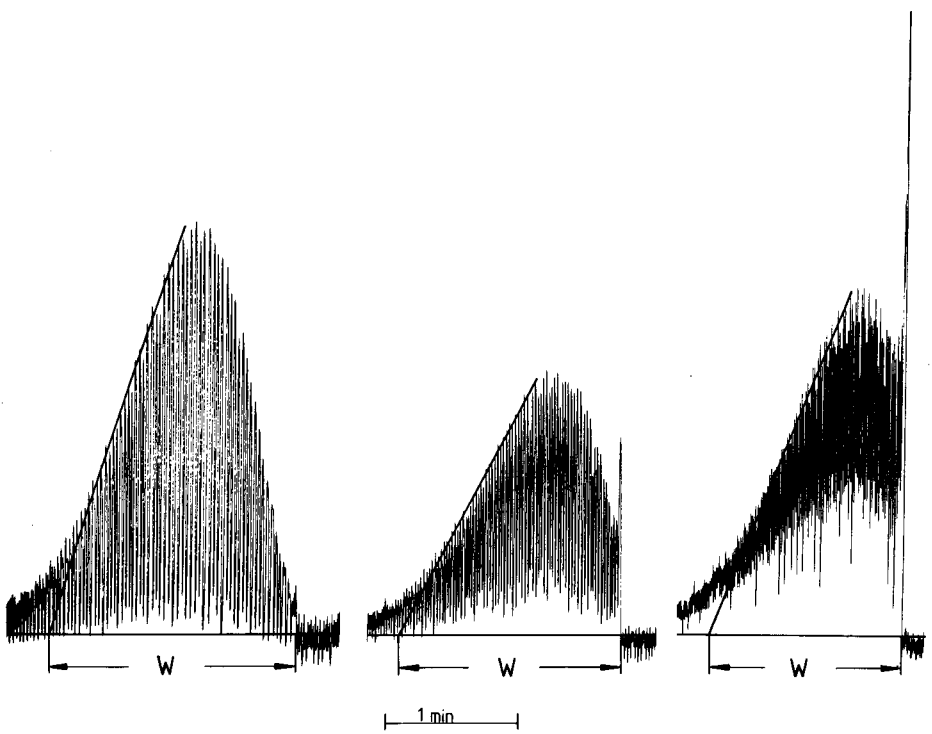

Fig. 3. Peaks resulting from injections of 2 μl of a pentanol solution of BCG into a single pentanol segment. Tubing: 2 m, 0.7 mm i.d., PTFE. Flow velocities from left to right: 0.8; 1.2; 2.0 cm s^{-1}. The first peak to the right was recorded with double sensitivity.

f.i.a. are normally skewed, rising quickly to an apex and then returning more slowly to the baseline. The discrepancy between $W/4$ and σ increases when the peaks become more skewed, so that $W/4$ is less than σ. However, the baseline width measure, $W/4$, is easily calculated and it is therefore a convenient estimation of the peak standard deviation, σ. The $W^2/16$ values obtained for independent portions of flow-injection systems are additive, similarly to their corresponding variance values.

Photographic technique

In order to find experimental evidence for film formation in the liquid/liquid segmented system, a photographic technique was applied. It was also possible to establish the flow pattern within the segments by this technique. A thin-wall PTFE tube (i.d. 0.7 mm, o.d. 0.9 mm) was placed under a transmission microscope (Nikon, Model S, Japan), equipped with a camera. A magnification factor of 10 was used. To reduce light refraction at the tube surface, diffuse light was used and the PTFE tube was placed in a glass cell filled with glycerine. The segmented stream passed through the tube at a linear velocity in the range 0—25 cm s^{-1}. Flash exposures of 10^{-5} s duration were required to achieve sharp contours.

RESULTS AND DISCUSSION

Film formation in the liquid/liquid segmented system

Figure 4 shows graphical reproductions of photographs taken of the pentanol/water (Fig. 4A) and chloroform/water systems (Fig. 4B). The upper panels in the Figures illustrate the physical conditions at zero flow rate. No film formation was observed under these circumstances. Neither of the phases wetted the tubing wall, consequently the boundary between the organic and water phases was sharp. When the segment started to move, the sharp boundaries at the tubing wall faded and a thin film of organic phase started to accumulate on the wall. This film formation is best

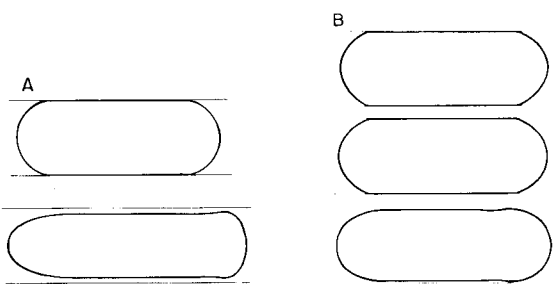

Fig. 4. Segment shape and organic film formation. (Flow direction from right to left; PTFE tubing, 0.7 mm i.d.) A, A pentanol/water system, with flow velocities of 0 and 11 cm s^{-1}; film thickness 0.055 mm (11 cm s^{-1}), B, A chloroform/water system with flow velocities of 0, 5 and 23 cm s^{-1}; film thickness 0.014 mm (23 cm s^{-1}).

illustrated in Fig. 4A for the pentanol/water system but it was also easily observed for the chloroform/water system. An increased flow velocity resulted in a thicker film. When the flow was stopped, the film disappeared either by joining the original, large segments or by forming new, small segments. Indisputably, the film formation was directly related to the flow velocity. When PTFE was used, the film comprised the organic phase exclusively in both the pentanol and chloroform systems. The phenomenon seems to be due to the higher affinity for the tubing material shown by the organic phase. This manifested itself in the fact that the contact angle (i.e., the angle between the solid/liquid and the liquid/liquid interfaces) was smaller for the organic phase than for the aqueous phase. As shown in Fig. 4, this smaller contact angle gave a starting point for the film formation. Conversely, in hydrophilic tubing material (glass), the aqueous phase will form the film.

Figure 5 shows the film thickness as a function of the flow velocity for the pentanol/water system in PTFE tubing. When illuminating and photographing such a system, light refraction creates darker bands in the region of the PTFE/pentanol and the pentanol/water interfaces. This introduced a constant error that accounts for the fact that the extrapolated straight line has a positive intercept although it was clearly seen from all the photographs that there is no film at zero flow rate.

There is no previous theory for film formation in liquid/liquid segmented systems. For gas/liquid systems, however, several equations describing film formation have been derived [25, 26]. These have the form

$$d_f = \text{const.}\ d_t\ (u\,\eta/\gamma)^a \qquad (1)$$

in which values of a of 1/2 or 2/3 have been used. Other symbols are defined in Table 1. This equation describes the film thickness behind one plug of

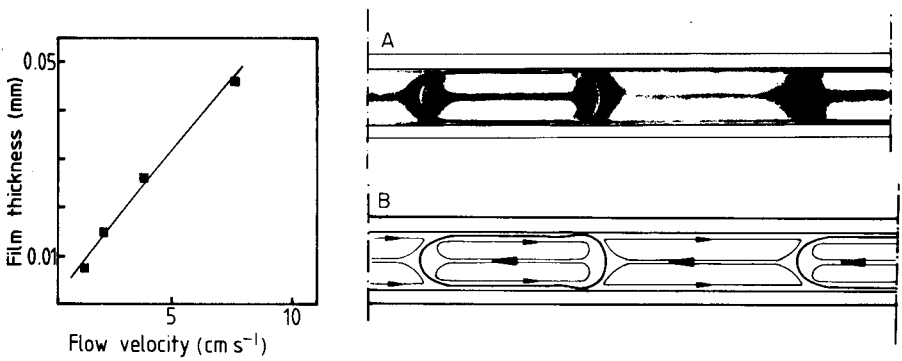

Fig. 5. Film thickness as a function of the flow velocity with pentanol as the organic phase and 0.7 mm i.d. PTFE tubing.

Fig. 6. A, Photographic reproduction of the analyte distribution in a pentanol/water segmented system in PTFE tubing. B, Schematic depiction of the streamlines in the pentanol/water system; flow from right to left.

TABLE 1

List of symbols

σ_s, σ_v, σ_l, σ_t	Peak standard deviation in segments, volume, length and time
W_s, W_v, W_l, W_t	Peak width in segments, volume, length and time
d_f	Film thickness (cm)
d_t	Inner diameter (cm)
u	Flow velocity (cm s^{-1})
η	Viscosity (poise)
γ	Surface tension (dyne cm^{-1})
L	Tubing length (cm)
L_s	Segment length (cm)
D_m	Diffusion coefficient (cm^2 s^{-1})

liquid that is forced through a capillary and where the liquid phase wets the surface of the capillary. Although these conditions are different from those existing in a liquid/liquid segmented flow system, it was of interest to examine whether Eqn. 1 could be used to predict the performance of different phases in extraction systems in f.i.a.

Snyder and Adler [24] have used this type of equation in the form

$$d_f = 0.67\,\pi\, d_t\, (u\,\eta/\gamma)^{2/3} \qquad (2)$$

to calculate the film thickness in air-segmented flow systems. If Eqn. 2 is used but η is taken as the viscosity of the film-forming phase and γ as the interfacial tension for the aqueous/organic system, it is possible to calculate a theoretical film thickness in a liquid/liquid segmented system from literature data [27]. When data for chloroform and pentanol were unavailable, η and γ were estimated from benzene, octanol and butanol data. When Eqn. 2 was used to calculate the film thickness for pentanol/water and chloroform/water systems in 0.7 mm i.d. tubing, the theoretically calculated film thicknesses were between 3 and 6 times higher than the experimentally measured values. Thus Eqn. 2 does not seem to be useful for prediction of absolute film thickness values in liquid/liquid segmented systems. The film thickness in a pentanol/water system was about 8 times that for a chloroform/water system (u = 11 cm s^{-1}, d_t = 0.7 mm, PTFE). In Eqn. 2, $(\eta/\gamma)^{2/3}$ describes the influence of the physical properties of the film-forming phase on the film thickness. For pentanol, $(\eta/\gamma)^{2/3}$ was 15 times that of chloroform. This means that the quotient η/γ is useful as a guide for comparing different film-forming phases. In order to obtain as thin a film as possible, the quotient between viscosity and interfacial tension should be minimized.

The results in Figs. 4 and 5 empirically establish some fundamental properties of film formation in liquid/liquid segmented systems: the film thickness depends on the flow velocity. The higher the flow rate, the thicker the film. The relationship is linear. Secondly, both the viscosity of the film-forming phase and the interfacial tension influence film thickness in such a way that high viscosity in combination with low interfacial tension results in a thick film.

Dispersion mechanism in the liquid/liquid segmented system

Figure 6A is a graphical reproduction of photographs showing the distribution of analyte in the organic and aqueous phases (pentanol/water system, PTFE). First, the system was photographed after an injection of dyed organic phase and under such conditions that no extraction occurred. The distribution solely in the organic phase was thus obtained. When the experiment was repeated under conditions that gave extraction to the aqueous phase, the resulting photograph showed the distribution in this phase. Figure 6A is a montage of these two photographs. The segments shown are about 10 segments after the original segment where dye was introduced. The first observation was that analyte distribution within a segment resulted from the type of flow shown in Fig. 6B. The analyte was retained in the stationary film and then partly mixed into the next segment by diffusion and convection. Thus, some analyte lagged behind the sample zone giving rise to dispersion.

In unsegmented systems under the same flow conditions, laminar flow prevails. A Reynolds number (Re) of 10 was calculated for pentanol (5 cm s^{-1}, 0.7 mm i.d.). Turbulent flow conditions are accepted to exist at $Re > 2000$. In the segmented case, the flow in the centre of a segment was also laminar.

The flow velocity should be zero at the tubing wall and convective mixing between streamlines should be negligible. These conditions were actually observed in a segmented system in which one of the organic segments was dyed. When the dyed segment was travelling forward, a region at the tubing wall developed which had no visible colouration. The thickness of this region corresponded to the film thickness of the organic phase.

Snyder and Adler [24] have derived equations which describe the dispersion in an air-segmented system. The fundamental assumptions are that there is a stationary film throughout the tube and that the analyte is transferred between the film and the segments by diffusion and convection. An "effective diffusion coefficient" was used in order to take the convective mixing into account. By rearranging the derived equations an expression for the peak variance, σ_s^2, was obtained

$$\sigma_s^2 = 4 d_f L/(d_t L_s) + 4L d_f^2 u/(9 D_m L_s^2) \quad (3)$$

In Fig. 7 the peak variance, σ_s^2, is plotted vs. the flow velocity, u, using Eqn. 3 (broken line). The film thicknesses were taken from Fig. 5, the diffusion coefficient was 10^{-6} cm^2 s^{-1}, and it was assumed that convective mixing did not contribute. The solid line shows the experimentally found relationship. The discrepancy between the two curves indicates that the influence of convective mixing cannot be neglected. Furthermore, the degree of convective mixing seems to vary with the flow velocity. The most probable regions for convective mixing are those at the segment boundaries where the streamlines reverse sharply, particularly the head region in the organic segment (in the flow direction). These sharp turns can be clearly observed in Fig. 6A; in these regions whirls may occur.

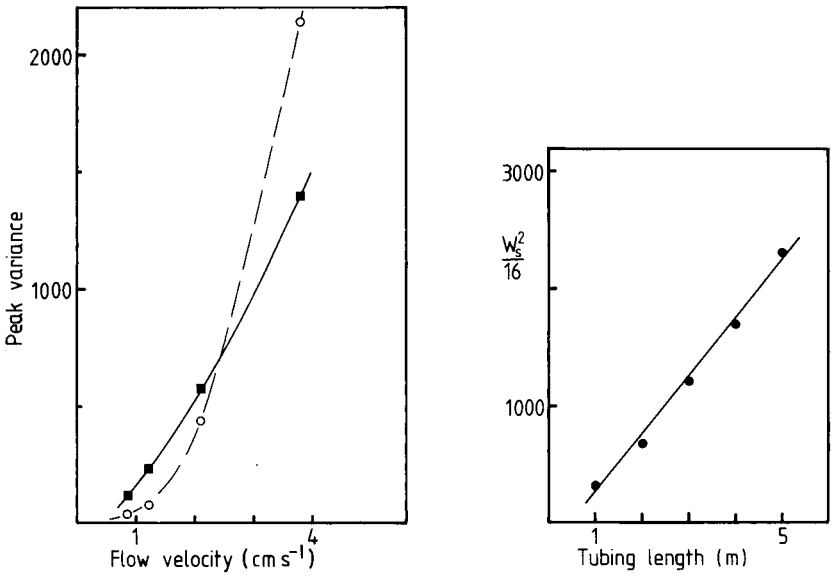

Fig. 7. Peak variance (segments²) as a function of flow velocity: (○) calculated from Eqn. 3; (■) found experimentally. Conditions: pentanol as organic phase, 2 m, 0.7 mm i.d. PTFE tubing, 10 mm segment lengths; 3 μl of a pentanol solution of BCG injected into a single pentanol segment.

Fig. 8. Total peak variance ($W_s^2/16$, segments²) as a function of tubing length. Conditions as for Fig. 7, except for flow velocity (4.0 cm s^{-1}) and injected sample size (5 μl).

Figure 3 shows typical recorder traces from experiments where dye was injected into a single segment. One interesting feature is that at high flow velocities an absorbance minimum occurred between the initial segment and the rest of the peak. This shows that the initial segment was washed out more slowly than the other segments. One possible explanation for this phenomenon was that the dye was originally evenly distributed in the first segment whereas for the following segments the dye was introduced via the film and was contained mainly in the boundary area (Fig. 6A). This suggests that a portion of the dye in the first segment was trapped and only reached the film through diffusion while the exchange between the film and the following segments was faster because of both short diffusion distances and convective mixing.

The influence of the manifold and flow variables on the dispersion process

Figure 8 depicts the total peak variance, $W_s^2/16$, as a function of coil length, L, for a pentanol/water system. The flow velocity and segment length were held constant. The variance was directly proportional to the tube length. This agrees with the additivity principle of variances for independent components of a system.

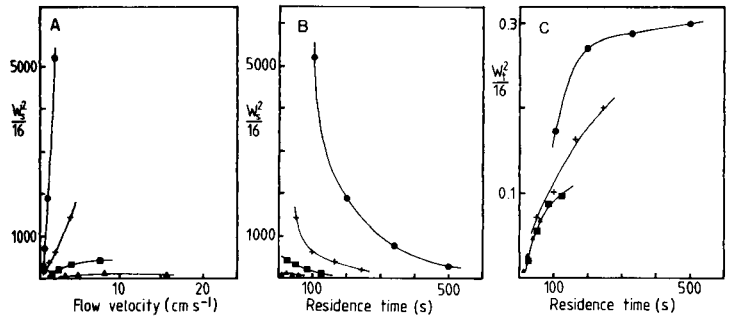

Fig. 9. A, Peak variance ($W_s^2/16$, segments^2) as a function of flow velocity. B, Peak variance ($W_s^2/16$, segments^2) as a function of residence time. C, Peak variance ($W_t^2/16$, min^2) as a function of residence time. Tubing: (•) 2 m, 1.0 mm i.d.; (+) 2 m, 0.7 mm i.d.; (▪) 2 m, 0.5 mm i.d.; (▲) 2 m, 0.35 mm i.d., all PTFE. Segment volume 3 μl; pentanol organic phase; 2 μl of pentanol solution of BCG injected into a single pentanol segment.

Figure 9A shows the peak variance, $W_s^2/16$, in a pentanol/water system, as a function of flow velocity; $W_s^2/16$ is proportional to the volume variance $W_v^2/16$, because $W_v = W_s V_s$ and V_s was kept constant. The inner diameters were varied while the coil length and the segment volume (V_s) were kept constant. The dispersion increased with both increased linear flow velocity (u) and tubing inner diameter (d_t). Comparing these results with those in Fig. 7, the immediate conclusion is that convective mixing cannot be excluded for any of the tube diameters. In fact, the plots obtained for the two smallest diameters were concave whereas Eqn. 3 predicts a convex shape.

Increased flow velocity caused additional dispersion in two ways: (a) the film thickness increased thus increasing the mass flow of analyte backwards from the sample zone; and (b) the analyte in the film had a shorter period of time for diffusion into the segment bulk. This means that the analyte moved a greater distance from the initial segment, before it was mixed into a new segment. When the tube inner diameter was increased, the film thickness increased at constant flow velocity. In addition, the diffusion distance from the film into the bulk of the segment will be longer. Figure 9A shows that the flow velocity has less influence on the dispersion at smaller inner diameters. The obvious explanation is that the convective part of the mass transfer becomes relatively larger as the diameter decreases.

In flow systems where a complete extraction is desired, the extraction kinetics determine the residence time required in the extraction coil. Therefore, the residence time is a suitable base for comparison, when the influence of design parameters such as flow rate (Q) and inner diameter (d_t) on dispersion are studied. Figure 9B and C shows the effect of decreased dimensions, i.e., d_t and Q, of the segmented system. The volume variance decreases dramatically but the time variance decreases only slightly as a consequence of varying inner diameter at a fixed residence time. This suggests that miniaturization of the segmented system leads to decreased sample

dilution but improves the sampling frequency only marginally. However, it should be stressed that only sample dispersion was studied. The influence of system dimensions on the mass transport between the phases (i.e., the extraction rate) may give stronger arguments for miniaturization.

Effect of coiling the extraction tubing

The influence of the coil diameter was investigated for the pentanol/water system. PTFE tubing (L = 3 m, i.d. = 0.7 mm) was used, both straight and coiled (coiling diameter 10 mm). A pentanol solution of BCG (5 μl) was injected into a single segment as described earlier. At flow velocities of 3.8 and 7.6 cm s^{-1}, no differences in the measured peak widths could be detected between the coiled and the straight case. However, there was a change in peak shape, in that the high absorbance of the first segment disappeared or decreased greatly when a coiled tube was employed. This indicates that coiling affected the intrasegment mixing although it did not substantially influence dispersion.

Influence of tubing material on dispersion

Table 2 shows the total variance for a pentanol/water system with tubes of PTFE, glass and steel (3 m, 0.7 i.d.). The sample was injected into a single aqueous or organic segment and, as in previous experiments, a reference system of PTFE tubing was connected to the tubes to be examined. This arrangement made it possible to exclude effects of components other than the tube. When the dye was contained in the organic phase (acidic conditions) there was no significant difference between the reference system only and the glass or steel tube systems. This means that the dispersion in these tubes was negligible. In the PTFE tube the dispersion increased substantially.

When the dye was contained in the aqueous phase (alkaline conditions) and injected into an aqueous segment, the first observation was that

TABLE 2

Total variance ($W_s^2/16$, segments^2) for tubes of glass, steel and PTFE (flow velocity 3.7 cm s^{-1}).

	Reference system only	Reference system + 3 m, 0.7 mm i.d. tubing of		
		Steel	Glass	PTFE
Analyte in aqueous phase[a]	5	270	160	—
Analyte in organic phase[b]	430	500	430	4100

[a]Dispersion in aqueous phase: alkaline conditions, injection of an aqueous BCG solution into a single aqueous segment. [b]Dispersion in organic phase: acidic conditions, injection of a pentanol BCG solution into a single pentanol segment.

dispersion in the reference system of PTFE was very small. When steel or glass tubes were added, dispersion increased. It was clear from these results that when the analyte is contained solely in the organic phase, a polar tubing material such as glass or steel (aqueous film formation) should be used to minimize dispersion. When the analyte is in the aqueous phase, the very low dispersion of the reference system indicates that a non-polar tubing material which generates a film of organic phase will give very low dispersion. The aqueous segments are completely enclosed by organic phase and thus isolated from each other in such a system. The same is true for steel or glass tubes when the analyte exists only in the organic phase.

Figure 10 shows the effect of the flow velocity on dispersion expressed in $W_s^2/16$ on a pentanol/water system with BCG injected as an alkaline aqueous solution. Steel and glass tubes were tested. It was observed that the dispersion was considerably lower for the glass tube, most notably at higher flow velocities. A possible explanation for this was the difference in the film thickness. When the inner surfaces of steel and glass tubes were examined under a microscope, the glass surface was found to be very smooth whereas the steel surface was rough or almost grooved. It is probable that the surface roughness gave a thicker water film for steel.

The dispersion was smaller when the analyte was contained in the aqueous

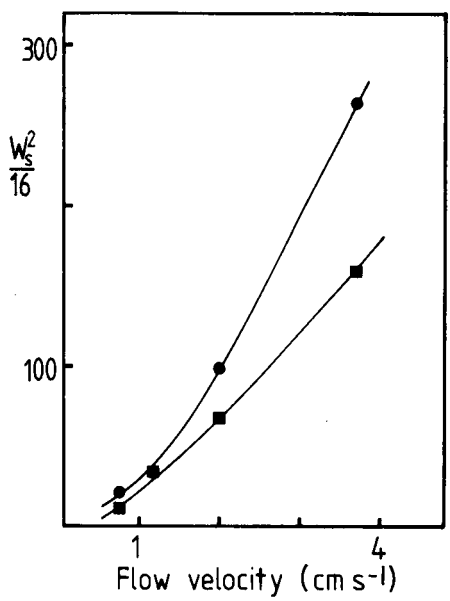

Fig. 10. Peak variance ($W_s^2/16$, segments^2) as a function of flow velocity. Tubing: (•) 3 m, 0.7 mm i.d., steel; (▪) 3 m, 0.7 mm i.d., glass. Conditions: pentanol as organic phase; segment length 10 mm; 2 μl of aqueous BCG solution in 0.01 M NaOH injected into a single aqueous segment.

phase and when steel or glass tube was employed compared to when the pentanol contained the analyte and PTFE tube was used. This observation can also be attributed to film thickness. The viscosity of pentanol is approximately 4 times that of water, suggesting that the organic film should be about 4 times thicker than the water film.

Dispersion in flow-injection extraction systems

Figure 11 shows the influence of tubing material on peak height during the extraction of BCG into pentanol. Because pentanol leaves a thick film resulting in a large dispersion, this solvent was used in this study. Different lengths of PTFE, polypropylene (PP), steel and glass tubing were tested. For non-polar tubing material (PTFE and PP), the loss in sensitivity was considerable even with the optimum extraction coil length. For steel tubing, no additional dispersion can be detected after the point where the analyte is completely extracted into the organic phase. The fundamental difference between the types of tubing materials, is that for steel, dispersion takes place in the aqueous phase prior to extraction but for PTFE and PP, the analyte is dispersed in the organic phase after extraction.

Figure 12 shows the influence of tubing diameter and segment length on

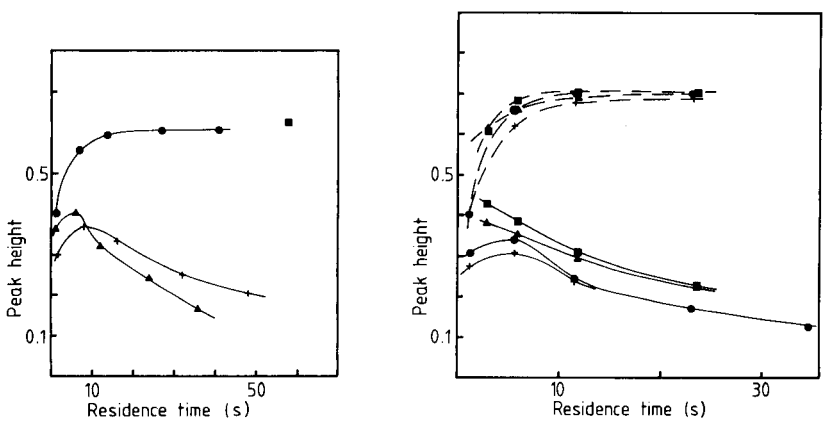

Fig. 11. Flow-injection extraction of BCG: influence of coil material on dispersion. Extraction coils: (▪) glass, 0.9 mm i.d.; (•) steel 0.76 mm i.d.; (▲) PTFE 0.7 mm i.d.; (+) polypropylene 0.8 mm i.d. Flow rates: aqueous = 0.9 ml min^{-1}, organic = 1.1 ml min^{-1}. Sample: 126 mg l^{-1} BCG in 0.015 M nitric acid.

Fig. 12. Flow-injection extraction of BCG: influence of tubing diameter and segment length on dispersion. (---) Continuous pumping of sample; (—) f.i.a. Extraction coils: (▪) and (▲) 0.5 mm i.d. PTFE; (•) and (+) 0.7 mm i.d. PTFE. Segment volumes: (▪) and (•), 2.5 μl; (▲) and (+) 5.0 μl. Flow rates: 1.1 ml min^{-1} pentanol, 0.9 ml min^{-1} aqueous phase. Sample: BCG in 0.015 M nitric acid, 126 mg l^{-1} (f.i.a.) and 63 mg l^{-1} (continuous pumping).

peak height. Extraction coils of PTFE with 0.5 and 0.7 mm i.d. were used with segment volumes of 2.5 and 5 μl. Peak height was plotted vs. calculated residence time in order to compare the two different inner diameters. The upper curves in Fig. 12 relate to continuous pumping of the sample solution into the system, which completely eliminates dispersion. It can be concluded (from the upper curves) that extraction in the 0.5 mm i.d. tubing is slightly faster than in the 0.7 mm i.d. tubing. Moreover, shorter segment lengths give faster extraction. The lower curves relate to samples injected into the system. The dispersion curves for 0.5 mm i.d. tubing reach higher maxima and drop more slowly than those for 0.7 mm i.d. tubing. The shortest segment length gives the highest maximum. The extraction rate should influence the overall dispersion in a system where extraction and dispersion occur simultaneously. As a consequence, higher extraction rates would allow less time for the dispersion process to act on the sample zone. This means that the maxima in Fig. 12 should be displaced to the left and the overall dispersion should decrease.

Figure 13 shows the results of a study of the extraction of caffeine into chloroform with a PTFE extraction coil (0.7 mm i.d.). The segment length had a very small influence on dispersion, a fortyfold increase giving only about 10% decrease in peak height (Fig. 13A). This was also valid when dispersion was large, i.e., for pentanol (Fig. 12). Figure 13B shows the influence of the flow velocity on dispersion. For a low flow velocity, dispersion was almost negligible but increased for higher flow velocities, because of increasing film thickness.

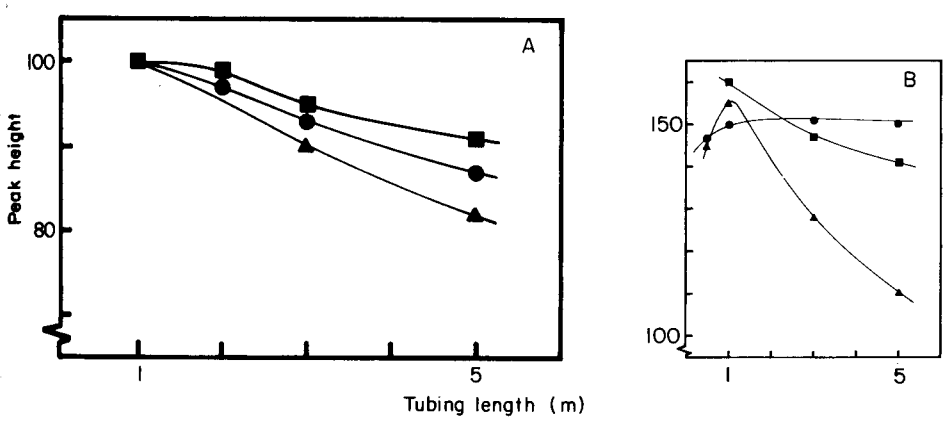

Fig. 13. Flow-injection extraction of caffeine. A, Influence of segment length on dispersion for segment lengths of: (■) 1 mm; (●) 5 mm; (▲) 40 mm. B, Influence of flow velocity on dispersion for flow velocities of: (●) 2.7 cm s^{-1}; (■) 5.4 cm s^{-1}; (▲) 17.8 cm s^{-1}. Conditions: 0.7 mm i.d. PTFE tubing; 10^{-4} M caffeine; 0.75 ml min^{-1} aqueous phase and 0.57 ml min^{-1} chloroform for A; segment length 6 mm for B.

CONCLUSIONS

The following parameters should be considered in designing an extraction system for f.i.a.: tubing material, length, and inner diameter; flow rate and flow ratio of organic/aqueous phases; the nature of the organic phase (viscosity, interfacial tension, density, boiling point); the nature of the extractant; sample volume and concentration; segment length and separator design.

This work makes it possible to summarize some recommendations, the object being to control the dispersion in order to optimize the sample throughput and the sensitivity for an extraction system. First, the organic phase selected should form a thin film; such organic solvents are characterized by a low viscosity/interfacial tension ratio. If, for any reason, a solvent with a viscosity higher than water has to be selected for the extraction, a coil material of steel or glass should be considered. Secondly, for the parts of any liquid/liquid segmented system in which no extraction occurs or in which extraction is complete and has reached equilibrium, dispersion can be prevented by selecting a coil material onto which the phase carrying the analyte does not form a film.

Thirdly, the volume dispersion in an extraction system can be decreased by decreasing the inner diameter of the extraction tube and by decreasing the flow rate simultaneously to maintain a constant residence time. The sample throughput and the time dispersion remain essentially constant. This conclusion assumes a fixed sample volume and a fixed flow-detector configuration. However, an overall decrease of the system dimensions will lead to a decrease of the time dispersion.

Fourthly, when the total flow rate in an extraction system is decreased, the volume dispersion decreases when all other system parameters are kept constant, including the flow ratio of the organic and aqueous phases.

Finally, a change of the segmentation pattern, for a given design of a system, towards smaller and more segments will lead to a slight decrease of the volume dispersion.

The authors are indebted to Prof. F. Ingman, Dr. B. Bubnis and Prof. G. Pacey for valuable discussions. This work was supported by the Swedish National Board for Technical Development.

REFERENCES

1 B. Karlberg and S. Thelander, Anal. Chim. Acta, 98 (1978) 1.
2 H. Bergamin F°, J. X. Medeiros, B. F. Reis and E. A. G. Zagatto, Anal. Chim. Acta, 101 (1978) 9.
3 K. Kina, K. Shiraishi and N. Ishibaski, Talanta, 25 (1978) 295.
4 B. Karlberg, P. A. Johansson and S. Thelander, Anal. Chim. Acta, 104 (1979) 21.
5 J. Kawase, A. Nakae and M. Yamanaka, Anal. Chem., 51 (1979) 1640.
6 B. Karlberg and S. Thelander, Anal. Chim. Acta, 114 (1980) 129.
7 P. A. Johansson, B. Karlberg and S. Thelander, Anal. Chim. Acta, 114 (1980) 215.

8 O. Klinghoffer, J. Růžička and E. H. Hansen, Talanta, 27 (1980) 169.
9 L. Nord and B. Karlberg, Anal. Chim. Acta, 118 (1980) 285.
10 J. Kawase, Anal. Chem., 52 (1980) 2124.
11 T. Imasaka, T. Harada and N. Ishibaski, Anal. Chim. Acta, 129 (1981) 195.
12 D. C. Shelly, T. M. Rossi and I. M. Warner, Anal. Chem., 54 (1982) 87.
13 L. Fossey and F. F. Cantwell, Anal. Chem., 54 (1982) 1693.
14 K. Ogata, K. Taguchi and T. Imanari, Anal. Chem., 54 (1982) 2127.
15 T. M. Rossi, D. C. Shelly and I. M. Warner, Anal. Chem., 54 (1982) 2056.
16 L. Nord and B. Karlberg, Anal. Chim. Acta, 125 (1981) 199.
17 L. Nord and B. Karlberg, Anal. Chim. Acta, 145 (1983) 151.
18 K. Bäckström, L.-G. Danielsson and L. Nord, Analyst (London), 109 (1984) 323.
19 R. W. Frei, in R. W. Frei (Ed.), Chemical Derivatization in Analytical Chemistry, Vol. 1, Plenum, New York, 1981, p. 269.
20 J. Růžička and E. H. Hansen, Flow Injection Analysis, Wiley, New York, 1981.
21 E. H. Hansen, J. Růžička, F. J. Krug and E. A. G. Zagatto, Anal. Chim. Acta, 148 (1983) 111.
22 B. Karlberg, in R. W. Frei (Ed.), Chemical Derivatization in Analytical Chemistry, Vol. 2, Plenum, New York, 1982, p. 24.
23 I. Cockshott, personal communication.
24 L. R. Snyder and H. J. Adler, Anal. Chem., 48 (1976) 1017, 1022.
25 P. Concus, J. Phys. Chem., 74 (1970) 1818.
26 M. Novotny and K. D. Bartle, J. Chromatogr., 93 (1974) 405.
27 R. C. Weast (Ed.), Handbook of Chemistry and Physics, CRC Press, Boca Raton, 1982.

Analytica Chimica Acta, 164 (1984) 251—256
Elsevier Science Publishers B.V., Amsterdam — Printed in The Netherlands

ENHANCED SPECTRUM MATCHING OF MIXED MASS SPECTRA BY MEANS OF QUALITY FACTORS

W. M. SHACKELFORD* and D. M. CLINE

U.S. Environmental Protection Agency, Environmental Research Laboratory, Athens, GA 30613 (U.S.A.)

(Received 7th June 1984)

SUMMARY

A system of computer programs for recognizing impure or mixed spectra was assembled that provided automatic subtraction of reference mass spectra from a mixed spectrum. The software was 99% successful in recognizing pure spectra for the cases tested. Subtractions were done on mixed spectra in 70% of the cases tested. Spectrum subtraction enhanced the ability of the matching program to match components of a multicomponent mixture correctly, whereas quality factors were a great aid in the evaluation of the overall match validity.

The matching of mass spectra with a library of reference spectra involves special problems when the spectra acquired from gas chromatography/mass spectrometry (g.c./m.s.) data are not pure. For field samples, impure spectra must be dealt with quite often. Rosenthal [1] has demonstrated that, even when 1-s scans and capillary g.c. columns are used, overlapping components are a virtual certainty for such samples.

Faced with impure spectra as a routine problem, the analyst spends much time trying to unravel both the mixed spectra and the matched results generated from the mixed spectra. In this work, an attempt was made to automate much of this unravelling through the use of quality factors as developed by the McLafferty group [2] and automated spectrum subtraction.

The use of reverse searching to identify components of a mixed spectrum has been reported by several workers [3—5]. The subtraction of a matched spectrum from a mixed spectrum has been reported previously also [6]. An inherent problem in both of these approaches, however, lies in establishing whether the spectrum is pure or impure. Even though match parameters may indicate spectrum purity, the differences in instrument or acquisition conditions between the unknown and reference spectra may result in misleading purity calculations (see Fig. 1).

In this work, quality factors as previously proposed [2] for the determination of purity of reference spectra were applied to the results of spectrum matches by using the probability based matching (PBM) system [7] to estimate spectrum purity. Spectrum subtraction was applied only if the quality

0003-2670/84/$03.00

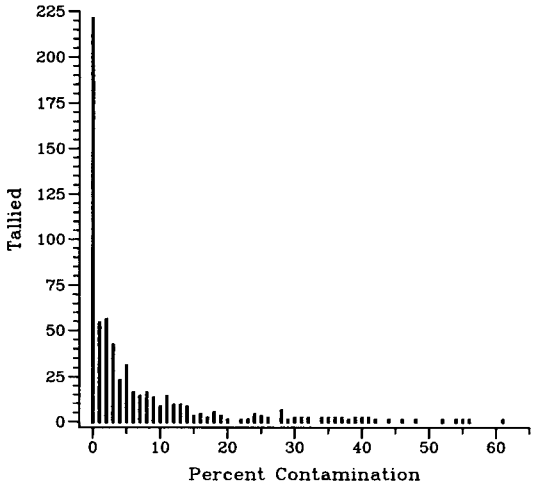

Fig. 1. Distribution of percent contamination for 609 pure spectra calculated by PBM.

factor test was failed. All stages of the matching system were handled automatically.

EXPERIMENTAL

The spectra used for unknowns in this study were obtained from the Research Triangle Institute, Research Triangle Park, NC [8]. All 609 pure spectra represented compounds, the spectra of which were contained in the reference library used for matching in this laboratory [9]. To produce the mixed spectra, a computer program was written to combine linearly and renormalize binary, ternary, and quaternary mixtures. Spectra were mixed in groups of nine. Within each group, spectrum numbers 3 and 6 were mixed to form the binary mixtures. Spectrum numbers 2, 5, and 8 were mixed for the ternary mixtures and spectrum numbers 1, 4, 7, and 9 were mixed for the quaternary mixtures. Thus, from the 609 pure spectra, 67 groups of nine spectra resulted in 603 mixed spectra. Table 1 shows the distribution of mixtures in the set of mixed spectra. As can be seen, component concentrations within mixed spectra ranged from 20% to 80%.

Computer algorithms and hardware

For spectrum matching, the PBM [7] system was used as modified in this laboratory [9]. To calculate the quality factors, code was obtained from the McLafferty group at Cornell University and modified in this laboratory. Only quality factor QF3, which measures contaminant peaks above the molecular weight of the reference compound, and QF4, which measures the extent of illogical neutral losses, were used. Other quality factors discussed earlier [2] do not give as direct a measure of spectrum impurity as QF3 and QF4.

In order to match a spectrum, the PBM was first run and QF3 and QF4

TABLE 1

Distribution of mixed spectra (67 spectra for each case)

Number of components	Ratio	Number of Components	Ratio
2	1:1	3	1:1:1
2	1:2	3	1:2:1
2	1:3	3	1:2:2
2	1:4	4	1:1:1:1
		4	1:1:1:2

were calculated for each of the ten best matches assuming the identity of the unknown spectrum to be each of the compounds generated by the match results. The match results were then scanned to ensure that the best match had more positive than negative match quality. For matches of sufficient quality (see below), the product of QF3 and QF4 was scanned to look for any values less than 0.70. If a value less than 0.70 was found, the best matched reference spectrum (the spectrum with the highest match correlation) was subtracted from the unknown spectrum and the PBM was run on the residual. This process could be repeated for a maximum of four PBM runs.

Because a number of poorly matched compounds can show up in a list of matches for even pure spectra, logic was devised to let the computer judge whether the best spectrum match was of sufficient quality to disregard any subsequent matches that might have the product, QF3XQF4, less than 0.70. The best match for the unknown was the key to further action. If the best match showed K (positive correlation) greater than ΔK (negative correlation) and a calculated contamination less than 30%, the spectrum was deemed pure. If the contamination percentage was greater than 30% but less than 40%, spectrum purity was conceded only if the molecular ion also was found. For cases with contamination percentage greater than 40%, the spectrum was deemed to be contaminated and a match with the quality factor product less than 0.70 was sought. If such a match was found, the best matched spectrum was subtracted from the unknown and the whole process was restarted. If at any point in the process the spectrum was deemed pure, no further processing took place.

Spectrum subtraction was achieved by subtracting the condensed [7] reference spectrum from the unknown spectrum after multiplying the reference spectrum by the purity factor calculated by PBM. Although in earlier work [6] the complete reference spectrum was used for subtraction, storage restrictions made the retention of both a condensed reference data base and the full-spectrum data base on line at one time impractical. Because each condensed spectrum contains between 16 and 26 m/z intensity pairs, it was considered sufficient for this work. After spectrum subtraction occurred, the residual spectrum was renormalized.

All operations were done with a Digital Equipment Corporation PDP 11/70 computer.

RESULTS AND DISCUSSION

To test the use of quality factors as a measure of unknown spectrum purity, both pure and mixed spectra were studied. The collection of 609 pure spectra and 603 mixed spectra were run through the matching routine and statistics were kept to establish the best logic for automatic determination of spectrum purity.

In Fig. 2A, the distribution of values for QF3 are shown for the pure spectra. As expected, essentially all spectra show no contaminant peaks above the molecular weight. In Fig. 2B, the distribution of values for QF4 are shown. Again, although there is some scatter, all values lie essentially near the perfect score of 1.0. Thus, it can be seen that, for pure spectra acquired under routine g.c./m.s. conditions, the quality factors accurately describe purity.

Using quality factors alone, however, does not address the situation in which the components have molecular weights that differ more than the range of illogical neutral losses used in the QF4 calculation, 38 daltons. In these cases, the heavier component will show no interference above its molecular weight and no illogical neutral losses, because the QF4 calculation will not consider losses of greater than 38 daltons. Although the lighter of the components will definitely have QF3 < 1, the heavier component may well look as if it is pure. In the case when the heavier component also is the best matched component, the computer cannot make the decision to subtract without additional data.

To aid the computer at this point, a second parameter is examined to determine spectrum purity; the second parameter is the value calculated by the PBM for contamination percentage. In Fig. 1 the distribution of values for the pure spectra is shown. The 80th percentile of all values for the pure

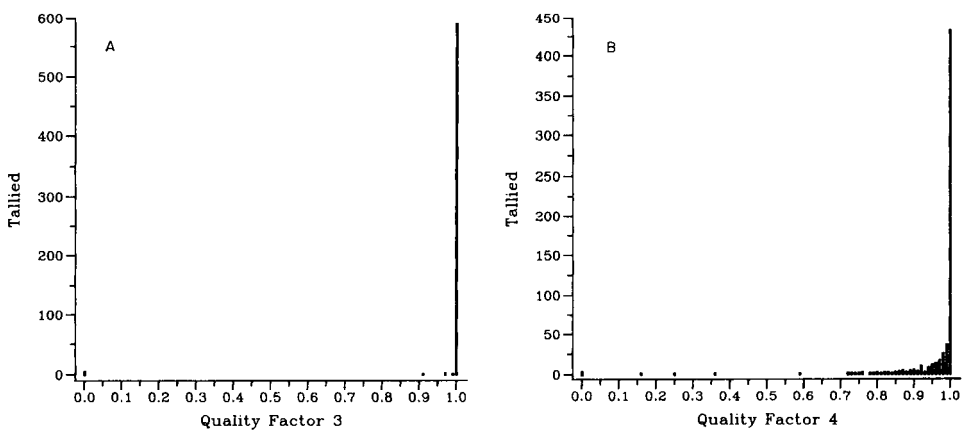

Fig. 2. Distribution of quality factor values for 609 pure spectra: (A) quality factor 3; (B) quality factor 4.

spectra is reached at the 30% level. This was set as the level below which, barring any indications from QF3 and QF4, a spectrum was deemed pure. At intermediate levels, 31–40%, if the molecular ion were present as well, purity was indicated. At contamination levels greater than 40%, all matches were examined for low quality factor values. If any low values were found, the best match in the reference library was subtracted from the unknown spectrum and the process repeated.

Of the 609 pure spectra sent to the matching routine, 605 were seen to be pure by the above logic. Of the 603 mixed spectra sent to the matching routine, 422 were correctly seen to be mixed. The compounds that consistently gave problems to the logic were heavily halogenated aromatics. Because of their relatively high molecular weights and characteristic isotope clusters, these compounds had very low contamination matches and exhibited almost no effects on their quality factors. Overall, although about 30% of the mixed spectra were incorrectly classified as to purity, much computer time was saved by avoiding unnecessary spectrum subtraction of the pure spectra.

In Table 2 are shown the matching results for the pure and mixed spectra. For this work, a correct answer corresponds to a Class 2 [7] match (the correct compound or an isomer differing by a shift of only one carbon position) of the unknown as the best PBM match. Thus, although the reference library contained spectra corresponding to each of the pure spectra, there were cases in which these spectra were not the best match. For pure spectra, 92% were matched.

For the mixtures, the results were promising. As can be seen in Table 2, spectrum subtraction improved the number of compounds that were matched in mixtures over what could be expected for a single matching step. It is evident from Table 2 that, as the number of compounds within the mixture increases or the relative proportion of a compound within a mixture decreases, the ability of the system to retrieve correct matches decreases.

TABLE 2

Spectrum matching results

Number of components	Ratio	Correct answers	Percentage correct	Expected percentage correct
1	N/A	562	92	100
2	1:1	115	86	50
2	1:2	91	68	50
2	1:3	76	57	50
2	1:4	69	51	50
3	1:1:1	109	57	33
3	1:2:1	92	48	33
3	1:2:2	83	43	33
4	1:1:1:1	98	37	25
4	1:1:1:2	89	33	25

This decrease comes from both the inability of the matching program to retrieve a good initial match (in the case of three- and four-component mixtures) as well as the first match appearing pure (in the case of 1:3 and 1:4 binary mixtures).

As shown in Table 2, automatic spectrum subtraction resulted in a 36% increase in identifications for unweighted binary mixtures, a 23% increase for unweighted tertiary mixtures and a 12% increase for unweighted quaternary mixtures over the expected identification rate.

Conclusions

Use of quality factors for automating spectrum subtraction in conjunction with the matching of mixed spectra is a valid approach to save operator time. Improvement in the identification rate of compounds is greatest in binary mixtures, which are by far the most frequently encountered in real samples, but is noticeable in ternary and quaternary mixtures.

We thank Prof. F. W. McLafferty, of Cornell University for the quality factor FORTRAN code, Richard Bowen for programming help and Laura Folwell for collation of results.

REFERENCES

1 D. Rosenthal, Anal. Chem., 54 (1982) 63.
2 D. D. Speck, R. Venkataraghavan and F. W. McLafferty, Org. Mass Spectrom., 13 (1978) 209.
3 F. P. Abramson, Anal. Chem., 47 (1975) 45.
4 F. W. McLafferty, R. H. Hertel and R. D. Villwock, Org. Mass Spectrom., 9 (1974) 690.
5 B. E. Blaisdell and C. C. Sweely, Anal. Chim. Acta, 117 (1980) 18.
6 B. A. Fell, R. Venkataraghavan and F. W. McLafferty, Anal. Chem., 51 (1979) 1945.
7 G. M. Pesyna, R. Venkataraghavan, H. E. Dayringer and F. W. McLafferty, Anal. Chem., 48 (1976) 1362.
8 J. T. Bursey and E. D. Pellizzari, EPA Report EPA-600/S4-83-028, 1983.
9 W. M. Shackelford, D. M. Cline, L. Faas and G. Kurth, Anal. Chim. Acta, 146 (1983) 15.

Analytica Chimica Acta, 164 (1984) 257—262
Elsevier Science Publishers B.V., Amsterdam — Printed in The Netherlands

Short Communication

COMPARATIVE EVALUATION OF TWO SUBSTRATES FOR URINARY DETERMINATION OF *p*-AMINOBENZOIC ACID BY ROOM-TEMPERATURE PHOSPHORIMETRY

H. THOMAS KARNES and S. G. SCHULMAN

College of Pharmacy, University of Florida, Box J-4, J. Hillis Miller Health Center, Gainesville, FL 32611 (U.S.A.)

J. D. WINEFORDNER*

Department of Chemistry, University of Florida, Gainesville, FL 32611 (U.S.A.)

(Received 7th June 1984)

Summary. Filter paper (S & S 903) impregnated with diethylenetriaminopentaacetic acid, and Whatman DE-81 anion-exchange paper are evaluated for quantitation of urinary *p*-aminobenzoic acid. The two substrates are compared with respect to drying characteristics, pH variations, heavy atom effect, and some other variables. Impregnated S & S 903 paper is superior in terms of drying characteristics and background interferences but DE-81 has several advantages including lower detection limit, wider pH range, and ready availability. Although both substrates seem applicable to clinical application, DE-81 is probably more useful.

The urinary determination of *p*-aminobenzoic acid (PABA) which has been enzymatically cleaved from *N*-benzoyl-L-tyrosyl-*p*-aminobenzoic acid (bentiromide) has recently been proposed as a reliable screening test for pancreatic function [1—3]. The PABA marker is specifically cleaved by the pancreatic endopeptidase chymotrypsin, absorbed in the small bowel, metabolized and excreted in the urine. The recovery of urinary PABA is therefore proportional to chymotrypsin activity and low activity is indicative of pancreatic deficiency.

Quantitation of urinary PABA has classically been accomplished by colorimetric methods [4, 5] which detect total aromatic amines and thus suffer from a lack of selectivity with respect to certain drugs and other compounds which may be present in the urine samples [6]. Room-temperature phosphorimetry (r.t.p.) has been shown to be a sensitive and potentially selective method for PABA [7]; here, r.t.p. is proposed as a possible alternative to colorimetric methods. The choice of solid substrate is a critical factor affecting the success of r.t.p. methodology and two substrates, S & S 903 impregnated with diethylenetriaminopentaacetic acid (DTPA) and DE-81 anion-exchange filter papers, were evaluated for application to urine samples.

Currently accepted r.t.p. theory suggests that rigid binding of the analyte to substrate material decreases the probability of non-radiative deactivation

0003-2670/84/$03.00

and enhances intersystem crossing, thus contributing to observed phosphorescence intensity [10, 11]. Diethylenetriaminepentaacetic acid-treated S & S 903 filter paper is thought to be less porous than untreated paper and penetration of the analyte into the paper is minimized, resulting in greater surface adsorption and higher phosphorescence intensity [12]. Relatively high phosphorescence intensity observed from DE-81 anion-exchange paper is attributed to the interaction of substrate functional groups with analyte molecules [8]. Both of these substrates appear superior for r.t.p. quantitation of PABA; they were therefore compared with regard to pH-dependence, drying characteristics, heavy atom effect, and background interference with application to urine samples.

Experimental

Instrumental. Phosphorescence measurements were made with a modified spectrophotofluorimeter (Aminco-Bowman model SPF100) equipped with a rotating can phosphoroscope, ratio photometer (American Instrument Co., Silver Springs, MD) and a Hamamatsu IP21 photomultiplier tube. A solid sample bar constructed in this laboratory [9] was used and a 150-W xenon arc lamp provided excitation energy.

Reagents and materials. Solvents used for dilutions were "nanopure" deionized water (Barnstead System, Sybron Co.) and absolute ethanol (U.S. Industrial Chemical Co.). All reagents except PABA (Sigma Chemical Company) were analytical grade (Fisher); DE-81 paper was from Whatman Chemical Separation; S & S 903 (Schleicher and Schüll) was treated with DTPA (Sigma Chemical Company) as previously described [12].

Procedure. A 3-μl sample or blank solution with or without 2 μl of 1 mol l^{-1} potassium iodide was applied to a 0.25-in diameter filter paper disc contained in the sample bar by use of an SMI micropipetter. The sample bar was placed in the phosphorimeter sample compartment and allowed to dry under dry nitrogen for 15 min. Phosphorescence intensity was measured from each position on the sample bar with the excitation and emission wavelengths set at 295 and 432 nm, respectively. Adjustment of pH and pH dependence studies were accomplished by adding very small amounts of concentrated sulfuric acid and saturated sodium hydroxide solution to aqueous analyte solutions (25 mg l^{-1}) containing 0.01 M potassium dihydrogenphosphate. The pH was measured with a Markson pH meter (Markson Science Inc., Del Mar, CA) prior to application onto the solid substrate.

Results and discussion

Drying characteristics. The drying characteristics of the two substrates were compared by measuring phosphorescence intensity of PABA solutions (25 mg l^{-1}) vs. time under a dry nitrogen flow. The resultant drying histograms consisted of 3 regions, the time it took the r.t.p. signal to reach a maximum, the plateau region in which the signal remained constant, and the decay region where the phosphorescence intensity decreased at a rate dependent on

TABLE 1

Effect of solvent and substrate on drying characteristics for PABA quantitation

Substrate	Solvent[a]	Rise time (min)	Plateau time (min)	Fall rate[b] (RI min^{-1})
DE-81	0.01 M KH_2PO_4	14.4	9.4	1.8
S & S 903 (DTPA)	0.01 M KH_2PO_4	13.0	17.0	1.6
DE-81	50% ethanol in 0.01 KH_2PO_4	14.0	13.4	2.5
S & S 903 (DTPA)	50% ethanol in 0.01 KH_2PO_4	10.6	18.0	1.3

[a]All at pH 6.4. [b]Relative intensity.

the conditions and substrate. Two solvents were used for each substrate; the results are shown in Table 1. These observations suggest that the optimal drying time is only slightly lessened and the plateau time slightly increased by the addition of ethanol. The rise and plateau times for the two substrates are significantly different, with DTPA-soaked S & S 903 showing better characteristics. This may be due to decreased porosity of the DTPA-soaked S & S 903 substrate or possibly to the interaction of water molecules with functional groups on the DE-81 substrate.

pH dependence. The dependence of phosphorescence intensity on pH is shown in Fig. 1 for each substrate studied. The r.t.p. signal from the DTPA-soaked S & S 903 substrate falls sharply below pH 3.3 and above pH 6.6. The DE-81 substrate, however, demonstrates a much wider range of relatively stable r.t.p. intensities between pH 2.3 and 11.7. Von Wandruszka and Hurtubise [7] proposed that decreased phosphorescence at low pH may

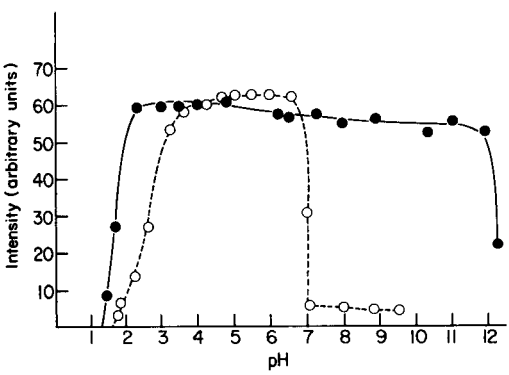

Fig. 1. Dependence of PABA (25 mg l^{-1}) room-temperature phosphorescence intensity on pH: (•) DE-81; (○) DTPA-soaked S & S 903.

be due to protonation of the functional groups on PABA which prevents strong binding to the substrate. In alkaline solutions, the decreased intensity was thought to be due to precipitated sodium hydroxide on the substrate upon evaporation. Possibly, the quaternary ammonium exchanger groups on DE-81 have some buffer capacity, in that excess of H^+ may be bound to the OH^- counter ion of the substrate. At high pH, excess of hydroxide may be bound by the quaternary ammonium group preventing precipitation of sodium hydroxide.

Phosphorescence intensity and the effect of heavy atom. Su and Winefordner [8] showed that the iodide heavy-atom perturber is optimal for enhancement of PABA phosphorescence intensities; iodide was therefore chosen for this comparative evaluation. The r.t.p. intensities of pooled blank urine (pH 6.4) from fasting volunteer donors 0—6 h after their first morning voiding and the same urine containing 25 mg l^{-1} PABA were compared for both substrates with and without the addition of heavy atom. The results of this study are presented in Table 2. The DTPA-soaked S & S 903 paper demonstrated significantly greater r.t.p. signals than DE-81 in both blank ($P < 0.0025$) and spiked samples ($P < 0.0025$) as compared by the t-statistic. However, DE-81 paper showed a significantly greater heavy atom effect in both blank ($P < 0.0025$) and spiked urines ($P < 0.0025$).

Blanks in randomly collected urine samples. Urine from non-fasting persons may contain certain substances which cause background interference. These interferences could be minimized by the selectivity of the substrate for PABA. This potential interference was evaluated by collecting urine samples randomly from 13 non-fasting subjects and measuring r.t.p. signals from these samples, with and without iodide ion (Table 3). Each sample was evaluated individually by a paired *t*-test, which showed that r.t.p. intensities without iodide added were significantly higher for DTPA-impregnated S & S 903. The DE-81 demonstrated higher background when iodide was added, which follows the trend established for samples of pooled fasting subjects. The low background signals indicate good selectivity of the method.

TABLE 2

Comparison of phosphorescence intensities on DE-81 and DTPA-soaked S & S 903 substrates with and without heavy atoms[a]

Substrate	Blank urine				Urine with 25 μg ml^{-1} PABA			
	No I^-		1.0 M I^-		No I^-		1.0 M I^-	
	Mean RI	S.d.	Mean RI	S.d.	Mean RI	S.d.	Mean	S.d.
DE-81	1.1	0.2	3.3	0.6	65.7	4.4	429.8	8.0
S & S 903 (DTPA)	1.3	0.4	1.7	0.4	83.5	7.7	409.3	16.0

[a]RI, relative phosphorescence intensity; S.d., standard deviation (for $n = 10$).

TABLE 3

Background results for randomly collected urine samples from non-fasting subjects ($n = 13$)

	DE-81		S & S 903 (DTPA)		Paired t-test[a]
	Mean	S.d.	Mean	S.d.	
No I^-	1.3	0.3	1.5	0.3	($P < 0.005$)
1.0 M I^-	7.0	4.2	3.4	1.1	($P < 0.005$)

[a]P is the probability that the difference between means occurred by chance.

Linearity, recovery and detection limits. The standard graph for both substrates was linear over the range of approximately 0—40 mg l^{-1} for buffered aqueous standards. The ratio of the slope of the calibration curve of the phosphorescence of PABA, spotted from buffered aqueous solutions, to that spotted from urinary solution was 0.93 for DTPA-impregnated S & S 903 and 0.96 for DE-81, indicating good recovery of the method. The limit of detection in spotted aqueous samples was 0.26 mg l^{-1} with iodide and 1.70 mg l^{-1} without iodide for DE-81. The DTPA-impregnated S & S 903 paper demonstrated detection limits of 0.26 mg l^{-1} and 1.30 mg l^{-1} with and without iodide, respectively.

Conclusions

This study indicates that both types of filter papers are rather promising substrates for quantitation of urinary PABA, with DE-81 being superior in terms of pH variations; this is an important consideration because urine samples must be hydrolyzed in either strongly acidic or alkaline solution to convert PABA metabolites to PABA. Although DE-81 does show significantly higher background signals in the presence of iodide ion, these levels are a small fraction of the analyte signal and would not cause significant interference with regard to clinical interpretation. Impregnated S & S 903 paper has somewhat better drying characteristics but must be prepared, adding another step to the procedure. The DE-81 paper is inexpensive and commercially available. If all factors are considered, DE-81 seems slightly better suited for the described purpose although either substrate should be adequate.

This research was partly supported by NIH-5-R01-GM-11373-21.

REFERENCES

1 C. Arvanitakis and N. Greenberger, Lancet, i (1976) 663.
2 C. Lang, K. Gyr, G. A. Stalder and D. Gillessen, Br. J. Surg., 68 (1981) 771.
3 P. P. Toskes, Gastroenterology, 85 (1983) 565.
4 H. W. Smith, N. Finkelstein, L. Aliminosa, B. Crawford and M. Graber, J. Clin. Invest., 24 (1945) 388.
5 C. Yamato K. Kinoshita, Anal. Biochem., 98 (1979) 13.

6 C. Arvanitakis and A. R. Cooke, Gastroenterology, 74 (1978) 932.
7 R. M. A. von Wandruszka and R. J. Hurtubise, Anal. Chem., 98 (1977) 2164.
8 S. Y. Su and J. D. Winefordner, Can. J. Spectrosc., 28 (1983) 21.
9 J. L. Ward, R. P. Bateh and J. D. Winefordner, Analyst (London), 107 (1983) 335.
10 J. N. Miller, Trends Anal. Chem., 1 (1981) 31.
11 R. T. Parker, R. S. Freedlander and R. B. Dunlap, Anal. Chim. Acta, 119 (1980) 189.
12 R. P. Bateh and J. D. Winefordner, Talanta, 29 (1982) 713.

Analytica Chimica Acta, 164 (1984) 263—266
Elsevier Science Publishers B.V., Amsterdam — Printed in The Netherlands

Short Communication

SIMPLIFICATION OF THE ROBINSON-BIGGS SPECTROPHOTOMETRIC TREATMENT OF OVERLAPPING PROTOTROPIC EQUILIBRIA BY USE OF ISOSBESTIC POINTS

JEFFREY S. O'NEAL and STEPHEN G. SCHULMAN*

University of Florida, College of Pharmacy, Box J-4, J. Hillis Miller Health Center, Gainesville, FL 32610 (U.S.A.)

(Received 23rd January 1984)

Summary. The appearance and disappearance of isosbestic points between acid—base conjugate pairs of a diprotic acid with changing pH can be used to simplify the resolution of individual overlapping equilibria. Absorbance vs. pH data at an isosbestic wavelength can be treated in the same way as those from a monoprotic acid by using the Henderson—Hasselbalch equation. Application of the method is illustrated for hydroxy *N*-heterocycles having overlapping equilibria. Good precision and reasonable agreement with literature values was obtained for acidity constants determined by the method.

The traditional Robinson-Biggs spectrophotometric treatment of overlapping diprotic acid equilibria [1] involves simultaneous solutions at several H^+ concentrations of the equation

$$(a - \epsilon_{H_2A} C_T l)(H^+)^2 + (a - \epsilon_{HA} C_T l) K'_{a1} (H^+) + (a - \epsilon_A C_T l) K'_{a1} K'_{a2} = 0 \qquad (1)$$

in which C_T is the fixed formal concentration of the acid, H_2A, a is the absorbance, and K'_{a1} and K'_{a2} are the experimentally determined conditional acidity constants, uncorrected for ionic strength effects. Equation 1 is extremely tedious to solve for a substantial number of points. Moreover, this method suffers from a decrease in precision as overlap of the two inflection regions becomes smaller. This occurs as a result of the relative dominance of two of the three acid-base conjugates at any given pH in this pH range. As a result, the Robinson-Biggs approach works well when $pK'_{a2} - pK'_{a1} < 1.5$ and is unnecessary when $pK'_{a2} - pK'_{a1} > 4$ but leaves a great deal to be desired when $1.5 < pK'_{a2} - pK'_{a1} < 4$. Simplifications of the Robinson-Biggs approach have been developed [2, 3] but these apply to special cases. Attempts to reduce the Robinson-Biggs approach to the treatment of two separate monoprotic equilibria tend to be non-systematic and the limits of the validities of the approximations are usually uncertain.

This communication describes an alternative method which takes advantage of the appearance and disappearance, with changing pH, of isosbestic points between conjugate acid—base pairs. At high pH values, data at isosbestic wavelengths (where $\epsilon_{H_2A} = \epsilon_{HA}$) which are present at low pH may be used to

0003-2670/84/$03.00

obtain K'_{a2}. At these wavelengths, and at higher pH when new isosbestic points are formed, confirming the absence of H_2A, Eqn. 1 can be reduced to

$$(a - \epsilon_{HA}C_T l)K'_{a1}(H^+) + (a - \epsilon_A C_T l)K'_{a1}K'_{a2} = 0 \quad (2)$$

Equation 2 reduces, upon rearrangement, to the absorptiometric form of the Henderson-Hasselbalch equation:

$$pK'_{a2} = pH - \log [(a - a_{HA})/(a_A - a)] \quad (3)$$

in which a_{HA} is the absorbance when the isosbestic point is maintained (i.e., when $[H^+] \ll K'_{a2}$) and a_A is the absorbance at high pH, (i.e. $a_{HA} = \epsilon_{HA}C_T l$ and $a_A = \epsilon_A C_T l$) of the isolated conjugate base. It should be noted that the absorbance measurements in Eqn. 3 are all made at the isosbestic wavelength occurring at low pH. The isosbestic points appearing at high pH are simply a guide to when H_2A becomes experimentally negligible.

At low values of pH, data at wavelengths at which isosbestic points are formed at high pH can be treated similarly to obtain values for pK'_{a1}. At these wavelengths, the Robinson-Biggs equation reduces to

$$(a - \epsilon_{H_2A}C_T l)(H^+)^2 + (a - \epsilon_{HA}C_T l)K'_{a1}(H^+) = 0 \quad (4)$$

which can be rewritten as

$$pK'_{a1} = pH - \log [(a - a_{H_2A})/(a_{HA} - a)] \quad (5)$$

where $a_{H_2A} = \epsilon_{H_2A}C_T l$ is the absorbance when $(H^+) \gg K'_{a1}$ and $a_{HA} = \epsilon_{HA}C_T l$ is the absorbance when $(H^+) \ll K'_{a1}$.

Use of Eqns. 3 and 5 greatly simplifies the data analysis in two ways. First, the complex 3-component 2-equilibrium treatment entailed in the Robinson-Biggs equation is reduced to two 2-component, single-equilibrium problems. The range of pH over which each 2-component equilibrium can legitimately be treated as such is clearly indicated by the appearance and disappearance of isosbestic points. Secondly, the Robinson-Biggs equation contains three unknowns, namely, K'_{a1}, K'_{a2} and, because HA cannot be isolated at any given pH, ϵ_{HA}. Previous simplifications of the Robinson-Biggs equation [2, 3] in effect reduced the 3-parameter equations to two 2-parameter equations, one containing K'_{a1} and ϵ_{HA} as unknowns and the other containing K'_{a2} and ϵ_{HA} as unknowns. However, in the present treatment, because $\epsilon_{H_2A} = \epsilon_{HA}$ at one of the isosbestic points and $\epsilon_{HA} = \epsilon_A$ at the other, the absorptivities measured at the low and high pH extremes of pH will give ϵ_{HA} unequivocally in each case. Hence, the reduction of the Robinson-Biggs equation here is from an equation with three unknowns to two equations, each with one unknown. The limitations of the proposed method are the possibility of only a single wavelength for which calculations can be done if not more than one isosbestic point can be located at each pH extreme (as for small aromatic systems) and the usual errors inherent to spectrophotometry at a single nominal wavelength.

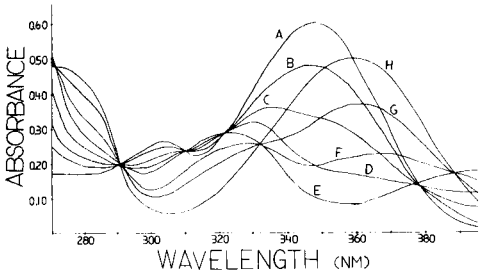

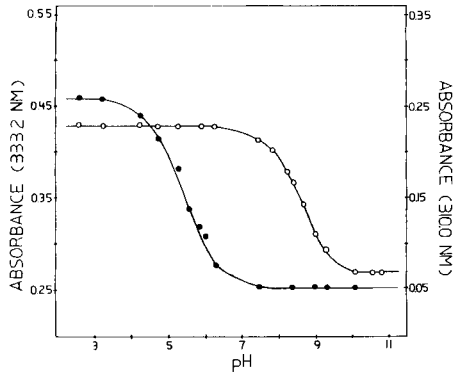

Fig. 1. Dependence of the electronic absorption spectra of 7-quinolinol on pH. pH values: (A) 2.80; (B) 4.82; (C) 5.29; (D) 6.05; (E) 6.22; (F) 8.47; (G) 9.04; (H) 11.01.

Fig. 2. Variation of absorbance with pH of 7-quinolinol at the isosbestic wavelengths of 333.2 nm (•) and 310.0 nm (○).

Experimental

5-Quinolinol and 5-isoquinolinol were obtained from Aldrich Chem. Co. The 5-quinolinol was preparatively purified on Mallinckrodt Silicar special-grade silica gel with chloroform/methanol (99:1) as mobile phase. The 5-isoquinolinol was similarly purified but with a gradient mobile phase from 100% chloroform to chloroform/methanol (80:20). Thin-layer chromatography showed a single spot on Whatman MK6F silica plates with a chloroform/methanol (95:5) mobile phase. 7-Quinolinol (Pfaltz and Bauer) was preparatively purified on the above-mentioned Silicar gel with 100% chloroform mobile phase. 3-Pyridinol (Pfaltz and Bauer) was recrystallized three times from ethanol.

Absorption spectra were obtained with a Beckman Model 25 spectrophotometer, at 21°C, at a constant ionic strength of 0.010 M (sodium perchlorate).

Results

A representative set of pH-dependent absorption spectra of 7-quinolinol illustrates the pertinent isosbestic points used for calculations (Fig. 1). Absorbance vs. pH data for 7-quinolinol at the isosbestic wavelengths of 333.2 nm and 310.0 nm are depicted in Fig. 2. Some pK_a values calculated by the proposed method are listed in Table 1. These pK_a values are in reasonable agreement with literature values obtained by the potentiometric method at 20°C [4, 5] and demonstrate the precision typical of dissociation constants derived from spectrophotometric evaluations of monoprotic equilibria.

TABLE 1

Values of pK_a calculated for several compounds at several isosbestic wavelengths

Compound	Isosbestic point (nm)	No. of data points used This work	pK_{a1} This work[a]	pK_{a2} This work[a]	pK_a Literature value[b]
3-Hydroxypyridine	234.5	(7)	8.70 ± 0.02		8.72 [4]
	279.0	(5)	4.91 ± 0.05		4.86 [4]
5-Isoquinolinol	346.6	(6)		8.35 ± 0.05	8.45 [5]
	264.5	(9)	5.30 ± 0.05		5.40 [5]
5-Quinolinol	326.5	(6)	5.18 ± 0.04		5.20 [4]
	270.0	(6)	5.17 ± 0.06		
	338.0	(6)		8.33 ± 0.02	8.54 [4]
7-Quinolinol	271.8	(5)	5.47 ± 0.03		5.48 [4]
	333.2	(6)	5.48 ± 0.09		
	310.0	(7)		8.61 ± 0.05	
	374.0	(7)		8.61 ± 0.04	8.85 [4]

[a] ± 95% confidence interval; corrected by Debye—Hückel approximation for ionic strength effects. [b] Reference is given in brackets.

REFERENCES

1 R. A. Robinson and A. I. Biggs, Aust. J. Chem., 10 (1957) 128.
2 B. J. Thamer and A. F. Voigt, J. Phys. Chem., 56 (1952) 225.
3 K. P. Ang, J. Phys. Chem., 62 (1958) 1109.
4 A. Albert and J. N. Phillips, J. Chem. Soc., (1956) 1294.
5 S. F. Mason, J. Chem. Soc., (1958) 674.

Analytica Chimica Acta, 164 (1984) 267—271
Elsevier Science Publishers B.V., Amsterdam — Printed in The Netherlands

Short Communication

A SPECTROSCOPIC STUDY OF DYES: MECHANISM OF DETECTION OF NONABSORBING ANALYTES IN REVERSE-PHASE CHROMATOGRAPHY WITH THE AID OF CHROMOPHORES

G. K. VEMULAPALLI*

Department of Chemistry, University of Arizona, Tucson, AZ 85721 (U.S.A.)

T. GNANASAMBANDAN

Department of Pharmaceutical Sciences, University of Arizona, Tucson, AZ 85721 (U.S.A.)

(Received 3rd April 1984)

Summary. In order to understand the mechanism by which dyes assist chromatographic detection in reverse-phase systems, absorption spectra of brilliant green and methylene blue were investigated. It is shown that dye-assisted chromatographic detection depends on the ability of the analyte to shift the monomer-dimer equilibrium of the dyes toward greater monomer concentrations. Monomers have higher molar absorptivities than dimers. Equilibrium constants and molar absorptivities for monomeric and dimeric forms of the dyes are reported.

Compounds that do not absorb in the visible-ultraviolet part of the spectrum or absorb at widely different wavelengths offer special difficulties for detection following chromatographic separation. In the first case, detection by absorption becomes impossible and in the second case, cumbersome. Such compounds are usually detected by monitoring the refractive index of the eluted sample. A method that promises higher sensitivity and greater ease of detection involves using dyes or other molecules with chromophores as probe molecules [1—3] in the mobile phase. It was recently shown that the absorption of methylene blue and brilliant green can be used for detection of aliphatic compounds that are separated on a chromatographic column [1]; the enhanced absorption of the probe molecule in the presence of the nonabsorbing compounds in the eluate is detected.

While the technique is known to work reliably, the mechanisms by which probe molecules affect separation and facilitate detection have not been systematically investigated. It has been realized that dyes are adsorbed on the stationary phase of the chromatographic column and hence dyes could affect the separation. Complex formation between probe molecule and analyte has been suggested as an explanation for enhanced absorbance but this has not been proved experimentally. A spectroscopic investigation that shows conclusively the function of dyes in the detection of analytes is

0003-2670/84/$03.00

presented below. The results indicate that the dyes dimerize appreciably at the concentrations used in the chromatographic experiments and that dimerization leads to reduction of apparent molar absorptivity. Aliphatic compounds enhance the absorbance of dye solutions by reducing the dimer concentration and increasing the monomer concentration. Although it is known that dyes and many other organic molecules dimerize in aqueous media [4—8], the relation between dimer equilibrium and chromatographic detection has not been studied previously.

Experimental

Analytical-grade methylene blue (J. T. Baker) and brilliant green (Eastman) were used as received. Baker Analyzed grade analytes were used. A Cary 219 u.v.-visible spectrophotometer (Varian Associates) was used with 0.1-, 1- and 10-cm path-length cells.

Working solutions were prepared by diluting stock 10^{-3} M solutions. Monomer—dimer equilibria were established rapidly for methylene blue solutions but not for brilliant green solutions. The latter, therefore, were diluted one day prior to measurements. All measurements were made at ambient temperature ($\approx$24°C).

Results and discussion

Brilliant green. The absorption spectrum of brilliant green in the visible region (Fig. 1) includes a broad peak at 624 nm and a shoulder at 580 nm. The absorbance does not follow Beer's law even at moderately low concentrations. Because molar absorptivity should not depend on concentration in the absence of significant intermolecular interactions, the deviation from Beer's law is attributed to formation of dimeric dye molecules. This hypothesis quantitatively accounts for the observed concentration dependence of the molar absorptivity. Dimerization leads to lowering of the apparent molar absorptivity (hypochromism) and sometimes to marked splitting of the monomer absorption band.

Deviation from Beer's law was found to be insignificant at brilliant green concentrations of $\leqslant 5 \times 10^{-6}$ M. Hence, the molar absorptivity of the monomer form at 624 nm, ϵ_M, was found to be $(1.04 \pm 0.03) \times 10^5$ l mol^{-1} cm^{-1} from the absorbance values at and below concentrations of 5×10^{-6} M. Absorbance of brilliant green is related to concentration by $A = [M]\epsilon_M + 2[D]\epsilon_D$, when the path length is 1.0 cm; $[M]$ and $[D]$ are the concentrations of the dye monomer and dimer and ϵ_D is the molar absorptivity per monomer unit in the dimer. Because both the absorptivity and the concentration of dimer are unknown, the equilibrium constant for dimerization cannot be directly calculated from the absorbance values. To circumvent this, the following approach was adopted.

The equilibrium constant, K_{BG}, for dimerization of brilliant green is given by $K_{BG} = [D]/[M]^2 = ([T] - [M])/2[M]^2$ where $[T]$ is the total concentration of the dye if it were to exist completely as the monomer. A series

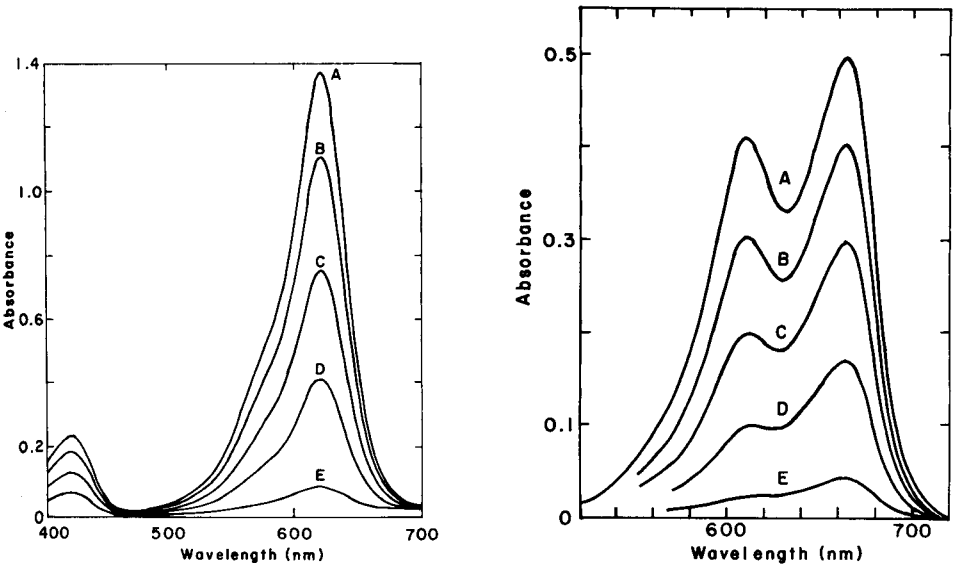

Fig. 1. Absorption spectrum of brilliant green in deionized water. Path length 1 cm. Concentration (10^{-5} M): (A) 2.0; (B) 1.5; (C) 1.0; (D) 0.5; (E) 0.1.

Fig. 2. Absorption spectrum of methylene blue in deionized water. Path length 0.1 cm. Concentration (10^{-5} M): (A) 20; (B) 15; (C) 10; (D) 5.0; (E) 1.0.

of trial values was assumed for K_{BG}, and $[M]$ and $[D]$ were calculated from this equation. From these values and the above absorbance expression, ϵ_D values were calculated. This was done for $[T] = 1 \times 10^{-4}$ M and 1×10^{-5} M. When the trial K_{BG} values were plotted against calculated ϵ_D values, these two concentrations gave different curves, which intersected at $K_{BG} = 1.4 \times 10^4$ l mol^{-1} and $\epsilon_D = 29\,400$ l mol^{-1} cm^{-1}. These should be the correct values for the equilibrium constant and the molar absorptivity of the dimer. These values of K_{BG}, ϵ_M and ϵ_D were then used to calculate absorbance at four other concentrations. The calculated and the experimental values of absorbance did not differ significantly (average deviation between experimental and calculated was 5.6%), which indicates that aggregates higher than dimers are not formed in any appreciable concentrations.

According to the exciton theory, hypochromism in dimers results from interaction of the transition dipoles of the two molecules in the dimer [5, 6]. If $\vec{M}$ is the transition moment of the dimer and $\vec{m}_1$ and $\vec{m}_2$ are the transition moments of the molecules in the dimer, then $\vec{M} = \vec{m}_1 \pm \vec{m}_2$. From this, the angle θ between the transition moments of the two molecules is $\theta/2 = \cos^{-1}(M/2m)$. When the transition moments determined from the spectra are substituted into this expression, the value obtained is 120°. The transition moment of brilliant green at 624 nm is very likely in the plane of the three rings. Hence one possibility for the structure of the dimer is a stack of

two molecules, one plane on top of the other, with the ethylamino groups of the two molecules at 120° from each other. Other structures consistent with $\theta = 120°$ could also be proposed.

Methylene blue. Dimerization of this dye and thionine was investigated in the pioneering work of Rabinowitch and Epstein [4]. Equilibrium constant and absorptivities were obtained in this study by extrapolating the absorbance values, from a relatively small range of concentrations, to zero and infinite concentration. The equilibrium constant and absorptivities were redetermined using the procedure outlined above.

Figure 2 shows the absorption spectrum of aqueous solutions of methylene blue at different concentrations; there are two broad peaks at 660 and 605 nm. The relative intensities of these bands depend on the concentration of the dye and Beer's law is severely violated at both wavelengths. At low concentrations, the 660-nm band is very prominent; at higher concentrations, the 605-nm band becomes more intense and is assigned to a dimer of methylene blue. Because the absorbance at 605 nm nearly disappears at low concentrations ($\leqslant 5 \times 10^{-7}$ M), this band does not belong to monomer spectrum. Hence $A_{605} = 2\epsilon_{D,605}[D]$. As before, several trial values for K_{MB} were assumed and C_M, C_D and $\epsilon_{D,605}$ were calculated for two different total concentrations ($C_T = 1 \times 10^{-4}$ M and 1×10^{-5} M). These calculations gave the values $K_{MB} = 3.2 \times 10^6$ l mol^{-1} and $\epsilon_{D,605} = 2.1 \times 10^4$ l mol^{-1} cm^{-1}.

Molar absorptivity values were calculated for four other concentrations of methylene blue using the above K_{MB} value. The average of these values was $2.05 \pm 0.06 \times 10^4$ l mol^{-1} cm^{-1} which is in good agreement with the above value of molar absorptivity. Therefore, aggregates higher than dimers play no significant role in methylene blue spectrum. The values reported by Rabinowitch and Epstein were $\epsilon = 1.57 \times 10^4$ and $K_{MB} = 3.6 \times 10^3$.

Absorbance at 660 nm is given by $A_{660} = [M]\epsilon_{M,660} + 2[D]\epsilon_{D,660}$ for a 1-cm path length. From this equation and $K = 3.2 \times 10^6$, the values obtained were $\epsilon_{D,660} = 1.7 \times 10^4$ and $\epsilon_{M,660} = 3.1 \times 10^5$ l mol^{-1} cm^{-1}. These results cannot be compared with those reported by Rabinowitch and Epstein because they assumed that the dimer does not absorb at 660 nm. From the equation for $\theta/2$, $\epsilon_{D,605}$ and $\epsilon_{M,660}$, the angle between the two transition moments is 150°. A structure for the dimer that is consistent with this result is one in which the planes of the two molecules are parallel to each other and the nitrogen-sulfur axes of the molecules are at 150° to one another.

Interactions with hydrocarbons. The effects of the progressive addition of several aliphatic compounds to methylene blue and brilliant green solutions were studied. In the case of methylene blue, the dimer peak at 660 nm decreases and the peak at 605 nm increases with the addition of the aliphatic compounds. For example, absorbances in 1-cm cells for 10^{-5} M solutions of methylene blue increased linearly from 0.525 to 0.730 as the 2-propanol concentration was increased from zero to 5.2×10^{-3} M.

In the case of brilliant green, absorbance of the band at 624 nm increases with increasing concentration of aliphatic compounds. For example,

absorbances of 10^{-4} M solution of brilliant green in a 0.1-cm cell increased linearly from 0.428 to 0.505 as the n-butanol concentration was increased from zero to 8.6×10^{-2} M. As was shown earlier, both monomer and dimer absorb at this wavelength with the monomer having a higher molar absorptivity.

No new visible or near-ultraviolet bands were observed when aliphatic compounds were added to methylene blue or brilliant green solutions.

These observations are attributed to a shift (by aliphatic compounds) of the monomer—dimer equilibrium of the dyes toward greater monomer concentration. The results indicate that specific interactions between the dyes and aliphatic compounds are insignificant. It is suggested, therefore, that aliphatic compounds shift the monomer—dimer equilibrium towards formation of monomer and thus enhance the absorbance of the dyes, and that this is the mechanism by which aliphatic compounds are detected in dye-assisted chromatography.

Conclusions

The work reported here suggests the possibility of lowering the detection limits very significantly. It is well known that dyes used in tunable lasers (brilliant green is one such dye) exhibit monomer—dimer equilibria. The laser action is solely due to monomers because dimers have very low fluorescence quantum yields [9]. Detection of the analytes depends on their ability to increase monomer concentration. Hence these analytes, if present in the cavity of dye laser, could significantly alter lasing properties.

We are indebted to Professor M. F. Burke for encouragement and Professor Quintus Fernando for encouragement and constructive criticism.

REFERENCES

1 T. Gnanasambandan and H. Freiser, Anal. Chem., 53 (1981) 909.
2 L. Hackzell and G. Schill, Chromatographia, 15 (1982) 437.
3 T. Gnanasambandan and H. Freiser, Anal. Chem., 54 (1982) 1282.
4 E. Rabinowitch and L. Epstein, J. Am. Chem. Soc., 63 (1941) 69.
5 E. G. McRae and M. Kasha, Physical Processes in Radiation Biology, Academic Press, New York, 1964, p. 23.
6 A. R. Monahan, N. J. Germano and D. F. Blossey, J. Phys. Chem., 75 (1971) 1227.
7 K. K. Rohatgi and G. S. Singhal, J. Phys. Chem., 70 (1966) 1695.
8 J. E. Selwyn and J. I. Steinfeld, J. Phys. Chem., 76 (1972) 762.
9 K. H. Drexhage, in F. P. Schäfer (Ed.), Dye Lasers, Springer-Verlag, Berlin, 1977, p. 158.

Analytica Chimica Acta, 164 (1984) 273—277
Elsevier Science Publishers B.V., Amsterdam — Printed in The Netherlands

Short Communication

MICROBIOLOGICAL ASSAY OF ANTIBIOTICS BASED ON INHIBITION OF AMMONIA PRODUCTION MONITORED WITH AN AMMONIA ELECTRODE

D. L. SIMPSON and R. K. KOBOS*[a]

Department of Chemistry, Virginia Commonwealth University, Richmond, VA 23284 (U.S.A.)

(Received 5th January 1984)

Summary. A potentiometric method with an ammonia gas sensor is described for the microbiological assay of tetracycline hydrochloride, gentamicin, streptomycin, and neomycin in pharmaceutical preparations. The method is based on the inhibiting effect of antibiotics on the production of ammonia by a suspension of *Escherichia coli* in a nutrient solution.

Traditional microbiological assays for antibiotics which are based upon the inhibition of growth of a sensitive microorganism require incubation times of 18—24 h [1]. However, changes in metabolic activity which occur in the presence of these inhibiting substances can be detected long before any cell growth can be observed. Therefore, the amount of time required for a microbiological assay can be significantly reduced by monitoring a metabolic process that is affected by the antibiotic. For example, respirometric assays based on spectrophotometric [2—6] and electrochemical [7, 8] measurements have been developed which provide results within 2 h. A respirometric method for antibiotics based on a potentiometric carbon dioxide sensor was recently reported [9, 10]. Other potentiometric methods have been reported for antibiotics and amino acids [11—14].

This communication describes the development of a novel microbiological method for the assay of pharmaceutical preparations. The method is based on antibiotic inhibition of ammonia production by a suspension of *Escherichia coli* in a nutrient solution with potentiometric detection of ammonia. This method is more sensitive for the antibiotics studied than the previously reported method [9, 10].

Experimental

Apparatus. An Orion Model 95-10 ammonia gas sensor was used with a Corning Model 130 pH/mV meter to monitor the ammonia produced by the bacterial cells. Potentiometric measurements were made in a sealed cell

[a]Present address: E. I. duPont de Nemours and Co., Experimental Station, Biomedical Products Dept., Wilmington, DE 19898.

0003-2670/84/$03.00

thermostated at 25.0 ± 0.5°C. Prior to the ammonia measurement, the bacterial cell suspensions were incubated with peptone—antibiotic mixtures in a Lab-Line Orbit shaker bath at a selected temperature controlled to ±1°C. Bacterial cell suspensions were standardized and measured by turbidimetry with a Beckman Model DB-G spectrophotometer with 1-cm silica cells [10].

Reagents. All chemicals used were of reagent grade. Solutions were prepared in distilled-deionized water. The antibiotics tested were reference-grade gentamicin sulfate (10 mg ml^{-1}; Sigma Chemical Company), streptomycin sulfate (740 $\mu g\ mg^{-1}$), neomycin sulfate (681 $\mu g\ mg^{-1}$) and tetracycline hydrochloride (980 mg g^{-1}); all from ICN Life Sciences. The Schering Garamycin Pediatric Dose (10 mg ml^{-1}), which was used for the bioassay of a gentamicin pharmaceutical preparation, was obtained from the Medical College of Virginia Commonwealth University. Freeze-dried sera used in optimization studies were Normal Human Serum Control Type 1A (Sigma Chemical Company) and Validate Normal and Abnormal Human Controls (General Diagnostics). The human blood plasma used in the optimization studies and the gentamicin bioassays was obtained from the Medical College of Virginia Commonwealth University. The bacteria used were *Escherichia coli* ATCC 9637, 25922, and 23716 (American Type Culture Collection, Rockville, MD).

Procedures. The bacteria *E. coli* ATCC 9637 and 23716 were grown in nutrient broth at 37°C for 20—24 h, whereas the *E. coli* ATCC 25922 was grown in trypticase soy broth at 37°C for 20—24 h. The bacterial cell suspensions were prepared and stored as previously described [9].

The response of the system was optimized for tetracycline hydrochloride and gentamicin as previously described [9, 10]. Prior to the potentiometric measurements, sodium hydroxide was added to the measurement cell to adjust the pH to >12. The ammonia concentrations were obtained from the measured potentials and the average of two daily calibration curves.

The method was tested by assaying a pharmaceutical preparation of gentamicin sulfate under the conditions found to be optimal for gentamicin. A 2 × 2 parallel line bioassay [9, 10, 15] was done using two dose levels each for standard and sample solutions.

For the assays of gentamicin in blood, a separate study of the log dose/response curve was done as a function of plasma or serum type, plasma dilution level, bacterial cell concentration, and peptone concentration to establish the optimum assay conditions. The plasma gentamicin assays were based on a calibration curve [10].

Results and discussion

Because the proposed method has no literature basis, several bacterial strains had to be screened for their ability to produce ammonia and their sensitivity to antibiotics. The bacterium used earlier, *E. coli* ATCC 9637, was found to be unsuitable in the new system because of its very narrow range of response; *E. coli* 23716 was found to produce the best response to the antibiotics tested. Consequently, this strain was used in all further studies.

A study of the effects of incubation parameters demonstrated that the optimum conditions for the bioassay of pharmaceutical preparations of gentamicin are: temperature 37°C, time 120 min, stock cell concentration 1.6×10^8 cells ml^{-1}, stock peptone concentration 6%, and pH 7.8. The effect of cell concentration on the gentamicin log dose/response curve is shown in Fig. 1. The optimum cell concentration of 1.6×10^8 cells ml^{-1} was chosen because it provided the highest sensitivity over the widest concentration range. The incubation pH, in the range of 7.0—7.8, had little effect on the gentamicin log dose/response curve. A pH of 7.8 was chosen because the recommended pH range for the bioassay of gentamicin is 7.8—8.0 [16]. As shown in Fig. 2, a reduction in pH from 7.8 to 7.0 produced a significant increase in the linear range and the slope of the tetracycline hydrochloride log dose/response curve. Therefore, a pH of 7.0 is optimal for a tetracycline HCl bioassay. The log dose/response curves for streptomycin and neomycin were established under the conditions optimal for gentamicin.

The linear ranges and slopes of the log dose/response curves obtained for the antibiotics tested are shown in Table 1. The results for the previously reported (CO_2) system [9, 10] are provided for comparison. As can be seen, the sensitivities, given by the slopes, are greater by a factor of 1.4—2.1 for the new ammonia system. The linear ranges are also changed, but not in a consistent manner. The range for gentamicin was diminished in the ammonia system because of an increase in the lower limit of detection.

The results of the bioassay of gentamicin in a pharmaceutical preparation are presented in Table 2. The potency found was in excellent agreement with the label claim and is well within the uniformity of content for individual

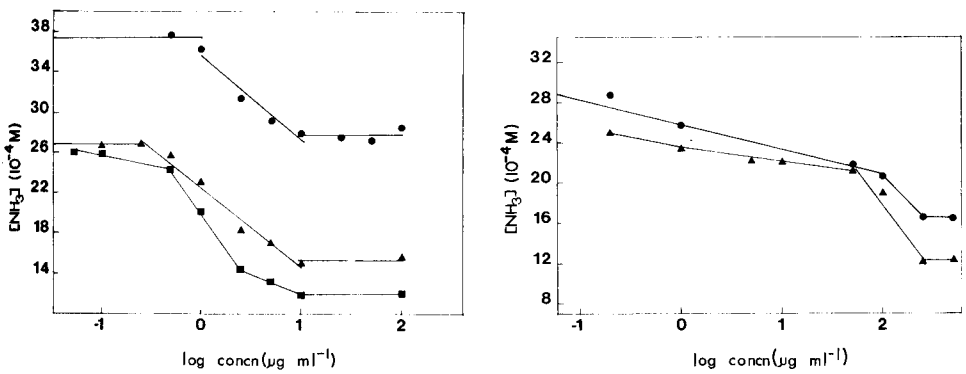

Fig. 1. Log dose/response curves for gentamicin with *E. coli* ATCC 23716 at different stock cell concentrations: (■) 0.8×10^8; (▲) 1.6×10^8; (●) 3.2×10^8 cells ml^{-1}. Experimental conditions: 2-h incubation, 37°C, pH 7.8, μ = 0.1 M, stock peptone concentration 6%.

Fig. 2. Log dose/response curves for tetracycline hydrochloride with *E. coli* ATCC 23716: (▲) at pH 7.0; (●) at pH 7.8. Experimental conditions: 2-h incubation, 37°C, μ = 0.1 M, stock peptone concentration 6%, stock cell concentration 1.6×10^8 cells ml^{-1}.

TABLE 1

Comparison of slopes and ranges for antibiotics and measurement systems

Antibiotic	System	Slope[a] (10^{-4} M/decade)	Range ($\mu g\ ml^{-1}$)
Tetracycline HCl	CO_2	−6.26 (0.93)	33—167
	NH_3	−13.3 (0.98)	16.7—83.3
Gentamicin	CO_2	−3.80 (0.95)	0.017—3.33
	NH_3	−7.97 (0.99)	0.083—3.33
Streptomycin	CO_2	−3.74 (0.96)	0.33—16.7
	NH_3	−5.24 (0.99)	0.33—33.3
Neomycin	CO_2	−6.88 (0.98)	0.17—3.33
	NH_3	−13.1 (0.998)	0.33—3.33

[a]Figures in parentheses are correlation coefficients for least-squares treatment.

TABLE 2

Results of bioassay of gentamicin in Schering Garamycin Pediatric Dose (10 mg ml^{-1}, 2 ml)

Sample	Run no.	Slope (10^{-4} M/decade)	Potency (mg ml^{-1})	Label claim (%)
Reference	1	−8.28		
Sample	1	−7.58	10.02	100.2
Pooled	1	−7.93		
Reference	2	−9.06		
Sample	2	−8.86	9.78	97.8
Pooled	2	−8.96		
Reference	3	−7.40		
Sample	3	−7.87	9.72	97.2
Pooled	3	−7.14		
Reference	Ave	−8.25 ± 0.83[a]		
Sample	Ave	−7.77 ± 1.02	9.84 ± 0.19[b]	98.4 ± 1.9[b]
Pooled	Ave	−8.01 ± 0.91		

[a]Standard deviation. [b]95% Confidence limits.

capsules as defined by U.S.P. [17]. Furthermore, the results obtained in the gentamicin bioassay are more accurate and precise than those obtained with the potentiometry-based respirometry system [10]. The validity of the gentamicin bioassay was verified by an analysis of variance (ANOVA) [15].

The preliminary studies for the bioassay of gentamicin in blood were done with three types of freeze-dried sera and a frozen plasma sample. Because *E. coli* 23716 does not possess urease activity and the ammonia level in blood is normally very low, pretreatment of the blood samples to remove urea or ammonia was not necessary. This is an advantage of the ammonia

system over the previously reported system [10], which required the removal of hydrogencarbonate.

The effect of the presence of blood on the slope and linear range of the log dose/response curve and the total ammonia produced varied with the type of blood sample used. This effect is not understood at this time, although similar results were obtained with the earlier system [10]. In the case of the plasma sample, dilution (1 + 4) was required to cover the therapeutic gentamicin range (1—20 μg ml^{-1}); optimum response was obtained with a stock bacterial cell concentration of 3.2×10^8 cells ml^{-1} and a stock peptone concentration of 9%. The linear range for these conditions was 1—25 μg ml^{-1}.

The results of the bioassay of gentamicin in two plasma samples were less satisfactory. The precision obtained in the assays was good but the accuracy was poor. For example, in two separate samples, the gentamicin potencies were found to be 4.93 ± 0.83 and 16.0 ± 1.26 μg ml^{-1} (mean and standard deviation of 3 determinations) whereas the actual values were 7.41 and 19.6 μg ml^{-1}, respectively. Further study is obviously needed.

Although the potentiometric bioassay method reported here was specifically designed to determine antibiotics, the method is a general one which could be applied to the determination of other antimicrobial agents such as environmental pollutants, toxins, and chemical warfare agents. The method could also be useful for the rapid screening of potential therapeutic agents.

We thank Berry Kline, Department of Pharmacy and Pharmaceutics, for his suggestions and encouragement. We acknowledge the financial support of Philip Morris, Inc. and the National Science Foundation (Grant No. CHE-8215809). D. L. S. was on sabbatical leave from Philip Morris, Inc.

REFERENCES

1 F. Kavanagh, in J. H. Hash (Ed.), Methods in Enzymology, Vol. 43, Academic Press, New York, 1975, p. 55.
2 R. Dewart, F. Nandts and W. Lhoest, Ann. N.Y. Acad. Sci., 130 (1965) 686.
3 W. H. Shaw and R. E. Duncombe, Ann. N.Y. Acad. Sci., 130 (1965) 647.
4 W. H. Shaw and R. E. Duncombe, Analyst (London), 88 (1963) 694.
5 V. J. Greely, W. W. Hall, T. P. Michaels and L. P. Sinotte, Ann. N.Y. Acad. Sci., 130 (1965) 657.
6 T. A. Haney, J. R. Gerke, M. E. Madigan and J. F. Pagano, Ann. N.Y. Acad. Sci., 93 (1962) 627.
7 I. Karube, T. Matsunaga and S. Suzuki, Anal. Chim. Acta, 109 (1979) 39.
8 R. K. Kobos, Trends Anal. Chem., 2 (1983) 154.
9 D. L. Simpson and R. K. Kobos, Anal. Lett., 15 (1982) 1345.
10 D. L. Simpson and R. K. Kobos, Anal. Chem., 55 (1983) 1974.
11 T. Matsunaga, I. Karube and S. Suzuki, Anal. Chim. Acta, 99 (1978) 233.
12 S. Faine and D. C. Knight, Lancet, 2(7564) (1968) 375.
13 T. Matsunaga, I. Karube, N. Teraoka and S. Suzuki, Anal. Chim. Acta, 127 (1981) 245.
14 P. Noone, J. R. Pattison and J. R. Samson, Lancet, 2(7714) (1971) 16.
15 A. Goldstein, Biostatistics: An Introductory Text, Macmillan, New York, 1964, Ch. 4.
16 B. Arret, D. P. Johnson and A. Kirshbaum, J. Pharm. Sci., 60 (1971) 1689.
17 United States Pharmacopeia, United States Pharmacopeial Convention, Rockville, MD, 1980, 20th Rev., p. 956.

Analytica Chimica Acta, 164 (1984) 279—282
Elsevier Science Publishers B.V., Amsterdam — Printed in The Netherlands

Short Communication

DETERMINATION OF SELECTIVITY COEFFICIENTS OF ION-SELECTIVE ELECTRODES BY A MATCHED-POTENTIAL METHOD

V. P. Y. GADZEKPO[a] and G. D. CHRISTIAN*
Department of Chemistry BG-10, University of Washington, Seattle, WA 98195 (U.S.A.)
(Received 29th February 1984)

Summary. A new method is proposed for the determination of selectivity coefficients of ion-selective electrodes. A reference solution of the primary ion is used and potential changes are measured after adding either the primary ion or secondary ion. Increasing concentrations of the secondary ion are added to provide the same potential change as obtained for a fixed added concentration of the primary ion. The ratio of the primary-to-secondary ion concentrations for this potential change represents the selectivity coefficient. This method is illustrated by the use of a sodium glass electrode and a potassium valinomycin electrode. Results obtained are compared with those from conventional determinations of selectivity coefficients. The advantages of this method are discussed.

The selectivity coefficient ($K^{Pot}_{A,B}$) is used to express the degree of selectivity of an ion-selective electrode for an interfering ion, B, with respect to the primary ion, A. $K^{Pot}_{A,B}$ is defined by the general equation

$$E = E^0 \pm 2.303\, RT/z_A F \log (a_A + \sum K^{Pot}_{A,B} a_B^{z_A/z_B}) \quad (1)$$

where z_A and z_B are the charges on the ions A and B and E^0 is the standard potential of the electrode or a constant. The selectivity coefficient will be less than unity if the electrode is more responsive to ion A than to ion B and greater than one if it is more responsive to ion B in comparison with A. The value of $K^{Pot}_{A,B}$ is generally not constant for all activities of A and B [1]. Moody et al. [2] showed a typical spread of $K^{Pot}_{A,B}$ values with the calcium ion-selective electrode. The variations in $K^{Pot}_{A,B}$ have been explained [3] as being due to the changing environment of the ion in solution and to the mechanism of the electrode response. Selectivity coefficient values are therefore very dependent on the method used to determine them, making it very difficult to apply or rely on $K^{Pot}_{A,B}$ values quoted in the literature, and it is very important to know the details of the method of determining any quoted values.

To develop ion-selective electrodes for real situations, the $K^{Pot}_{A,B}$ may be deceptive because the matrices are often different. It is important to have a

[a]Present address: Department of Applied Chemistry, UWIST, Cardiff, Great Britain.

0003-2670/84/$03.00

parameter that could clearly give the user an idea of the performance of the electrode in terms of selectivity. The determination of selectivity coefficient by a matched-potential method is proposed here.

Selectivity coefficients evaluated by this method are reported for potassium, calcium and magnesium relative to sodium for a sodium glass electrode and for sodium, calcium and magnesium relative to potassium for a potassium valinomycin electrode. The values obtained are compared with the values from the mixed solution and separate solution methods. The values obtained for the potassium valinomycin electrode are compared with values reported in the literature.

Principle of method

Selectivity coefficients can be defined as the ratio of the primary ion concentration to the interfering ion concentration which gives the same potential change in a reference solution. This definition is similar but not identical to that of Rechnitz et al. [4] who defined the selectivity coefficient as the ratio of interferent ion concentration to primary ion concentration required to yield the same cell e.m.f. under otherwise identical conditions. To determine the selectivity coefficient by the proposed method, one would measure the change in potential upon changing the primary ion concentration. The interfering ion would then be added to an identical reference solution until the same potential change is obtained. The change in potential must be produced in a constant initial background of the primary ion and must be the same in both cases.

In this method, both monovalent and divalent ions are treated in the same manner. There is no need to take the valence of the ions into consideration as indicated by Moody et al. [2]. This method, therefore, does not assume that the slope for both primary and interferent ions are the same nor even Nernstian.

Experimental

The electrodes used were a sodium glass electrode and potassium valinomycin electrode (Beckman Instruments). The e.m.f. was measured with a Beckman Model 4500 digital pH meter.

Chloride salts were used as source of the cations studied and all stock solutions were prepared from reagent-grade chemicals and deionized water. Concentrated stock solutions were used for spiking so that volume changes could be neglected.

Selectivity coefficients were determined by the mixed-solution method [5, 6], the separate-solution method [2, 7] and the matched-potential method. For the separate-solution method with the interferent ion being a divalent cation, and with equal concentrations of the primary and interfering ions, the following equation was used

$$\log K^{\mathrm{Pot}}_{\mathrm{A,B}} = [(E_{\mathrm{B}} - E_{\mathrm{A}})/2.303\, RT/z_{\mathrm{A}}F] + 1/2 \log a$$

where E_{B} is the potential of the electrode in a solution containing only the

divalent interferent ion, E_A is the potential of the cell containing only the primary ion, and a is the activity of the ions used for measurements; z_A is unity.

For the mixed-solution method, potentials were measured in a constant background of the particular interferent ion. The concentrations of interferent ions were such as would be found in blood serum, i.e., K^+ (5.5×10^{-3} M), Na^+ (0.140 M), Ca^{2+} (2.5×10^{-3} M) and Mg^{2+} (2.4×10^{-3} M).

Results and discussion

The selectivity values given in Table 1 emphasize the variations in selectivity for the sodium glass electrode evaluated by the different methods. The values from the matched-potential method are consistently lower than the other values, i.e., higher selectivities toward sodium. This may be due to the fact that little rearrangement occurs on the membrane surface because the membrane has been soaked in the primary ion solution before use and the reference solution contains primary ions. In most other methods, the electrode is exposed to the interfering ion alone for a period of time, even before being spiked by the primary ion in the case of the mixed-solution method. This causes the membrane surface to rearrange, causing more active sites to be occupied by the interfering ion and also displacing some of the primary ions. Accordingly, the electrode becomes more selective toward the interfering ion and so less selective for the primary ion.

This method of selectivity evaluation offers a number of advantages. It does not assume that the slope of the electrode response for the interferent is equal to or a multiple of that for the primary ion, nor that the response of either is Nernstian. It is not affected by drifts or changes in E_A^0 or E_B^0 between measurements because a change in potential from the reference solution potential is all that is measured; in fact, the potentiometer reading could be adjusted to the same initial reading in the reference solution if desired. This method provides a measure of selectivity under defined quantitative conditions, and provides the actual concentration of interferent that would appear as equal to the primary ion.

Use of this definition of the selectivity coefficient would allow values to be reproduced from one study to another within a reasonable percentage

TABLE 1

Selectivity coefficients ($K^{Pot}_{Na,M}$) for the sodium glass electrode

Interferent ion	Mixed-solution method	Separate-solution method[a]	Separate-solution method[b]	Matched-potential method
K^+	0.018	0.27	0.12	7.6×10^{-3}
Mg^{2+}	9.5×10^{-4}	2.8×10^{-3}	2.0×10^{-3}	3.5×10^{-4}
Ca^{2+}	1.8×10^{-3}	3.2×10^{-3}	2.2×10^{-4}	7.1×10^{-4}

[a]Equal concentrations of A and B. [b]Unequal concentrations of A and B.

TABLE 2

Selectivity coefficients ($K^{Pot}_{K,M}$) for the potassium valinomycin electrode

Interferent ion	Mixed-solution method	Separate-solution method[a]	Separate-solution method[b]	Matched-potential method
Na^+	2.9×10^{-4}	7.0×10^{-3}	6.8×10^{-4}	$8.3(\pm 0.8) \times 10^{-5}$ [c]
Mg^{2+}	—	1.2×10^{-4}	2.0×10^{-4}	$2.6(\pm 0.6) \times 10^{-4}$ [d]
Ca^{2+}	—	1.8×10^{-4}	2.1×10^{-4}	$3.7(\pm 0.4) \times 10^{-4}$ [e]

[a]Equal concentrations of A and B. [b]Unequal concentrations of A and B. [c]$n = 6$. [d]$n = 4$. [e]$n = 2$.

error for a given set of conditions; alternatively, a fixed concentration or activity of primary ion could be adopted for the reference solution in reporting results. This method would obviously be limited to those conditions in which the selectivity for the primary ion is not large, because the solubility of the secondary ion salt may be exceeded before an equal potential change is reached (with subsequent appreciable ionic strength changes). But this is the exact situation in which one would need to know the relative response of the electrode to the interfering ion most accurately. For larger selectivities, the range of measurements by this matched-potential method could be extended by using a more dilute reference solution or smaller primary ion increment.

This case is illustrated for the potassium valinomycin electrode. In the evaluation of selectivity coefficients for this electrode by the matched-potential method (Table 2), 1.2×10^{-5} M KCl was used as the reference solution. This is equivalent to diluting a serum sample 400 times. For potential changes of 12, 21, 27, and 32 mV, $K^{Pot}_{K^+,Na^+}$ values were 8.6, 7.0, 9.2, and 8.6 $\times 10^{-5}$, respectively. The magnitude of the potential change does not appreciably affect the selectivity obtained by this method. The selectivity values obtained by this method are within the range of values reported by other workers [8—11].

REFERENCES

1 R. P. Buck, Anal. Chim. Acta, 73 (1974) 321.
2 G. J. Moody, R. B. Oke and J. D. R. Thomas, Analyst (London), 95 (1970) 910.
3 K. Camman, Anal. Chem., 50 (1978) 936.
4 G. A. Rechnitz, M. R. Kresz and S. B. Zamochinick, Anal. Chem., 38 (1966) 973.
5 L. P. Bailey, Analysis with Ion-Selective Electrodes, 2nd edn., Heyden, 1980, pp. 49—50. pp. 49—50.
6 M. F. Wilson, E. Haikala and P. Kivalo, Anal. Chim. Acta, 74 (1975) 397.
7 K. Srinivasan and G. A. Rechnitz, Anal. Chem., 41 (1969) 1203.
8 M. Mascini and F. Pallozzi, Anal. Chim. Acta, 73 (1974) 375.
9 U. Fiedler and J. Růžička, Anal. Chim. Acta, 67 (1973) 179.
10 R. W. Cattrall, S. Tribuzio and H. Freiser, Anal. Chem., 46 (1974) 2233.
11 F. S. Nakayama and B. A. Rasnick, Anal. Chem., 39 (1967) 1022.

Analytica Chimica Acta, 164 (1984) 283—286
Elsevier Science Publishers B.V., Amsterdam — Printed in The Netherlands

Short Communication

ELECTROCHROMATOGRAPHY—A PRELIMINARY STUDY OF THE EFFECT OF APPLIED POTENTIAL ON A CARBONACEOUS CHROMATOGRAPHIC COLUMN

ROBERT F. ANTRIM, ROBERT A. SCHERRER and ALEXANDER M. YACYNYCH*

Department of Chemistry, Rutgers, The State University of New Jersey, New Brunswick, NJ 08903 (U.S.A.)

(Received 16th April 1984)

Summary. The preparation of a trimethylchlorosilane-modified carbon support material and the construction of a three-electrode high-performance liquid chromatographic column are described. The effects of applied potential on the capacity factors are described. The capacity factors decrease by factors of 8 for toluene, 2 for phenol, and 1.1 for pyridine as the applied potential is changed from + 0.8 to —0.8 V vs. Ag.

In modern high-performance liquid chromatography (h.p.l.c.), the analyst has a plethora of variables from which to choose when optimizing a separation. However, it is difficult to change the stationary phase without changing the column. This communication describes preliminary results of a study in which the properties of the stationary phase are changed by the application of an electrical potential. This was accomplished with an electrically conductive, carbonaceous, trimethylchlorosilane-modified support as the packing material with the column serving as the working electrode in a three-electrode system. It is known that changes in the potential of an electrode produce changes in its interfacial characteristics [1], which in turn change the surface interactions of the electrode with solutes [2—4]. The effect of applied potential in chromatography has been demonstrated in the case of low-pressure separations. In these studies, it was shown that the application of a potential could deposit solutes, which could then be stripped at different potentials [5—10]. This communication describes the construction, and preliminary results obtained for toluene, phenol, and pyridine with a controlled-potential chromatographic column.

Experimental

Preparation of carbon. The carbonaceous material used as the chromatographic support was Ambersorb XE-347 (Rohm and Haas, Philadelphia, PA). After milling, a 270—325-mesh fraction was used. To remove impurities, this material was washed with 6 M nitric acid by stirring overnight, rinsed with distilled/deionized water until neutral, dried overnight at 120°C, and

0003-2670/84/$03.00

extracted in a Soxhlet apparatus with ethanol for 24 h and then dried overnight at 120°C. The material was then oxidized using a radio-frequency-generated oxygen plasma (Harrick Scientific, Ossining, NY) at 0.2 Torr, and reduced with lithium aluminum hydride (Aldrich Chem. Co., Milwaukee, WI).

This support was silated in a 500-ml, 3-neck round-bottom flask containing 10 g of sized carbon, 250 ml of dry toluene, obtained by distillation over sodium, and 5 ml of trimethylchlorosilane (C_3; Aldrich). This mixture was refluxed overnight, with nitrogen purging to remove generated hydrogen chloride. The carbon was then removed and dried at 120°C for 8 h. It was extracted with acetonitrile in a Soxhlet apparatus overnight, then dried at 120°C. This material was used to pack the column.

Column construction. The three-electrode column (Fig. 1) allows application of a potential to the stationary phase without hindering the chromatography. It is constructed of commercially available components except for the 0.25/0.5-in. reducer and female connectors. The two female connectors are important because they insulate the column electrically from the pump and detector. The inner column consisted of two 3-in. pieces of 316 stainless steel welded to an 18-in., 5-μm porous stainless steel tube (Mott Metallurgical Corp., Farmington, CT). The porosity of the column was further decreased by polymerizing acrylamide into the pores. This was accomplished by placing a previously dried column into a 25-mm by 48-cm glass tube which was in an ice bath. Then 130 ml of cooled (ca. 0°C) 0.1 M sodium perchlorate containing 45 g of acrylamide (Aldrich), 0.5 g of ammonium persulfate (Matheson Coleman & Bell, Norwood, OH), and 2.5 ml of 1:10 (v/v) *N,N,N′,N′*-tetramethylethylenediamine (Aldrich)/0.1 M sodium perchlorate were added to the tube, which was immediately placed under vacuum. Polymerization was allowed to continue for 1 h under vacuum, then the tube was placed in an

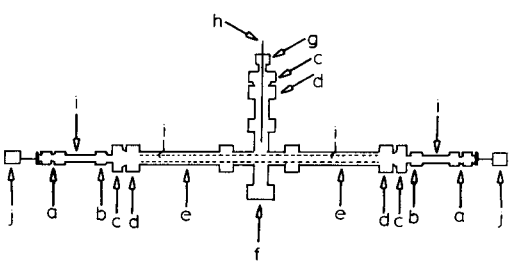

Fig. 1. Schematic diagram of the chromatographic column. (a) 0.25-in. low-internal-dead-volume column end fitting; (b) 0.25-in. NY tube nut-drilled to accept 0.25-in. tubing; (c) 0.25/0.5-in. NY reducing union drilled to accept 0.5-in. tubing; (d) 0.5-in. SS tube nut; (e) 0.5-in. SS tubing (auxiliary electrode); (f) 0.5-in SS union cross; (g) 0.25-in. SS plug drilled to accept silver wire (pseudo-reference electrode); (h) 20-gauge silver wire silver soldered in (g); (i) separation column (working electrode), see text for details; (j) NY insulators, 0.5-in. round stock drilled through with a 10-thou wire drill and tapped to accept 1/16-in. i.d. nut (NY-nylon, SS-type 316 stainless steel); (a—i) obtained from Parker Fluid Connectors, Huntsville, AL.

ice bath overnight. The excess of polyacrylamide was scraped from the column and the inner bore. The complete column was assembled, and the support material was slurry-packed, using ethanol, at 2000 psi with a model DSTV-122 Haskel pump (Haskel, Burbank, CA). The mobile phase was 0.1 M sodium perchlorate (G. Frederick Smith, Columbus, OH) in acetonitrile (h.p.l.c.-grade; Baker Chemical Co., Phillipsburg, NJ). The flow rate was 2.0 ml min^{-1} for all studies of k'.

Procedures. Potential was applied to the column by attaching the column (working electrode), the 0.5-in. SS jacket (auxiliary electrode), and a silver wire pseudo-reference electrode, to a potentiostat (model 550; ECO, Cambridge, MA).

Initially, a potential was applied and the current was allowed to reach steady state. The pump was then started, and the current was again allowed to reach a steady state. Solutes (5 μl) were injected and absorbance was monitored at 254 nm.

Results and discussion

Because there are no commercially available carbonaceous supports [11], a suitable support had to be made. Ambersorb XE-347 was used because it has suitable mechanical stability and the necessary conductivity for construction of a three-electrode electrochemical column. The column was checked for its pressure capability and hardness of support material by increasing the flow rate in steps and recording the pressure. The results indicated a linear relationship as expected from the equation [12], $u = K^0P/nL$, where u is the mobile phase velocity, K^0 is the column permeability, P is the pressure drop, n is the viscosity of the mobile phase, and L is the length of the column. Pressures up to 3000 psi were tested by constricting the flow after the column.

Because the column is very slightly porous and contains polyacrylamide in the pores of the walls, tests were done to establish if these factors had a deleterious effect on the chromatography. A 316 stainless steel column of identical length and internal diameter was packed with C_3-modified carbon and compared to the three-electrode column. Samples were injected under identical conditions and their retention times and capacity factors (k') were determined. The retention time and k' values showed that both types of columns compare very favorably, indicating that the polyacrylamide has no effect on the chromatography.

Data in Table 1 show an increase in k' as the potential is poised at increasingly positive values. One of the drawbacks to the use of carbonaceous supports is the relatively small range of solvent strength available when compared to the alkyl-modified silicas [13, 14]. Because it appears that retention time changes with applied potential, this approach may help to overcome this disadvantage of carbonaceous supports. Reasons for the dependence of k' on applied potential are not clear at this time but will be the subject of future studies.

TABLE 1

Effects of potential on capacity factors for toluene, phenol, and pyridine

Potential (V vs. Ag)	Capacity factor (k')		
	Toluene	Phenol	Pyridine
+0.8	1.3	16	16.6
+0.4	0.9	8.6	15.5
−0.8	0.6	2.0	15.0

R. F. A. thanks Rutgers University for a Morgan Graduate Fellowship. We thank R. A. Hartwick and H. J. Wieck for very helpful discussions and suggestions.

REFERENCES

1 J. O'M. Bockris and A. K. N. Reddy, Modern Electrochemistry, Vol. 2, Plenum Press, NY, 1976, p. 626.
2 P. Delahay, Double layer and Electrode Kinetics, Interscience, NY, 1967.
3 A. J. Bard and L. R. Faulkner, Electrochemical Methods, Fundamentals and Applications, Wiley, NY, 1980.
4 E. Gileade, E. Kirowa-Eisner and J. Perciner, Interfacial Electrochemistry, Addison-Wesley Pub. Co. Inc., Reading, MA, 1975.
5 W. J. Blaedel and J. H. Strohl, Anal. Chem., 36(7) (1964) 1245.
6 J. H. Strohl and T. A. Polutanovich, Anal. Lett., 2(8) (1969) 423.
7 T. Fujinaga, Pure Appl. Chem., 25 (1971) 709.
8 T. Fujinaga and S. Kihara, Crit. Rev. Anal. Chem., 7 (1977) 223.
9 J. H. Strohl and K. L. Dunlap, Anal. Chem., 44(13) (1972) 2166.
10 J. L. Hern and J. H. Strohl, Anal. Chem., 50(14) (1978) 1954.
11 K. K. Unger, Anal. Chem., 55 (1983) 361A.
12 L. R. Snyder and J. J. Kirkland, Introduction to Modern Liquid Chromatography, 2nd edn., Wiley Interscience, NY, 1979, p. 36.
13 H. Colin, C. Eon and G. Guiochon, J. Chromatogr., 122 (1976) 223.
14 H. Colin, G. Guiochon and P. Jandera, Chromatographia, 15 (1982) 133.

Analytica Chimica Acta, 164 (1984) 287—291
Elsevier Science Publishers B.V., Amsterdam — Printed in The Netherlands

Short Communication

THE EFFECTS OF ERRORS IN MEASURING THE INDEPENDENT VARIABLE IN LEAST-SQUARES REGRESSION ANALYSIS

LOUIS MEITES*[a] and H. C. SMIT

Laboratorium voor Analytische Scheikunde, Universiteit van Amsterdam, Nieuwe Achtergracht 166, 1018WV Amsterdam (The Netherlands)

G. KATEMAN

Laboratorium voor Analytische Scheikunde, Universiteit van Nijmegen, Toernooiveld, 6525ED Nijmegen (The Netherlands)

(Received 6th April 1984)

Summary. It is well known that linear regression analysis gives unbiased estimates of the slope and intercept of a straight line if the dependent variable y is subject to random errors of measurement while the independent variable x is not. It is much less well known that, if x is also subject to random errors of measurement, linear regression analysis yields an underestimate of the slope and a correspondingly biased estimate of the intercept. These errors cannot be removed by weighted regression. Similar errors arise in non-linear regression when the independent variable is afflicted by random errors of measurement.

Suppose that some dependent variable y is related to an independent one x by an equation of the form $y = ax + b$, and that a number of hypothetically error-free measurements of their values are used to evaluate the parameters α and β in the regression equation $\hat{y} = \alpha x + \beta$. The values of α and β may be found by combining those two equations and differentiating to obtain

$$d\Sigma(y - \hat{y})^2/d\alpha = d\Sigma(ax + b - \alpha x - \beta)^2/d\alpha$$
$$= 2(\alpha - a)\Sigma x^2 - 2(b - \beta)\Sigma x$$

Equating this to zero to minimize the sum of the squares of the residuals gives

$$\alpha = [(b - \beta)\Sigma x/\Sigma x^2] + a \quad (1)$$

and the expression

$$\beta = (a - \alpha)\Sigma x + b \quad (2)$$

may be obtained by equating $d\Sigma(y - \hat{y})^2/d\beta$ to zero in similar fashion.

[a]Permanent address: Department of Chemistry, George Mason University, 4400 University Drive, Fairfax, VA 22030, U.S.A.

0003-2670/84/$03.00

Combining Eqns. 1 and 2 yields $\alpha = a$ and $\beta = b$. In this hypothetical case, the values of α and β are exactly equal to those of the parameters a and b.

Another familiar route to the same conclusion is as follows. If a residual r is defined by the equation $r = y - \hat{y}$, the variance σ_r^2 of the residuals is given by

$$\sigma_r^2 = \Sigma(y - \hat{y})^2 = \Sigma(y - \alpha x - \beta)^2$$

$$= \alpha^2\sigma_x^2 - 2\alpha\sigma_{xy} + \sigma_y^2 + (\mu_y - \alpha\mu_x - \beta)^2 \tag{3}$$

where σ_x and σ_y denote the variances and μ_x and μ_y the means of x and y, respectively, and σ_{xy} denotes the covariance of x and y. Minimizing σ_r^2 with respect to both α and β by writing

$$d\sigma_r^2/d\alpha = 0 = 2\alpha\sigma_x^2 - 2\sigma_{xy} - 2\mu_x\mu_y + 2\beta\mu_x + 2\alpha\mu_x^2 \tag{4}$$

and

$$d\sigma_r^2/d\beta = 2\beta - 2\mu_y + 2\alpha\mu_x = 0 \tag{5}$$

and combining Eqns. 4 and 5 yields

$$\alpha = \sigma_{xy}/\sigma_x^2 \tag{6}$$

$$\beta = \mu_y - \alpha\mu_x \tag{7}$$

Now suppose that each measured value of y, denoted by the symbol y', contains a random error of measurement p whose value is independent of x or y, so that $y' = y \pm p$. The estimate of α will become

$$\alpha' = \sigma_{xy'}/\sigma_x^2 = \Sigma[(x - \mu_x)(y - \mu_y \pm p)]/\Sigma(x - \mu_x)^2$$

$$= \Sigma[(x - \mu_x)(y - \mu_y) \pm p(x - \mu_x)]/\Sigma(x - \mu_x)^2$$

$$= \Sigma[(x - \mu_x)(y - \mu_y)] \pm p\Sigma(x - \mu_x)/\Sigma(x - \mu_x)^2$$

But $\Sigma(x - \mu_x) = 0$, and therefore

$$\alpha' = \Sigma[(x - \mu_x)(y - \mu_y)]/\Sigma(x - \mu_x)^2 = \sigma_{xy}/\sigma_x^2$$

which is identical with the expression for α given by Eqn. 6. Accordingly, the latter is unbiased in this situation, as has long been known.

If, however, it is x rather than y that is subject to errors of measurement, so that $x' = x \pm p$, the estimate of α becomes

$$\alpha' = \sigma_{x'y}/\sigma_{x'}^2 = \Sigma[(x - \mu_x \pm p)(y - \mu_y)]/\Sigma(x - \mu_x \pm p)^2$$

$$= \Sigma[(x - \mu_x)(y - \mu_y) \pm p\Sigma(y - \mu_y)]/\Sigma[(x - \mu_x)^2 \pm 2p(x - \mu_x) + p^2]$$

$$= \Sigma[(x - \mu_x)(y - \mu_y) \pm p\Sigma(y - \mu_y)]/[\Sigma(x - \mu_x)^2 \pm 2p\Sigma(x - \mu_x) + \Sigma p^2]$$

Because both $\Sigma(y - \mu_y)$ and $\Sigma(x - \mu_y)$ are equal to zero, the result is

$$\alpha' = \sigma_{xy}/(\sigma_x^2 + \sigma_p^2) \tag{8}$$

which may be compared with Eqn. 6 to yield

$$\alpha'/\alpha = \sigma_x^2/(\sigma_x^2 + \sigma_p^2) < 1 \tag{9}$$

In this situation the estimated value of α is too small, and the resulting bias is of course propagated onto the value of β, which according to Eqn. 7 will be overestimated if $\alpha\mu_x$ is negative and underestimated if $\alpha\mu_x$ is positive. Although α' gives the smallest sum of the squares of the residuals and should therefore be used in calculating interpolated or extrapolated values of y, its value is wrong and should be corrected, in the manner suggested by Eqn. 9, whenever the purpose of the experiment is to evaluate α rather than to permit predictions of y. At least an approximate value of σ_p is needed in making this correction.

If both x and y are subject to error, so that $x' = x \pm p_x$ while $y' = y \pm p_y$, similar reasoning gives

$$\begin{aligned}
\alpha' &= \sigma_{x'y'}/\sigma_{x'}^2 \\
&= \Sigma[(x - \mu_x \pm p_x)(y - \mu_y \pm p_y)]/\Sigma(x - \mu_x \pm p_x)^2 \\
&= \{\Sigma[(x - \mu_x)(y - \mu_y)] \pm p_y\Sigma(x - \mu_x) \pm p_x\Sigma(y - \mu_y) + \Sigma(\pm p_x)(\pm p_y)\}/ \\
&\quad \{\Sigma(x - \mu_x)^2 \pm 2p_x\Sigma(x - \mu_x) + \Sigma p_x^2\} \\
&= \sigma_{xy} + \Sigma(\pm p_x)(\pm p_y)/(\sigma_x^2 + \sigma_{p_x}^2)
\end{aligned}$$

The product $p_x p_y$ of the sum of the errors will be positive when the errors have the same sign, and negative when they have opposite signs; on the average, $\Sigma p_x p_y$ will be equal to zero, and in the absence of experimental bias it will certainly be much smaller than the term Σp_x^2 in the denominator, which is necessarily always positive. Hence a biased estimate of α is always to be anticipated when the measured values of x are subject to error.

This situation must be sharply distinguished from the one discussed by Beckson [1], which though related is very different in principle. There are some practical situations in which the successive values of x are controlled (i.e., preassigned). Beckson proved that the method of least squares can be used to fit such data to a straight line as though x were free from error, even though its individual values may differ from the nominal or pre-assigned ones.

In the situation under discussion here, where the values of x are not pre-assigned, any given uncertainty in the value of the independent variable at any particular point gives rise to an uncertainty in the corresponding value of the dependent variable, and the magnitude of the latter uncertainty depends on the slope of the curve at the point in question. This is the principle of weighted regression analysis, in which one minimizes a quantity of the form

$$\Sigma\{(y - \hat{y})^2/[s_y^2 + s_x^2(\mathrm{d}y/\mathrm{d}x)^2]\}$$

If, as was assumed above, $y = ax + b$, the denominator of this quantity is

constant no matter what the standard errors of measurement, s_x and s_y, may be, and the bias of the least-squares estimate is therefore immune to weighted analysis.

Because weighted regression analysis is associated with uncertainties in the measured values of the independent variable, the fact that it cannot remove bias in the simplest case suggests that it may always yield biased results. Such propositions are ill suited to proof or disproof by numerical calculations, but the following results may be of interest. Twenty-five points on the theoretical titration curve for the titration of a strong acid with a strong base were synthesized in the manner previously described [2], using the values c_a^0 = 0.01 M (the initial concentration of the acid titrated), $\log_{10} K_t$ = 14 (the decadic logarithm of the concentration constant $1/[H^+][OH^-]$), and y_{H^+} = 1 (the apparent single-ion activity coefficient of hydrogen ion). They were subjected to both unweighted and weighted regression analysis, using a general computer program [3] written in FORTRAN and executed in double precision on a Hewlett-Packard HP-1000 computer. Exact equations were used throughout and are given in detail elsewhere [2]. The value c_b = 0.01 M (the concentration of the base used as reagent) was also assumed, both in synthesizing the "data" and in the regression analyses.

Unweighted regression (which is tantamount to assuming that there are no errors in the measured volumes), in which the calculations were initialized differently and performed in different modes so that they would take different courses, gave the following average values: c_a^0 = 0.010 000 000 005 M, $\log K_t$ = 14.000 000 077, and y_{H^+} = 0.999 999 934. Errors of this magnitude are inherent in the nature of a search for a minimum on a four-dimensional error surface and in the errors of the arithmetic routines employed; no individual result was affected by even quite substantial changes in the extraordinarily stringent conditions that were set for termination.

Similar calculations by weighted regression gave the following average values: c_a^0 = 0.010 000 000 010 M, $\log K_t$ = 14.000 000 211, and y_{H^+} = 0.999 999 932. Weighting has no detectable effect on the average value for y_{H^+}, but the average values of the other two parameters are definitely and systematically higher in weighted than in unweighted regression.

Although the errors that arise in this example are far too small to have any experimental significance, there is no reason to suppose that that will always be true. In every experiment, the measurements of the independent variable are subject to some uncertainty, and experimenters should be aware that this introduces a bias into the results of proper statistical treatment of the data. Generally similar conclusions have been reached by others [4] but have been widely overlooked.

This work was made possible by the generous support of the Nederlandse Organisatie voor Zuiver Wetenschappelijk Onderzoek, and was aided in part by grant number CHE-8106103 from the National Science Foundation.

REFERENCES

1 J. Beckson, J. Am. Stat. Assoc., 45 (1950) 164.
2 H. C. Smit, L. Meites and G. Kateman, Anal. Chim. Acta, 153 (1983) 121.
3 L. Meites, The General Non-Linear Regression Program CFT4A, privately published, 1983.
4 P. M. E. M. van der Grinten and J. M. H. Lenoir, Statistische Procesbeheersing, Het Spectrum, Amsterdam, 1973.

Analytica Chimica Acta, 164 (1984) 293—297
Elsevier Science Publishers, B.V., Amsterdam — Printed in The Netherlands

Short Communication

QUANTIFYING CHEMICAL COMPOSITION FROM TWO-DIMENSIONAL DATA ARRAYS

AVRAHAM LORBER

Nuclear Research Centre-Negev, P.O. Box 9001 Beer-Sheva, 84190 (Israel)

(Received 4th June 1984)

Summary. Many analytical instruments (e.g., videofluorimeter and liquid chromatographs with spectrometric detectors) can produce two-dimensional data arrays. Rank-annihilation factor analysis enables chemical composition to be quantified from such an array. Solution by this method requires a search for a minimum value of an eigenvector which cannot be calculated even iteratively. The problem is presented here as a generalized eigenvalue problem and a direct solution is found by using singular value decomposition.

When a spectrum is acquired by a multichannel detector at several time intervals during a chromatographic separation, the resulting data serve to construct an image. The spectrum/time scales are the frame of the picture and the intensity is the gray scale. In mathematical terms, an image can be constructed if the object under scrutiny gives rise to more than one type of response when subjected to perturbations [1]. The above spectra/time example is one example where the instrument produces an image. Another example is the emission/excitation image produced by the videofluorimeter [2]. Quantification of chemical composition from images produced by instruments or by kinetic experiments has been studied in detail in recent years because of the increasing number of instruments that can produce such images. Most of the numerical methods suffer from one or more of the following limitations: (a) quantification requires a unique response for one or more of the components [3—7]; (b) mixtures of only up to three components can be handled [8—11]; (c) prior assumptions are necessary [12—15]. A method that does not suffer from the above limitations is rank-annihilation factor analysis (r.a.f.a.) [16]. The method has been successfully applied to video-fluorimetry [16—18] and liquid-chromatography with ultraviolet detection [19].

While r.a.f.a. makes it possible to quantify an individual component which contributes to a compound image produced by several components, it does not require any knowledge of the identity or amount of the others. Also quantification does not require a unique response or any assumption. However, implementation of r.a.f.a. does demand three prerequisites. First, the image of the quantified component must not be expressed by a linear sum of images of the other components in the sample, i.e., its contribution to the image of the sample must raise the rank of the data matrix. Secondly,

0003-2670/84/$03.00

the image of an individual component must be expressed as a matrix product of two vectors. For the spectrum/time example, one vector is its spectrum and the other is its chromatogram, i.e., the rank of the individual component data matrix should be unity. Thirdly, the image of the quantified component must be known in advance. If the first two requirements are combined, it is clear that subtracting the known image of the quantified component will result in a rank reduction only in the case that the image of the known component is multiplied by a scalar equal to the ratio amount in sample/amount in standard. Thus quantification reduces to the problem of finding a scalar value that will reduce the rank of the sample data matrix.

The scalar value can be established by examining the effect of varying the scalar value on the smallest significant eigenvalue. Ho et al. [16] succeeded in reducing the large amount of computation necessary to compute the eigenvalues by examining the eigenvalues of a matrix of the same order as the number of components instead of solving for the full data matrix. However, even with this simplification, a lot of computational work remains because the correct value of the scalar cannot be computed either directly or iteratively. In this communication, it will be shown that the scalar value can be computed directly.

Reformulation of the method

In r.a.f.a., the two-dimensional data matrix, $\mathbf{N}_k$, for each component should obey the rule $\mathbf{N}_k = \mathbf{x}_k \mathbf{y}_k^{\mathrm{T}}$, where $\mathbf{x}_k$ is a column vector with elements $x_{k,i} (i = 1, \ldots m)$ and $\mathbf{y}_k$ is a column vector with elements $y_{k,j} (j = 1, \ldots n)$; subscript k denotes the kth component. Throughout this communication, superscript T denotes the operation of matrix transposition. A scalar which expresses the quantum efficiency, molar absorptivity, and concentration should multiply the right-hand side of the equation. For convenience, this scalar is absorbed into $\mathbf{x}_k$ and $\mathbf{y}_k$. The matrix $\mathbf{N}_k$ is considered as a standard matrix at a concentration of C_k^0. The data matrix of a mixture composed of N_c components ($k = 1, \ldots N_c$) should also be expressed by a linear sum over the data matrices of all contributors

$$\mathbf{D} = \sum_{k=1}^{N_c} \mathbf{x}_k \mathbf{y}_k^{\mathrm{T}} / \lambda_k$$

The scalar λ_k is the ratio of the concentration of kth component in the standard solution to its value in the mixture. The ingenuity of the r.a.f.a. method is the observation that when the value λ_k is found, the matrix $\mathbf{M}$, which is obtained by $\mathbf{M} = \mathbf{N}_k - \lambda_k \mathbf{D}$, is a matrix of rank $N_c - 1$. This observation suggested that examining the effect of varying λ_k on the eigenvalues of the matrix $\mathbf{M}$, will yield quantitative results on the concentration of the kth component.

In conventional mathematical treatment, the problem of reducing the rank of a matrix is equivalent to saying that the determinant of the matrix is zero. Thus, the problem may be formulated as $|\mathbf{N}_k - \lambda_k \mathbf{D}| = 0$. This problem is also known as the generalized eigenvalue/eigenvector problem

$\mathbf{N}_k\mathbf{z} = \lambda_k\mathbf{D}\mathbf{z}$. Here, z is the eigenvector and λ_k is the eigenvalue. However, the present situation differs from the conventional eigenvalue problem in the following respects: (a) the matrices $\mathbf{N}_k$ and D are very probably rectangular; (b) the matrix $\mathbf{N}_k$ is singular; and (c) the matrix D or $\mathbf{D}^T\mathbf{D}$ is not an identity matrix. Solution of the problem is possible, however, by using decomposition techniques. The singular value decomposition will serve here to find the solution.

The singular value decomposition

It is well known in linear algebra that any real matrix may be decomposed into three matrices, $\mathbf{D} = \mathbf{USV}^T$, where U is an $m \times m$ orthonormal matrix (i.e., $\mathbf{U}^T\mathbf{U} = \mathbf{I}_m$, where $\mathbf{I}_m$ denotes the identity matrix of dimension m); V is an orthonormal square matrix of order n, and S is an $m \times n$ matrix. Its upper $n \times n$ matrix is a diagonal matrix (only the diagonal elements may differ from zero), with elements $s_1, s_2, \ldots s_p, \ldots s_n$ for which $s_1 \geqslant s_2 \geqslant, \ldots s_p \geqslant, \ldots s_n$. These scalars are the non-zero singular values of the matrix D. The singular values are unique, and are the square roots of the eigenvalues of the matrix $\mathbf{D}^T\mathbf{D}$. The subscript p denotes the smallest significant eigenvalue, $p \leqslant N_c$. The lower $(m - n) \times n$ part of S is a zero matrix. This decomposition into three matrices is referred to as the singular value decomposition (SVD) [20].

The second step in the analysis of the data matrix is to determine p, the number of significant eigenvalues. This step is called abstract factor analysis (a.f.a.). Methods of determining p are available [21]. When p is determined, an approximation, $\bar{\mathbf{D}}$, to the data matrix, D, which is reproduced from the p significant eigenvalues and eigenvectors is obtained by $\bar{\mathbf{D}} = \bar{\mathbf{U}}\bar{\mathbf{S}}\bar{\mathbf{V}}^T$. Now $\bar{\mathbf{U}}$ is a $m \times p$ matrix containing the first p eigenvectors that span the space of $\mathbf{DD}^T$; $\bar{\mathbf{V}}^T$ is a $p \times n$ matrix containing the first p eigenvectors that span the space of $\mathbf{D}^T\mathbf{D}$; $\bar{\mathbf{S}}$ is a diagonal matrix with the first p singular values as the diagonal elements. As a.f.a. assumes that nonsignificant eigenvalues and eigenvectors are due to random error, the matrix $\bar{\mathbf{D}}$ is free from random errors except for "imbedded errors" [21].

Solution of the problem

The eigenvalue problem is rewritten by using the SVD of the data matrix, D, as

$$\mathbf{x}_k\mathbf{y}_k^T\mathbf{z} = \lambda_k\bar{\mathbf{U}}\bar{\mathbf{S}}\bar{\mathbf{V}}^T\mathbf{z} \tag{1}$$

Using the orthogonal property of the matrix, $\bar{\mathbf{U}}$, gives

$$\bar{\mathbf{U}}^T\mathbf{x}_k\mathbf{y}_k^T\mathbf{z} = \lambda_k\bar{\mathbf{S}}\bar{\mathbf{V}}^T\mathbf{z} \tag{2}$$

The eigenvector Z is replaced by $\mathbf{z}' = \bar{\mathbf{S}}\bar{\mathbf{V}}^T\mathbf{z}$, which makes it possible to write

$$\bar{\mathbf{U}}^T\mathbf{x}_k\mathbf{y}_k^T\bar{\mathbf{V}}\bar{\mathbf{S}}^{-1}\mathbf{z}' = \lambda_k\mathbf{z}' \tag{3}$$

This relation is obtained by inserting the matrix $\bar{\mathbf{V}}\bar{\mathbf{S}}^{-1}\bar{\mathbf{S}}\bar{\mathbf{V}}^T$ into the left-hand side of Eqn. 1. The term $\bar{\mathbf{V}}\bar{\mathbf{V}}^T$ is not the same as the identity matrix unless

$n = p$. However, the matrix $\bar{\mathbf{V}}\bar{\mathbf{V}}^T$ is a projection matrix [22] and the following relations are in force: $\mathbf{y}_k^T\bar{\mathbf{V}}\bar{\mathbf{V}}^T = \mathbf{y}_k^T$ and $\bar{\mathbf{V}}\bar{\mathbf{V}}^T\mathbf{z} = \mathbf{z}$. In order to simplify the notation, the terms $\mathbf{a} = \bar{\mathbf{U}}^T\mathbf{x}_k$, and $\mathbf{b} = \bar{\mathbf{V}}^T\mathbf{y}_k$ are defined. These two vectors have p elements, a_i and $b_i (i = 1, \ldots p)$, and are called orthogonal rotation vectors [21, 22]. In this notation Eqn. 1 is rewritten as $\mathbf{ab}^T\bar{\mathbf{S}}^{-1}\mathbf{z}' = \lambda_k\mathbf{z}'$. In determinant notation, the final result is $|\mathbf{ab}^T\bar{\mathbf{S}}^{-1} - \lambda_k\mathbf{I}| = 0$, which is the familiar eigenvalue problem.

Because the rank of the matrix $\mathbf{ab}^T\mathbf{S}^{-1}$ is unity, there are $(p - 1)$ zero solutions for the eigenvalue. The only nontrivial solution is the sum of diagonal elements of the matrix (also known as the trace). Thus the solution is

$$\lambda_k = \sum_{i=1}^{p} a_i b_i / s_i \tag{4}$$

The concentration, C_k, of the kth constituent is then simply found by $C_k = C_k^0/\lambda_k$.

Discussion

The benefits of this solution of the r.a.f.a. problem are not limited to reduction of computation time. The solution overcomes the difficulties associated with deciding which of the eigenvalues should be scrutinized for the minimum that indicates rank annihilation. When r.a.f.a. was applied to a six-component sample [17], it was observed that the sixth eigenvalue did not show a minimum in the concentration interval examined; instead, several other eigenvalues exhibited minima. The proposed solution avoids this difficulty. The effect of taking into account more eigenvectors than there are real factors in the data matrix was examined by Ho et al. [17] who found that it had negligible effect on the result. This result, although it has no theoretical basis, ensures that, when the transformations are done, the number of factors will have a marginal effect.

The above-mentioned problem of deciding which of the eigenvalues to follow is a consequence of a more troublesome situation, rank deficiency. Rank deficiency arises from the combined effects of poorly resolved spectra and error in the data matrix. The outcome is error propagation: the experimental errors in the collected data are amplified to produce larger errors in the concentration determined. This problem is not unique to the r.a.f.a. method but is characteristic of all multivariate methods. Methods developed for estimating error limits for the conventional least-squares problem are not adequate for r.a.f.a., because error limits are expressed by vector norms of the concentrations [20] whereas in r.a.f.a. error limits should be placed for each component separately. Suitable error limits are now under investigation.

Ho et al. [16] also used the SVD (which they called biorthogonal expansion) to reduce the computational time needed to transform an $m \times n$ matrix to an $N_c \times N_c$ matrix. However, they did not observe that the transformations enable the direct solution to be found. Ho et al. [18] also developed an iterative method for the simultaneous determination of all components in

the solution. The proposed solution does not allow this benefit to be duplicated because when the standard matrix contains data for more than one component, the resultant eigenvalues cannot be assigned to specific components. Nevertheless, when one considers that the SVD computation is the main time consumer in the calculation, once the SVD has been done, quantifying each component requires only about $p \times (m + n)$ multiplications plus additions. Thus, there is no need to determine all components simultaneously.

The author thanks M. Glouberman for his help in the preparation of the manuscript.

REFERENCES

1 M. G. Moran and B. R. Kowalski, Anal. Chem., 51 (1979) 776A.
2 D. W. Johnson, J. B. Callis and G. D. Christian, Anal. Chem., 49 (1977) 747A.
3 W. H. Lawton and E. A. Sylvestre, Technometrics, 13 (1971) 617.
4 N. Ohta, Anal. Chem., 45 (1973) 553.
5 F. J. Knorr and J. H. Futrell, Anal. Chem., 51 (1979) 1236.
6 E. R. Malinowski, Anal. Chim. Acta, 134 (1982) 129.
7 P. C. Gillette, J. B. Lando and J. L. Koenig, Anal. Chem., 55 (1983) 630.
8 M. A. Sharaf and B. R. Kowalski, Anal. Chem., 53 (1981) 518.
9 M. A. Sharaf and B. R. Kowalski, Anal. Chem., 54 (1982) 1291.
10 J. H. Chen and L. P. Huans, Anal. Chim. Acta, 133 (1981) 271.
11 E. Spjotvoll, H. Martens and R. Volden, Technometrics, 24 (1982) 173.
12 J. J. Kankare, Anal. Chem., 42 (1970) 1322.
13 E. A. Sylvestre, W. H. Lawton and M. S. Maggio, Technometrics, 16 (1974) 353.
14 F. J. Knorr, H. R. Thorsheim and J. M. Harris, Anal. Chem., 53 (1981) 821.
15 S. D. Frans and J. M. Harris, Anal. Chem., 56 (1984) 466.
16 C.-N. Ho, G. D. Christian and E. R. Davidson, Anal. Chem., 50 (1978) 1108.
17 C.-N. Ho, G. D. Christian and E. R. Davidson, Anal. Chem., 52 (1980) 1071.
18 C.-N. Ho, G. D. Christian and E. R. Davidson, Anal. Chem., 53 (1981) 92.
19 M. McCue and E. R. Malinowski, J. Chromatogr. Sci., 21 (1983) 229.
20 C. L. Lawson and R. J. Hanson, Solving Least-Squares Problems, Prentice-Hall, Englewood Cliffs, NJ, 1974.
21 E. R. Malinowski and D. G. Howery, Factor Analysis in Chemistry, Wiley, New York, 1980.
22 A. Lorber, Anal. Chem., 56 (1984) 1004.

ANALYTICA CHIMICA ACTA, VOL. 164 (1984)

AUTHOR INDEX

(Continued from outside back cover)

CONTENTS

(Abstracted, indexed in: Anal. Abstr.; Biol. Abstr.; Chem. Abstr.; Curr. Contents Phys. Chem. Earth Sci.; Life Sci.; Index Med.; Mass Spectrom. Bull.; Sci. Citation Index; Excerpta Med.)

(Continued on inside back c